Late Quaternary climate in the Indo-Pacific Warm Pool reconstructed from the raised coral reefs of Sumba, Indonesia

Ding-Chuang QU

RESEARCH SCHOOL OF EARTH SCIENCES
THE AUSTRALIAN NATIONAL UNIVERSITY

A thesis submitted for the degree of Doctor of Philosophy of the Australian National University

MAY 2009

Except where otherwise indicated, this thesis is my own work.

ABSTRACT

A wealth of high-quality *Porites* coral cores have been retrieved from the Mondu raised reefs on the north coast of Sumba, Indonesia. The main aim of this thesis was to explore the U-series geochronology and palaeoclimatologic significance of the oxygen isotope and carbon isotope signals in Sumba corals from the penultimate deglaciation (Termination II) and the Holocene. These corals provided the opportunity to investigate the history of important climate systems in the Indo-Pacific Warm Pool region, such as the El Niño-Southern-Oscillation (ENSO), the Asian-Australian Monsoon, and the Indonesian Throughflow.

Multiple measurements of U-series isotopes in skeletal sub-samples within a single *Porites* coral were made to explore the diagenetic behaviour of U-series isotopes in fossil corals from the raised reefs of Sumba, Indonesia. Detailed analysis of two diagenetic stages and corresponding changes in U-series isotopic composition has revealed two distinct processes of U-series isotope diagenesis in this single coral colony. Both of them are different from those suggested before. The earlier process involved addition of allochthonous dissolved ^{234}U and ^{238}U together with addition of detrital non-radiogenic ^{230}Th, while the later process was clearly connected to loss of ^{234}U and ^{238}U occurring along to loss of detrital-bound ^{230}Th. Locally radiogenic ^{230}Th appears to have played an important role in maintaining a constant $^{234}U/^{230}Th$ when percolating groundwater with allochthonous U and a high $\delta^{234}U$ value entered the coral at the earlier stage. On the other hand, detritus-bound ^{230}Th was critical to maintain a fixed $^{234}U/^{230}Th$ when percolating meteoric water dissolved coral skeletal U at the later-stage. The results suggest that a mechanism like diffusion or osmosis controlled the addition or loss of dissolved U and detrital Th in the coral by way of a solute concentration gradient. This mechanism explains the constant $^{234}U/^{230}Th$ ratios in situations involving either the addition or loss of U. Model correction ages could be determined for both processes and they yield essentially the same age of 133.6 ka for the early highstand of Termination II.

This detailed study serves to substantiate the isochron model, and provides insight into the way by which the $^{234}U/^{230}Th$ ratio can remain constant when U is added to or lost from corals during diagenesis.

Initial U-series measurements on the Sumba corals demonstrated that reliable conventional ^{230}Th ages could not always be obtained from *Porites* corals and other robust thick-walled coral species older than the Holocene. However, fifty-four measurements of the U/Th isotopic composition of corals from the same reefs, and sub-samples from a single coral colony, form two distinct groups on a $^{234}U/^{238}U$ – $^{230}Th/^{238}U$ plot. Analysis of the $^{234}U/^{238}U$ – $^{230}Th/^{238}U$ plot shows that the data within the two groups comprise two parallel arrays of lines. The lines within the array associated with the older corals have larger slopes than the lines associated with the younger corals. Stratigraphic analysis demonstrates that the slopes of the lines reflect the burial/exposure history of the reefs and could serve to help determine the age of the reefs.

An isochron model was used to determine corrected ages for most of the Mondu raised reefs. All of the corrected ages are consistent with the stratigraphic analysis carried out in this study based on detailed topographic surveys and field observations. The corrected ages for the Mondu raised coral reefs fall within marine isotope sub-stages 5a-5e, early-stage highstands during Termination II and MIS 6, and a late-stage highstand during MIS 8. This study supports a near-constant uplift rate of 0.49 m/kyr in the Mondu area since ~260 ka (thousand years ago), even though the rate may have been slightly higher during MIS 5a and slightly lower during MIS 5c.

This study demonstrates that the Sumba corals are excellent recorders of climate and ocean dynamics in the Indo-Pacific Warm Pool. The Sumba coral $\delta^{18}O$ has recorded the mean climate conditions of the warm pool and indicates that surface seawater was enriched in ^{18}O by 0.3–0.5‰ during the mid-Holocene (3.7-5.7 ka), relative to the present time, despite the mid-Holocene sea surface temperature (SST) being within $0.5^{o}C$ of the modern SST. The Sumba coral records also show that the warm pool SST

was 2.4^{o}C cooler (relative to the mid-Holocene) when the sea level was -18 m lower at 134 ka during the early highstand of Termination II. It is likely that the seawater $\delta^{18}O$ value at that time was similar to the relatively high Holocene value, rather than the modern value.

High-resolution analysis of $\delta^{18}O$ and $\delta^{13}C$ in the fossil corals was used to interpret the influences of ENSO, the Asian-Australian monsoon and remote equatorial Indian Ocean forcing on the local climate and oceanography of Sumba. Distinctive signals in the coral $\delta^{18}O$ and $\delta^{13}C$ climatologies were utilized to disentangle the local climatologic imprints of the three climate systems. The Sumba coral $\delta^{18}O$ record shows the dominant control of ENSO in austral winter whereby the interannual variability of the winter $\delta^{18}O$ serves as a good index for ENSO events. In austral summer and autumn (November through May), the coral $\delta^{18}O$ is overwhelmingly controlled by the tropical Indian Ocean winds and the monsoon. The results suggest that the somewhat complicated relationship between ENSO and Asian-Australian monsoon varied during background climate states with different mean SST and seawater $\delta^{18}O$ values. When the Asian-Australian monsoon was relatively strong at ~134 ka during Termination II, the El Niño was suppressed. During the Holocene, both the ENSO and monsoon were relatively strong at 4.8 ka. At 3.7 ka the ENSO was weaker than at 4.8 ka and modern times, but the monsoon was still stronger than it is at present. Taken together, the Sumba coral records indicate that the modern monsoon is the weakest on record. However, El Niño events were 40% less frequent at 134 ka, 23% more frequent at 4.8 ka, and 11% less frequent at 3.7 ka, relative to modern El Niño activity.

The high-resolution Sumba modern *Porites* coral $\delta^{18}O$ provides evidence for the routine penetration of the South Java Current (SJC) in austral summer and remote forced equatorial Indian Ocean Kelvin wave in autumn into the Savu Sea, which results in distinct freshening of the surface ocean during the austral autumn. By sensitively recording variability of sea surface temperature and salinity in this important exit of the Indonesian Throughflow (ITF), the Sumba coral $\delta^{18}O$ revealed active oceanic current

activity in Sumba Strait since 134 ka. In austral winter, westward currents generally flow in the Sumba Strait and the ITF brings Pacific source-water with moderate salinity. In summer, the more saline SJC enters the Savu Sea from the west until around March. After March, two causes gradually lower the seawater salinity: the gradual weakening of the eastward SJC owing to the weakening of northwest monsoon winds, and the arrival of a remotely forced Kelvin wave with very warm and fresh water during April-July. Input of Indian Ocean water into the Savu Sea by the summer SJC and autumn Kelvin wave could have significantly influenced the transport of the Indonesian Throughflow

Detailed correlations between annual skeletal density banding and the high-resolution coral $\delta^{13}C$ record show that the low skeletal density band coincides with peak summer monsoonal rainfall and maximum depletion in skeletal $\delta^{13}C$. This correlation was attributed to the large input of terrigenous nutrients linked to peak summer monsoonal rainfall. This relationship could be applied to explore local monsoon variability in a more economical and efficient way by simply measuring the coral density.

ACKNOWLEDGEMENTS

My sincere thanks go firstly to my supervisor Mike Gagan. Thank you so much for leading me into the fantastic domain of paleoclimatology and paleoceanography through this wonderful PhD project. None of it would have been possible without your remarkable scientific insight. Thanks for knowing exactly how to guide me in the right direction and for providing support whenever I needed it. Thank you for everything.

I would also like to thank my advisor Malcolm McCulloch for being generous with instrument time and offering helpful in advice and suggestions. Sincere thanks also go to my other advisors, John Chappell, Wahyoe Hantoro, and Gavin Dunbar for all their help along the way. An extra giant thanks to Gavin Dunbar for being both a mentor and friend over the years.

Thanks to everyone at RSES for being great people to work with. Thanks especially go to Heather Scott-Gagan, Joe Cali, Joan Cowley, Graham Mortimer, Sue Kesson, Tony Phimphisane, and Harri Kokkonen for their technical expertise that kept my research flowing smoothly. Thanks also to the other RSES PhD students who I have really enjoyed getting to know, and especially to Nerilie Abram, Helen McGregor, Rose Berdin, and Erica Hendy for their wonderful opinions and help.

I would like to thank Wahyoe Hantoro and Bambang Suwargadi from the Indonesian Institute of Sciences, Mike Gagan and Gavin Dunbar from RSES, and the many local supporters for their amazing support during the 2003 coral drilling expedition to Sumba, Indonesia.

Thanks also go to Ulrich Radtke for supporting my visit to the Department of Geography at the University of Cologne for training and collaborative measurements of electron spin resonance for dating corals. I am very grateful to the Radtke family and to everyone in the Department of Geography for making me feel so welcome and offering

their friendship and guidance during my stay.

Last, but certainly not least, heaps of thanks to Jian-xin Zhao at the University of Queensland for support during the final stages of the thesis writing. Special thanks go to his wife Liu Fang and his team for being so encouraging and helpful.

TABLE OF CONTENTS

CHAPTER 1

RATIONALE AND AIMS

1.1 RATIONALE

The primary goal of this PhD project is to reconstruct the natural bounds of Late Quaternary ocean/climate variability in the Indo-Pacific Warm Pool. The Indo-Pacific Warm Pool-Indonesian Maritime Continent region is a key component of global climate system. The Warm Pool is a major source of moisture and latent heat for the global atmosphere and plays a fundamental role in driving the globally important meridional Hadley circulation and zonal Walker circulation [*Keenan et al.*, 2000]. Recent studies indicate that changes in sea surface temperature (SST) and atmospheric convection in the tropical Indo-Pacific region contribute to the interannual to decadal climate variability observed in extra-tropical regions [*Cane*, 1998; *Hoerling et al.*, 2001]. Changes in the Warm Pool region may also play an important role in driving glacial-interglacial cycles [*Visser et al.*, 2003] and possibly millennial-scale climate change [*Cane and Clement*, 1999; *Stott et al.*, 2002]. Important tropical climate systems with global impact, such as the El Nino-Southern Oscillation (ENSO), Asian-Australian Monsoon and Indian Ocean Dipole (IOD), interact within this region. The Indonesian Throughflow from the Pacific to the Indian Ocean also contributes to the thermal conditions and local hydrological cycles of this region [*Gordon et al.*, 2003; *Gordon*, 2005].

Despite its profound importance, little is known about the natural bounds of past ocean/climate variability of the Warm Pool because of the limited historical database in this region. The available instrumental records for the Warm Pool region are too short and scarce to adequately characterise its natural variability. The problem of sparse data is exacerbated by the fact that many scientists believe that human activity has already influenced modern sea surface temperature and climate variability [e.g. El Niño/La Niña phenomena, *Trenberth and Hoar*, 1996] through the injection of fossil fuel CO_2 into the atmosphere [*Hansen and Lebedeff*, 1987]. Proxy records of climate provide the only means for extending the Warm Pool ocean/climate records to pre-anthropogenic time.

Also, paleoclimate reconstructions provide the only way to understand how climate behaves during periods when climate boundary conditions were much different from those of the present day. Knowing the natural bounds of past ocean-atmosphere variability in the Warm Pool region will improve our understanding of the role of the tropics in global climate change at different time scales, and enhance our ability to predict climate change in the future.

Modern and fossil *Porites* corals provide one of the most promising natural archives for the reconstruction of ocean-atmosphere climate variability on seasonal to interannual timescales. *Porites* corals provide unparalleled temporal resolution for reconstructing past climate and are capable of recording the physical and chemical properties of their growth environment. Surface-ocean temperature and salinity are the two most important parameters for understanding the role of ocean-atmosphere interactions in global climate change. Measurements of stable isotopic compositions and element ratios in coral skeletons allow for the simultaneous tracking of SST, concentration of ^{18}O in surface seawater, input of nutrients, and incoming radiation on seasonal to interannual timescales. The $\delta^{18}O$ of coral skeletons is a function of the combined effects of seawater $\delta^{18}O$ and the temperature at which the coral aragonite precipitates, while coral $\delta^{13}C$ is usually closely connected to the ambient nutrient isotopic composition and incoming solar radiation which reflect local rainfall and cloud cover. Given a period of time when global ice volume is relatively stable, the local sea-surface hydrological balance between precipitation and evaporation can be extracted from coral records. Such records provide reliable and detailed histories of the Warm Pool climate and insights into how the ocean and atmosphere interact as background climate changes.

Coral geochemistry has long been applied to reconstruct changes in mean climate and ENSO variability in the tropics [*Cole and Fairbanks*, 1990; *McCulloch et al.*, 1994; *Dunbar et al.*, 1996; *Beck et al.*, 1997; *Quinn et al.*, 1998; *Hughen et al.*, 1999; *McCulloch et al.*, 1999; *Urban et al.*, 2000; *Tudhope et al.*, 2001; *Cobb et al.*, 2003; *Watanabe et al.*, 2003; *Woodroffe et al.*, 2003; *Gagan et al.*, 2004; *Kilbourne et al.*, 2004; *McGregor and Gagan*, 2004; *D'Arrigo et al.*, 2006; *Juillet-Leclerc et al.*, 2006; *Quinn et*

al., 2006]. Coral records also show potential to record the variability of monsoonal rainfall in the tropical monsoon regions [*Charles et al.*, 1997; *Charles et al.*, 2003; *Pfeiffer et al.*, 2004; *Sun et al.*, 2005; *Yu et al.*, 2005; *Chakraborty*, 2006; *D'Arrigo et al.*, 2006; *Abram et al.*, 2007; *Morimoto et al.*, 2007]. While some of these records were high-resolution and shed light on the variability of important climate systems at a seasonal timescale, they are mostly limited to the Holocene epoch. More high-resolution coral records are needed, especially for periods before the Holocene.

The island of Sumba is located within this key region of atmospheric and oceanic exchange and a wealth of modern and Late Quaternary corals have been collected there. The coral reefs of Sumba are situated in the southern sector of the Indonesian maritime continent where the El Niño-Southern Oscillation (ENSO) has a strong impact [*Nicholls*, 1981; 1984; *Ropelewski and Halpert*, 1996; *Haylock and McBride*, 2001; *McBride et al.*, 2003]. Sumba corals are also in the migration path of the Asian-Australian monsoon convective centre [*Meehl*, 1987; *Chang et al.*, 2005]. A 1 million-year-long sequence of raised coral terraces has been found in Cape Laundi in the central north Sumba [*Pirazzoli et al.*, 1991]. The geological and depositional setting of a recently discovered suite of fossil coral terraces located at Mondu village, west of Cape Laundi, appears to be particularly well suited for the *in situ* preservation of large coral colonies. Two fieldtrips during 1995 and 1998 have produced many long cores from the Holocene and modern reefs, and reconnaissance-style drilling of the older raised reefs has revealed the prospect of high-quality fossil corals suitable for palaeoclimate reconstruction.

1.2 AIMS

Specifically, this project has the following research aims:

1. ***To explore the Mondu area for raised coral reefs, retrieve long cores from Porites corals, and U-series date the reefs and coral cores***. To achieve this aim, detailed topographic surveys, field observations, and stratigraphic analysis were carried out to

determine the relative ages of the raised reefs and fossil corals. Collecting robust coral samples with thick well-preserved walls facilitated the U-series dating. High-precision U-series isotope measurements were applied to try to achieve reliable ages. Studies of diagenesis and its effects on the distribution of U/Th isotopes in the fossil coral skeletons served to support the dating strategy.

2. ***To explore the climatologic and oceanographic significance of the Sumba coral $\delta^{18}O$ and $\delta^{13}C$ records by characterizing them using instrumental records of local climate phenomena***. Towards this end, high-resolution coral $\delta^{18}O$ and $\delta^{13}C$ records were extracted from modern Sumba corals and compared with the available instrumental records of local climate. Statistical transformation and analysis involved characterizing the coral records, local instrumental records, and remote detection indices. I focused on the seasonal characteristics and interannual variability of the climate parameters. Where possible, sections of records were duplicated within a given time-slice to demonstrate the level of reproducibility of climate signals.

3. ***To reconstruct climate variability since the middle Holocene.*** A wealth of coral cores have been collected from the Holocene reefs which provides an excellent opportunity to reconstruct sea surface temperature and evaporation/precipitation at high temporal resolution. The Holocene coral records will improve our understanding of the natural bounds of climate variability for important systems, such as the ENSO, Asian-Australian Monsoon, and Indonesian Throughflow.

4. ***To reconstruct climate variability during background conditions distinct from the modern and Holocene.*** This aspect of the project was highly exploratory and aimed to find and drill cores from well-preserved corals older than the Holocene, U-series date them, and produce high-resolution paleoclimate records. The Late Quaternary coral records document variations in the prevailing climatic and oceanographic systems during distinctly different background climate states.

CHAPTER 2

CORAL AS A TOOL FOR RECONSTRUCTING PAST CLIMATE

Annually banded massive corals have unique attributes that make them exceptional archives of environmental change in the tropics through the Late Quaternary. These include the proven ability of large corals to yield high-resolution (up to weekly) multidecadal to multicentury records of past climate variability in the Late Quaternary , and the ability to directly date corals by high-precision U-series techniques [reviewed by *Druffel*, 1997; *Dunbar and Cole*, 1999; *Gagan et al.*, 2000; *Correge*, 2006; *Eakin and Grottoli*, 2006; *Grottoli and Eakin*, 2007, and so on.].

2.1 CORAL CHRONOMETERS

2.1.1 Density banding

The most significant characteristics contained in most hermatypic coral skeletons are annual density bands that consist of a high and low density couplet per year discernible by x-ray of a thin slab cut parallel to the axis of upward corallite growth. Barnes and Lough have noted that almost all the published papers on coral density banding describe the annual pattern as one band of higher density and one of lower density [*Barnes and Lough*, 1989], even in corals with 12 or more fine bands which group together to form an annual band couplet [*Buddemeier*, 1974; *Barnes and Lough*, 1989; *Gill et al.*, 2006]. Annual variations in skeletal density represent changes in both the rate of linear extension and calcification. Massive *Porites* corals in the tropics usually grow continuously at rates of 6-25 mm/yr, producing annual density bands that provide time markers for the development of long chronologies [*Knutson et al.*, 1972]. Density bands provide an inexpensive, fast, and precise chronology of skeletal growth with many coral records having absolute annual chronologies. Where banding is absent or poorly defined, the seasonal cycling of detailed oxygen or carbon isotope records [*Fairbanks and*

Dodge, 1979; *Cole et al.*, 1993; *Gagan et al.*, 1996; *Evens et al.*, 1998] can be used to fill gaps in coral growth records or even to establish relatively long chronologies. Just as dendrochronologists cross-date wood samples to extend tree-ring chronologies, distinctive growth bands in corals (e.g stress bands) have been used as time-markers to improve the accuracy of coral chronologies [*Druffel*, 1997]. Application of cross-dating and multiple age-specific tracers should allow most coral records to achieve true annual chronologic precision [*Hendy et al.*, 2003].

It is likely that the sensitivity of corals to their environment varies with species and location [*Lough and Barnes*, 1997], and skeletal extension, density and calcification do not necessarily increase or decrease in concert with changes in environmental conditions [*Dodge and Brass*, 1984]. However, many studies agree that, at least for *Porites*, extension rate is inversely related to average skeletal density [*Lough and Barnes*, 1992; *Scoffin et al.*, 1992; *Lough and Barnes*, 2000] and directed linked to calcification rate [*Dodge and Brass*, 1984; *Grigg*, 1997; *Lough and Barnes*, 2000].

Density variations in corals have been explored as a proxy for variations in environmental conditions, such as sea surface temperature [*Lough and Barnes*, 1990; 1997; 2000; *Carricart-Ganivet*, 2007; *Worum et al.*, 2007], even though the relationships between them are complex [*Aharon*, 1991].

2.1.2 UV fluorescent banding

UV fluorescent banding is commonly observed in coral slabs placed under long-wave ultra-violet (UV) light. Isdale [1984] first described UV fluorescent banding in an inshore Great Barrier Reef (GBR) *Porites* colony and recognized it as an annual maker, consistent with the region's seasonal river runoff. Slices cut from skeletons of massive *Porites* display two types of fluorescence when illuminated by UV light: (1) faint fluorescent banding associated with annual skeletal density banding and (2) narrow lines of strong fluorescence associated with monsoonal runoff of fresh water from

nearby land [*Barnes and Taylor*, 2005]. The timing, width and intensity of the fluorescent bands correlate strongly with summer monsoon rainfall [*Lough*, 1991] and the magnitude of coastal discharge from Queensland's largest river, the Burdekin [*Isdale*, 1984; *Lough*, 1997; *Isdale et al.*, 1998]. The fluorescent lines were attributed to terrestrial humic substances transported in river flood plumes to the GBR lagoon and then incorporated into the coral skeleton [*Boto and Isdale*, 1985; *Susic et al.*, 1991]. In contrast, marine organic matter is the proposed source of the diffuse fluorescent bands in corals distant from freshwater input, such as those from southern Oman [*Tudhope et al.*, 1996] and the outer GBR [*Susic et al.*, 1991]. Ramseyer et al. [1997] concluded that fluorescence results from skeletal construction of less densely-packed aragonite crystals which, in turn, traps more organic matter. This is consistent with evidence from Scoffin et al. [1989] and Barnes and Taylor [2005] that fluorescent lines coincide with low density bands in the coral skeleton. Barnes and Taylor [2001] presented an alternative model in which fluorescent bands in coral skeletons are the result of reduced calcification as the coral responds to low salinity conditions associated with coastal runoff.

UV fluorescent banding is usually applied with density banding as a complementary tool to help with the recognition of annual cycles of coral growth. However, Hendy et al. [2003] successfully established an absolute chronology for the past 373 years by cross-dating characteristic patterns of fluorescent bands in eight long coral cores from the GBR. They also used fluorescence in corals as a proxy for freshwater influx to the GBR to gain insight into regional rainfall variability and ENSO teleconnection patterns over the past several centuries.

2.1.3 Uranium-series dating

Dating of modern and fossil corals by uranium-series methods provides excellent absolute age control for the Late Quaternary and Holocene [*Quinn and Tudhope*, 2000]. Uranium-series dating methods originate from two separate decay chains parented by

^{238}U and ^{235}U [*Edwards et al.*, 2003]. These parent isotopes are separated from their daughter products, including ^{230}Th and ^{231}Pa respectively, during the weathering process because uranium is soluble in most natural waters, while ^{230}Th and ^{231}Pa are essentially insoluble. Thus carbonates precipitated from natural waters will contain some uranium, but essentially no thorium or protactinium [*Broecker*, 1963; *Broecker and Thurber*, 1965]. The in-growth of ^{230}Th from the decay of ^{238}U is the backbone of the main chronometer, which finds one of its optimal applications in fossil corals due to the high concentration of uranium (~3 ppm) in coralline skeletal aragonite. The half-life of ^{230}Th is ~75,000 years, which allows the technique to be applied back to ~450,000 years ago for coral that has been perfectly preserved. ^{231}Pa has a half-life of ~33,000 years, and an applicable range of ~200,000 years. High-precision techniques utilizing thermal ionization mass spectrometry (TIMS) yield analytical precisions ranging from two years for a 100-year old sample to 10,000 years for a 350,000-year old sample [*Edwards et al.*, 1987]. The recent use of multi-collector inductively coupled plasma mass spectrometry (MC-ICP-MS) has yielded even higher analytical precision [*Luo et al.*, 1997; *Stirling et al.*, 2001; *Andersen et al.*, 2004; *Potter et al.*, 2005].

Many studies have employed ^{230}Th dating of fossil corals to study a wide range of problems including neo-tectonics, ^{14}C-calibration, and reconstructing past sea levels and palaeoclimate [*Bard et al.*, 1996; *Stirling et al.*, 1998; *Esat et al.*, 1999; *McCulloch et al.*, 1999; *Tudhope et al.*, 2001; *Cutler et al.*, 2003; *Fairbanks et al.*, 2005]. For older corals especially, the limitation is not usually the precision of the determined age, but the preservation of the sample, as most older corals come from uplifted reefs subject to meteoric diagenesis [*Bard et al.*, 1992; *Stirling et al.*, 1995; *Scholz et al.*, 2004].

Coralline aragonite can be altered to calcite and aragonite by meteoric waters, thus potentially changing the U-series isotopic composition and shifting the ^{230}Th age from its true value [*Stein et al.*, 1993]. Screening for calcite is a first-order check for alteration, however measuring the uranium isotopic composition provides a means of testing for subtle diagenesis. ^{234}U, another daughter of ^{238}U, is also fractionated from its parent and is present in excess in ocean water. The modern marine $^{234}U/^{238}U$ ratio is

1.144 to ~1.149 [*Chen et al.*, 1986; *Edwards et al.*, 1986/87; *Chen et al.*, 1991; *Ludwig et al.*, 1991; *Gallup et al.*, 1994; *Szabo et al.*, 1994; *Cheng et al.*, 2000; *Stirling et al.*, 2001; *Muhs*, 2002; *Robinson et al.*, 2004] (the ratio would be 1 if there was no fractionation), whereas some uplifted fossil corals older than 100,000 years have $^{234}U/^{238}U$ ratios that imply an initial marine value exceeding 1.2. Seawater $^{234}U/^{238}U$ ratios exceeding ~1.17 are highly unlikely to have occurred in the last 200,000 years [*Hamelin et al.*, 1991b; *Richter and Turekian*, 1993], given the ~400,000 year residence time of U in the ocean ([~ 400,000 years; *Ku et al.*, 1977]. Such elevated $^{234}U/^{238}U$ ratios imply that the corals have been altered by diagenesis. Further, several studies have suggested that the marine $^{234}U/^{238}U$ ratio has not changed significantly over the last 200,000 to 400,000 years [*Henderson and Cohen*, 1993; *Gallup et al.*, 1994; *Henderson*, 2002]. As a result, checking the $^{234}U/^{238}U$ ratio has become a standard means for testing the quality of a coral sample, and thus the reliability of the ^{230}Th age [*Stirling et al.*, 1995; *Scholz and Mangini*, 2007]. Recently, ^{231}Pa dating has become important as an independent chronometer, providing a test of concordance between ^{230}Th and ^{231}Pa ages [*Edwards et al.*, 1997; *Gallup et al.*, 2002; *Edwards et al.*, 2003].

Even though some researchers have found no general correlation between coral $\delta^{234}U$ value (activity ratio for $^{234}U/^{238}U$ which is reformulated into δ-notation as $\delta^{234}U = ((^{234}U/^{238}U) / (^{234}U/^{238}U_{eq}) - 1) \times 10^3$, with $(^{234}U/^{238}U_{eq})$ as the atomic ratio at secular equilibrium and equal to $\lambda^{238}/\lambda^{234}$ where λ^{238} and λ^{234} are the decay constants for ^{238}U and ^{234}U respectively), measured $^{230}Th/^{238}U$ activity ratio, and calculated ^{230}Th age [such as *Chen et al.*, 1991], many others found some correlation between $\delta^{234}U$ and ^{230}Th age [*Stein et al.*, 1993; *Zhu et al.*, 1993; *Fruijtier et al.*, 2000] and $^{230}Th/^{238}U$ [*Bender et al.*, 1979; *Hamelin et al.*, 1991b; *Bard et al.*, 1992; *Gallup et al.*, 1994; *Stirling et al.*, 1995; *Cheng et al.*, 1998; *Henderson et al.*, 2001; *Stirling et al.*, 2001; *Thompson et al.*, 2003; *Villemant and Feuillet*, 2003; *Potter et al.*, 2004; *Scholz et al.*, 2004]. Various models have been developed to explain U-series isotopic anomalies in reef corals. Some authors showed the effects of gain and loss of ^{238}U and ^{230}Th [*Chen et al.*, 1991; *Hamelin et al.*, 1991a; *Bar-Matthews et al.*, 1993; *Henderson and Cohen*,

1993]. Ku et al. [1990] suggested a model which takes into account gain or loss of both ^{234}U and ^{238}U through continuous exchange with uranium in groundwater or soil water. Bender et al. [1979] and Gallup et al. [1994] presented models where ^{234}U and ^{230}Th are continuously added to corals, while Cheng et al. [1998] modelled continuous/episodic uranium gain and loss relative to ^{230}Th, or continuous addition of ^{234}U and ^{230}Th. The latter study showed that if a suite of samples of the same age experience different degrees of one of the above-mentioned processes, the data will fall along a curve that is close to a straight line near the upper intercept in a concordia diagram whereby the upper intercept will the true age of crystallization.

Recently three models have been published to try to produce accurate U-series correction ages. Villemant and Feuillet [2003] propose a model that takes into account possible initial ^{230}Th excess where continuous selective redistribution (gain or loss) of ^{234}U, ^{234}Th and ^{230}Th is controlled by recoil processes. Thompson et al. [2003] present a quantitative model where the positive correlation between $^{234}U/^{238}U$ and $^{230}Th/^{238}U$ activity ratios is explained by coupled addition of particle-reactive ^{234}Th and ^{230}Th, which is produced by decay of dissolved uranium and α-recoil mobilisation of uranium daughters. Scholz et al. [2004] have developed a new model which combines uranium uptake and loss, the latter being proportional to the amount of uptake, that explains their data and produces characteristic isochrons. They show that the 'true' age of the coral can be calculated from the intersection of the isochron and the seawater evolution curve.

2.1.4 Radiocarbon dating

Radiocarbon (^{14}C) is produced in the upper atmosphere by bombardment of atmospheric nitrogen atoms with cosmic ray neutrons. The ^{14}C atoms are rapidly oxidized to $^{14}CO_2$, which diffuses downwards and mixes with the pool of atmospheric carbon dioxide and enters into all pathways of the biosphere. Plants and animals assimilate ^{14}C into their tissues through photosynthesis and respiration; the ^{14}C content of these tissues is in equilibrium with that of the atmosphere because there is a constant exchange of new ^{14}C

as old cells die and are replaced. However, as soon as an organism dies this exchange and replacement of ^{14}C ceases. From that moment on the ^{14}C content of the organism declines as the ^{14}C decays to nitrogen with a half-life of 5,730 years, and the ^{14}C content is henceforth purely a function of time. The age of organic material can be determined by measuring the ratio of ^{14}C to ^{12}C or ^{13}C [*Gupta and Polach*, 1985]. Now accelerator coupled mass spectrometers (AMS) are often used to measure the concentrations of individual ions of ^{14}C, ^{13}C and ^{12}C and only 1 mg of carbon is required for analysis.

The ^{14}C content of the mixed layer of the surface ocean where corals grow is different to that in the atmosphere due to slow isotopic exchange between the atmosphere and surface ocean and the ^{14}C dilution effect due to mixing with older ^{14}C-depleted deep water. Therefore, corals formed in the ^{14}C-depleted surface-ocean reservoir will yield apparent ages that are older than their true age. A correction for this apparent age anomaly is possible when the reservoir-atmosphere offset in ^{14}C is known. On average the radiocarbon ages of samples formed in the surface ocean are 400 years older than those formed in isotopic equilibrium with northern hemisphere atmospheric CO_2 [*Bard et al.*, 1993; *Stuiver and Braziunas*, 1993]. This 400 year offset for the surface ocean is known as the global oceanic reservoir effect. Regional variations in the oceanic reservoir effect can occur due to the upwelling of ^{14}C-depleted water as well as regional differences in the ^{14}C content of the atmosphere [*Stuiver and Braziunas*, 1993].

Since the activity of ^{14}C in the atmosphere has not remained constant over time, the radiometric time scale is not an absolute time scale. However, conventional radiocarbon ages can be converted into calibrated calendar years (cal BP relative to 1950 AD) by applying internationally agreed calibration curves based on carefully screened data with updates at 4-6 year intervals [Klein et al., 1982; Stuiver and Reimer, 1986; 1993; Stuiver et al., 1998]. The current internationally-ratified calibration curves are IntCal04, SHCal04, and Marine04, for Northern Hemisphere terrestrial, Southern Hemisphere terrestrial, and marine samples, respectively [*Hughen et al.*, 2004; *McCormac et al.*, 2004; *Reimer et al.*, 2004]. These calibration curves can now be accessed through the program Calib5 [*Stuiver et al.*, 2005, available on http://calib.qub.ac.uk/calib/].

2.2 CLIMATE PROXIES

2.2.1 Oxygen isotopes

The oxygen isotopic composition of coral skeletons is the most frequently used coral climate proxy. The oxygen isotopic composition of a sample is generally expressed as a departure of the $^{18}O/^{16}O$ ratio from an arbitrary standard ($\delta^{18}O$), as follows:

$$\delta^{18}O = 1000 \times (^{18}O/^{16}O_{sample} - {}^{18}O/^{16}O_{standard}) \div {}^{18}O/^{16}O_{standard}$$

The resulting values are expressed in per mil (‰) units. The isotopic composition of carbonates is determined by the isotopic composition of the fluid and the thermodynamic isotope fraction during crystallization [*McCrea*, 1950]. Therefore, coral $\delta^{18}O$ reflects environmental conditions (mainly temperature and seawater $\delta^{18}O$) in the ambient seawater during skeletal aragonite precipitation. On timescales for which ice sheet variability is negligible, coral $\delta^{18}O$ mainly reflects the local sea surface temperature (SST) and the local hydrological conditions (sea surface salinity (SSS) resulting from evaporation, precipitation and runoff).

The temperature-dependent fractionation of oxygen isotopes in biological carbonate was first found in mollusk aragonite by Epstein et al. [1953], where $\delta^{18}O$ decreases by ~0.22‰ for each 1°C increase in temperature. Weber and Woodhead [1972] subsequently demonstrated that the $\delta^{18}O$ of coralline aragonite also varied inversely with SST though different genera were offset by constant amounts from this $\delta^{18}O$ vs. SST relationship. Seasonal variations in $\delta^{18}O$ along the growth axis of a coral and their relationship to seasonal SST variations were first reported by Fairbanks and Dodge [1979]. Subsequently, Dunbar and Wellington [1981] showed that finely sampled corals can provide an intra-annual record of SST. Since then, many researchers have shown that in oceanic settings where the oxygen isotope composition of seawater is constant, coral skeletal $\delta^{18}O$ records SST variability. The isotopic composition of coralline

aragonite is offset by a biological non-equilibrium effect that appears to be stable through time, as long as a consistent, maximum growth axis is sampled within a coral colony [*McConnaughey*, 1989; *Winter et al.*, 1991; *Shen et al.*, 1992; *Gagan et al.*, 1994; *Leder et al.*, 1996; *Swart et al.*, 1996a; *Wellington et al.*, 1996; *Cohen and Hart*, 1997]. For the genus *Porites*, a $\delta^{18}O$-SST relationship has been established by Gagan et al. [1994] with a 0.18‰ increase in $\delta^{18}O$ per 1°C decrease in SST. Other $\delta^{18}O$-SST relationships have been suggested for different regions, such as 0.172‰/°C by Quinn et al. [1998], 0.15‰/°C by Boiseau et al. [1998], 0.164‰/°C by Felis et al. [2000].

The other important influence on coral $\delta^{18}O$ is the isotopic signature of seawater, which is related to the salinity of the surface water set by the balance of evaporation, precipitation, runoff, and water advection [*Swart and Coleman*, 1980; *Dunbar and Wellington*, 1981; *Cole et al.*, 1993; *Gagan et al.*, 1994; *Linsley et al.*, 1994]. In oceanic settings where seawater $\delta^{18}O$ correlates with rainfall, long records of coral $\delta^{18}O$ have been used to reconstruct precipitation [*Cole et al.*, 1993; *Linsley et al.*, 1994].

A recently developed technique involving tandem measurements of $\delta^{18}O$ and Sr/Ca (SST proxy) in corals allows for the simultaneous tracking of SST and sea surface hydrological balance, which are the two most important parameters for understanding the role of ocean-atmosphere interactions in global climate change [*McCulloch et al.*, 1994; *Gagan et al.*, 1998; *Hendy et al.*, 2002]. The proxy used to determine the surface-ocean hydrological balance is referred to as the residual $\delta^{18}O$ ($\Delta\delta^{18}O$).

2.2.2 Carbon isotopes

The carbon isotope signal in corals is less straightforward to interpret in climatic terms because coral $\delta^{13}C$ (the per mil deviation of the ratio of $^{13}C/^{12}C$ relative to Vienna-Peedee Belemnite Limestone Standard) generally has a complicated relationship with environmental and physiological variables that interact. Variables potentially affecting coral $\delta^{13}C$ mainly include the $\delta^{13}C$ value of dissolved inorganic carbon (DIC)

in reef water [*Swart et al.*, 1996b], light related photosynthetic modulation of the isotopic composition of the coral internal DIC pool [*Weber and Woodhead*, 1970; *Fairbanks and Dodge*, 1979; *Swart*, 1983; *McConnaughey*, 1989; *Wellington and Dunbar*, 1995; *Swart et al.*, 1996b], the symbiotic relationship between corals and zooxanthellae [*Porter et al.*, 1989; *Carriquiry et al.*, 1994; *Allison et al.*, 1996], heterotrophic vs autotrophic feeding [*Carriquiry et al.*, 1994; *Swart et al.*, 1996b; *Felis et al.*, 1998], coral spawing [Gagan et al., 1994], colony topography [Cohen and Hart, 1997], and kinetic effects associated with the rate of coral growth and calcification [*McConnaughey*, 1989; *de Villiers et al.*, 1995; *Allison et al.*, 1996; *Cohen and Hart*, 1997; *McConnaughey*, 2003].

The control of light on coral $\delta^{13}C$ has been observed by many researchers [*Weber and Woodhead*, 1970; *Erez*, 1978; *Fairbanks and Dodge*, 1979; *Swart*, 1983; *McConnaughey*, 1989; *Wellington and Dunbar*, 1995; *Swart et al.*, 1996b] and it is generally believed that light intensity affects coral calcification as it takes place from an internal inorganic carbon pool [*Erez*, 1978; *Swart*, 1983; *McConnaughey*, 1989]. This internal pool is composed of carbon derived from the ambient seawater and coral respiration and modified by fractionation during CO_2 uptake by photosynthesis. Zooxanthellar photosynthesis preferentially fixes ^{12}C and leaves behind ^{13}C, thus increases in the rate of photosynthesis enrich the carbon isotope ratio of the skeleton. Incoming short-wave radiation is highly correlated with incoming photosynthetically active radiation, thus any change in incoming short-wave radiation would change the photosynthetic activity of the endosymbiotic zooxanthellae and hence the $\delta^{13}C$ of the coral skeleton.

Although the symbiotic algae are capable of providing their coral host with up to 100% of its daily metabolic energy requirements [*Muscatine et al.*, 1981; *Grottoli et al.*, 2006], it has been demonstrated that zooxanthellar photosynthetic activity can decrease or even cease under some environmental stresses, such as elevated temperature and light [*Porter et al.*, 1989; *Jokiel and Coles*, 1990; *Fitt et al.*, 2000]. A decrease in zooxanthellar

photosynthetic activity could decrease the intake of ^{12}C from the coral DIC pool and increase of proportion of ^{12}C precipitated in coral skeleton [*Swart*, 1983; *McConnaughey*, 1989]. Recently, Grottoli et al. [2006] found that some coral species meet more than 100% of their daily metabolic energy requirements by markedly increasing their feeding rates and CHAR (per cent contribution of heterotrophicaaly acquired carbon to daily animal respiration) when they lose photosynthetic energy input from the symbiotic zooxanthellae. *Porites* colonies can switch from autotrophy to heterotropy depending on food availability and this plays an important role in interannual skeletal $\delta^{13}C$ variability [*Felis et al.*, 1998]. Anthony [1999; 2000] found that corals from the inshore GBR have a greater capacity to feed on suspended sediment than the same species living in the mid-shelf, suggesting a heterotrophic adaptation to the turbid coastal conditions. Risk et al. [1994] discovered that the coral $\delta^{13}C$ trend across the GBR shelf may result from shifting levels of autotrophy with changes in water turbidity.

2.2.3 Strontium/Calcium

Owing to their chemical similarity to Ca, elements such as Sr, Mg, U, Ba, and Cd are co-precipitated in coral skeletal aragonite. Many studies have shown that the relative concentration of such elements often provides a palaeoclimatic or palaeoceanographic signal [e.g.: *Smith et al.*, 1979; *Shen and Sanford*, 1990]. The coralline Sr/Ca ratio provides one of the most powerful approaches to reconstruct sea surface temperature. The groundwork for Sr/Ca thermometry was laid by Smith et al. [1979] who showed that the Sr/Ca ratio in coralline aragonite correlated with temperature. A significant improvement was made by Beck et al. [1992] who used thermal ionization mass spectrometry (TIMS) to dramatically enhance the signal-to-noise ratio for this proxy. Their results showed that the coral Sr/Ca records track SST with an apparent accuracy of better than ± 0.5°C.

Since then, many studies have shown that Sr/Ca in coral can be a high-fidelity

temperature proxy [*de Villiers et al.*, 1994; *McCulloch et al.*, 1994; *Min et al.*, 1995; *Shen*, 1996; *Alibert and McCulloch*, 1997; *Gagan et al.*, 1998] and a number of Sr/Ca-SST relationships have been established. The slopes of most of the calibration equations are similar, with a mean value of 0.062±0.014 based on data published before year 2000 [*Gagan et al.*, 2000], or 0.0607±0.0089 based on data published before 2006 [*Correge*, 2006].

The Sr/Ca palaeothermometer is based on two key assumptions in that biological controls on skeletal Sr/Ca up-take and changes in the Sr/Ca content of seawater are assumed to be negligible. Even though most studies support these assumptions, there are some who disagree. De Villiers et al. [1994; 1995] found that variations in skeletal extension rate caused variations of 2-4°C in the calculated temperature. Also, de Villiers et al. [1994] reported variation in seawater Sr/Ca that could lead to errors in temperature estimates of up to 0.7°C. This effect is most pronounced in areas where upwelling brings water enriched in Sr to the surface [*de Villiers*, 1999]. Furthermore, modeling by Stoll and Schrag [*Stoll and Schrag*, 1998] suggested that changes in sea level leading to recrystallization of exposed aragonite have caused fluctuations in the seawater Sr/Ca ratio during glacial-interglacial cycles. These fluctuations could produce errors in palaeotemperatures of up to 1.5°C.

Sub-weekly to daily sampling of coralline material reveals spikes in Sr/Ca ratios unrelated to temperature [*Allison*, 1996; *Hart and Cohen*, 1996; *Sinclair et al.*, 1998]. Reproducibility on coral samples suggests that these inhomogeneities in the Sr/Ca distribution can produce uncertainties of around 0.3°C in fine-scale measurements.

2.3 DIAGENESIS

Biogenic coral aragonite is subject to post-depositional diagenetic alteration in the marine and vadose environments [*James*, 1974; *Bathurst*, 1975; *Hubbard and Swart*, 1982; *Aissaoui et al.*, 1986; *Constanz*, 1986; *Martin et al.*, 1986; *Purser and Schroeder*,

1986; *Potthast*, 1992; *Bar-Matthews et al.*, 1993; *Stein et al.*, 1993; *Tribble*, 1993] and exchange and removal of elements and isotopes during diagenesis have the potential to affect the veracity of coral proxies [*Guilderson et al.*, 1994; *McCulloch et al.*, 1996; *Esat et al.*, 1999; *Hughen et al.*, 1999; *Woodroffe and Gagan*, 2000; *Guilderson et al.*, 2001; *Tudhope et al.*, 2001; *Felis et al.*, 2004; *Brachert et al.*, 2006].

Several recent studies have investigated the paleoclimatic implications of diagenetic transformations in corals [*Enmar et al.*, 2000; *Muller et al.*, 2001; *McGregor and Gagan*, 2003; *Muller et al.*, 2004; *Quinn and Taylor*, 2006]. McGregor and Gagan [2003] found that diagenetic transformation of aragonite to calcite and addition of calcite cements in environments with meteoric water decreases Sr/Ca, $\delta^{18}O$ and $\delta^{13}C$ in corals, which is consistent with early observations [*Siegel*, 1960; *Martin et al.*, 1986; *Stein et al.*, 1993; *Zhu et al.*, 1994; *Wei et al.*, 1998]. They also showed that lower Sr/Ca and $\delta^{18}O$ in diagenetically altered corals would produce warm SST artefacts of up to 1.5^{o}C and 0.2^{o}C, respectively, for reconstructed paleotemperatures [*McGregor and Gagan*, 2003]. Recent studies have also showed that secondary aragonite added to coral skeletons during early marine diagenesis would produce significantly higher bulk Sr/Ca, $\delta^{18}O$ and $\delta^{13}C$ relative to pristine corals [*Enmar et al.*, 2000; *Muller et al.*, 2001; *Muller et al.*, 2004; *Gallup et al.*, 2006; *Quinn and Taylor*, 2006]. Conversion of these altered coral Sr/Ca and $\delta^{18}O$ compositions to SST using standard equations yielded anomalous palaeotemperature estimates that are ~4-5^{o}C [*Muller et al.*, 2001], 2.5^{o}C ($\delta^{18}O$-SST) or 6^{o}C (Sr/Ca-SST) [*Quinn and Taylor*, 2006] cooler than those estimated from unaltered portions of the same coral.

CHAPTER 3

GEOLOGY, CLIMATOLOGY, AND OCEANOGRAPHY AROUND SUMBA

3.1 THE STUDY AREA

3.1.1 Location and tectonic setting

The study area for this PhD project is located around Mondu village, ~10 km west of Cape Laundi, on the central part of the north coast of Sumba Island, Indonesia (Figure 3.1).

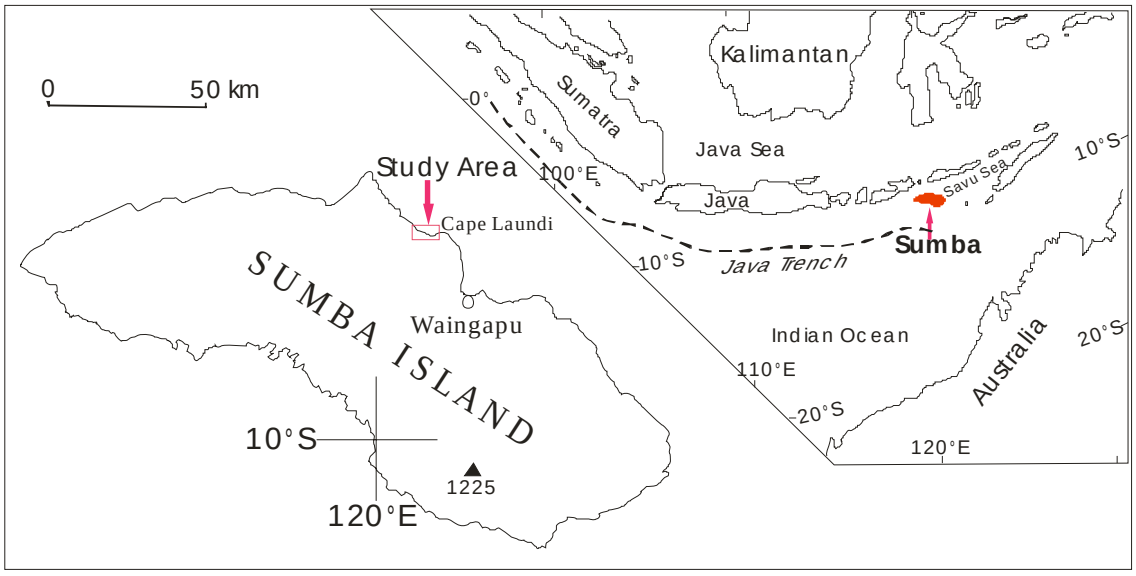

Figure 3.1 Location of Sumba, Cape Laundi, and the study area

Sumba is situated at the southwest end of a tectonic inflexion where the Sunda Arc passes eastward into the Banda Arc. The island is an exposed part of the outer arc ridge produced by the active subduction of the Indian-Australian plate beneath the Pacific plate [*Fitch and Hamilton,* 1974]. Sumba is separated from Australia by the Java Trench-Timor Trough, and from the volcanic ridge of the Sunda-Banda island-arc to the north by an outer arc basin (the Savu Sea). The collision of the plates and the upheaval of the outer arc ridge resulted in uplift of the palaeo-reefs and the formation of flights of raised coral terraces on the north coast of Sumba.

3.1.2 A 1 million-year-long sequence of coral terraces

An exceptional sequence of coral-reef terraces is developed near Cape Laundi between sea level and an ancient patch reef 475 metres above sea level [*Pirazzoli et al.*, 1991]. Figure 3.2 shows the flight of coral terraces on the western side of Cape Laundi. Using uranium-series and electron spin resonance dating, Pirazzoli et al. [1991; 1993] and Bard et al. [1996] deduced a local uplift rate of 0.49 m/kyr and concluded that most terraces correspond to specific interglacial stages, with the oldest terrace formed about 1 million years ago. Their dating has been successful because of the relatively low levels of diagenesis in the Sumba fossil corals. In particular, the relatively low annual rainfall and pronounced winter dry-season tends to slow down the processes of diagenesis in fossil corals, leaving some of them almost unrecrystallized after 600 ka [*Pirazzoli et al.*, 1993].

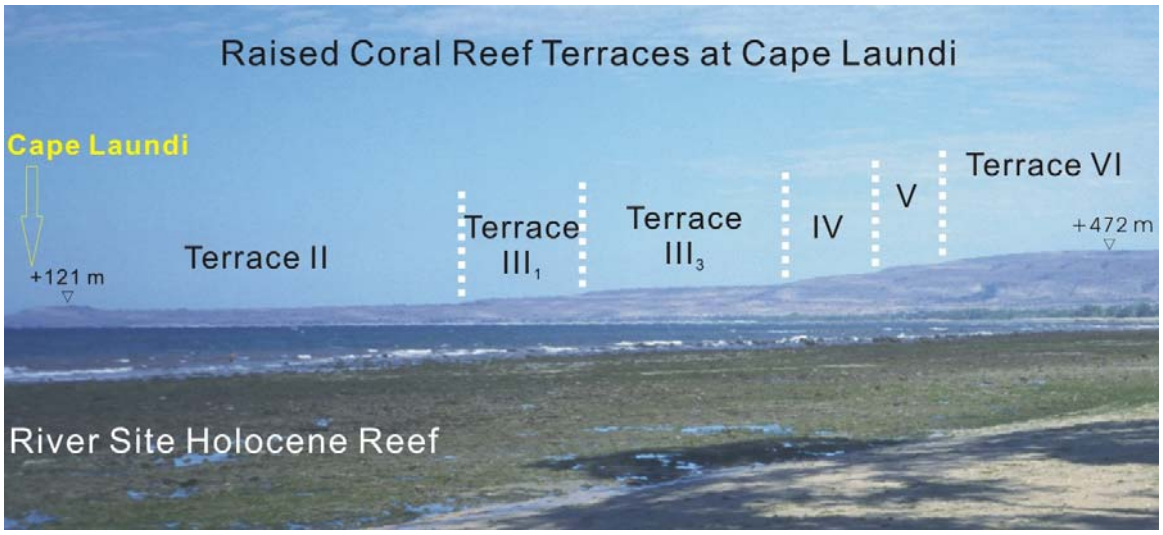

Figure 3.2 Coral terraces on the western side of Cape Laundi viewed from River Site Holocene raised reef in the Mondu area. The numbering of the terraces is in accord with Pirazzoli et al. [1993].

Unlike Pirazzoli et al. [1991; 1993] who focused on the terraces of Cape Laundi, my fieldwork area around Mondu village (~10 km west of Cape Laundi) has more extensive palaeo-reef terraces developed between 0 m and 80 m above sea level. This palaeo-reef setting provides an excellent opportunity to study the reef development between these altitudes and find more massive *Porites* corals suitable for palaeoclimate reconstruction.

All the coral cores for this climate study were drilled from reefs below 60 m above sea level, thus the altitudes of our corals are no higher than Pirazzoli et al.'s Terrace II_3. During our surveys, we did not find any corals suitable for climate reconstruction on or above the upper terraces corresponding to Pirazzoli et al.'s Terrace II_4 and Terrace II_5.

3.1.3 Local instrumental records

The study area has an annual mean sea surface temperature (SST) of 28.2°C. The local mean SST is close to or above 29°C for up to six months per year and drops sharply below 26.5°C for only one month around mid-August (Figure 3.3).

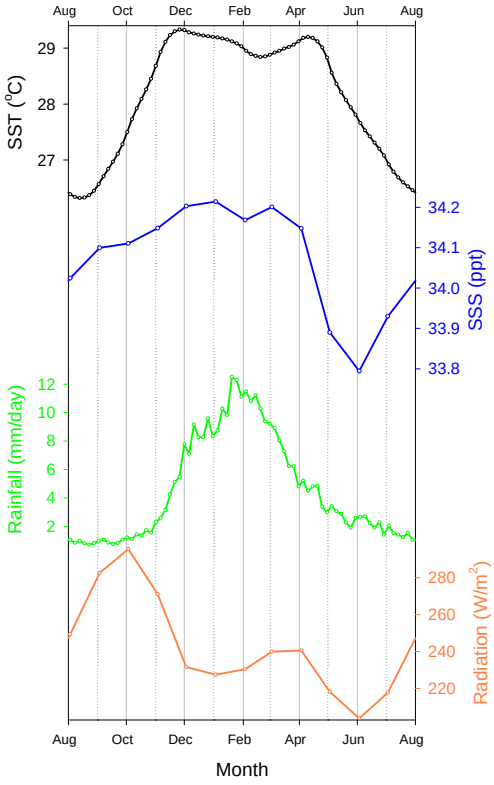

Figure 3.3 The annual climatologies around Sumba, Indonesia. The climatologies are as follows: IGOSS sea surface temperature (SST, black curve, [*Reynolds et al.*, 2002], Carton-Giese SODA dataset V1.4.2 sea surface salinity (SSS, parts per thousand, blue curve, [*Carton et al.*, 2005], CMAP rainfall (green curve, [*Xie and Arkin*, 1997], and Atlas of Surface Marine Data 1994 incoming short-wave radiation (orange curve, [*da Silva et al.*, 1994]. The original data can be found at: http://iridl.ldeo.columbia.edu/SOURCES/.IGOSS/.nmc/, http://iridl.ldeo.columbia.edu/SOURCES/.CARTON-GIESE/SODA/.v1p2/, http://iridl.ldeo.columbia.edu/SOURCES/.NOAA/.NCEP/.CPC/.Merged_Analysis, and http://iridl.ldeo.columbia.edu/SOURCES/.DASILVA/.SMD94/.climatology/.shortrad/.

Even though most of Indonesia lies in the wet tropics, Sumba is relatively dry with a mean annual rainfall of 1655 mm (1979 to 2005) and most of the rain falls during the wet season from December to March. The mean rainfall in January or February is 15 times higher than that in August, which marks the peak of the eight-month dry season from April to November when monthly mean rainfall is as low as 22 mm (Figure 3.3).

The climatology of the local sea surface salinity is consistent with the low-salinity characteristic of the Indo-Pacific Warm Pool [annual average < 34.2 ppt (parts per thousand)]. In spite of that, it still shows some intra-annual variability including freshening during May to July with low SSS of 33.8 ppt in June. Surprisingly, Figure 3.3 shows that the most saline surface water coincides with the summer monsoon peak during December to March, indicative of little effect of local rainfall on sea surface salinity even though the summer monsoon is as strong as 330 mm/month. Similarly, Figure 3.3 suggests that the local incoming surface radiation has little effect on the seasonality of the local sea surface temperature.

3.2 THE OCEAN-ATMOSPHERE SYSTEM AND SUMBA

Sumba is located in the south-central sector of the Indo-Pacific Warm Pool (Figure 3.4), which is of global importance for Earth's climate system. Several important components of the tropical ocean-atmosphere system interact in the Warm Pool region, including the El Niño-Southern Oscillation, the Asian-Australian Monsoon, the Indian Ocean Dipole, the Indonesian Throughflow, and the South Java Current.

3.2.1 Indo-Pacific Warm Pool

The Indo-Pacific Warm Pool (IPWP) is a huge reservoir of warm ocean water around the Indonesian Maritime Continent. The IPWP is the largest expanse of warm surface-ocean water on our planet (mean SST >28°C), and is 2-5°C warmer than any other equatorial region [*Yan et al.*, 1992]. It is also often referred to as the Western

Pacific Warm Pool (WPWP), even though it extends well into the tropical eastern Indian Ocean. During the northern summer, SSTs in the IPWP average 29-30°C. In winter, SSTs cool to 26-27°C. Precipitation over the IPWP is highest in northern summer, with roughly 80% of annual rainfall occurring between June and October. Rainfall averages between 300 and 400 mm/month during summer and between 50 and 100 mm/month during winter. As a result of this precipitation pattern, sea surface salinities vary seasonally by about 1.5‰. The annual precipitation pattern is tied to the migration of the Intertropical Convergence Zone (ITCZ) over the site and the timing of the northern summer monsoon. During El Niño and La Niña events, the western tropical Pacific experiences dramatic differences in precipitation. For example, summer precipitation over northern Indonesia can be diminished by as much as 60% during a major El Niño.

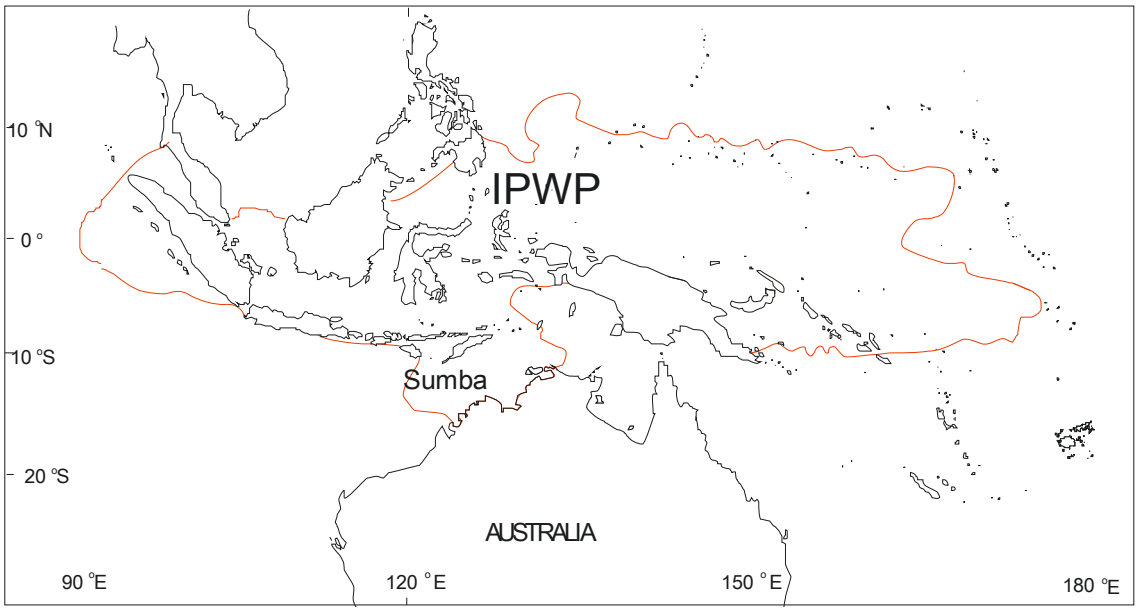

Figure 3.4 Location of Sumba and the Indo-Pacific Warm Pool (mean SST >28°C inside red curve, [*Yan et al.*, 1992]

The IPWP is a key component of the global climate system because it is a major source of latent heat and moisture for the global atmosphere. The heat and moisture play a fundamental role in driving the zonal Walker circulation and meridional Hadley

circulation [*Keenan et al.*, 2000]. An intense low-pressure cell above the IPW forms the rising branch of the Walker circulation, which produces high rainfall throughout the Indonesian region [*Bjerknes*, 1969]. With its high precipitation and tectonically active mountainous topography, this region contributes a large amount of water, solutes, and sediment to the coastal ocean. The overall balance of high precipitation exceeding evaporation results in relatively low sea surface salinity (SSS) in the IPWP. The IPWP is also a key area with respect to the exchange of water between two major oceans by the Indonesian Throughflow. The transfer of water from the Pacific to the Indian Ocean is crucial to the transport of heat and freshwater for the global ocean. Therefore, any changes in the nature of the Indo-Pacific Warm Pool and Indonesian Throughflow will certainly affect global energy transfers and climate.

The major control of Australasian monsoon circulation, with the Warm Pool below its centre, is the recurrent shift in the intensity of the highly mobile Indonesian Low. Any changes in physiochemical sea surface parameters and vegetation would modify this seasonal monsoon circulation. And on inter-annual timescales during an El Niño, for example, the IPWP and the Indonesian Low migrate eastward to the central Pacific, upsetting the equilibrium of Earth's climate and altering weather patterns around the world. During these warm ENSO episodes, cooler SSTs and less rainfall are the major characters of the climate in the Indonesian region.

The IPWP is now generally regarded as the source area for a substantial proportion of Earth's inter-annual climate variability. However, the role of the tropical oceans in longer-term climate changes is less clear and, until recently, has been largely neglected by palaeoclimatologists since the 1970s when a major study of global climate found that the tropical oceans had apparently cooled little during the last ice age while the rest of the world slipped into a deep freeze [*CLIMAP Project Members*, 1976]. Thinking that such climatological inertia implied a minor role for the tropics in climate change, researchers focused instead on the high latitudes, especially the North Atlantic, as the place where long-term climate changes are initiated [*Kerr*, 2001]. But now that new

research results have revealed the dynamic nature of tropical climate [*Rind and Peteet*, 1985; *Lyle et al.*, 1992; *Guilderson et al.*, 1994; *Thompson et al.*, 1995; *Schrag et al.*, 1996; *Beck et al.*, 1997; *McCulloch et al.*, 1999; *Pelejero et al.*, 1999; *Crowley*, 2000; *Lea et al.*, 2000; *Lea et al.*, 2006], climatologists are now suggesting that the tropical Indian and Pacific oceans participate in, and possibly drive, long-term climate change [*Cane*, 1998; *Cane and Evans*, 2000; *Pierrehumbert*, 2000; *Lea*, 2002]. Indeed, recent studies indicate that changes in sea surface temperatures and atmospheric convection in the tropical Indo-Pacific region are responsible for the decadal climate variability observed in extra-tropical regions [*Hoerling et al.*, 2001] and also play an important role in driving glacial-interglacial cycles [*Visser et al.*, 2003] and possibly millennial-scale climate changes [*Stott et al.*, 2002].

Therefore, utilizing modern and fossil corals to reconstruct the natural range of variability in sea surface temperature and hydrological cycle of the IPWP will be of great significance for understanding, modeling and predicting global climate change.

3.2.2 El Niño-Southern Oscillation

The El Niño-Southern Oscillation (ENSO) is the dominant coupled atmosphere-ocean mode of interannual climate variability, affecting most of the tropics and subtropics and many mid-latitude regions of North and South America and eastern Asia.

A. ENSO term and mode

The term El Niño means ‘the boy child’ and was first used by Peruvian fishermen in the late 1800s to describe the warm current appearing off the west coast of Peru around Christmas time [*Enfield*, 1989]. Today El Niño describes the warm phase of a naturally occurring sea surface temperature oscillation in the tropical Pacific Ocean. This oscillation is associated with the atmosphere, and thus the term ENSO – which incorporates the Southern Oscillation phenomenon – is commonly used.

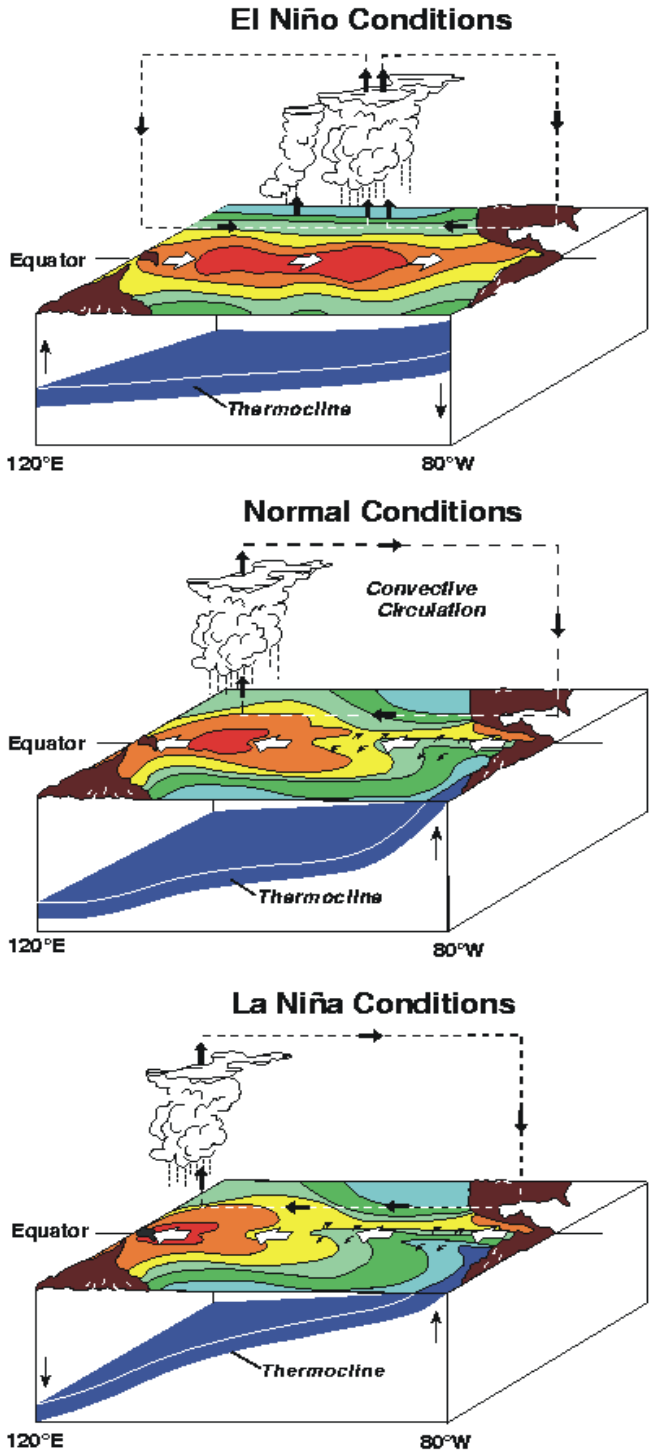

Figure 3.5 Schematic of the El Niño-Southern Oscillation. (By NOAA/PMEL/TAO)

Southern Oscillation (introduced by Sir Gilbert Walker) refers to a seesaw shift in surface air pressure at Darwin, Australia and the South Pacific island of Tahiti. When the pressure is high at Darwin it is low at Tahiti, and vice versa. El Niño, and its sister

event – La Niña – are the extreme phases of the Southern Oscillation, with El Niño referring to a warming of the eastern tropical Pacific, and La Niña a cooling [*Philander*, 1990; *Trenberth et al.*, 2002; *Cane*, 2005].

Distinct climatic changes occur in both the atmosphere and ocean during periods of El Niño and La Niña. On average, sea surface temperatures are ~6-8°C warmer in the western tropical Pacific than in the eastern tropical Pacific.

This east-west temperature difference is generally maintained by easterly trade winds that blow across the tropical Pacific and move the warm surface water from east to west. Because of this zonal temperature gradient, the trade winds typically blow towards the west across the tropical Pacific. However, during an El Niño event when the zonal temperature gradient is reduced, the trade winds typically slacken or reverse. Also, mean sea level is typically 0.5 m higher in the western tropical Pacific because the trade winds move water from east to west. This movement of water causes the thermocline to be deeper in the west than in the east, and as a result upwelling typically occurs in the eastern tropical Pacific. During an El Niño event, when the trade winds typically slacken or reverse, less water is moved from east to west and SST, sea level and the thermocline all increase in the east. During an El Niño event, surface air pressure is typically higher in the western tropical Pacific than in the eastern tropical Pacific.

Much of the basic physics of the ENSO cycle is now reasonably well known and the coupled atmosphere-ocean mode has been established, as shown in Figure 3.5. The cool phase of ENSO is characterized by the zonal Walker circulation in which easterly winds occur at the surface, Indonesian Low convection is maximal, and westerly flow aloft brings dry subsiding air over the eastern and central Pacific. The transition to the warm phase of ENSO occurs when the trade winds relax west of the date line, which allows the western Pacific warm pool to move eastward. The Indonesian Low convective maximum migrates to the equatorial region near the date line, upwelling in the eastern Pacific is suppressed, and trade winds are weak because of the diminished zonal SST

gradient. Rainfall patterns across the tropical Pacific shift as the Indonesian Low migrates northeast and convection develops over newly warmed waters [*Philander*, 1990; *Cole et al.*, 1993].

B. Global impacts of ENSO

El Niño events occur every three to seven years, and arise naturally through the strong interaction between the ocean and atmosphere in the tropical Pacific. The effects are felt worldwide (Figure 3.6) because the tropical Pacific is a powerful source of heat for driving atmospheric circulation. Even small changes in the sea-surface temperature in this region have major repercussions for global climate. Dry conditions in the western Pacific, warmer-than-average conditions in the northern United States and wetter-than-average conditions to the south, and suppressed hurricane development in the Atlantic, are all indicators of an El Niño event. Consequently, when the ENSO cycle is particularly strong, as occurred in 1982–83 and again in 1997–98, the changed weather patterns have profound social, economic and ecological consequences.

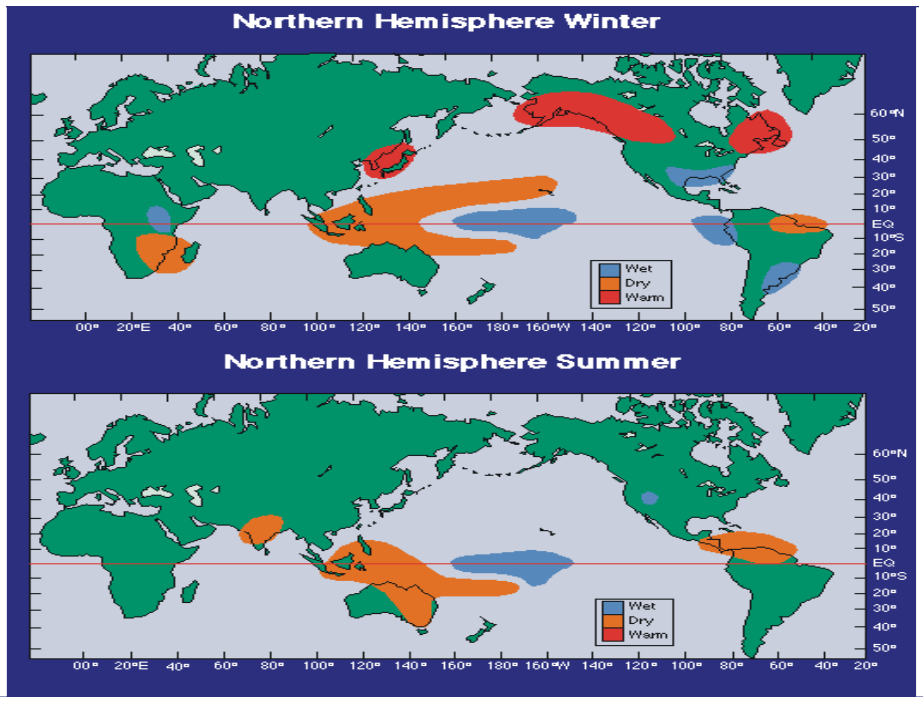

Figure 3.6 Precipitation anomalies during El Niño events in northern summer and winter (from NOAA/PMEL/TAO).

The ENSO of the tropical Pacific has a strong influence over the rainfall and sea surface temperature in the Indonesian Maritime Continent on interannual timescales. During an El Niño event, eastern Indonesian rainfall is suppressed and the SST is cooler, with the converse happening during a La Niña [*Nicholls*, 1981; 1984; *Ropelewski and Halpert*, 1996; *Haylock and McBride*, 2001; *McBride et al.*, 2003]. Also, it is now well known that there is a strong seasonal variation in the association between Indonesian rainfall and the ENSO [*Nicholls*, 1981; *Hastenrath*, 1987; *Haylock and McBride*, 2001; *McBride et al.*, 2003]. That is, rainfall in the Maritime Continent is strongly related to the ENSO during the dry half of the year (July to November) but has a weak association with ENSO during the summer wet-season months.

C. Measurement of recent ENSO events

Instrumental measures of ENSO are either atmospheric [the Southern Oscillation Index (SOI)] or oceanic (e.g. tropical Pacific SSTs) and extend back to the mid-19th century [*Philander*, 1990].

The SOI measures the monthly/seasonal fluctuations in surface air pressure differences at Tahiti and Darwin (equation = Tahiti – Darwin) and thus the SOI usually has a negative value during an El Niño event. Other frequently used measures of ENSO events are the NINO 3 and NINO 3.4 indices which are area averages of eastern equatorial Pacific SST anomalies over the regions 5°N-5°S, 90°W-150°W and 5°N-5°S, 120°W-170°W, respectively. Positive SST anomalies in these regions reflect El Niño conditions and negative anomalies mark La Niña conditions.

A multivariate ENSO Index (MEI) based on six main observed variables over the tropical Pacific has been developed for research purposes [*Wolter and Timlin*, 1998]. The six variables are: sea-level pressure (P), zonal surface wind (U), meridional surface wind (V), sea surface temperature (S), surface air temperature (A), and total cloudiness fraction of the sky (C). Figure 3.7 shows all the ENSO events since 1950 and the comparison of their intensities based on the MEI index.

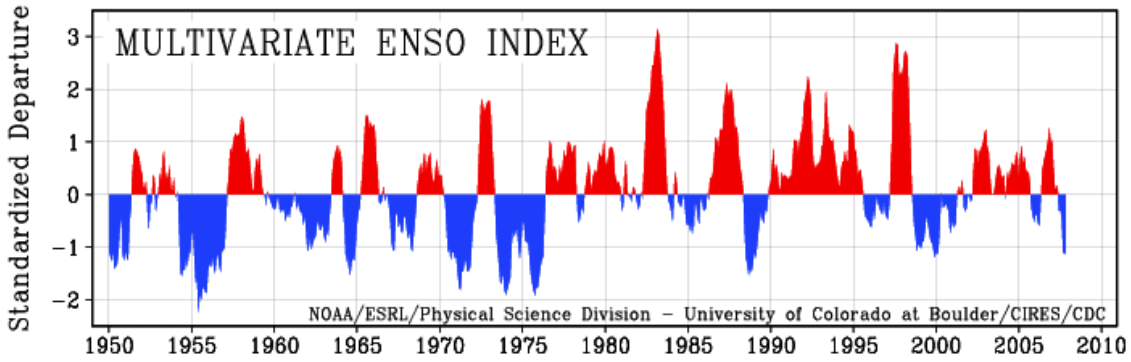

Figure 3.7 ENSO events from 1950 to 2007 based on the MEI index (from NOAA-CIRES-CDC). El Niño events are in red and La Niñas in blue.

D. ENSO variability

Most of the instrumental records of tropical Pacific climate span in detail only the past few decades. The few longer records that exit suggest that tropical Pacific climate is complex, including decoupling of the eastern and western Pacific ENSO components, significant decadal variability in ENSO, and changes in the overall strength of the Southern-Oscillation and its teleconnections [*Cole et al.*, 1993].

Many proxies have also been used to reconstruct the El Niño variability, such as corals, ice cores, varved sediments, tree rings, sclerosponges, and historical documents. These proxy records extend the length of the climate record beyond the short period of instrumental coverage and reveal long-term climatic trends more reliably. Long coral records indicate that ENSO has varied considerably in strength over the past millennium, with changes occurring rapidly on timescales of decades. Given this long-term perspective, ENSO events in the twentieth century appear to have been relatively strong, but not exceptionally so [*Cobb et al.*, 2003]. There is increasing evidence that the ENSO cycle may have been weak, or even absent, between about 14,000 and 5,000 years ago [*Sandweiss et al.*, 1996; *Rodbell et al.*, 1999; *Tudhope et al.*, 2001; *Moy et al.*, 2002; *McGregor and Gagan*, 2004; *Brijker et al.*, 2007]. Other researches also indicated a general increase in interannual variability to the late Holocene [*McGlone et al.*, 1992;

Shulmeister and Lees, 1995; *Sandweiss et al.*, 2001]. Moy et al. [2002] and Woodroffe et al. [2003] suggested that warm ENSO events become more frequent over the Holocene until about 1,200 years ago. ENSO may also have been generally weaker during the cooler conditions of the last glacial period (100,000–20,000 years ago) [*Tudhope et al.*, 2001]. Coral records also show that in the last interglacial period (124,000 year ago), when the global climate was slightly warmer than at present, the ENSO was robust and ENSO frequency was similar to that in modern instrumental records before the mid-1970s, but distinct from the most recent period [*Hughen et al.*, 1999].

Apart from the above-mentioned variability at the decadal, centennial, and longer-term timescales, ENSO-like variability at millennial timescale has also been found in tropical regions. Moy et al. [2002] found that periods of relatively high and low ENSO activity alternated at a timescale of 2,000 years and Stott et al. [2002] showed that the salinity of the western Pacific Warm Pool varied in accord with the millennial timescale Dansgaard/Oeschger cycles over Greenland.

E. Cause and origin of ENSO variability

There are different interpretations on the observed behaviours of the ENSO in the past. A modeling study has suggested that ENSO variability over the middle to late Holocene was largely a response to orbitally driven changes in the seasonal cycle of solar radiation in the tropics [*Clement et al.*, 2000]. The model results even suggested that under certain orbital configurations of the past, variability associated with El Niño-Southern Oscillation physics can abruptly lock to the seasonal cycle for several centuries, producing a mean sea surface temperature change in the tropical Pacific that resembles a La Niña. This change in SST would have a global impact and abrupt events, such as the Younger Dryas, may have been the outcome of orbitally driven changes in the tropical Pacific [*Clement et al.*, 2001]. Another model which simulated a reduced ENSO intensity in the early and mid-Holocene also showed that suppression of the

ENSO was caused by higher insolation and resulting intensification of the Asian summer monsoon or a warm water subduction from the south Pacific into the equatorial [*Liu et al.*, 2000].

Tudhope et al. [2001] proposed a dual control for ENSO consisting of a "glacial dampening" component and an orbital precession component would explain all the major features of the observed palaeo-ENSO data. The evolution from weak ENSO in the early-middle Holocene to strong and variable ENSO today was related to processional effects. Moderate ENSO strength around 38 to 42 ka, 85 ka, and 130 ka was the net result of the competing effects of glacial dampening and processional enhancement. The relatively weak ENSO around 112 ka resulted from neutral procession effects and strong glacial dampening.

Moy et al. (2002) attributed the long-term trend of weakening ENSO over the Holocene to orbitally induced changes in insolation, and suggested internal ENSO dynamics as a possible cause of the millennial variability.

Based on the high-resolution coral climate record during the last millennium, Cobb et al. (2003) found that the inferred changes in ENSO strength did not appear to be correlated with documented changes in Northern Hemisphere regional climate — for instance, the Little Ice Age (seventeenth to nineteenth centuries) or the Medieval Warm Period (eleventh to fourteenth centuries). Nor did they seem to tie in with reconstructions of volcanic and solar behavior that might drive climate change. They concluded that the majority of ENSO variability over the last millennium may have arisen from dynamics internal to the ENSO system itself.

F. The future of ENSO

The recent unusual behavior of ENSO, including the exceptionally strong warm events of 1982-83 and 1997-98 and the predominance of El Niño-like conditions during the past two decades [*Trenberth and Hoar*, 1996], has highlighted the possibility that ENSO

may be influenced by anthropogenic forcing. Research has indicated that ENSO could vary significantly on its own even during a period of relatively little global climate change, such as the last millennium [*Cobb et al.*, 2003]. Also, palaeo-ENSO records have shown that the ENSO system is sensitive to background climate, such as differences between glacial and interglacial periods [*Tudhope et al.*, 2001] and even over Holocene [*Moy et al.*, 2002]. Considering that the future is almost certainly going to be radically different, with predictions of a 1.5–6.0°C rise in global mean temperature within the next 100 years being almost as large as the change since the last glacial period [*Cubash and A.*, 2001], it is reasonable that ENSO may well respond to future greenhouse warming.

The realistic hope for predicting the response of ENSO to this warming lies in the use of coupled ocean–atmosphere climate models. Some of the best of these models now generate a realistic ENSO cycle but produce a wide range of predicted outcomes for ENSO in a warmer world, ranging from a significant strengthening of the cycle to no effect, or even a weakening. In order to obtain more successful modeling, more proxy climate records, like those from fossil corals, are crucial.

3.2.3 The Asian-Australian monsoon

The term monsoon was originally applied to the seasonal reversals of wind directions along the shores of Indian Ocean. Now its definition has been broadened to include almost all of the phenomena associated with the annual weather cycle on the tropical and subtropical continents of Asia, Australia, and Africa and adjacent seas and oceans [*Webster et al.*, 1998]. The inherent seasonality of the monsoon results in cool/dry winters and warm/wet summers over the continents. These seasonal changes in atmospheric circulation and precipitation also affect the ocean, leading to strong seasonality in current strength and direction, sea-surface temperature (SST) and salinity patterns [*Wang et al.*, 2005].

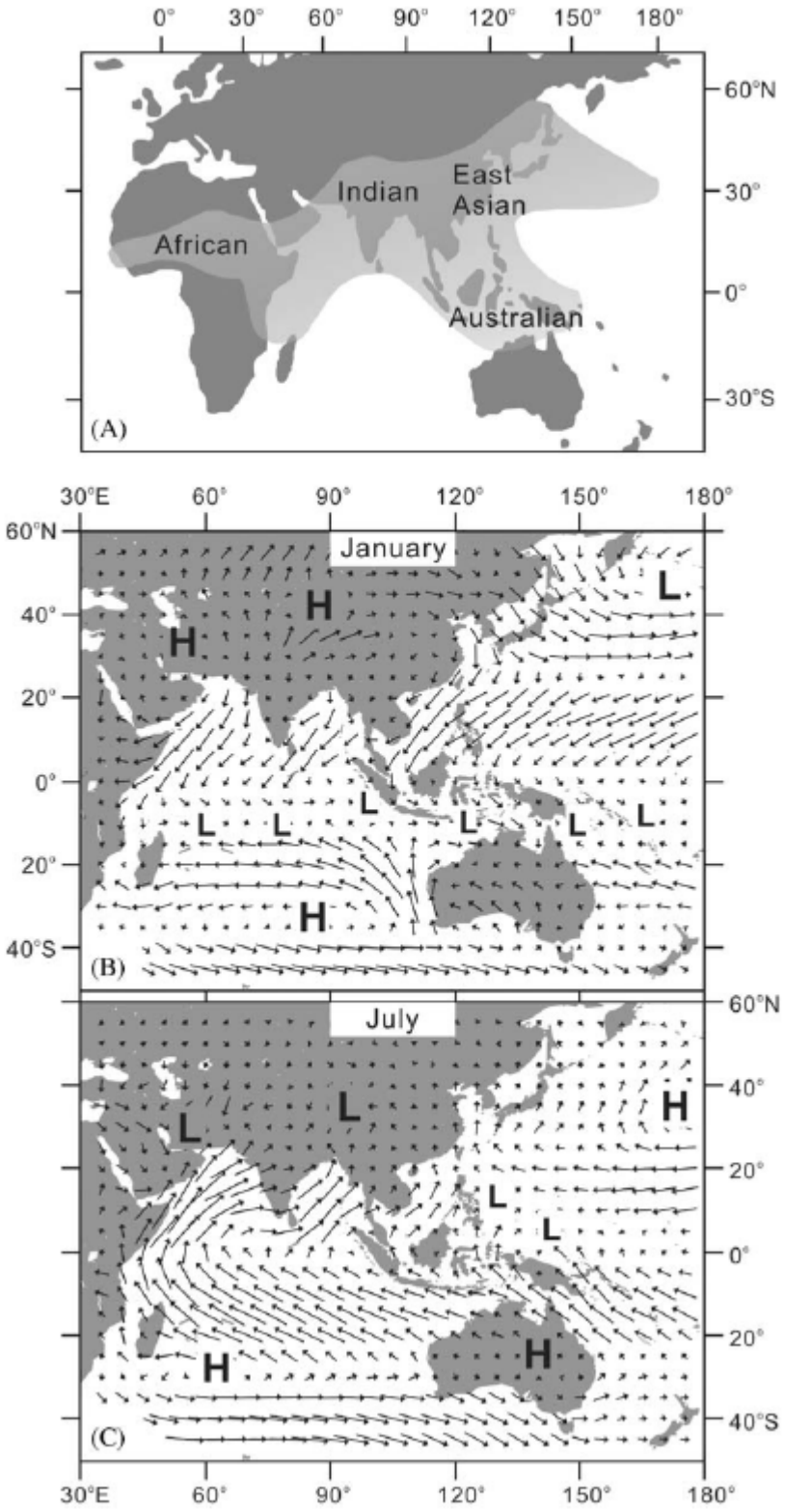

Figure 3.8 The modern monsoon system. (A) distribution of modern monsoonal regions in Asia, Africa and Australia ([*Black*, 2002]). (B) pressure and surface wind patterns in winter and (C) in summer [*Wang et al.*, 2005]

Even though early studies considered the monsoon to be a regional physical entity, the trend in modern monsoon studies has been toward an understanding of the 'global' monsoon by studying the dynamic links between regional subsystems [*Meehl*, 1987; *McBride*, 1998; *Webster et al.*, 1998; *Trenberth et al.*, 2000; *Clemens et al.*, 2003; *Chang et al.*, 2004], The most active Indian, East Asian, and Australian monsoons are now often referred as one macroscale phenomenon of the Asian-Australian monsoon with the tropical convective maximum undergoing an annual migration from over north India in July to Indonesia and northern Australia in January [*Meehl*, 1987; *Hung et al.*, 2004; *Chang et al.*, 2005]. A quasi-biennial variability (2 – 3 year period centred at 2.6 years, referred as the tropospheric biennial oscillation – TBO) has been found to be a fundamental characteristic for the Asian-Australian monsoon rainfall in all the India, East Asia, Indonesia, and Australia subsystems [*Meehl*, 1997; *Webster et al.*, 1998 and references there; *Meehl and Arblaster*, 2002]. There is considerable seasonal persistence from the south Asian to Australian monsoon with a strong south Asian or Indian monsoon tending to precede a strong northern Australian monsoon and vice versa for weak monsoons [*Meehl and Arblaster*, 2002; *Loschnigg et al.*, 2003; *Hung et al.*, 2004].

Sumba is located in the pathway of the annual migration of the Asian-Australian monsoon convective centre. The Intertropical Convergance Zone (ITCZ) migrates from over the South Asian subcontinent in July to Sumatra in November, to Java in December, and then to Sumba and north Australia in January and early February [*Meehl*, 1987; *Huang and Mehta*, 2004; *Chang et al.*, 2005].

3.2.4 Indian Ocean Dipole

The recently discovered Indian Ocean Dipole (IOD) mode is a coupled air-sea interaction within the Indian Ocean. During these events, an interannual climate anomaly is characterized by a sea surface temperature anomaly (SSTA) of opposing sign in the western and eastern tropical Indian Ocean [*Saji et al.*, 1999] and strong zonal wind anomalies in the equatorial Indian Ocean region [*Saji et al.*, 1999; *Webster et al.*,

1999; *Murtugudde et al.*, 2000]. Satellite-derived and *in situ* observations have confirmed that these events are associated with sea level [*Rao et al.*, 2002; *Feng and Meyers*, 2003] and rainfall anomalies [*Saji et al.*, 1999; *Saji and Yamagata*, 2003] having a structure similar to the SSTA.

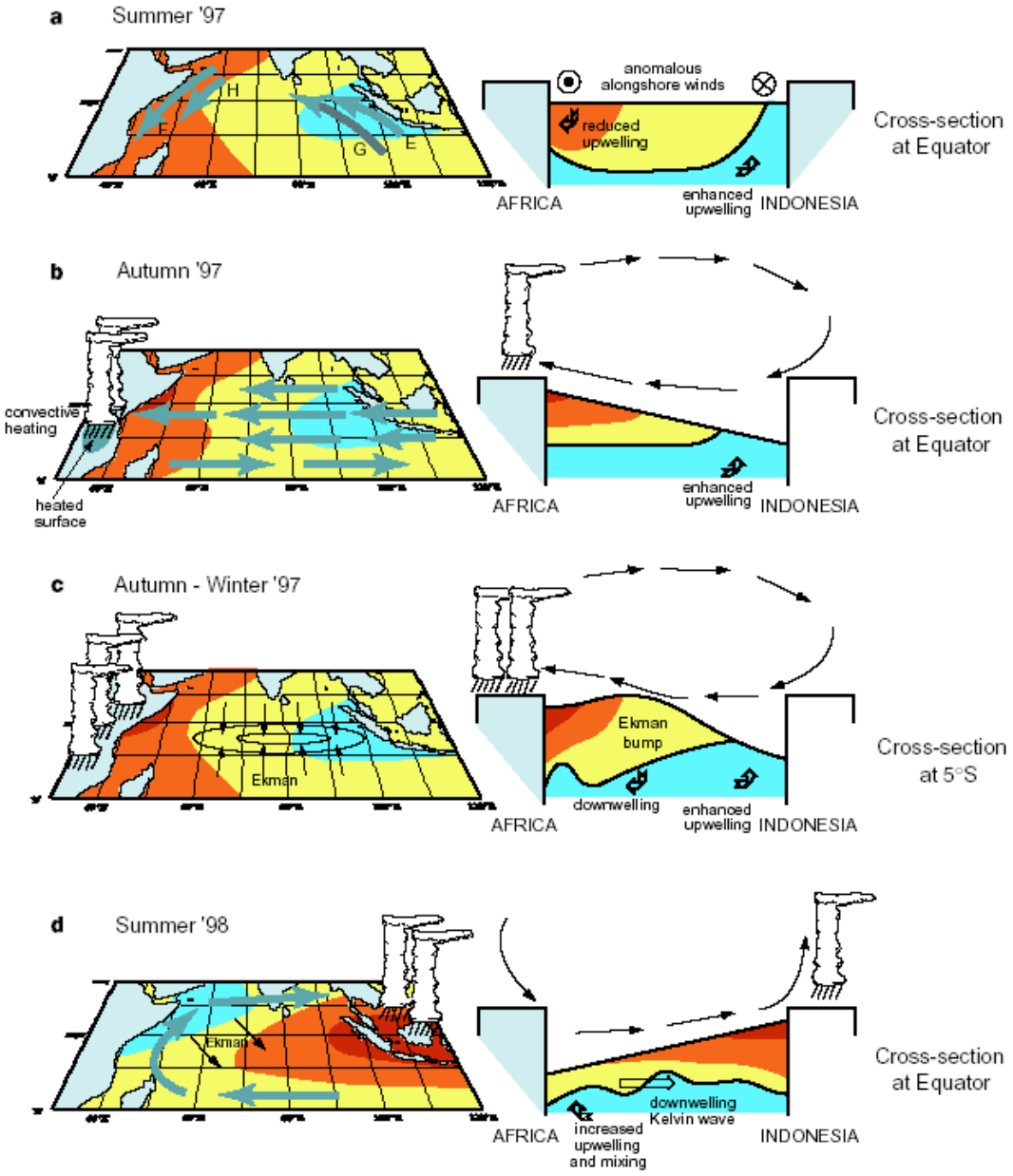

Figure 3.9 The Indian Ocean Dipole Mode [*Webster et al.*, 1999].

A mode has been presented to account for Indian Ocean Dipole events by Webster et al.

[1999], as shown in Figure 3.9. Initiation of an IOD event involves an unusual intensification of the southeasterly monsoon winds off the southwestern Indonesian coast which enhances local upwelling, raises the thermocline, and reduces the SST. Cooler waters in the eastern Indian Ocean gives rise to easterly winds along the equator (these winds are normally westerly) enhancing the cooling in the eastern equatorial Indian Ocean and promoting warming in the western equatorial Indian Ocean. The western warming involves the generation of an Ekman ridge around 10°S which then propagates westward. Westward propagating Rossby waves contribute to the warming process in the west by suppressing local upwelling. Kelvin waves are speculated to play a role in the initial elevation of the eastern thermocline. This mode implies an out-of-phase development of the SST extrema in the eastern and western Indian Ocean, so the Indian Ocean Dipole mode is also referred as Indian Ocean Zonal Mode (IOZM; Clark et al., 2003).

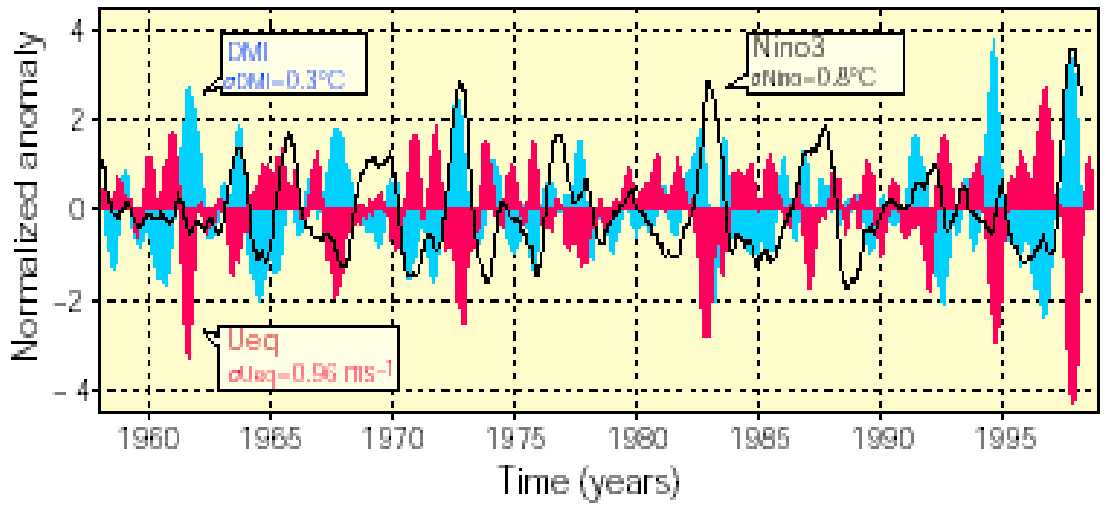

Figure 3.10 Comparison of Indian Ocean Dipole events and ENSO for the period 1958-1998 [*Saji et al.*, 1999]. The dipole mode index (DMI, plotted in blue) is moderately correlated with the ENSO (represented by Nino3 SST anomalies, black line). On the other hand, zonal wind anomalies across the equatorial Indian Ocean (Ueq, plotted in red) coevolves with the DMI.

The Indian Ocean Dipole can be identified using a simple index, the Dipole Mode Index (DMI), which describes the difference in SST anomaly between the tropical western Indian Ocean (10°N-10°S, 50°E-70°E) and the tropical south-eastern Indian Ocean

(Equator-10°S, 90°E-110°W) [1999]. The zonal wind anomaly (U_{eq}) over the equatorial central and eastern Indian Ocean (5°N-5°S, 70°E-90°E) is also a feature of dipole events. During 1958 to 1998, large amplitudes of the dipole occurred in 1961, 1967, 1972, 1982, 1994, and 1997, as shown in Figure 3.10. The IOD appears to have a complicated relationship with ENSO, occurring at times of ENSO extrema and at other times when the Pacific Ocean was not anomalous (as shown in Figure 3.10). Saji et al. [1999] and Webster et al. (1999) suggest that this mode results from the air-sea interactions of the Indian Ocean itself and is independent of the ENSO. Coupled atmosphere-ocean general circulation modelling (CGCM) results suggest that the coupled Indian Ocean-Monsoon system itself is capable of producing the Indian Ocean dipole mode without forcing from ENSO. However, ENSO is capable of changing the dominant timescales of the Indian Ocean dipole mode [*Yu et al.,* 2002]. Model experiments also show that the Indian Ocean-Monsoon system can modulate the amplitude and frequency of ENSO and produce interdecadal ENSO variations [*Yu et al.,* 2002]. The further work of Saji and Yamagata [2003] indicates that the IOD is not a part of ENSO evolution in the tropical Indian Ocean but both phenomena may interact. They note that ENSO events co-occurring with IOD events are much stronger compared to independent events. And IOD events that are independent of ENSO have the same strength as those that co-occur with ENSO. But the relationship between the IOD and ENSO is still controversial because some researchers have found that the zonal SST gradient anomaly is significantly correlated with ENSO during the boreal fall [*Hendon,* 2003] and that East African coastal rainfall and SST in the Indian Ocean correlates strongly with ENSO during the “short rain” season [*Clark et al.,* 2003].

The relationship between IOD and the Asian Monsoon is still unclear. Of the two largest dipole events on record, the1961 event was associated with the heaviest Indian monsoon in 150 years [*Saji et al.*, 1999], whereas during the 1997 IOD, rainfall over India was normal. In fact, Saji et al. [1999] found no statistical relationship between monsoon rainfall and the dipole. But it has been found that ENSO-Monsoon relationship is less "typical" and more irregular when the role of the Indian Ocean is considered [*Yu et al.,*

2002]. Modeling by Ashok et al. [2001] shows that the IOD plays an important role as a modulator of Indian monsoon rainfall, and influences the correlation between the monsoon and ENSO. Their result indicates that whenever the ENSO-monsoon correlation is low (high), the IOD-monsoon correlation is high (low).

Recent research also indicates that IOD events may even have important impacts on global climate. The strong local coupling of variables with the Indian Ocean suggests that the IOD may be an important determinant of regional climate fluctuations on interannual timescales [*Saji and Yamagata*, 2003]. Whenever the Indian Ocean Dipole Mode Index is positive, it leads to drought over the Indonesian region and heavy rain over East Africa [*Saji et al.*, 1999]. Black et al.[2003] and Clark et al. [2003] have shown that the IOD may significantly modulate rain over many African countries during boreal fall and early winter. Ashok et al. (2001a) and Ashok and Saji (2007) have demonstrated that positive IOD events may enhance summer monsoon rainfall over India. Zubair et al. [2003] showed a strong and robust association between the Sri Lankan "Maha" rainfall and the IOD from 1869 to 2000. Saji and Yamagata [2003] also showed that land temperature and rainfall are anomalously high over countries west of the Indian Ocean and anomalously low to its east; enhanced rainfall is found over the Asian monsoon trough, extending from Pakistan up to southern China. Also noted by Saji and Yamagata are IOD impacts on several regions remote from the Indian Ocean; a strong correlation was found over Europe, northeast Asia, North and South America and South Africa concurrent with IOD events. Over these regions, positive IOD events are associated with warm land surface anomalies and reduced rainfall. Modeling by Ashok et al. [2003] showed that the IOD has significant impact on the winter rainfall of western and southern Australia. Recent research has revealed a strong positive correlation between SSTs in the tropical eastern Indian Ocean and Australian rainfall, particularly winter rainfall in the southeast of the continent [*Nicholls*, 1989; *Ansell et al.*, 2000].

Abram et al. [2003] confirmed that modern corals could be used to reconstruct Indian

Ocean Dipole events. Their study also showed that Holocene coral records preserve similar signals and provide the first evidence that the Indian Ocean Dipole has operated since at least the mid-Holocene. The fossil coral records provide evidence that the Indian Ocean Dipole system can operate independently of the ENSO, with dipole events continuing in the mid-Holocene when ENSO is thought to have been substantially weaker than at the present [*Abram et al.*, 2007].

3.2.5 Indonesian Throughflow

The Indonesian Throughflow (ITF) between the western Pacific and the eastern Indian Ocean spreads across the Indonesian archipelago [*Wyrtki*, 1987] (Fig. 2.4). The main route for the upper low-salinity, well-ventilated water masses of northern Pacific origin passes through the Celebes Sea and the Makassar Strait from the Mindanao current, while deeper more saline water masses of southern Pacific origin enter the eastern Indonesian Seas through the Molucca and Halmahera Seas [*Gordon and Fine*, 1996]. Then three main passages open the Indonesian waters to the Indian Ocean. The Lombok Strait involves the upper layers 0-350 m; the Ombai Strait (3250 m deep) between Alor and Timor Islands, and the Timor Passage (1890 m) between Roti Island and the Australian continental shelf, allow deeper transports [*Molcard et al.*, 2001a].

The magnitude of the Indonesian Throughflow has strong seasonal and interannual variations. Maximum flow occurs during the northern hemisphere summer (August) and minimum flow during winter (February). ENSO variability is recognized as a dominant cause of interannual variability of the Throughflow [*Molcard et al.*, 2001a]. The estimated volume of water transport from the Pacific to the Indian Ocean varies between 2 and 24 SV (1 Sverdrup, Sv $=10^6$ m^3s^{-1}) [*Tomczak and Godfrey*, 1994] or, more conservatively, 7 to 18.6 Sv [*Murray and Arief*, 1988]. Direct measurements had been made in three normal years (weak ENSO years) and the yearly total transports through the three main outflow passages were 11.2 Sv, including Lombok Strait, 1.7 Sv [*Murray and Arief*, 1988]; Timor Passage, 4.5 ± 1.5 Sv [*Molcard et al.*, 2001a] and

Ombai Strait, 5 ± 1 Sv [*Molcard et al.*, 2001a] with an uncertainty of the order of 3 Sv.

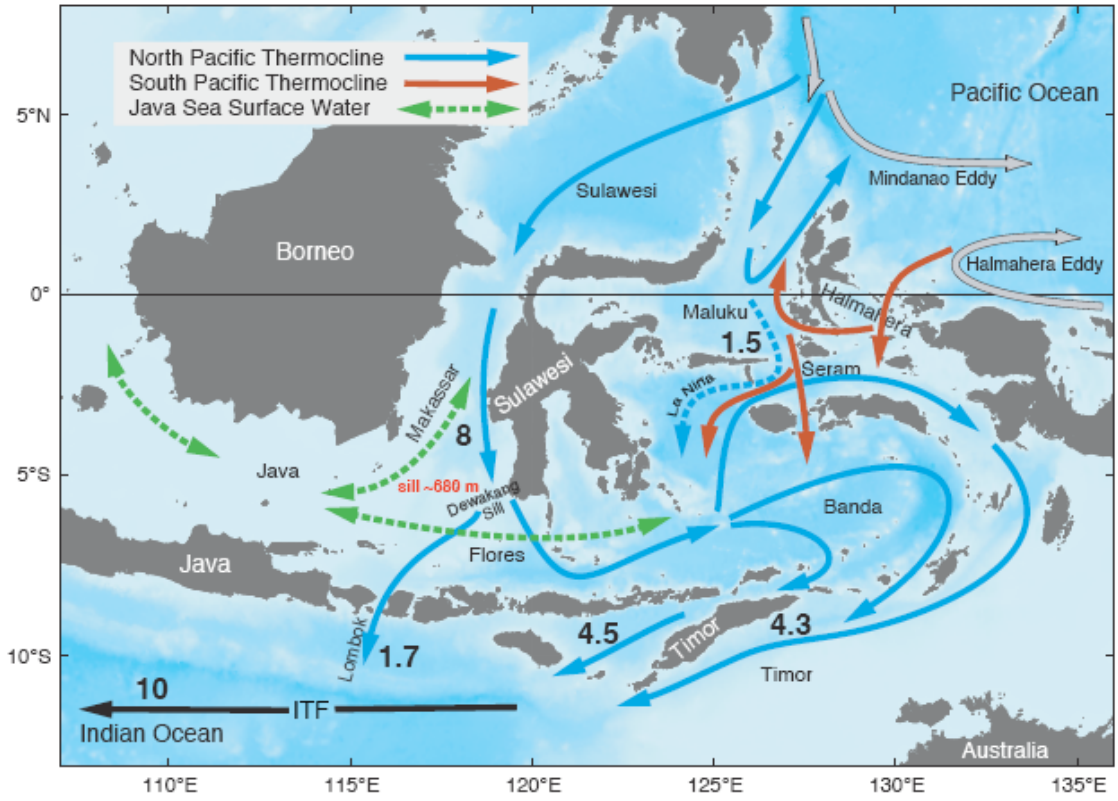

Figure 3.11 Pathways of the Indonesian Throughflow [*Gordon*, 2005].

The Indonesian Throughflow has long been a focus of considerable research interest from local, regional and global perspectives. Locally, there are large changes in water-mass structure within the Indonesian Seas, because of surface freshwater input, bottom friction, and mixing by vigorous tidal currents over sills. Regionally, it is important to understand how the throughflow and its variability relate to neighboring current systems in the western Pacific and near Australia, particular regarding the Leeuwin Current. Globally, it is considered one of the choke points of the global ocean circulation system, and its variability is believed to affect climate on interannual and longer time scales [*Schott and McCreary*, 2001]).

The Indonesian Throughflow modifies the heat and fresh-water budgets and air-sea heat fluxes of the Pacific and Indian Oceans, and may exercise a role in the El Niño/Southern Oscillation and Asian monsoon climate phenomena [*Wajsowicz and Schneider*, 2001].

The Indonesian Throughflow shifts the Indo-Pacific Warm Pool and centre of deep atmospheric convection to the west by increasing surface temperatures in the eastern Indian Ocean and reducing temperatures in the equatorial Pacific. This control on sea surface temperature and deep convection affects atmospheric pressure in the entire tropics and, via atmospheric teleconnections, in the mid latitudes. As a result, surface wind stresses in the entire tropics change and meridional and zonal gradients of the tropical thermocline and associated currents increase in the Pacific and decrease in the Indian Ocean. The response includes an acceleration of the equatorial undercurrent in the Pacific, and a deceleration in the Indian Ocean. Thus the Indonesian Throughflow exerts significant control over the global climate in general, and the tropical climate in particular. An example of this impact is that recent research indicates that during the boreal winter monsoon, the wind drives buoyant, low-salinity Java Sea surface water into the southern Makassar Strait, creating a northward pressure gradient in the surface layer of the strait. This surface layer "freshwater plug" inhibits the warm surface water from the Pacific Ocean from flowing southward into the Indian Ocean, leading to a cooler Indian Ocean sea surface, which in turn may weaken the Asian monsoon [*Gordon et al.*, 2003].

Given that it is located in one of the most important ocean-flow pathways, the SST and salinity around Sumba will be strongly affected by the variability of the Indonesian Throughflow and it will be directly recorded by the Sumba corals.

3.2.6 South Java Current and remote forced Kelvin waves

During northwestern monsoon season, heavy rainfall and strong input of runoff from the Indonesian islands such as Sumatra and Java make the surface salinity near the coast is up to 3 psu lower than in the open Indian Ocean [*Wyrtki*, 1973]. The published data demonstrate a very warm, fresh surface layer in the coastal water and the salinity is 33.8 psu which is much fresher than the Indonesian inner sea Banda Sea Water (salinity is 34.4 psu) [*Fieux et al.*, 1994b; *Bray et al.*, 1997; *Sprintall et al.*, 1999; *Sprintall et al.*,

2000]. The reduced salinity gives rise to a cross-shore pressure gradient, driving a south-easterly baroclinic coastal jet [*Quadfasel and Cresswell*, 1992]. The monsoonal winds, in turn, force an eastward or westward boundary current during the summer and winter, respectively. That is the formation of the semi-annually reversing South Java Current (SJC) [*Quadfasel and Cresswell*, 1992] (Figure 3.12).

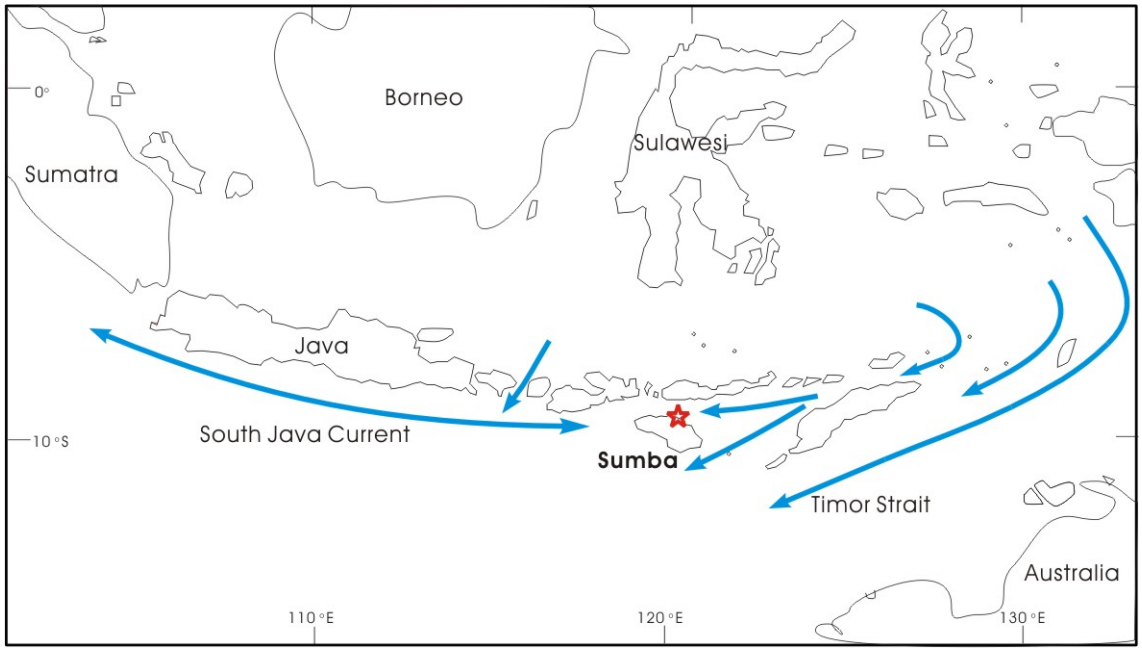

Figure 3.12 Oceanic currents around Sumba: the South Java Current (SJC, blue double headed arrow) and outflows of the Indonesian Throughflow (ITF, blue arrows). The red star marks the study area: the southern side of Sumba Strait.

The SJC is particularly interesting as it is closely related to the sea-level along the south coast of the lava - Nusa Tenggara island chain, and thus affects the overall pressure difference from the western Pacific that is widely thought to govern the mean throughflow and its low frequency variations [*Sprintall et al.*, 1999]. The SJC reverses to south-eastward flow semi-annually around May and November, probably through the propagation of coastal and equatorial Kelvin waves forced by westerly wind bursts during the monsoon transitions in the equatorial Indian Ocean. At these times, the SJC has been found to consist of narrow cores of accelerated flow extending to depths of ~ 150-250 m, and 90 nm south of Java to ~ 10^{o}S and the boundary with the westward

flowing South Equatorial Current (SEC) [*Fieux et al.*, 1994a; *Meyers et al.*, 1995]. South of Java, historical data reveal the occurrence of a very warm, fresh surface layer (salinities ~ 33.8) [*Sprintall et al.*, 1999], too fresh to be the Throughflow Banda Sea Water (~ 34.4) [*Fieux et al.*, 1994b]. Below this freshcap, in the thermocline and at depth, relative saline (~ 34.65) North Indian Intermediate Water is often found [*Bray et al.*, 1997]. During the south-east monsoon period (June-October) the SJC is north-westward, slower and in the same direction as the SEC and throughflow [*Sprintall et al.*, 1999].

In summary, the changing monsoon winds and the variations of the freshwater flux from the Indonesian archipelago are responsible for the annual cycle of the flow, while the actual reversals between the seasons are strongly influenced by remote forcing through equatorial and coastal long waves from the central Indian Ocean [*Quadfasel and Cresswell*, 1992].

During the monsoon transition periods of April/May and October/November. westerly wind bursts in the equatorial western Indian Ocean force the semiannual eastward Wyrtki Jet [*Wyrtki*, 1973]. The source waters of the jet stem from the western tropical Indian Ocean, delivered into that region by the SEC. The Wyrtki jet is weaker during the October/November transition period when the Somali Jet in the Arabian Sea appropriates some of the SEC flow [*Wyrtki*, 1973]. The equatorial and surface-confined Wyrtki Jet generally sets up within a week after the westerly wind onset, and the oceanic adjustment to the wind forces an associated downwelling Kelvin wave. Directly observed speeds of the jet have ranged from 0.7 to 2.1 m/s [*Wyrtki*, 1973; *Michida and Yoritaka*, 1996], which is roughly commensurate with the first model baroclinic mode equatorial Kelvin wave speed of 19 m/s, which may have been modified by the mean currents. The Kelvin wave transits from the western equatorial Indian Ocean in about a month to impinge the west coast of Sumatra on the equator in Indonesia. Subsequently, it excites a reflected Rossby wave back into the Indian Ocean as well as northward and southward propagating coastally trapped Kelvin waves that correlate directly with

observed coastal sea level rises along the coasts of Sumatra and Java [*Clarke and Liu*, 1993; 1994]. The fate of the southward propagating coastally trapped Kelvin waves once it reaches the south coast of java and its impact on the Indonesian internal seas and the throughflow are areas of active debate [*Murtugudde et al.*, 1998; *Qiu et al.*, 1999]. The main issues of contention are twofold: (1) the nature of the "gappy" island boundary of southern Indonesia and whether it permits the Kelvin waves to enter and affect the circulation of the interior Indonesian seas and (2) the modulation of the Kelvin wave signal by the semiannually reversing South Java Current and the throughflow itself. In addition, the role of local versus remote forcing within the Indonesian seas remains a controversial issue [*Sprintall et al.*, 2000].

Even though early studies have noticed that the eastward flow of the semi-annually reversing boundary current SJC could reduce the transport of the ITF [*Meyers et al.*, 1995], it had not been confirmed if the Indian Ocean water enters into the Indonesian seas through the Sumba Strait for a long time until the recently reported eastward flows in the Ombai Strait [*Molcard et al.*, 2001b] and in the Sumba Strait [*Hautala et al.*, 2001] measured using current metres in December 1995, May 1997, and March 1998. Question that still remains is, did those detections disclose a routine penetration or just an occasional incursion of the SJC/the remote forced Kelvin waves into the Savu Sea? A historical record is needed to answer this question.

CHAPTER 4

TWO DISTINCT PROCESSES OF U-SERIES ISOTOPIC DIAGENESIS IN A SINGLE FOSSIL CORAL COLONY AND MODEL CORRECTION AGE

ABSTRACT

Multiple measurements of U-series isotopes in skeletal sub-samples within a single *Porites* coral were made to explore the diagenetic behaviour of U-series isotopes in fossil corals from the raised reefs of Sumba, Indonesia. Detailed analysis of two diagenetic stages and corresponding changes in U-series isotopic composition has revealed two distinct processes of U-series isotope diagenesis in this single coral colony. Both of them are different from those suggested before. The earlier process involved addition of allochthonous dissolved ^{234}U and ^{238}U together with addition of detrital non-radiogenic ^{230}Th, while the later process was clearly connected to loss of ^{234}U and ^{238}U occurring along to loss of detrital-bound ^{230}Th. Locally radiogenic ^{230}Th appears to have played an important role in maintaining a constant $^{234}U/^{230}Th$ when percolating groundwater with allochthonous U and a high $\delta^{234}U$ value entered the coral at the earlier stage. On the other hand, detritus-bound ^{230}Th was critical to maintain a fixed $^{234}U/^{230}Th$ when percolating meteoric water dissolved coral skeletal U at the later-stage. The results suggest that a mechanism like diffusion or osmosis controlled the addition or loss of dissolved U and detrital Th in the coral by way of a solute concentration gradient. This mechanism explains the constant $^{234}U/^{230}Th$ ratios in situations involving either the addition or loss of U. Model correction ages could be determined for both processes and they yield essentially the same age of 133.6 ka for the early highstand of Termination II. This detailed study serves to substantiate the isochron model [*Scholz et al.*, 2004], and provides insight into the way by which the $^{234}U/^{230}Th$ ratio can remain constant when U is added to or lost from corals during diagenesis.

4.1 INTRODUCTION

Since the U-series method was established to date coral using thermal ionisation mass spectrometry (TIMS) [*Edwards et al.*, 1986/87; *Edwards et al.*, 1987a], it has been widely applied to aid the reconstruction of sea levels [*Bard et al.*, 1996; *Stirling et al.*, 1998; *Esat et al.*, 1999; *Cutler et al.*, 2003] and paleoclimates [*McCulloch et al.*, 1999; *Tudhope et al.*, 2001]. The fundamental premise of U-series dating is that corals incorporate substantial seawater uranium and negligible thorium into their aragonite skeletons during growth, and remain subsequently closed to uranium and thorium loss or gain [*Broecker*, 1963]. While modern corals faithfully record seawater $^{234}U/^{238}U$ [*Chen et al.*, 1991], the fossil corals often do not reflect closed-system evolution from a modern seawater $^{234}U/^{238}U$ ratio [*Bender et al.*, 1979; *Edwards et al.*, 1987a; *Ku et al.*, 1990; *Bard et al.*, 1991; *Henderson and Cohen*, 1993; *Thompson et al.*, 2003]. Recently, U-series dating of U-rich continental slope sediments from the Bahamas suggested that seawater $\delta^{234}U$ has remained within 15‰ of the modern value (~145‰) for the last 360 ka [*Henderson*, 2002]. However, $\delta^{234}U$ measured in fossil corals spans a wide range of values, thus the established opinion is that the premise of closed system behaviour is not warranted [*Bard et al.*, 1992; *Stirling et al.*, 1995; *Scholz et al.*, 2004]. Even though some researchers have not found general correlations between $\delta^{234}U$ values, the measured $^{230}Th/^{238}U$ activity ratio, and calculated ^{230}Th age [such as *Chen et al.*, 1991], others have found correlations between $\delta^{234}U$, $^{230}Th/^{238}U$, and ^{230}Th age [*Bender et al.*, 1979; *Hamelin et al.*, 1991a; *Bard et al.*, 1992; *Stein et al.*, 1993; *Zhu et al.*, 1993; *Gallup et al.*, 1994; *Stirling et al.*, 1995; *Cheng et al.*, 1998; *Fruijtier et al.*, 2000; *Henderson et al.*, 2001; *Stirling et al.*, 2001; *Thompson et al.*, 2003; *Villemant and Feuillet*, 2003; *Potter et al.*, 2004; *Scholz et al.*, 2004].

Various scenarios have been developed to explain U-series isotopic anomalies in reef corals. Some authors have studied the effects of gain and loss of ^{238}U and ^{230}Th [*Chen et al.*, 1991; *Hamelin et al.*, 1991b; *Bar-Matthews et al.*, 1993; *Henderson and Cohen*,

1993]. Ku et al. [1990] developed a model which takes into account gain or loss of both ^{234}U and ^{238}U through continuous exchange with uranium in groundwater or soil water. Bender et al. [*Bender et al.*, 1979] and Gallup et al. [*Gallup et al.*, 1994] presented models where ^{234}U and ^{230}Th are continuously added to the corals, while Cheng et al. [1998] modelled continuous/episodic uranium gain and loss relative to ^{230}Th or continuous addition of ^{234}U and ^{230}Th. The models showed that if samples of the same age experience different degrees of one of the above-mentioned processes, the U-series data will fall along a curve that approximates a straight line near the upper intercept in a concordia diagram. In this case, the upper intercept will be the true crystallization age of the samples.

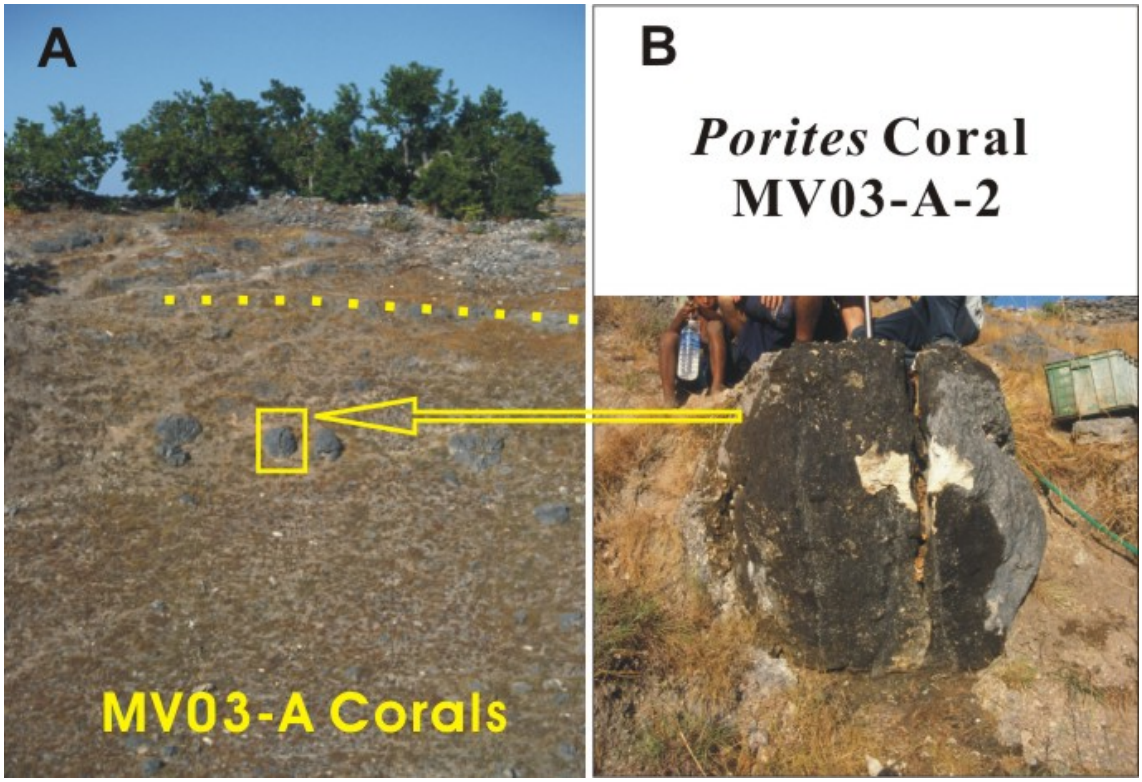

Figure 4.1 **(A)** Mondu V coral reef. Dotted line marks an erosion surface above the Mondu V coral reef. (**B)** The half exposed large *Porites* coral MV03-A-2 which is still in growth position. Note the big crack through the coral from top to bottom.

Recently three correction models have been published to more rigorously quantify open-system U-series ages. Villemant and Feuillet [2003] propose a model that takes into account possible initial ^{230}Th excess where continuous selective redistribution (gain or loss) of ^{234}U, ^{234}Th and ^{230}Th is controlled by recoil processes. Thompson et al. [2003] present a quantitative model where the positive correlation between $^{234}U/^{238}U$ and $^{230}Th/^{238}U$ activity ratios is explained by coupled addition of particle-reactive ^{234}Th and ^{230}Th, which is produced by decay of dissolved uranium and α-recoil mobilisation of uranium daughters. Scholz et al. [2004] have developed a new model which combines uranium uptake and loss, the latter being proportional to the amount of uptake, which explains their data and produces characteristic isochrons. They show that the 'true' age of the coral can be calculated from the intersection of the isochron and the seawater evolution curve.

In this chapter, I report on multiple measurements of U-series isotopes in skeletal sub-samples within a single fossil *Porites* coral to explore the diagenetic behaviour of U-series isotopes during two recognisable stages of post-depositional alteration. Detailed analysis of the relationship between the diagenetic stages and the corresponding changes in U-series isotopic composition has revealed two distinct processes of U-series isotope diagenesis in this single coral colony. Both of them are different from those previously reported in the literature.

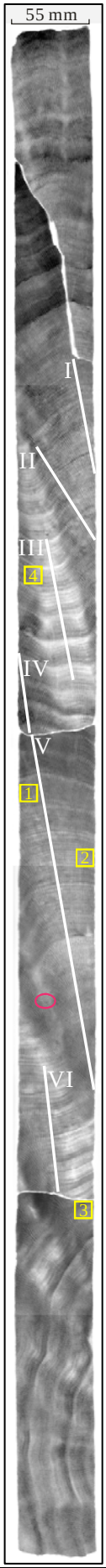

Figure 4.2 X-ray photo of 7 mm slab of core drilled into coral MV03-A-2c. Numbered yellow boxes denote positions of sub-samples collected for U-series dating. Red circle marks a calcite patch. White lines with Roman numerals indicate the sub-sampling transects for stable isotope analysis.

4.2 MATERIALS AND METHODS

4.2.1 Coral sampling

Four large *Porites* corals were found exposed in a steep wall of a deep valley ~1.5 km from the north coast of Sumba, Indonesia. The corals are positioned 39 m above modern mean sea level and still in their original growth positions (Figure 4.1). Colony MV03-A-2 is 1.2 m in diameter, 1.1 m in height and particularly well exposed. A prominent crack cuts through the coral from top to bottom (Figure 4.1B).

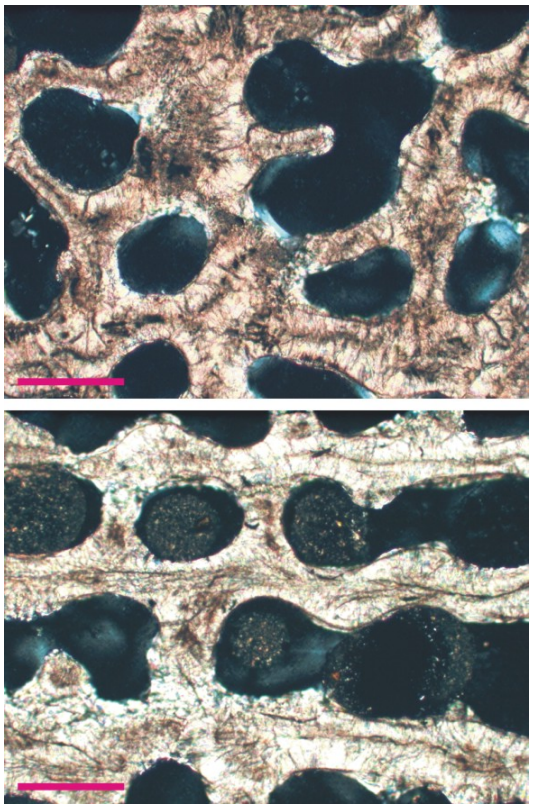

Figure 4.3 Optical microscopic image of petrographic thin-section of fossil coral MV03-A-2c (top) compared with image of modern local *Porites* coral RSM2b (bottom). Red bar represents 2 mm.

Two calcitized cores “a” and “b” were drilled before an exceptionally well-preserved core “c” was retrieved. The 1.1 m long core “c” was slabbed and one of the most pristine spots in the middle section was chosen to U-series date the coral (“c1” yellow

box in Figure 4.2). The ^{230}Th age of this sub-sample was not reliable enough so eight more sub-samples were selected to produce a model correction age for this coral (3 more from core c, 4 from core a, and 1 from core b).

4.2.2 Coral preservation

The coral slab show excellent preservation under natural and UV light with only one small patch of calcite (Figure 4.2).

Sub-samples from core c show only traces of calcite and aragonite content is >98%, as measured by X-ray diffraction at The Australian National University. Sub-samples from cores a and b were not measured by X-ray diffraction, but were chosen from the least altered parts of the cores where calcite contents were estimated to be <5% by visual check under UV light. Even though there is slight dissolution and slight calcite overgrowths in some parts of the core, the smooth septal walls and radial-fibrous structure of aragonite centres of calcification indicate excellent preservation of this coral skeleton. Figure 4.3 shows the impressive similarity between this fossil coral and a modern *Porites* coral (RSM2b) living on a nearby reef, indicative of extraordinarily good preservation for a very old *Porites* coral that has been exposed to both submarine and subaerial environments for a long time.

4.2.3 U-series isotopic measurement and age determination

The U-series method [*Edwards et al.*, 1986/87] was applied to obtain the U-series isotopic composition and ^{230}Th ages of different sub-samples in fossil coral MV03-A-2. However, both open-system [*Thompson et al.*, 2003] and isochron age [*Scholz et al.*, 2004] models failed to achieve a reliable age for this coral. Therefore, a detailed analysis of U-series isotopic characteristics of this coral was performed, which provided an excellent opportunity to understand the behaviour of U-series isotopes after the

coral's death. This analysis laid the foundation for the final determination of the age of this fossil coral by choosing appropriate correction models.

U-series measurements were performed using the multi-collector ICP-MS instruments at RSES, ANU and the Department of Geosciences, National Taiwan University following chemical procedures reported by Luo et al. [1997] and McCulloch and Mortimer [2008], or by Edwards et al. [*Edwards et al.*, 1987b], and MC-ICP-MS measurement protocols [Stirling et al., 2001; Shen et al., 2002; McCulloch and Mortimer, 2008]. The "U-2" mixed ^{229}Th and ^{233}U spike or double spike ^{233}U-^{236}U-^{229}Th were used to spike each dissolved coral sub-sample and a PE TRU or an anion exchange resin (BioRad 1-X8, 100 – 200 mesh, 0.6 – 1.0 ml column) ion exchange column was used to separate the elements. The ^{230}Th age and initial ^{234}U were calculated using ISOPLOT Excel add-in written by K.R. Ludwig with half-lives of 230Th, 234U, and 238U following Cheng et al. [2000]. The Isochron and open-system model ages were calculated according to Scholz et al. [2004] and Thompson et al. [2003].

4.3 RESULTS

A sub-sample from the most pristine part of core MV03-A-2c (sub-sample c1 in Figure 4.2) was first chosen to be dated and its conventional ^{230}Th age is 136.8 ± 1.5 ka with a back-calculated initial δ^{234}U value of 158.9‰ (Table 4.1, sub-sample c1). Given that this initial δ^{234}U value is near the range of δ^{234}U values measured for modern seawater and recent corals (136‰ to ~151‰, ave. 145-149‰ for different measurements) [*Chen et al.*, 1986; *Edwards et al.*, 1986/87; *Chen et al.*, 1991; *Ludwig et al.*, 1991; *Gallup et al.*, 1994; *Szabo et al.*, 1994; *Cheng et al.*, 2000; *Stirling et al.*, 2001; *Muhs*, 2002; *Robinson et al.*, 2004], the U-series age of this sub-sample should be close to the true age of this fossil coral. In fact, for old fossil corals many researchers have considered a ^{230}Th age to be reliable if its initial δ^{234}U is within the range of 149 ± 8-10‰ [For example, *Gallup et al.*, 1994; *Stirling et al.*, 1998; *Stirling et al.*, 2001; *Esat and*

Yokoyama, 2006] or 146 ± 8‰ [*Cutler et al.*, 2003]. Stirling et al. [1998] have also shown no significant difference for ^{230}Th age reliability for corals with initial δ^{234}U of 149 ± 10‰ and concluded that the 149 ± 10‰ range is acceptable for most coral dating studies.

Table 4.1

U-Th isotopic composition and calculated ages for sub-samples of fossil coral MV03-A-2

ID[1]	Distance (cm)[2]	^{238}U (ppb)	^{232}Th (‰)	$\delta^{234}U_m$[3] (‰)	[^{230}Th/^{238}U] (activity)	^{230}Th/^{232}Th (x10^{-6})[4]	^{230}Th age (ka)	$\delta^{234}U_i$[3] (‰)	O-S age (ka)[5]
c1	55	2541 ± 4	159	107.9 ± 1.7	0.805 ± 0.004	210374 ??????????????	136.8 ± 1.5	158.9 ± 2.4	131.7 ± 1.9
c2	60	3672 ± 4	276 ± 2	109.5 ±1.4	0.803 ± 0.002	176405 ± 1623	135.7 ± 0.8	160.8 ± 1.9	129.8 ± 1.4
c3	84	3902 ± 6	357 ± 3	135.6 ±1.7	0.854 ± 0.003	154194 ± 1166	145.5 ± 1.1	204.6 ± 2.3	121.8 ± 2.3
c4	40	3439 ± 5	271 ± 2	104.0 ± 1.8	0.843 ± 0.002	176626 ± 1649	151.3 ± 1.1	159.5 ± 2.5	145.7 ± 1.8
a1	54	3477 ± 6	234 ± 3	106.9 ± 1.3	0.841 ± 0.003	206577 ± 3061	149.9 ± 1.1	163.3 ± 1.9	142.7 ± 1.5
a2	63	3528 ± 6	360 ± 3	109.0 ± 1.2	0.847 ± 0.003	136944 ± 1366	151.3 ± 1.0	167.1 ± 1.7	142.5 ± 1.5
a3	68	3323 ± 6	285 ± 3	119.1 ± 1.4	0.888 ± 0.003	170655 ± 2094	163.7 ± 1.3	189.1 ± 2.1	145.3 ± 2.1
a4	75	3153 ± 5	196 ± 3	115.8 ± 1.3	0.911 ± 0.003	241960 ± 4069	175.0 ± 1.3	189.9 ± 1.9	155.9 ± 2.1
b1	46	3304 ± 7	221 ± 4	123.4 ± 1.8	0.877 ± 0.003	216830 ± 3533	157.8 ± 1.4	192.7 ± 2.5	138.2 ± 2.3

Measurements were isotope dilution runs using a mixed ^{233}U-^{229}Th tracer calibrated against the Harwell Uraninite (HU-1) secular equilibrium standard. Decay constants are 9.1577 x 10^{-6} yr^{-1} for ^{230}Th, 2.8263 x 10^{-6} yr^{-1} for ^{234}U, and 1.55125 x 10^{-10} yr^{-1} for ^{238}U (Cheng et al., 2000). Analytical errors are 2σ of the mean.

[1] Letters (a, b, c) indicate sub-sample is from core a, b, or c and data from different cores are separated by dotted lines. Measurement of sub-sample c1 was made using the MC-ICP-MS at RSES, ANU following chemical and instrumental protocols similar to Luo et al. [1997] and Stirling et al. [2001]. All the other sub-samples were analyzed using similar protocols by Chuan-Chou Shen and Chih-Wei Chen at the Department of Geosciences, National Taiwan University.

[2] Distance of sub-sample from the top of the core.

[3] $\delta^{234}U_m$ is measured value and $\delta^{234}U_i$ is back-calculated initial value.

[4] The degree of detrital ^{230}Th contamination is indicated by the [^{230}Th/^{232}Th] atomic ratio instead of the activity ratio.

[5] Open system (O-S) ages and errors were calculated using a spreadsheet provided by W. Thompson [*Thompson et al.*, 2003] with an assumed initial δ^{234}U value of 146.6‰ [*Stirling et al.*, 1998; *Robinson et al.*, 2004].

According to the observation of Gallup et al. [1994], the true age of coral MV03-A-2 might be only slightly younger than 136.8 ka. Gallup et al. [1994] suggested that if a coral hypothetically began with an initial δ^{234}U value of 149‰ but ultimately has a initial δ^{234}U value of 153‰, it has experienced open-system conditions and may be biased toward an older age by about 1000 yr. Accordingly, the age of coral MV03-A-2

might be between 133 ka and 134 ka [133.4 ka if a value of modern coral and seawater $\delta^{234}U$ of 148.9‰ [*Stirling et al.*, 1998] is applied, or 133.7 ka if a more recently measured value of 146.6‰ [*Robinson et al.*, 2004] is applied].

Whatever the true age of this coral is, it is probable that it grew in a very special period called Termination II (or penultimate deglaciation), which followed the penultimate glacial maximum (>140 ka) and ended at the Last Interglacial Maximum (< 128 ka) [*Martinson et al.*, 1987; *Muhs*, 2002; *Brauer et al.*, 2007]. There is now considerable evidence suggesting that sea-level and mean climate changed dramatically within a few thousands of years during the penultimate deglaciation [*Esat et al.*, 1999; *Gallup et al.*, 2002; *Antonioli et al.*, 2004; *Siddall et al.*, 2006]. Thus a highly accurate age for coral MV03-A-2 is needed to better understand the significance of the climatic and oceanic conditions recorded by this uncommon coral.

Towards this goal, more sub-samples from this core and other cores from the same coral colony were selected and analysed by MC-ICP-MS at the National Taiwan University. U-series isotopic compositions for all the sub-samples and calculated conventional ^{230}Th ages are listed in Table 4.1. The analyses revealed a range of U-series isotopic compositions for different parts of the same coral. The U contents vary from 2.5 ppm to 3.9 ppm and the ^{232}Th concentrations of the sub-samples vary by a factor of two. All the sub-samples were chosen from well preserved parts of the cores and most of them satisfied the so-called "strict" screening criteria (U 2.1-3.8 ppm, ^{232}Th <2 ppb, calcite <2%; [*Stirling et al.*, 1998; *Scholz and Mangini*, 2007]. The calculated conventional ^{230}Th ages changed from 136 ka to 175 ka for this single coral and have a surprising difference up to ~40 ka. The initial $\delta^{234}U$ values varied from 158.9 to 204.6, indicative of not only open-system behaviour for all the sub-samples but also significant differences in the degree of diagenetic alteration of U-series isotopes in this single coral.

As a result, among sub-samples in this single coral head there is no linear array on a $^{234}U/^{238}U$ and $^{230}Th/^{238}U$ isotope ratio diagram (Figure 4.4) which has been observed for many different corals of the same age on raised reefs worldwide [*Bender et al.*, 1979;

Hamelin et al., 1991a; *Bard et al.*, 1992; *Gallup et al.*, 1994; *Stirling et al.*, 1995; *Cheng et al.*, 1998; *Henderson et al.*, 2001; *Stirling et al.*, 2001; *Thompson et al.*, 2003; *Villemant and Feuillet*, 2003; *Potter et al.*, 2004; *Scholz et al.*, 2004]. Therefore, it is impossible to achieve a more reliable age for this coral by directly applying the newly published isochron model [*Scholz et al.*, 2004] where a single isochron line is needed to determine a model age. It is also difficult to obtain a reliable age from the other two correction models recently suggested by Thompson et al. [2003] and Villemant and Feuillet [2003], both of which explain the linear array by assuming that α-recoil controls the mobility of U-series isotopes. Table 4.1 lists the calculated open-system correction ages which showed discrepancies of up to 30 ka for the sub-samples. The result implies that this kind of decay-dependant addition of ^{234}Th and ^{230}Th should not be the only process involved in the diagenetic alteration of coral MV03-A-2.

In summary, the detailed analysis of the U-series isotopes in MV03-A-2 provided a good opportunity to explore the post-depositional alteration of the U-series isotopic composition in this coral. The following section discusses the characteristics and changes in U-series isotopic composition for the sub-samples. The correlation between U-series isotopic composition and sub-samples position, and degree of diagenetic alteration, will be explored. Two distinct post-depositional processes affecting U-series isotopes will be put forward followed by the determination of a more reliable age for this coral based on the new understanding of the diagenetic processes.

4.4 DISCUSSION

4.4.1 Two groups of U-series isotopic composition

Even though a consistent age could not be determined by direct application of any of the recently published correction models [*Thompson et al.*, 2003; *Villemant and Feuillet*,

2003; *Scholz et al.*, 2004], it seems that there are two groups of data on the $^{234}U/^{238}U$ - $^{230}Th/^{238}U$ diagram (Figure 4.4). Group one is comprised of sub-samples c1, c2, and c3 form core c. Group two includes all the sub-samples from core a (a1, a2, a3, and a4). Sub-sample c4 is also close to this group and the sub-sample from core b is between the two groups, but closer to group two.

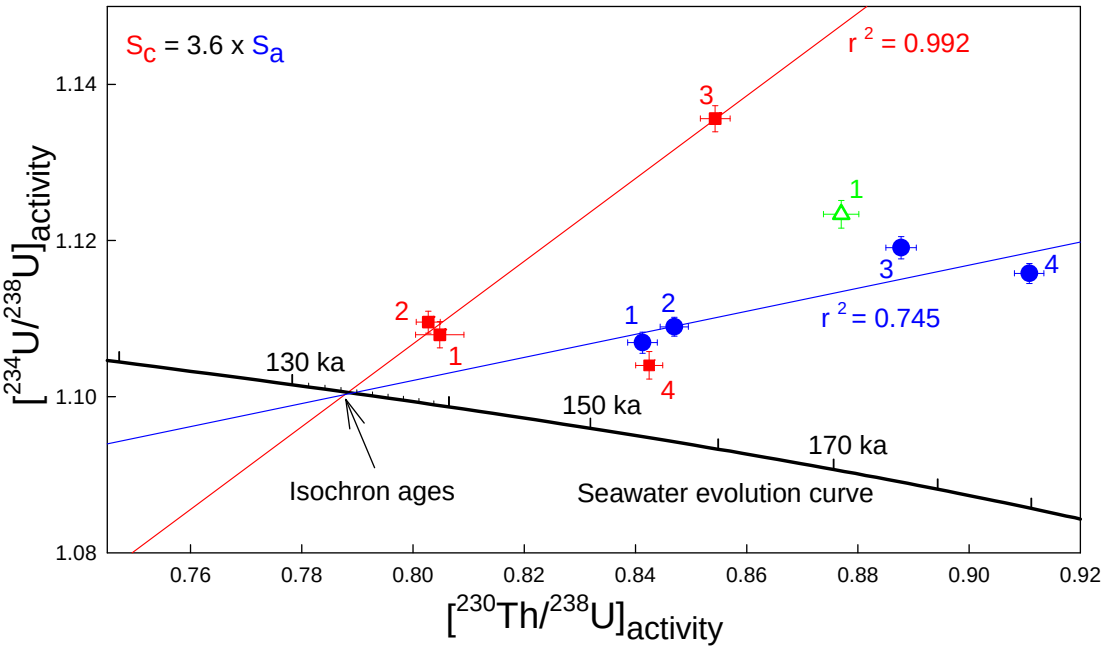

Figure 4.4 Correlation diagram of $^{234}U/^{238}U$ and $^{230}Th/^{238}U$ activity ratios in coral MV03-A-2. Analysis of two groups of sub-samples (red and blue) from different cores through the coral demonstrates that two distinct diagenetic processes have altered the $^{234}U/^{238}U$ and $^{230}Th/^{238}U$ activities. The red line is the linear regression for 3 sub-samples from core "c" while the blue line is the regression for all 4 sub-samples from core "a". The different slopes for the two data sets ($S_c = 3.6*S_a$) are indicative of two distinct diagenetic pathways. Independent "isochron" ages were determined by intersecting the regression lines with the seawater evolution curve. The results show that both sample groups yield essentially the same model age of 133-134 ka. Error bars for individual data points are 2σ.

There is a positive correlation of $^{234}U/^{238}U$ and $^{230}Th/^{238}U$ within each group, with two distinct slopes. Does the positive correlation imply a common mechanism of diagenesis for these sub-samples? One asks this question because there are only 3 or 4 points

within each group, which is not enough for us to conclude by the grouping behaviour in the $^{234}U/^{238}U$ - $^{230}Th/^{238}U$ projection. However, the different slopes of the correlations suggest there were two diagenetic processes involved in altering this single coral. What were they and how did they proceed?

Detailed analysis of all the data shows (apart from the grouping in the $^{234}U/^{238}U$ - $^{230}Th/^{238}U$ projection) that these sub-samples fall into distinct two groups in almost all aspects of the data (Figure 4.5), as follows:

1. Group one U content increases with depth of sub-samples in the coral, while it decreases with depth in Group Two, especially for a2, a3, and a4 (Table 4.1);

2. The ^{232}Th concentration has the same trends as for U content (Table 4.1);

3. All sub-samples show a strong correlation between U and ^{232}Th contents, but the correlation within each group is even stronger and the lines of fit have different slopes (Figure 4.5A);

4. ^{232}Th is strongly correlated with ^{230}Th within group two, including sub-samples c4 and b1, while group one shows strong correlation but with a dramatically different slope (Figure 4.5B);

5. Even though there is a strong correlation between ^{230}Th and ^{232}Th for both groups, group one shows a weak correlation between $^{230}Th/^{232}Th$ and ^{232}Th concentration, and in group two the ratio increases with decreasing ^{232}Th content.

6. U content strongly correlates with ^{230}Th within each group, but the two slopes differ by a factor of 3.6 (Figure 4.5D);

7. Figure 4.5E demonstrates strong correlation between $^{230}Th/^{238}U$ and ^{238}U within group two, but only a weak correlation within group one, and the slopes are very different.

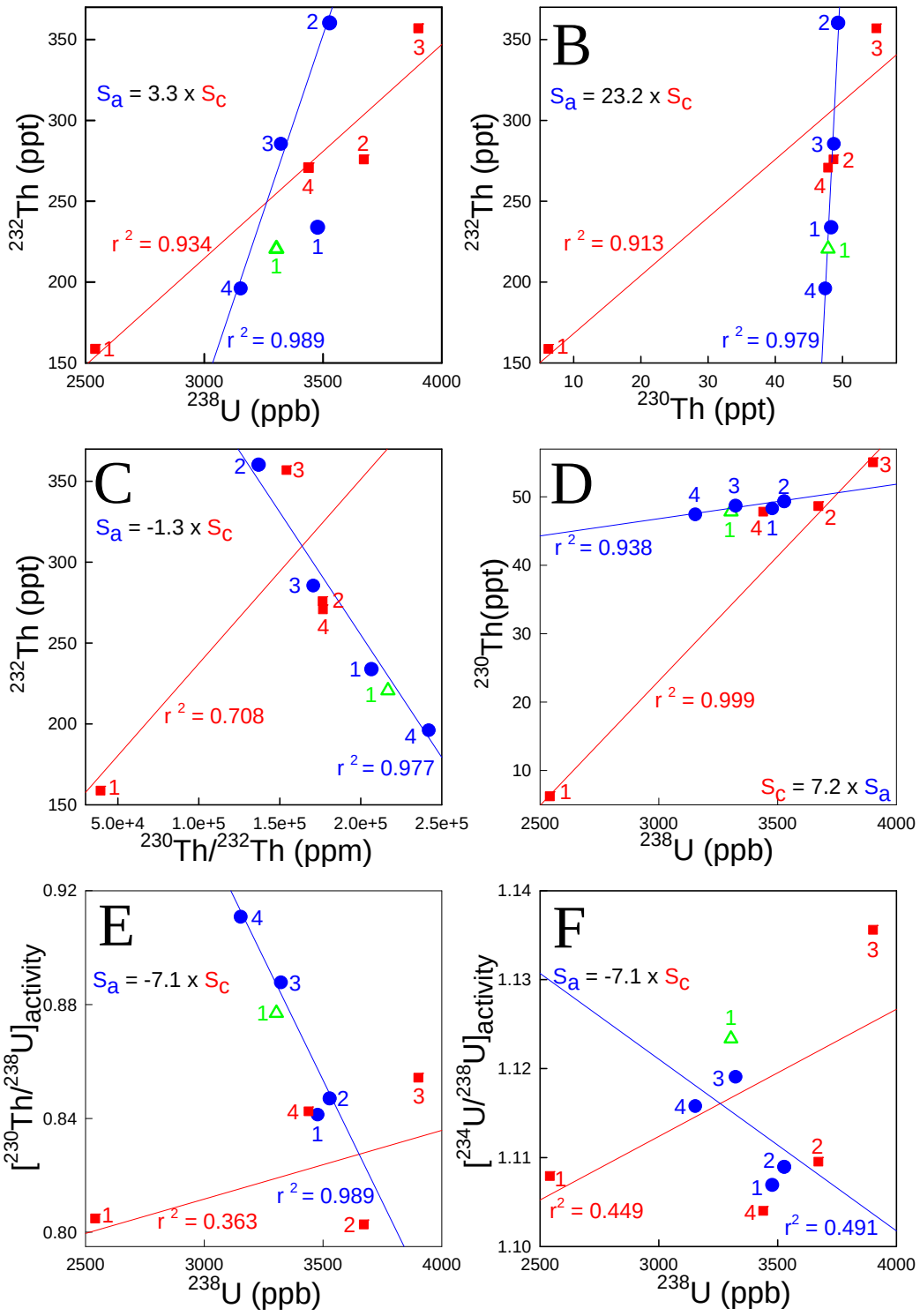

Figure 4.5 Two distinct groups of U-series isotopic behaviour have been displayed in the correlation diagrams of U-series isotopic ratios and their contents in fossil coral MV03-A-2. Numbered red squares represent sub-samples from core "c" and blue dots represent sub-samples from core "a". Green triangle denotes a sub-sample from core "b". Error bars are 2σ of the mean. Red thin lines are linear regression of data for 3 sub-samples from core "c" (c1, c2, and c3) and blue thin line are linear regression of data for 3 sub-samples from core "a" (excluding a1). Correlation coefficient r^2 is shown along with each regression line. The distinct difference between the two slopes of the regression lines in each plot is shown as an equation with S_c standing for slope of core "c" data, while S_a for slope of core "a".

8. In contrast to the behaviour of $^{230}Th/^{238}U$ and ^{238}U content, $^{234}U/^{238}U$ and ^{238}U content are moderately correlated in both groups with different slopes (Figure 4.5F).

9. When calculating open-system ages for the sub-samples applying the Thompson et al. model, there is somehow consistency within each group, but a significant discrepancy occurs between the two groups: in group one the corrected ages are younger than the preliminary age (133-134 ka) obtained for the most pristine sub-sample c1, while in group two the correction ages are older than the preliminary age (Table 4.1).

In summary, this detailed analysis of the U-series data has confirmed that there are two distinct modes of diagenesis influencing U-series isotopic behaviour in this coral.

4.4.2 Sample position, degree of alteration, and U/Th behaviour

When observing all the trends in the data, it is important to note that all the changes in ^{232}Th, ^{238}U, ^{230}Th, and even the calculated open-system ages keep two fixed orders: for group one all trends are in the order c1 → c2 → c3, and for group two in the order a2 → a3 → a4. These orders are the same as order of the sub-samples in the coral cores, and thus imply that the U-series isotopic processes are related to the position of the sub-samples in the coral. It also implies that the processes are related to the mobilization of the U-Th isotopes along certain paths within the coral after it was buried, rather than by initial uptake of ^{230}Th when the aragonite skeleton formed. This provides a good opportunity to explore how the diagenetic processes might connect the sub-samples with the directions of change in U-Th isotopes.

As shown in the photos in Figure 4.1, this coral had been buried for a long time before it was exposed. The extraordinarily well-preserved core c indicates that this coral colony has not been exposed for very long. Photo B also showed a large crack from the top to

the bottom of the colony. Given that core c is well-preserved, while other cores in the same colony are obviously diagenetic altered, it is likely that the crack developed after the coral was exposed. Figure 4.6 illustrates the positions of the cores and the sub-samples. Core a was drilled in the centre of this colony but was badly calcitized in many parts of the core. I could only find aragonite sub-samples for U-Th dating in the lower-middle section (sub-samples a1-a4 Figure 4.6B). Core b was then drilled close to core a, but closer to the crack. This core was seriously altered and, as a result, only one aragonite sub-sample could be selected for U-Th dating. Core c was also drilled close to core a, but farther away from the crack. This turned out to be a high quality core with only one small calcite patch in the lower middle section. At first we chose three well preserved sub-samples in the middle and lower sections (c1, c2, and c3 in Figure 4.2 and 4.6B), then we selected the forth sub-sample c4 in the upper section. Sub-sample c4 is slightly discoloured and appears slightly dissolved, as reflected by lower skeletal density in X-ray photos of the core (Figure 4.2).

Since the distance between the cores is only less than 20 cm, the big difference in diagenetic alteration between these cores demonstrates that the diagenetic process which calcitized the aragonite skeleton was strongly related to the crack. It also shows that aragonite skeleton only tens of centimetres away from the crack could effectively resist the diagenetic process.

Compared to all sub-samples, c1 appears to be the most unaltered in terms of pristine colour and texture. The U-series results are consistent with this observation in that sub-sample c1 has the (1) lowest detrital ^{232}Th content, (2) initial δ^{234}U value close to modern seawater and modern coral, and (3) lowest U content (2541 ppb) which is almost equal to that of modern corals in nearby Sumba reefs (range 2478-2663 ppb, M. Gagan unpublished data, Appendix C). Since some of other sub-samples are only tens of centimetres away from sub-sample c1 (e.g. c2 or a1 in Figure 4.6B), it is evident that the *Porites* aragonite skeleton is effective in resisting the incursion of both the diagenetic processes. Given its central position, the most likely candidate for another

diagenetic process (apart from that strongly related to the crack) should be a process entering the coral from outside by all directions. It is reasonable to imagine that the colony had been buried for a long time before the fossil reef was raised by tectonic uplift and then half exposed by valley incision followed by cracking because of its exposure. Therefore, it is plausible to think that the process which affected the core c sub-samples by invading the coral from outside occurred earlier than the process related to cracking of the coral which impacted the core a sub-samples.

4.4.3 Two distinct diagenetic processes

Owing to the strong correlation between the contents of U and detrital ^{232}Th (Figure 4.5A), and the fact that the U contents in other sub-samples are all higher than in local modern *Porites* corals, it is logical to suggest that some kind of uranium-rich groundwater had permeated through the coral and left some fine detritus (or some kind of colloid incorporated with detrital Th) within the aragonitic skeleton in a early stage when the coral was buried. Due to the resistance of the aragonite skeleton, and the fact that the groundwater would soak into the colony from the entire surface of the buried coral, the impact of this process should decrease symmetrically towards the central part having the least U and detritus contents. The source of the U-rich groundwater should be abundant in the fossil reef environment where this coral was buried. But when the coral was half exposed and cracked, this process would have been overpowered by meteoric water entering the coral, especially through the crack and the top surface. Accordingly, the permeation of the late-stage, relatively clean meteoric water would subsequently remove dissolved U and the fine detritus or colloid. This process would make the contents of U and detrital ^{232}Th lower in sub-samples closer to the surface or the crack, which is consistent with the U-series isotope results.

In summary, the evidence suggests that two distinct diagenetic processes were involved in the U-series isotopic post-depositional behaviour in coral MV03-2-A. Figure 4.5 illustrates both processes and they can be preliminarily described as follows:

- Process One: uranium-rich groundwater permeated into the buried coral through the outer surface from all directions at an early stage. The groundwater derived from the local fossil reefs and was rich in U and had a relatively high $\delta^{238}U$ value; it also transported fine detritus or colloids with foreign (non-radiogenic) ^{232}Th into the skeleton. The amount of additional U and detritus in the coral is proportional to the distance to the surface where the percolating water starts to enter the coral.

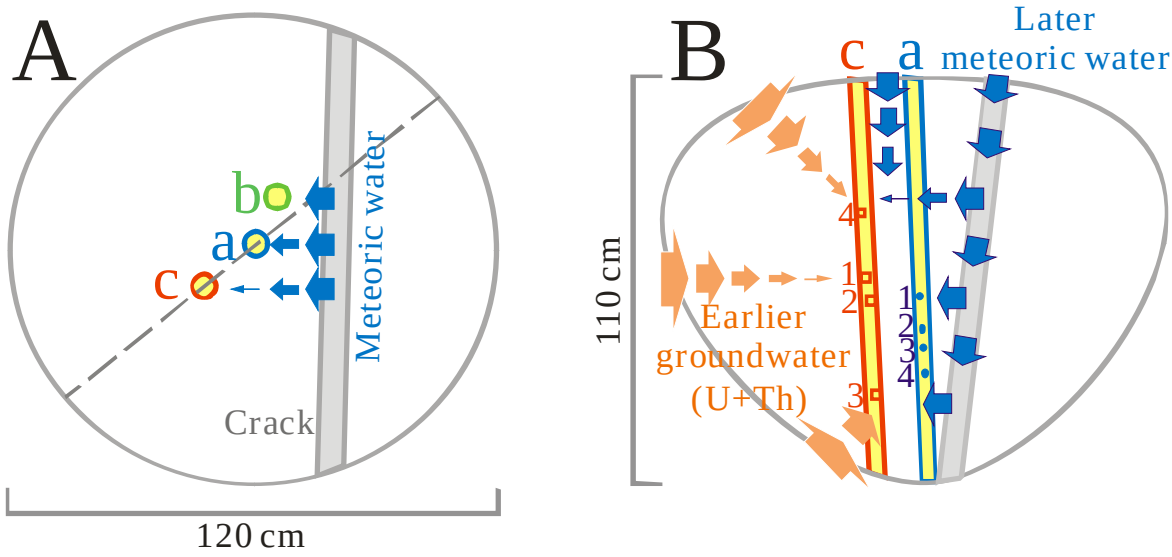

Figure 4.6 Cross-sections illustrating the position of the cores and sub-samples and two diagenetic processes that occurred after the burial of fossil coral MV03-A-2. **(A)** Top view of the coral colony. Grey bar represents the crack through the colony from top to bottom; Circles with letters represent cores “a”, “b”, and “c” extracted from the coral. Blue arrows show the incursion of meteoric water from the crack and the size of arrow depicts how the process impacted the sub-samples because of the resistance of the aragonite skeleton. Dashed line marks the position of the cross-section shown in panel B. **(B)** Cross-section of the coral colony. Orange and blue bars represent core “c” and “a”, respectively. Red squares show the position of sub-samples in core “c” and blue dots the sub-samples in core “a”. Orange arrows represent the incursion of U-rich groundwater from all directions in an earlier stage when the coral was still buried.

- Process Two: after the coral was half exposed and cracked as a result of tectonic uplift and valley incision at a later stage, meteoric water soaked into the colony mainly through the crack and the upper surface. Given that meteoric water would mainly result from rainfall or runoff from the upper slope of the valley, contents of

^{234}U, ^{238}U and the detrital Th should be very low or even zero in this water. Subsequently it would dissolve away U from the aragonite texture and remove detritus or colloids which had been taken into the coral by percolating groundwater during the earlier Process One, while radiogenic ^{230}Th remained in the aragonite skeleton due to its insolubility. The amount of U and detritus dissolved by the percolating meteoric water is also related to the distance of the spot in the coral to the surface or crack where the water started to enter the coral.

In the projections shown in Figures 4.4 and 4.5, the two diagenetic processes make the isotopic composition of the sub-samples change along distinct trends or directions. Detailed analysis and comparison of the distinct U-series isotopic behaviours of the two groups would provide opportunity for further understanding the mechanisms involved in diagenesis. Table 4.2 summarises the changes in U-series isotopes produced by the two distinct processes. The major aspects of the diagenetic mechanisms include the following:

1. Percolating water as a transport medium and osmosis rules followed

The transport medium for U-series isotopes was most likely the percolating water, which took dissolved U and fine detritus or colloids (Th was bound in it) into or out of the *Porites* coral down a solute concentration gradient following rules of diffusion, such as osmosis. Thus the addition of dissolved U and detritus into the coral would occur when the percolating water contains higher concentrations than the coral itself, while loss would occur when the percolating water has relatively low concentrations of dissolved U and detritus. It also means that the addition or loss of dissolved U into the coral aragonite should be a dynamic equilibrium process in which the addition and loss proceed at the same time, but the equilibrium should be controlled by the osmotic pressure. Not only would the osmotic pressure control the amount of percolating water (and the dissolved U and fine detritus) within the coral, but also the net amount of addition/loss into/out of the coral aragonite. This mechanism is the most plausible process that explains all the data, especially the strong correlation between the change in

U-series isotopic composition with distance of the sub-samples from the surfaces where percolating water entered the coral.

2. Remobilization of U and Th

Both allochthonous U and Th were transported into the coral at a relatively early stage in its burial history, while both U and Th were removed from the coral at a later stage, as shown in Figure 4.5A by the strong correlation between detrital ^{232}Th and ^{238}U. The results of this study show that ^{234}U, ^{238}U, ^{232}Th, and ^{230}Th were all involved in the addition or loss in both processes, with their redistribution being distinctly different in the two processes.

3. Large input of extraneous, locally radiogenic ^{230}Th in Process One

Figure 4.5B shows a strong correlation between the contents of ^{230}Th and detrital ^{232}Th, suggesting addition of extraneous ^{230}Th in Process One. The large difference in the slopes indicates a large amount of this input from an external source. If changes in the amount of ^{232}Th were fixed for both processes (addition or loss), then the change in amount of ^{230}Th in Process One would be 23.2 times greater than the change in Process Two (Table 4.2).

Figure 4.5C illustrates that in Process One the ^{230}Th/^{232}Th increased along with the increasing addition of ^{232}Th, while in Process Two it also increased during the loss of ^{232}Th (Figure 4.5B), which means that the contents of ^{230}Th apparently increased relative to ^{232}Th in both situations. The latter fact implies that the relative increase in ^{230}Th occurred due to loss of U, while the former confirms that extra ^{230}Th other than the non-radiogenic, detritus-binding ^{230}Th had been added into (in Process One) or lost from the aragonite (in Process Two). Since the insolubility of ^{232}Th in water is just like that of ^{230}Th, the probable cause of the relative increase in ^{230}Th in Process One should be the loss of dissolved ^{234}U and ^{238}U in the percolating groundwater, while in Process Two the apparent increase of ^{230}Th relative to ^{232}Th should result from dissolved ^{234}U and ^{238}U, which would have produced ^{230}Th if they had not been dissolved and taken

away from the aragonite. The plausible mechanism for the locally radiogenic ^{230}Th would be α-recoil decay from the dissolved ^{234}U and ^{238}U followed by absorbing to the aragonite texture owing to its particle-reactive character [*Henderson et al.*, 2001; *Thompson et al.*, 2003].

Radiogenic ^{230}Th directly decayed from extra ^{234}U should have played an important role in keeping the ^{234}U/^{230}Th ratio constant for the earlier-stage Process One.

Table 4.2

Comparison of changes in isotopes involved in the two processes of diagenesis

Nuclide if in fixed content	Nuclide or ratio in change	Comparison of rate of changing (Process One / Process Two)	Data source
	^{234}U/^{230}Th	3.6	Figure 4.4
^{232}Th	^{238}U	3.3	Figure 4.5A
^{238}U	^{230}Th	7.2	Figure 4.5D
^{232}Th	^{230}Th	23.2	Figure 4.5B
^{232}Th	^{230}Th	23.76 (= 3.3 x 7.2)	Calculated
^{238}U	^{234}U	25.92 (= 3.6 x 7.2)	Calculated
^{232}Th	^{234}U	83.52 (= 3.6 x 23.2)	Calculated
^{232}Th	^{234}U/^{238}U	25.3 (= 83.52 / 3.3)	Calculated
^{232}Th	^{230}Th/^{238}U	7.2 (= 23.76 / 3.3)	Calculated
^{232}Th	^{234}U/^{230}Th	3.5 (25.3 / 7.2)	Calculated

4. Input of allochthonous U with higher δ^{234}U in Process One

The large input of allochthonous locally radiogenic ^{230}Th in Process One implies even larger input of extraneous ^{234}U and ^{238}U. Actually, all the plots in Figure 4.4 and 4.5 reflect the likelihood that the early-stage percolating groundwater brought into the coral high concentrations of U and that its δ^{234}U value was higher than that of the coral aragonite.

The increase of ^{234}U/^{238}U activity ratio along with the addition of ^{238}U in Figure 4.4 is indicative of a higher δ^{234}U value in the percolating groundwater in Process One. Even

though the change in $^{234}U/^{230}Th$ ratio roughly keeps fixed values for both processes, the ratios are different for the two groups. The change in the $^{234}U/^{230}Th$ ratio in Process One is 3.6 times of that in Process Two, indicating that in Process One extra ^{234}U relative to both to ^{238}U and ^{230}Th was provided from the percolating water. However, in Process Two the percolating water did dissolve the same proportion of ^{234}U compared to ^{238}U and ^{230}Th as their addition in Process One. The most plausible source of the extra ^{234}U in Process One should be the dissolved ^{234}U in the percolating groundwater.

The difference in the slopes (Figure 4.5A) demonstrates that in Process One 3.3 times the amount of extraneous ^{238}U was added to the coral relative to the amount of ^{238}U dissolved in Process Two. In contrast, Table 4.2 shows that the change in the amount of ^{234}U in Process One would be 84 times larger than that in Process Two (3.6 x 23.2 = 83.52 or 3.6 x 23.76 = 85.53), if the involved ^{232}Th change was fixed for both processes. Accordingly, the change rate of $^{234}U/^{238}U$ ratio in Process One was 25.3 times that in Process Two if the ^{232}Th concentration was constant.

The U-rich groundwater and its relatively high $\delta^{234}U$ value should result from the local fossil coral reefs when it percolated through them before entering the buried coral. The higher $\delta^{234}U$ value might result from (1) the high $\delta^{234}U$ of fossil reefs because of their ages, and/or (2) the preferable entering of ^{234}U into the percolating water due to α-recoil decay of ^{238}U[*Moore*, 1967].

5. Percolating meteoric water as transport medium in Process two

The late-stage percolating water contained low U concentrations so it removed U from the coral aragonite and the earlier-stage removed detritus from (instead of added to) the coral down a solute concentration gradient according to the rules of osmosis. The most plausible source of the percolating water would be direct rainfall or runoff from the upper slopes of the coral terraces. When this meteoric water percolated through the coral, it would remove both ^{234}U and ^{238}U and their ratio should be similar to the ratio in the sub-samples because of their similar solubility and chemical characteristics.

6. Small amount of allochthonous non-radiogenic ^{230}Th involved

This study suggests that, even though allochthonous non-radiogenic ^{230}Th (binding in the fine detritus or colloid along with the detrital ^{232}Th) was involved in both processes, the amount was very small compared to detrital ^{232}Th. The loss of non-radiogenic ^{230}Th played an important role in deciding the ratio of ^{234}U/^{230}Th in Process Two; in contrast, it was insignificant in comparison with the extraneous radiogenic ^{230}Th in Process One. In both situations, both processes helped keep ^{234}U/^{230}Th constant and were important in model age determination.

Figure 4.5D clearly shows the loss of ^{230}Th in Process Two accompanying the loss of ^{238}U even though the amount of lost ^{230}Th is small. Due to its insolubility in water, the removed ^{230}Th must be adsorbed to fine detritus or colloids where detrital ^{232}Th was present. This was also confirmed by the data for this coral (Figure 4.5B) where ^{232}Th and ^{230}Th are strongly correlated. These results clearly demonstrate that, even though the amount of detrital ^{230}Th was small in comparison with the lost ^{232}Th and ^{238}U, the loss of ^{230}Th indeed happened in Process Two. The results demonstrate the ratio of ^{232}Th/^{230}Th in detritus would be 83.3 based on the slope. Considering that added non-radiogenic ^{230}Th in the early-stage Process One (if there was any) would remain together with the detritus due to its insolubility, and given the very high ^{232}Th/^{230}Th ratio in the detritus (83.3), the large discrepancy between the two slopes (23 times, as shown in Figure 4.5B) also implies that the content of non-radiogenic ^{230}Th in fine detritus or colloids along with detrital ^{232}Th is insignificant compared to content of radiogenic ^{230}Th decayed from ^{238}U or ^{234}U which added to coral during early-stage Process One.

To keep a roughly invariable ratio of ^{234}U/^{230}Th when both the ^{234}U and ^{238}U were increasingly removed, Process Two had to increasingly remove ^{230}Th from the coral. In despite of the insignificant contribution of the allochthonous non-radiogenic ^{230}Th to the ^{230}Th/^{238}U ratio in Process One because of the addition of high-concentration U, the contribution of detritus-bound ^{230}Th in Process Two is significant because its loss kept

the $^{234}U/^{230}Th$ ratio as a roughly constant value when ^{234}U was increasingly lost. It had impact because the lost U did not have high concentration in the percolating meteoric water in Process Two. It kept the $^{234}U/^{230}Th$ ratio constant because the removed U and detritus was roughly kept at a proportion which is reasonable if both of them were taken away by the percolating meteoric water. Even though the detritus-bound ^{230}Th would partly derived from the decay of U in the percolating water or coral, it is rational to deem that the added detritus or colloid in Process One at a earlier stage would contain small amount of allochthonous non-radiogenic ^{230}Th which was from the environmental fossil reefs and part of them had lost together with the detritus in Process Two at a later stage. The contribution of the non-radiogenic ^{230}Th would not affect the $^{234}U/^{230}Th$ ratio in Process One, but had significant effect on the ratio in Process Two.

7. Osmotic pressure, dynamic equilibrium, and fixed $^{234}U/^{230}Th$ ratios

The result has demonstrates that the contents of extraneous detrital ^{230}Th in Process One is insignificant compared with the extraneous but locally radiogenic ^{230}Th. So the $^{234}U/^{230}Th$ ratio in Process One (slope of the red line in Figure 4.4) is only affected by the $\delta^{234}U$ value of the percolating groundwater. Since both ^{234}U and ^{238}U decay to produce ^{230}Th, the U content should be too high to keep a roughly constant $^{234}U/^{230}Th$ value, if equal amount of ^{234}U, ^{238}U and their α-recoil decay-produced ^{230}Th were added into the aragonite texture. Scholz et al. [2004] suggested a explanation for a similar situation that a later loss of the added U occurred and speculated that the loss would be proportional to the earlier-stage addition and would be occurred at a same time for all the sub-samples. Since the result of this coral clearly exhibits an increase in U-content, an alternative explanation might be more possible for this coral: even though the high-concentration U groundwater kept entering the coral during the whole period when the Process One proceeded, the addition and loss of dissolved U into the aragonite texture would both happened because of U's solubility in water but would reach a dynamic equilibrium at some time point for a certain spot of the coral where the amount of addition and loss of U would be equal and no net addition of U would be occurring. The decay-produced ^{234}Th and ^{230}Th from the dissolved U would continue to be adding

to the texture because the percolating groundwater was still providing dissolved U, however, there was no loss of the added Th because of its insolubility. Therefore extra addition of Th relative to U would happen. Since the amount of entered groundwater into a specific spot followed the rules of osmosis (osmotic pressure), the amount of dissolved U and the then the decay-produced Th reached at this specific spot would be related to the distance of the spot from the surface where the water started to enter. Since the dynamic equilibrium was also controlled by the osmotic pressure, the net amount of added U into the aragonite texture would also be related to the distance of the spot from the surface where the groundwater started to enter, which was exactly shows by the data of this coral. Consequently, it would just look like that the loss of U is proportional to the addition of U.

Figure 4.4E shows very strong correlation between $^{230}Th/^{238}U$ activity ratio and ^{238}U content for Process Two ($r^2 = 0.99$) but only weak correlation ($r^2 = 0.36$) for Process One, further illustrate that the Process One was involved significant addition of extra ^{230}Th which has nothing to do with ^{238}U decay by path of ^{234}U and ^{234}Th. Unlike the $^{230}Th/^{238}U$ activity ratio - ^{238}U diagram, the $^{234}U/^{238}U$ activity ratio - ^{238}U projection illustrates that both processes have moderate correlation between $^{234}U/^{238}U$ activity ratio and ^{238}U contents (coefficients r^2 are 0.45 and 0.49 for Process One and Two respectively). For Process One, the reason is that there was an extra decay line (extraneous ^{234}U directly decayed) along with the ^{238}U decay line; for Process Two, it confirms that the same extra decay line contributed to the change in $^{234}U/^{238}U$ activity ratio, suggesting the taking away of ^{234}U along with the taking away of ^{238}U. It is reasonable given their similar dissolubility and chemical characters.

Owing to the very strong correlation between $^{230}Th/^{238}U$ activity ratio and the content of lost ^{238}U ($r^2 = 0.99$), and the moderate correlation between $^{234}U/^{238}U$ activity ratio and the content of lost ^{238}U ($r^2 = 0.49$), Process Two kept a strong correlation between $^{230}Th/^{238}U$ and $^{234}U/^{238}U$ ($r^2 = 0.74$ as shown in Figure 4.4A). The data of sub-samples which experienced both the earlier and later processes would array roughly to form a

straight line ("loss line") on the $^{230}Th/^{238}U$ - $^{234}U/^{238}U$ plot.

4.4.4 Model correction ages

This study presents two distinct processes of U-series isotopic diagenesis in a single coral colony. Both processes produced linear relationships in a $^{234}U/^{238}U$ - $^{230}Th/^{238}U$ activity ratio diagram whether or not U and Th are added to or lost from the coral. Since both the intersection points of the trend lines with the seawater evolution curve represent a coral which experiences no addition or loss of uranium and thorium, and the corresponding activity ratios represent a closed system, the true age of the coral could be calculated from either of the intersection points [*Gallup et al.*, 1994; *Cheng et al.*, 1998; *Scholz et al.*, 2004].

As shown in Figure 4.4, a linear regression line was fitted to data for 3 sub-samples in core c which experienced Process One to produce the "addition line" of allochthonous ^{234}U and ^{238}U. It intersects the seawater evolution curve at a point corresponding to 133.4 ka. Also, a linear regression line was fitted to data for 4 sub-samples of core a which experienced Process Two at a later stage to produce the "loss line" of U and Th. This line intersects the seawater evolution curve at a point corresponding to 133.7 ka.

Given the measurement errors, it is concluded that the distinct processes give the same model correction age, which reinforces the reliability of the model ages. Therefore, an average value of 133.6 ka is used to describe the age of this coral.

7.5 SUMMARY

Despite minor alteration of the mineralogy and petrology for nine sub-samples from a single fossil *Porites* coral which grew during the penultimate deglaciation in Sumba, Indonesia, the results of U-series isotopic measurements tell a different story. The data display diverse U-series isotopic compositions within the single coral and no consistent conventional ^{230}Th ages could be determined. No consistent correction ages could even be obtained for the sub-samples by applying any of the recently published correction

models [*Thompson et al.*, 2003; *Villemant and Feuillet*, 2003; *Scholz et al.*, 2004], indicative of the complicated diagenesis involved.

Given that this coral presents excellent stable isotopic records of the climate and oceanography in the Indo-Pacific Warm Pool, a more reliable date is highly desirable. In fact, the multiple measurements on sub-samples of this coral provided a good opportunity to explore the diagenetic behaviour of U-series isotopes in coral because it evidently experienced two distinct stages of post-depositional alteration. Detailed analysis of the relationship between the diagenetic stages and the corresponding changes in U-series isotopic composition has revealed two distinct processes of U-series isotope diagenesis in this single coral colony.

The results strongly suggest that a mechanism like diffusion or osmosis controlled the addition or loss of dissolved U and detrital Th into or out of the coral by water percolating down to a solute concentration gradient. The addition or loss of U-series isotopes is dependent on the concentration of the dissolved U and detritus in the percolating water. The amount of the added or lost U and detrital Th for a specific spot of the coral is controlled by the distance of the spot from the surface where the water starts to enter the coral. The absorption of dissolved U into the coral skeleton and the dissolution of the bound U from the coral proceed simultaneously and when they reach a dynamic equilibrium, the net addition or loss stops.

During the early stages of diagenesis, the percolating groundwater deposited into the coral a large amount of ^{238}U, and an even larger amount of ^{234}U, because of the relatively high concentration of U and ^{234}U in the percolating groundwater, which had filtered through the local fossil reefs. It also deposited in the coral fine detritus or colloids with detrital ^{232}Th and a small amount of ^{230}Th. The small amount of allochthonous non-radiogenic ^{230}Th is insignificant for the U/Th isotopic composition because of the large input of locally radiogenic ^{230Th}, a decay-product from the extraneous, highly concentrated dissolved ^{234}U and ^{238}U. The radiogenic ^{230}Th was absorbed into the aragonite texture owing to its particle-reactive nature and α-recoil.

Even though the dissolved ^{234}U and ^{238}U are the only significant sources of ^{230}Th, this process kept the $^{234}U/^{230}Th$ ratio constant in any spot in the coral. This constant ratio could be well explained by the osmosis mechanism: the osmotic pressure controlling net addition of U into the coral aragonite would stop when a dynamic equilibrium was reached, while the addition of radiogenic ^{230}Th would continue to increase as the groundwater continued to provide dissolved U and the added ^{230}Th would not redissolve due to its insolubility.

In the later stages of diagenesis, the coral was exposed and split because of tectonic uplift and valley incision. Meteoric water from rainfall or runoff from the slopes above soaked into the coral mainly from the crack and the top surface. Meteoric water contains no or low concentrations of U, detritus or colloids. Accordingly, following the osmosis rules, the percolating meteoric water dissolved away both ^{234}U and ^{238}U from the coral but left the insoluble ^{230}Th in the coral. The lost U had a $^{234}U/^{238}U$ close to that of the aragonite texture. The dilute meteoric water also took away detritus or colloids which entered the coral during earlier-stage diagenesis and bound ^{232}Th and small amount of ^{230}Th. Since this study shows apart from a comparable change in ^{232}Th the involved changes in ^{234}U, ^{238}U, ^{230}Th were much smaller in this process than that in the earlier process given a fixed amount of percolating water, the loss of detritus-bound ^{230}Th was no longer insignificant for the change of the U/Th isotopic composition; in contrast, it played an important role in keeping the $^{234}U/^{230}Th$ ratio roughly invariable among all the sub-samples whatever the amount of lost U and Th, because the amount of lost detritus-bound ^{230}Th very strongly correlated with the amount of lost ^{238}U and moderately correlated with that of lost ^{234}U following the osmosis rules.

Both diagenetic processes produced a linear relationship between $^{234}U/^{238}U$ - $^{230}Th/^{238}U$ in an activity ratio diagram when U and Th had been added to or lost from the coral. Given that the intersection of these trend lines with the seawater evolution curve represent a coral which experiences no addition or loss of uranium and thorium, and the corresponding activity ratios represent the closed system, the true age of the coral could

be calculated from the intersection points. Both intersection points give essentially the same model age of 133.6 ka.

This suggested mechanism explains the constant $^{234}U/^{230}Th$ ratios in situations involving either the addition or loss of U. This detailed study serves to substantiate the isochron model [*Scholz et al.*, 2004], and provides insight into the way by which the $^{234}U/^{230}Th$ ratio can remain constant when U is added to or lost from corals during diagenesis.

CHAPTER 5

LATE QUATERNARY HISTORY

OF THE MONDU RAISED CORAL REEFS IN SUMBA, INDONESIA

ABSTRACT

Large numbers of well-preserved *Porites* coral cores have been retrieved from the Mondu raised coral reefs of Sumba, Indonesia, indicating their potential as high-resolution paleoclimate records. Detailed topographic surveys and field observations provide new insights into the stratigraphic relationships and physiography of the raised reefs. Fifty-four coral samples have been measured for U-series isotopic composition, and the ages of these reefs have been determined by combining stratigraphic analysis and U-series age model corrections.

This study demonstrates that the isochron model of *Scholz et al.* [2004] could be well applied to determine the ages of the Mondu raised reefs. The results also indicate that the slopes of the isochrons of the reefs on the $^{234}U/^{238}U$ – $^{230}Th/^{238}U$ plot reflect their histories of burial and exposure. The slopes of the Mondu reefs display two distinct groups; steep isochrons are evidently connected to reefs experiencing long-term burial, while gentle isochrons are connected to reefs with no history of burial. This finding has served to help determine the ages of reefs whose ages could not be directly determined by the isochron model alone.

The results support a constant uplift rate of 0.49 m/kyr for the Mondu raised reefs since ~260 ka, although the rate may be higher during MIS 5a/5b and lower during 5c. This study demonstrates that some high-quality *Porites* cores have been retrieved from the exposed Mondu reefs. Promising time-periods for high-resolution palaeoclimate records include the interstadials and stadials of MIS 5, the early highstand during Termination II, highstands in glacial MIS 6, and even a late highstand during glacial MIS 8.

5.1 INTRODUCTION

Sumba is an exposed part of the outer arc ridge produced by the active subduction of the Indian-Australian plates beneath the Pacific plate [*Fitch and Hamilton*, 1974]. It is separated from Australia by the Java Trench - Timor Trough, and from the volcanic ridge of the Sunda-Banda island-arc to the north by an outer arc basin (the Savu Sea). The collision of the plates and the upheaval of the outer arc ridge result in the uplift of the palaeo-reefs and the formation of the flights of raised coral terraces on the north coast of Sumba. An exceptional 1-million-year-long sequence of coral reef terraces has been reported at Cape Laundi (Figure 5.1) between sea level and an ancient patch reef 475 metres above sea level [*Pirazzoli et al.*, 1991; *Pirazzoli et al.*, 1993]. Using uranium-series and electron spin resonance dating, they deduced a local uplift rate of 0.49 m/kyr which remained almost constant during at least the last million years and in any case at least until the last interglacial period. They credited the possibility of dating those very old fossil corals to the dry local climate, especially the pronounced winter dry-season which tends to slow down the processes of diagenesis in fossil corals, leaving some of them almost unrecrystallized after 600 ka.

Our research is focus on the area around Mondu village, about 10 km west of Cape Laundi, where much more extensive paleo-reef terraces developed between 0 m and 80 m above mean sea level (Figure 5.1) than that at Cape Laundi between the same altitudes, possibly due to the gentler underwater slope, more nutrition and sedimentary output through Mondu River. Three major field investigations in the past 14 years have been conducted in this area by Dr Michael Gagan and his team and a wealth of modern and fossil coral cores have been retrieved from the modern and raised reefs, providing an excellent opportunity for reconstruction of climate and oceanography.

Figure 5.1 (next page) Sumba Island and the Mondu Raised Coral Reefs (shown as red stars). The contour shows the topographic elevation and the numbers represent the altitudes of platforms in this area. The blue star is the village of Mondu and the blue line is the main road of this area. Transection AB (red line) is depicted in Figure 5.3.

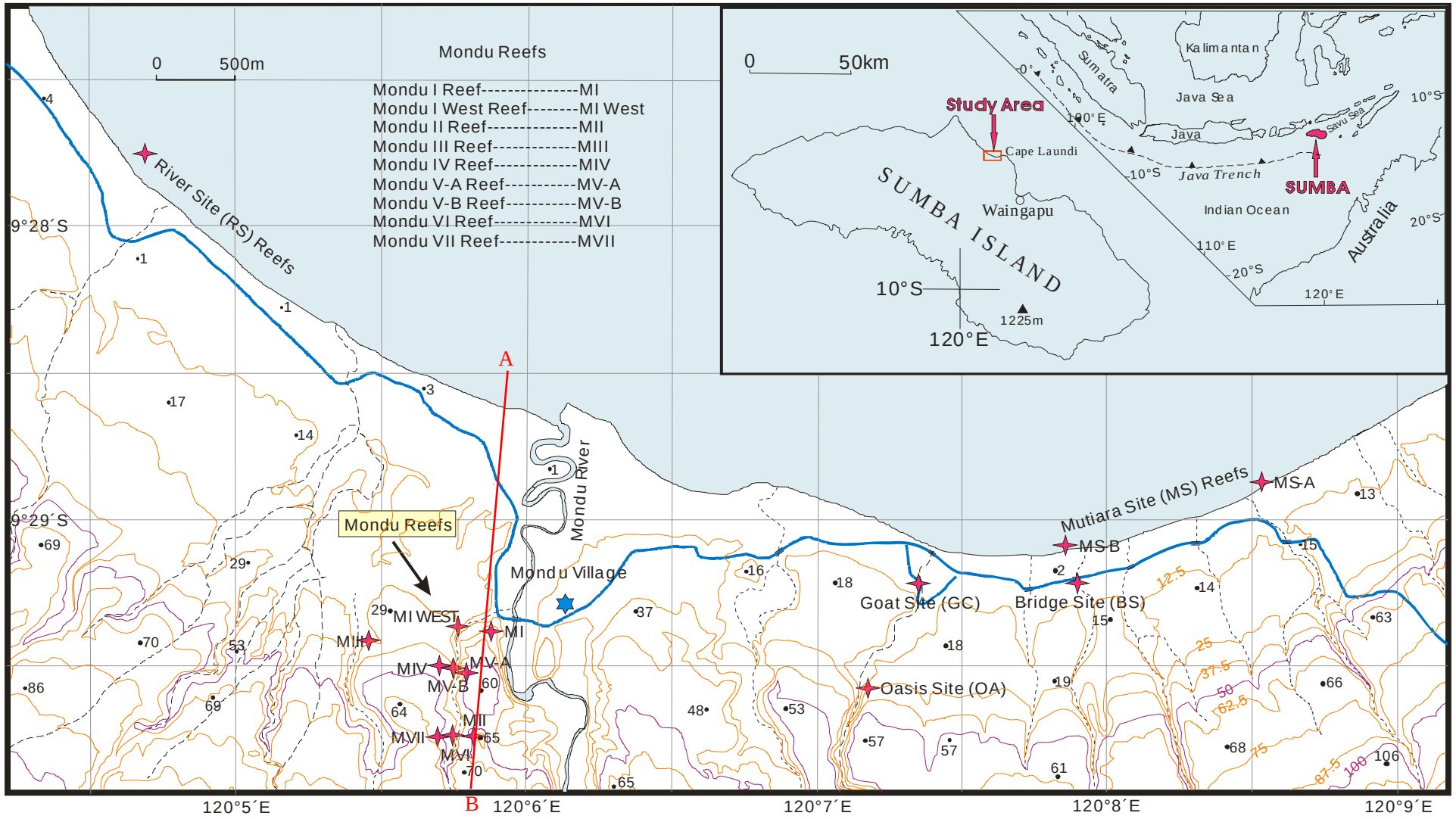
0 500m
Mondu Reefs
Mondu I Reef----------MI
Mondu I West Reef--------MI West
Mondu II Reef----------MII
Mondu III Reef----------MIII
Mondu IV Reef----------MIV
Mondu V-A Reef----------MV-A
Mondu V-B Reef----------MV-B
Mondu VI Reef----------MVI
Mondu VII Reef----------MVII
River Site (RS) Reefs
9°28´S
9°29´S
Mondu Reefs
Mondu River
Mondu Village
MI WEST
MI
MII
MIV
MV-A
MV-B
MVII
MVI
A
B
Mutiara Site (MS) Reefs
MS-A
MS-B
Goat Site (GC)
Bridge Site (BS)
Oasis Site (OA)
120°5´E
120°6´E
120°7´E
120°8´E
120°9´E
0 50km
Study Area
Cape Laundi
SUMBA ISLAND
Waingapu
10°S
120°E
1225m
Sumatra
Kalimantan
Java Sea
Java
Java Trench
Savu Sea
SUMBA
Indian Ocean
Australia
100°E
110°E
120°E
0°
10°S
20°S

The age determination of the corals is the basis for paleoclimate reconstruction and has always been a challenge for any effort to retrieve climate information from corals old than Holocene because most of the information is from the massive *Porites* coral which has loose texture and is more liable to the impact of diagenesis for its U-Th isotopes than the carriers of climate information: O/C isotopes and Sr/Ca elements [*Bard et al.*, 1992; *Stirling et al.*, 1995; *Edwards et al.*, 2003]. Tremendous efforts have been tried to achieve reliable ages for the U-series altered corals [*Gallup et al.*, 1994; *Henderson et al.*, 2001; *Thompson et al.*, 2003; *Villemant and Feuillet*, 2003; *Potter et al.*, 2004; *Scholz et al.*, 2004; *Thompson and Goldstein*, 2005; *Scholz and Mangini*, 2006; 2007; *Andersen et al.*, 2008] and three models have been published in recent years because of their successful application in different cases [*Thompson et al.*, 2003; *Villemant and Feuillet*, 2003; *Scholz et al.*, 2004]. In this chapter I will try to apply one of the models to aid to achieve reasonable ages for the cores and the surrounding reefs.

To determine the age of the coral cores which are of important potential for climate reconstruction and to provide guide for future exploration of more long cores, this chapter will generally summarize the distribution, elevation, and some stratigraphic features of the Mondu Raised Coral Reefs, and determine the age of the reefs by combination of using stratigraphic analysis and U-Th age correction models.

5.2 MATERIALS AND METHODS

5.2.1 Core drilling

To date, three field trips to the Mondu raised reefs have been carried out. The fieldtrip designed especially for my PhD research was in August/September, 2003. Other two expeditions were in 1995 and 1998.

1995 drilling: Cores were drilled from fossil *Porites* corals in the raised reefs at Goat Site, Mondu I, Mondu II, River Site, and Bridge Site (Figure 5.1) using a fuel-driven

Tanaka motor drill with a core diameter of 50 mm. This drilling was reconnaissance in style because the length of the cores was limited to the length of one core barrel (50 cm) (Appendix A.1).

1998 drilling: The large RSES water-driven drill was applied to collect 75 mm diameter cores from live corals (underwater) and Holocene reefs at River Site and Mutiara Site reefs. The portable Tanaka-driven drill (50 mm diameter cores) was also used to drill raised reef fossil corals at Mondu I, Mondu III and Mondu IV reefs. The genera of the sampled corals are *Porites* and *Diploastrea*. A total of 45 coral cores were collected from this trip. The longest core is up to 3 metres (MSM-3A). Some long Holocene cores were also collected, such as MS1b (2.17 m), RS8 (1.72 m) (Appendix A.2).

2003 drilling: The portable Tanaka-driven drill was used again to drill cores from all the raised reefs indicated on Figure 5.1, including the newly discovered reefs of Mondu V, Mondu VI, Mondu VII, Mondu I West, Oasis Site, and Goat Site. 65 coral cores were collected during this trip and the total length is up to 36 m. Several high quality fossil cores were drilled. Even though their age may be as old as MIS 5e or 6, no obvious recrystallized calcite spots have been observed under natural light. The MV03-A-2a, MV03-B-2b, MVI03-7a, GC03-1b, and RS03-4 are among the best cores for extracting palaeoclimate information. See Appendix A.3 for a summary of the cores.

5.2.2 Topographic Surveying

In order to get a better understanding of how the raised coral reefs developed, and their possible ages, topographic surveys were carried out using a theodolite during the 2003 field trip. The elevations of important coral heads, key features of the reefs, and main topographic marks have been included in this survey. To check the veracity of the results, routes for most of the surveys were designed to return to their starting points and the closure errors were calculated. The survey routes are shown in Table 5.1 and the good quality of the elevation survey has been proven by the small values of the closure errors (1 ~ 5.8 cm) also indicated in this table.

Table 5.1

Survey Routes and Closure Errors

Surveys	Route and Site	Closure Error (cm)
Goat Site	Mutiara Beach to Goat Site (and return)	1.0
Oasis Site	Goat Site to Oasis Site (and return)	3.6
Beach to Mondu I	River Site Beach to Mondu I (and return)	2.4
Mondu Raised Reefs	Mondu I to Mondu V-A to 60m Hill to Mondu VI East to Mondu II to +65 m Hill to Mondu VI West to "Favid" Reef to West 60 m Hill to Mondu V-B to Mondu V-A to Mondu V-B to Mondu IV to Mondu I West to Mondu I	2.0
Mondu I West to Mondu III	Mondu I West to Mondu III (and return)	5.8
Mondu II to Mondu VII	Mondu II to Mondu VI to Mondu VII	
Mutiara Site	Mutiara Holocene reef	
River Site	River Site Holocene reef	

5.2.3 Sampling for age determination

In addition to materials from *Porites* cores, well-preserved coral materials were collected by hammer and chisel from robust corals, such as *Favia*, *Favites*, *Platygyra*, *Symphllia*, or *Diploastrea*, to accurately determine the age of the reefs. These genera were chosen because they have thick and dense wall which would resist diagenetic alteration to the most extent. The samples are all *in situ* specimens within the same reefs containing the *Porites* cores.

5.2.4 Screening for diagenesis

Cores are initially examined under UV light to determine if calcite is present. Even minor amounts of calcite can be detected because it emits a distinctive pale-green fluorescence under UV light, whereas coralline aragonite emits a pale blue-mauve colour. For some samples X-ray diffraction were applied to determine the percentages of calcite in the cores. Some of the samples were also checked by thin section analysis and scanning electron microscopy.

To achieve the best results, the most pristine spots of the samples were selected for age determination. For corals with thick wall, dental drills were used to remove the loose

parts, such as thin walls or dissepiments.

5.2.5 U-Th dating

The U-series measurement was carried out using multiple-collector-ICP-MS at Research School of Earth Sciences, the Australian National University and Department of Geosciences, the National Taiwan University following chemical procedures reported by Luo et al. [1997] and McCulloch and Mortimer [2008], or by Edwards et al. [*Edwards et al.*, 1987], and MC-ICP-MS measurement protocols [*Stirling et al.*, 2001; *Shen et al.*, 2002; *McCulloch and Mortimer*, 2008].

"U-2" mixed ^{229}Th and ^{233}U spike was used to spike each dissolved coral sub-sample and a PE TRU ion exchange column was used to separate the elements. The ^{230}Th age and initial ^{234}U were calculated using ISOPLOT Excel add-in written by K.R. Ludwig with half-lives of ^{230}Th, ^{234}U, and ^{238}U following Cheng et al. [2000]. The Isochron and Open-system model ages were calculated according to Scholz et al. [2004] and Thompson et al. [2003].

11 Holocene *Porites* cores drilled during the 1995 and 1998 expeditions were conventional radiocarbon-dated by Abaz Alimanovic at the RSES Radiocarbon Dating Laboratory of the Australian National University. Also, sixteen Holocene and late Pleistocene *Porites* cores have been uranium-series dated by Dr Linda Ayliffe using the thermal ionisation mass spectrometry (TIMS) at the Laboratoire des Sciences du Climat et de l'Environnement, Gif-sur-Yvette Cedex, France. Both results will be applied here in this chapter (refer to Appendix B and C for the results).

5.3 RESULTS

5.3.1 Elevation of corals and reefs

Table 5.2 shows the survey results including the elevation of important coral heads and features of reefs. All elevations are defined relative to base of beach (approximately mean sea level).

Table 5.2

Elevation of coral colonies and features of reefs

Reefs	Reef ID	Coral ID or key features	Elevation (m)	Reefs	Reef ID	Coral ID or key features	Elevation (m)
Mutiara Site	MS	Seaward edge	-0.5	Mondu I	MI	MI-1	27.9
		MS2	-0.4			MI-4	28.5
		MS1	-0.3			MI-2	30.5
		MS5	-0.2			MI-3	33.5
		MS4	-0.2			MI-6	35.2
		MS03-B-1	-0.1			Undrilled *Porites*	26.5
		MS-7	-0.1			Undrilled *Porites*	27.6
		to PS-1	-0.1			Top *Porites*	40.3
		MS-9	0.0	Mondu VI	MVI-A	base of reef	36
		MS03-A-1	0.1			weathering surface	44
		MS-10	0.1		MVI-B	base of reef	34
		MS-8	0.1			weathering surface	44
River Site	RS	Seaward edge	-1.2		MVI-C	MVI03-2	37.9
		RS12	-1.0			MVI03-6	38.3
		RS13	-0.5			MVI03-7	38.7
		RS03-2	-0.4			MVI03-4	39.1
		RS8	-0.4			MVI03-3	39.5
		RS2	-0.3			MVI03-1	40.7
		RS14	-0.3			MVI03-5	40.8
		RS10	-0.1	Mondu V	MV	MV03-A-2	38.7
		RS1	-0.1			MV03-A-3	38.7
		RS3	-0.1			MV03-A-1	39.0
		RS15	0.0			MV03-B-2	37.5
		RS17	0.0			MV03-B-1	42.3
		RS6	0.0			Edge of top surface	48
		RS5	0.0	Mondu IV	MIV	Base	37
		RS7	0.0			MIV-1	40.1
		RS11	0.1			MIV03-1	41.5
Goat Site	GC	GC1	7.2			MIV03-2	42.1
		GC2	8.3			MIV-2	45.2
Oasis Site	OA	Base of reef	9	"Favid"		base	44
		OA03-4	11.2			top	52
		OA03-1	16.5	Mondu II	MII	W. base	50
		OA03-3	17.4			E. base of MII reef	51
		OA03-2	20.2			MII-10	52.4
Mondu III	MIII	Base of reef	19			MII-8	53.2
		MIII-3	22.9			MII-6	53.5
		MIII-2	23.6			MII-5	55.3
		Top of reef	26.5			MII-4	55.9
Mondu I West	MI West	base	20			MII-1	56.8
		MI03-B-1	25.6			MII-7	56.9
		Top surface	27			MII-9	58.6
Hills		Top of +60m hill	60			MII-2	59.0
						top of MII reef (W)	60
		Top of +65 m hill	64	Mondu	MVII	MVII03-1	54.5

5.3.2 U-Th ages and open-system model correction

Table 5.3 displays results of U-series dating for all the 54 fossil coral samples from Mondu raised reefs.

Even though all the Holocene corals show U-Th close-system behaviour (Appendix C), corals from higher raised reefs around the Mondu village exhibit obvious open-system behaviour. Only four of them show marginal initial $\delta^{234}U$ values, and only one coral (MI6-03-D-1) is within the usually used ± 8‰ range of acceptable age [*Stirling et al.*, 1998]. Therefore, the calculated conventional ^{230}Th ages could not serve as reliable ages for almost all the Mondu raised coral reefs, which means correction models have to be used to achieve reliable ages.

The open-system model [*Thompson et al.*, 2003] is applied to all the samples and the calculated ages are listed in Table 5.3. The model of Thompson et al. [2003] assumes that α-recoil mobilisation of thorium daughter isotopes ^{234}Th and ^{230}Th is the only U-Th alteration process operating within the reef, and there is no presence of initial ^{230}Th. However, the application of this model to the Mondu raised reefs shows that no consistent open-system correction ages could be achieved for any of the reefs. For example, the correction ages for Mondu I reef range from 74 ka to 263 ka. Even for subsamples from one single coral colony MV03-A-2, the correction ages change from 122 to 156 ka and the range of the ages is up to 25% of the average value of the correction ages. This result indicates the complexity of diagenetic alteration in the Mondu corals. The large discrepancy of the open-system correction ages within a single reef and even a single coral colony demonstrates that the open-system model is not applicable for age determination of the fossil corals in the Mondu raised reefs. It is likely that sytematic addition of ^{230}Th and ^{234}U through α-recoil might not be a dominant open-system process in the Mondu raised reefs. In contrast, the isochron correction model [*Scholz et al.*, 2004] shows good application in the correction of the coral ages.

Table 5.3 ^{230}Th ages and model correction ages for Mondu raised corals and reefs

Sample	$^{234}U/^{238}U$		$^{230}Th/^{238}U$		^{230}Th Age (ka)		Initial $d^{234}U$		O-S Age (ka)^		Corrected age (ka)$
MI03-B-2a*	1.246	± 0.002	1.468	± 0.006					263.3	± 42.9	**83.5**
MI1a*	1.228	± 0.002	1.480	± 0.004							
MI3-03a-D-1	1.173	± 0.001	0.958	± 0.003	171.6	± 1.3	280.8	± 2.0	117.9	± 3.9	
MI3c*	1.097	± 0.001	0.474	± 0.002	61.1	± 0.3	115.0	± 1.6	73.7	± 0.8	
MI6-03-D-1*	1.111	± 0.002	0.590	± 0.002	81.3	± 0.5	139.7	± 2.0	84.1	± 1.1	
MI6-03-D-2*	1.164	± 0.001	0.955	± 0.003	173.9	± 1.6	268.2	± 2.3	124.4	± 3.8	
MI6d#	1.101		0.623		89.7	± 0.0	130.0	± 0.0	96.6	± 0.0	
GC03-1b*	1.153	± 0.002	0.849	± 0.003	138.6	± 1.0	226.7	± 2.1	107.1	± 2.6	85.9
GC03-1b-3	1.170	± 0.003	0.888	± 0.004	146.7	± 1.4	256.9	± 3.6	103.7	± 3.6	
GC03-D-3	1.158	± 0.001	0.808	± 0.004	125.4	± 1.3	224.6	± 1.8	95.3	± 2.4	
GC03-D-4	1.144	± 0.001	0.811	± 0.003	129.6	± 1.0	207.6	± 1.3	105.5	± 1.9	
GC03-D-5	1.135	± 0.001	0.708	± 0.003	103.8	± 0.8	181.6	± 1.1	90.4	± 1.2	
GC3a*	1.137	± 0.002	0.756	± 0.002	115.5	± 0.7	190.5	± 2.0	98.3	± 1.7	
GC5b*	1.277	± 0.002	1.516	± 0.005					226.7	± 35.7	
GC6c#	1.161		1.330								**> 85?**
GC03-D-6	1.151	± 0.001	0.578	± 0.002	74.7	± 0.4	186.3	± 0.9	60.3	± 1.1	**< 85?**
MIV2#	1.116		0.760		121.3	± 0.0	162.9	± 0.0	114.7	± 0.5	**110-114**
OA03-2b*	1.087	± 0.001	0.684	± 0.002	106.3	± 0.7	116.9	± 1.9	119.3	± 1.2	**101.1**
OA03-D-2	1.171	± 0.001	1.099	± 0.003	252.6	± 2.9	349.4	± 2.9	163.2	± 6.1	
OA03-D-7	1.141	± 0.001	0.957	± 0.004	185.1	± 2.1	237.8	± 2.2	146.0	± 3.3	
OA03-D-3	1.145	± 0.001	0.916	± 0.003	165.3	± 1.5	232.0	± 1.5	129.9	± 2.8	
OA03-D-4	1.145	± 0.001	0.927	± 0.005	169.9	± 2.3	234.2	± 2.1	133.3	± 3.1	
OA03-1c*	1.252	± 0.001	1.106	± 0.004	202.0	± 1.8	446.4	± 2.7	91.7	± 7.1	**?**
MII9b*	1.289	± 0.002	1.635	± 0.005							**113-123**
MII2c#	1.223		1.344						209.2	± 17.6	
MII2c-D*	1.233	± 0.002	1.384	± 0.004					217.8	± 21.8	
MII03-D-1	1.186	± 0.002	1.396	± 0.004							
MII7a*	1.218	± 0.002	1.692	± 0.005							
MV03-A-2c-3	1.108	± 0.002	0.805	± 0.004	136.8	± 1.5	158.9	± 2.4	131.7	± 1.9	**133.6**
MVO3-A-2C-D-2*	1.110	± 0.001	0.803	± 0.002	135.7	± 0.8	160.8	± 1.9	129.8	± 1.4	
MVO3-A-2C-D-3*	1.136	± 0.002	0.854	± 0.003	145.5	± 1.1	204.6	± 2.3	121.8	± 2.3	
MVO3-A-2C-D-4*	1.104	± 0.002	0.842	± 0.002	151.3	± 1.1	159.5	± 2.5	145.7	± 1.8	
MV03-A-2a-D-1*	1.107	± 0.001	0.841	± 0.003	149.9	± 1.1	163.3	± 1.9	142.7	± 1.5	
MV03-A-2a-D-2*	1.109	± 0.001	0.847	± 0.003	151.3	± 1.0	167.1	± 1.7	142.5	± 1.5	
MV03-A-2a-D-3*	1.119	± 0.001	0.888	± 0.003	163.7	± 1.3	189.1	± 2.1	145.3	± 2.1	
MV03-A-2a-D-4*	1.116	± 0.001	0.911	± 0.003	175.0	± 1.3	189.9	± 1.9	155.9	± 2.1	
MV03-A-2b-D-1*	1.123	± 0.002	0.877	± 0.003	157.8	± 1.4	192.7	± 2.5	138.2	± 2.3	
MVO3-A-3-1a-D*	1.123	± 0.002	1.550	± 0.004							**?**
MVO3-A-3-1b-D*	1.139	± 0.001	1.317	± 0.004							
MVO3-A-3-D-1*	1.131	± 0.002	0.932	± 0.003	178.0	± 1.5	216.1	± 2.5	147.9	± 2.9	
MVO3-A-3-D-2*	1.152	± 0.002	0.818	± 0.002	129.7	± 0.8	219.4	± 2.4	101.3	± 2.4	
MVO3-A-3-D-3*	1.144	± 0.002	1.181	± 0.003					254.0	± 11.8	
MV03-B-2b-7	1.122	± 0.001	0.680	± 0.003	99.4	± 0.8	161.1	± 1.3	93.7	± 1.0	**83.5**
MV03-B-D-1_A	1.143	± 0.002	1.045	± 0.005	235.5	± 4.0	278.6	± 3.6	175.0	± 5.1	**175.0**
MV03-B-D-1_B	1.142	± 0.001	1.047	± 0.003	238.7	± 2.9	278.2	± 2.7	177.9	± 4.8	
MV03-B-D-2	1.118	± 0.001	0.947	± 0.006	191.7	± 3.1	203.0	± 2.4	166.2	± 3.1	
MV03-B-D-3	1.207	± 0.001	1.191	± 0.006					157.3	± 9.0	
MV03-B-D-5	1.174	± 0.001	1.081	± 0.003	236.2	± 2.3	340.2	± 2.3	152.9	± 5.7	
MVII03-B-D-1	1.173	± 0.001	0.868	± 0.003	139.5	± 0.9	256.1	± 1.8	97.4	± 3.1	**83.5**
MVII03-B-D-2	1.104	± 0.002	1.057	± 0.004	290.2	± 5.7	237.1	± 4.1	240.8	± 5.8	**258.1**
MVII03-B-D-3	1.122	± 0.001	1.146	± 0.002							
MVII03-D-4	1.188	± 0.000	1.273	± 0.002					230.1	± 15.2	
MVI03-7a-2	1.427	± 0.002	2.662	± 0.012							

Notes for Table 5.3:

All the ICP-MS measurements were isotope dilution runs using a mixed ^{233}U-^{229}Th tracer, which had been calibrated against the Harwell Uraninite (HU-1) secular equilibrium standard.

Decay constants are 9.1577 x 10^{-6} yr^{-1} for ^{230}Th, 2.8263 x 10^{-6} yr^{-1} for ^{234}U, and 1.55125 x 10^{-10} yr^{-1} for ^{238}U (Cheng et al., 2000).

Analytical errors are 2σ of the mean.

[#] The four samples were measured by Dr Linda Ayliffe using the thermal ionisation mass spectrometer at the Laboratoire des Sciences du Climat et de l'Environnement, Gif-sur-Yvette Cedex, France.

* Measurements were conducted at the Department of Geosciences, the National Taiwan University by Chuan-Chou Shen and Chih-Wei Chen, using MC-ICP-MS following chemical and instrumental protocols similar to Luo et al. [1997] and Stirling et al. [2001], while most of the other sub-samples were analyzed with similar protocols at Research School of Earth Sciences, the Australian National University (RSES, ANU).

^ "Open system" (O – S) ages and errors were calculated using a spreadsheet provided by W. Thompson [*Thompson et al.*, 2003] with an assumed initial $\delta^{234}U$ value of 146.6‰ [*Stirling et al.*, 1998; *Robinson et al.*, 2004].

[$] "corrected age" is achieved by combination of the isochron model correction and the stratigraphic analysis. The isochron age was obtained by linear regression of data on the $^{234}U/^{238}U$ - $^{230}Th/^{238}U$ plot for corals from the same reef or sub-samples from the same colony and its intersection with the seawater evolution curve corresponds to the true age of the reef or coral [*Scholz et al.*, 2004]. an seawater $\delta^{234}U$ value of 146.6‰ was applied for the seawater evolution curve [*Robinson et al.*, 2004]. There are corals from a reef excluded for isochron age correction on the base of further analysis as detailed in text.

5.3.3 Isochron model correction ages

Figure 5.2 displays a $^{234}U/^{238}U$ – $^{230}Th/^{238}U$ plot with all the data points for the Mondu fossil corals (one single massive *Porites* coral MV03-A-3 is excluded owing to its higher calcite content).

Careful observations reveal that, with few exceptions, the corals in reefs Mondu I, Goat Site, Mondu V-B, and Mondu VII, respectively, corals from a single reef form a very good array (with r^2 = 0.99, 0.80, 0.94, or 0.95, along the pink, red, blue, or green lines, Figure 5.2). The array of the corals within one reef means some common mechanism is involved in the diagenetic alteration of the U-series isotopes, and the isochron model [*Scholz et al.*, 2004] assumes that the intersection point between the array line and the seawater evolution curve corresponds to the true age of a coral within the reef. For the four reefs, the achieved isochron model ages are 83.5 ka, 85.9 ka, 175.0 ka, and 258.1 ka, respectively.

The U-series age correction of coral MV03-A-2 has been discussed in detail in the previous chapter since it provides a unique opportunity to explore U-Th open-system behaviours. Our study shows it involved two distinct processes of U-Th diagenesis and that correction ages could be achieved separately from both processes. Both corrections give an almost identical age of 133.6 ka, suggesting that reef MV-A developed during Termination II.

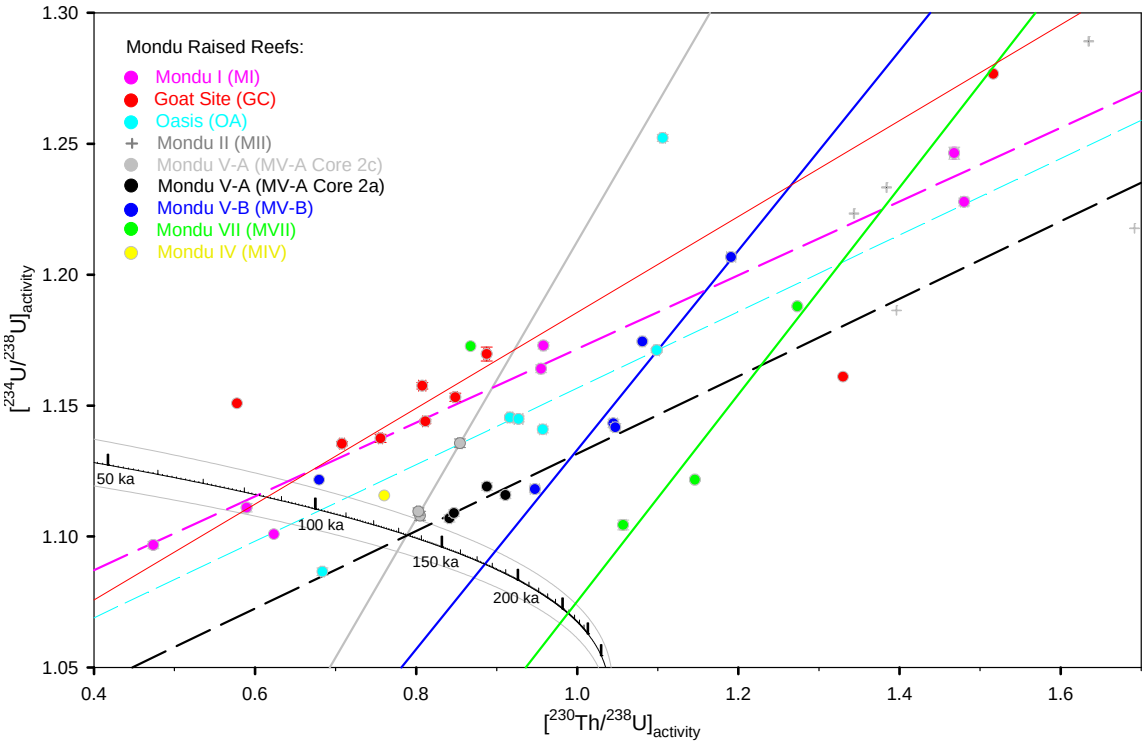

Figure 5.2 $^{234}U/^{238}U$ – $^{230}Th/^{238}U$ plot of the Mondu raised fossil coral reefs. The black curve with scales is the seawater evolution curve with a modern $\delta^{234}U$ value of 146.6‰ and the numbers along it represent the corresponding ages. The grey curves envelop a ±10‰ range for age reliability assessment. The coloured dots and crosses represent reef corals and the coloured thin lines show linear regression of data within one reef excluding one or two corals based on stratigraphic analysis (see text in Section 5.4 for details). Note that there seems to be two groups of the regression lines which are parallel to one another within one group: the group with older ages has larger slopes than the younger ones and the two groups seemed to separate around the last interglacial period or Termination II (around 130-140 ka) with the Termination II coral MV03-A-2c (134 ka) have both regression lines (details refer to Chapter 7 of this thesis). The array of the corals within one reef means some common mechanism involved in the diagenetic alteration of the U-series isotopes, and the Isochron Model [*Scholz et al.*, 2004] assumes that the intersection point between the array line and the seawater evolution curve corresponds to the true age of the corals within the reef. The calculated model correction ages are listed in Tables 5.3 and 5.4.

Even though as a whole the 6 corals in Oasis reef do not array in the $^{234}U/^{238}U$ – $^{230}Th/^{238}U$ plot, an isochron could still be achieved based on stratigraphic analysis and burial history (cyan line in Figure 5.2 and detailed description in Section 5.4). Also, since all the measured 5 corals from Mondu II reef are severely altered and located far away from the seawater evolution curve in the plot, no isochron correction age within reasonable error could be achieved for Mondu II reef, but the style of dispersing of the data points seems to constrain its age to 100-150 ka.

Sections 5.5 shows how the isochron model correction ages are consistent with stratigraphic relationships and physiographic features of the reefs. Section 5.4 summarizes the stratigraphic relationships and physiographic features of the Mondu raised reefs on the basis of topographic surveys and field observation.

5.4 STRATIGRAPHY OF THE MONDU RAISED REEFS

5.4.1 Composite cross-section of the major reefs

A schematic cross-section of the Mondu reef terraces has been synthesized in Figure 5.3, which captures the main stratigraphic relationships and elevations of most of the studied reefs.

The topographic features of the transect are those along the AB line through the central sector of the study area (red line “AB” in Figure 5.1). The elevations and stratigraphic relationships of the River Site, Mondu I, Mondu II, Mondu V-A, and Mondu VI reefs are what were observed along the AB line. Other reefs such as Mutiara Site, Bridge Site, Goat Site, Oasis Site, Mondu III (including Mondu I West), and Mondu VII, are also illustrated in this section on the basis of stratigraphic analysis and age determination (see Sections 5.4 and 5.5). The stratigraphic relationships involving Mondu V-B and Mondu IV reefs could not be included in this single cross-section and, instead, will be depicted in the text.

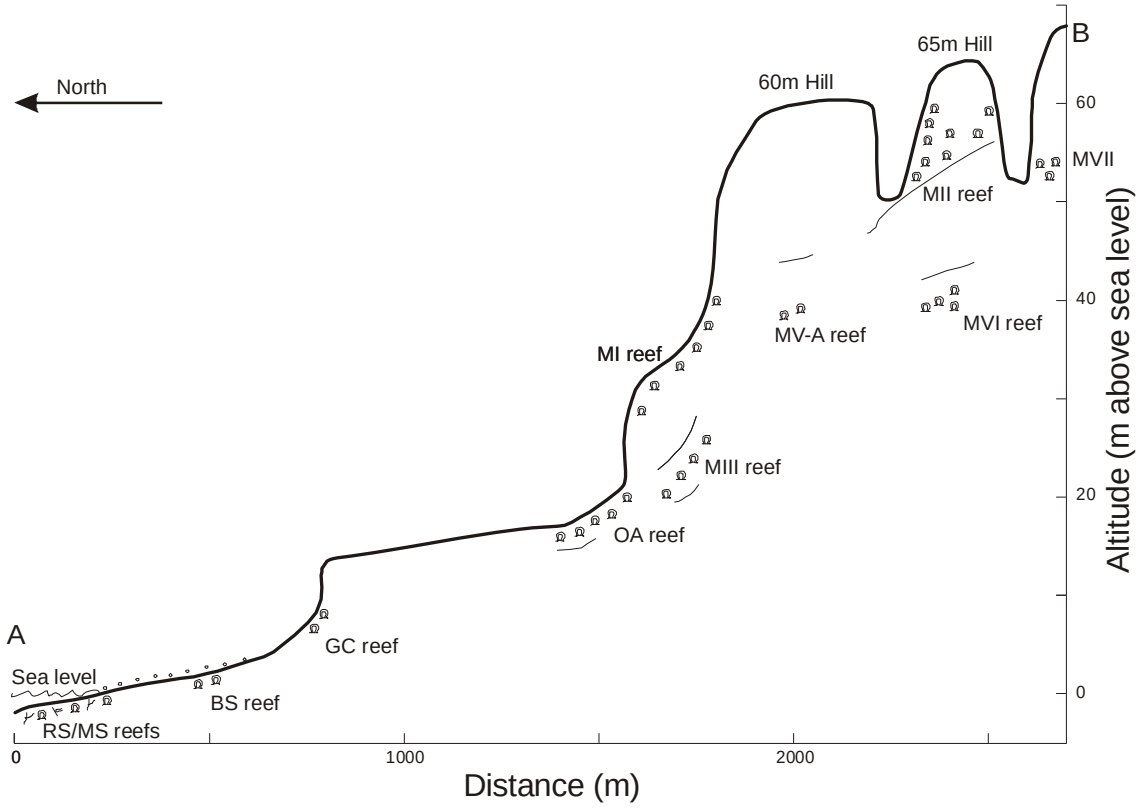

Figure 5.3 Schematic cross-section of the Mondu reef terraces. Thick black curve represents the topographic features across the central area of this study as shown by the red AB line in Figure 5.1. The reefs and associated erosion surfaces have been indicated by symbols and fine lines. Note: the vertical scale is obviously enlarged relative to the horizontal scale.

5.4.2 Features of the Mondu raised reefs

Holocene reefs

Extensive Holocene coral reef platforms have been developed along the coast. Reef platforms about 50 to 80 meters wide were exposed at low tide at both the Mutiara and River Site (Figure 5.1). Figure 5.4 shows the Holocene reef platforms.

Goat Site reef

Goat Site is about 250 to 500 m inland from the beach. All the corals are on the foot or in the middle of a steep cliff (Figure 5.5). This cliff is topped by an extensive platform with a typical carbonate surface that is very hard and flat but not smooth. According to our survey, the platform is about 12 to 21 m above the mean sea level.

Oasis Site reef

Oasis Site is 600m southwest of Goat Site, about 1 km from the beach line. The reef is located where the extensive platform above Goat Site ends and another higher terrace begins to rise steeply uphill which is about 21 m above sea level. The coral heads are distributed from just under the 21 m surface to a base 9 m above sea level (12 m in thickness). The preservation of the reef seems different from Goat Site corals; most of them are badly weathered. But we still retrieved a good core from coral OA03-1.

Mondu I reef

Mondu I reef is about 1.5 km inland from the beach line and is the most extensively exposed and developed of all the raised reefs we studied (Figure 5.6). The reef starts at 27 m and ends in 40 m above sea level (13m in thickness).

Many of the coral heads are still in good condition. Coral MI4 is particularly remarkable in that it has the original growth surface (as shown in the inset of Figure 5.6). But most of the corals show evidence of calcification.

Mondu I West and Mondu III reefs

Mondu I West reef is located on the west side of Mondu I reef; between them is a dry creek. The elevation of the reef is 18 to 27 m above sea level. Most of the corals are weathered.

Mondu III reef is located about 600m west of Mondu I West reef. It has almost the same elevation as Mondu I West reef and most of its corals are weathered.

Based on the stratigraphy, it is possible that the Mondu I West and Mondu III reefs developed during an old unknown stage. We believe this because there is a distinct erosion surface on the top of Mondu I West reef. It appears that Mondu I reef may have developed on the erosion surface.

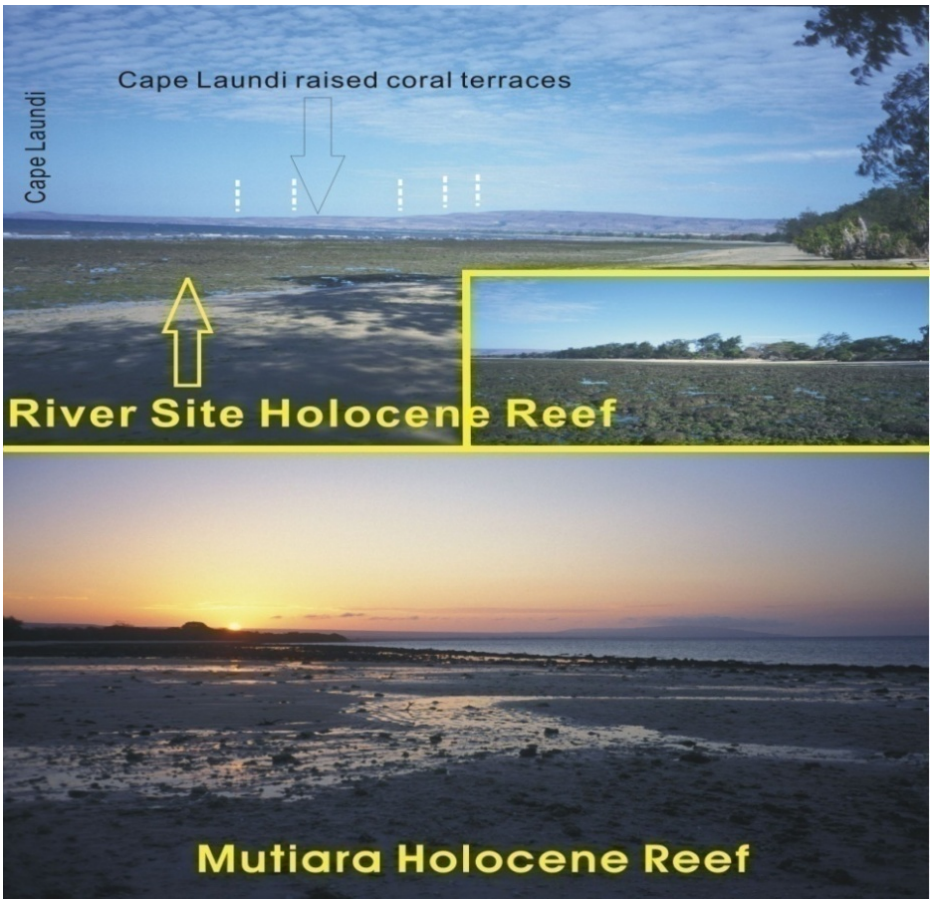

Figure 5.4 Holocene reefs in River Site (W. of Mondu River) and Mutiara Site (E. of Mondu River).

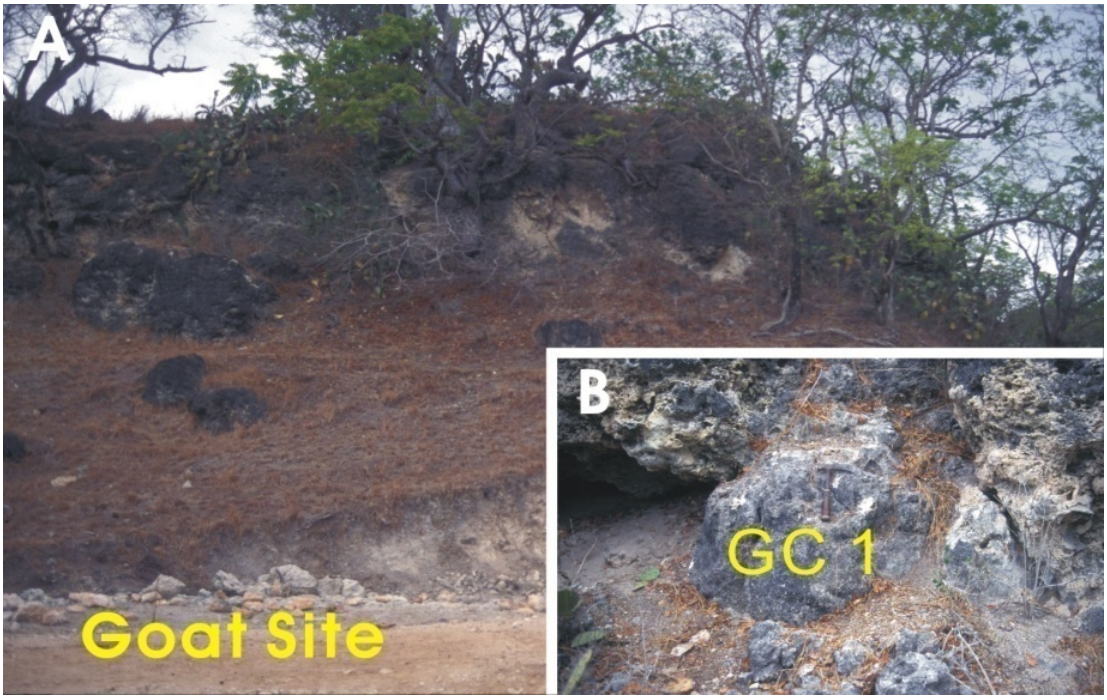

Figure 5.5 The Goat Site reef showing the cliff and fossil *Porites* coral GC1

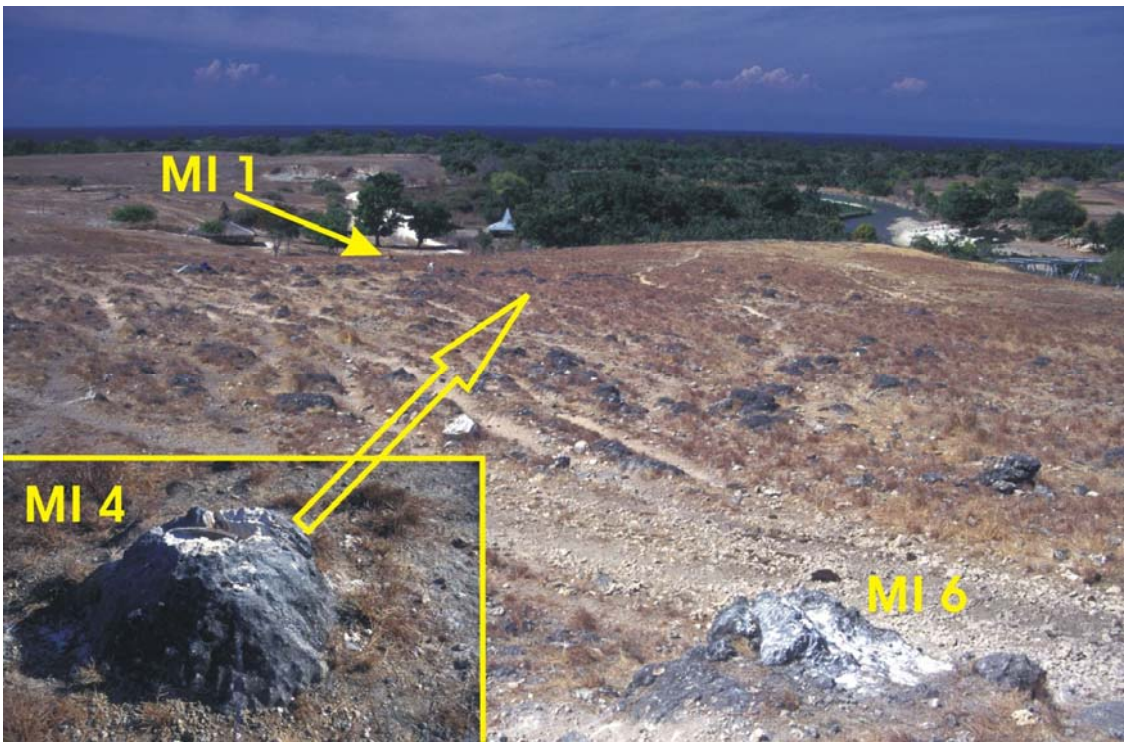

Figure 5.6 The Mondu I reef and well preserved coral MI4.

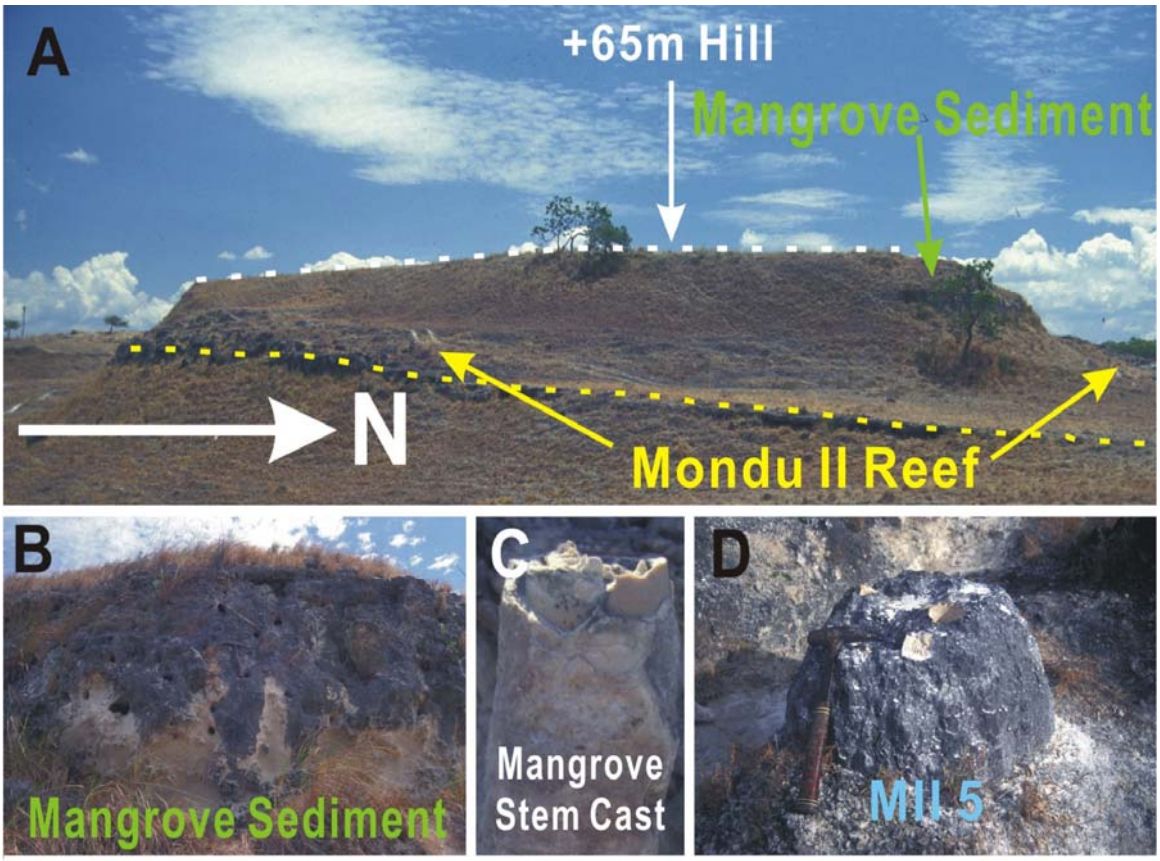

Figure 5.7 Panorama of the Mondu II reef (A) and close-ups of its sediment and coral head (B, C, and D).

Mondu II and VII reefs

Mondu II reef is located around a hill 65 m above sea level which we named "+65m Hill". This hill is about 2 km inland from the sea and 700 m south of Mondu I reef. Corals are abundant in the west and east side of the hill (Figs. 5.7 and 5.9). Their elevations are between 50 to 60 m above sea level (10 m in thickness). Figures 5.5 and 5.7 show clearly that this reef developed on an base surface (indicated by yellow dashed lines). Mangrove sediments (~ 4 m thick) are preserved between the reef and the hill top, as shown in Figure 5.7A and B. Many carbonate mangrove casts of stems and roots have been found among ivory white fine clastic sediment (Fig. 5.7C). Some of the corals are well preserved (as MII5 coral shown in Figure 5.7D), but many of them are weathered.

Mondu VII reef is further inland and 200 m southwest of Mondu II reef. Between them is a broad dry creek. They have the same elevation. There is a hard erosion surface on the top of the Mondu VII reef, and above that erosion surface, there seem to be other ancient reef or sediment but no coral samples were retrieved.

In Figure 5.1, we can see that there are 3 hills as high points around Mondu I and Mondu II reefs. All of them are top-flat around 60 m above sea level. Between the Mondu II reef and the top of the +65 m Hill, fine mangrove sediments with several meters in thickness have been found and many carbonate mangrove stem and root casts are among them. As a matter of fact, it is evident in Figure 5.1 that the 3 top-flat hills are later-incised parts of an extensively developed marine terrace (60 ~ 70 m above the sea level) around the Mondu area. This terrace is one of the three main terraces below 80 m above sea level in this area with an extension of 300 to 800 m (the other two extensively developed reef terraces are 0–5 m and 14–20 m above sea level, respectively, refer to Figures 5.1 and 5.3). These terraces all indicate lengthy periods of sea level stability producing terarces up to ~300 m wide. If an uplift rate of the nearby Cape Laudi is applied (0.49m/kyr) [*Pirazzoli et al.*, 1991], the development of this terrace might occur during MIS 5e, i.e., 128 to 119 ka.

Mondu V-A, V-B, and Mondu IV reefs

Mondu V-A and B reefs are exposed on each side of a deep creek located to the west of Mondu I +60m Hill (Figure 5.1). On the east side of the creek (the Mondu V-A reef) four *Porites* are very prominent and almost at the same elevation (39 m above sea level, Figure 5.8A). About 5 m above the corals there is an erosion surface which has an elevation of 44 m above sea level. All of these corals are in good condition. Dating of one of the MV-A coral (MV03-A-2 in Figure 5.8B) has been performed (see Chapter 4) by multiple U-series isotope measurements in skeletal sub-samples within this colony to explore the diagenetic behaviour of U-series isotopes in fossil corals from the Mondu raised reefs. A high-quality core and paleoclimate record has been reconstructed using this coral and is reported in Chapter 8.

On the west side of the creek (the Mondu V-B Site) many corals have been found and the elevations are between 37 to 42 m. On the top of Mondu V-B corals there is an erosion surface and the elevation is 48 to 51 m above sea level (Fig. 5.8C, yellow line). Coral MV03-B-2 has particularly high-quality material.

Figure 5.8C also shows the Mondu IV reef. It is located about 80 m west of Mondu V-B site. Most of the corals are 40 to 45 m above sea level, a little bit higher than the Mondu V-A and B corals. The Mondu IV reef seems to develop on edge part of the top of reef Mondu V-B, and in further inland, the reef MIV ends before the higher erosion surface (magenta line in Figure 5.8C).

Mondu VI reef

Figure 5.9 shows Mondu VI reef which is much lower than Mondu II reef. Around the Mondu II + 65 m Hill, there are 3 sites (MVI-A, B, C in Table 5.1) where reefs exposed. They have the same elevation, the same base and top, and under the same erosion surface. We think they are one single reef (named Mondu VI reef) buried beneath the Mondu II and V-A reefs.

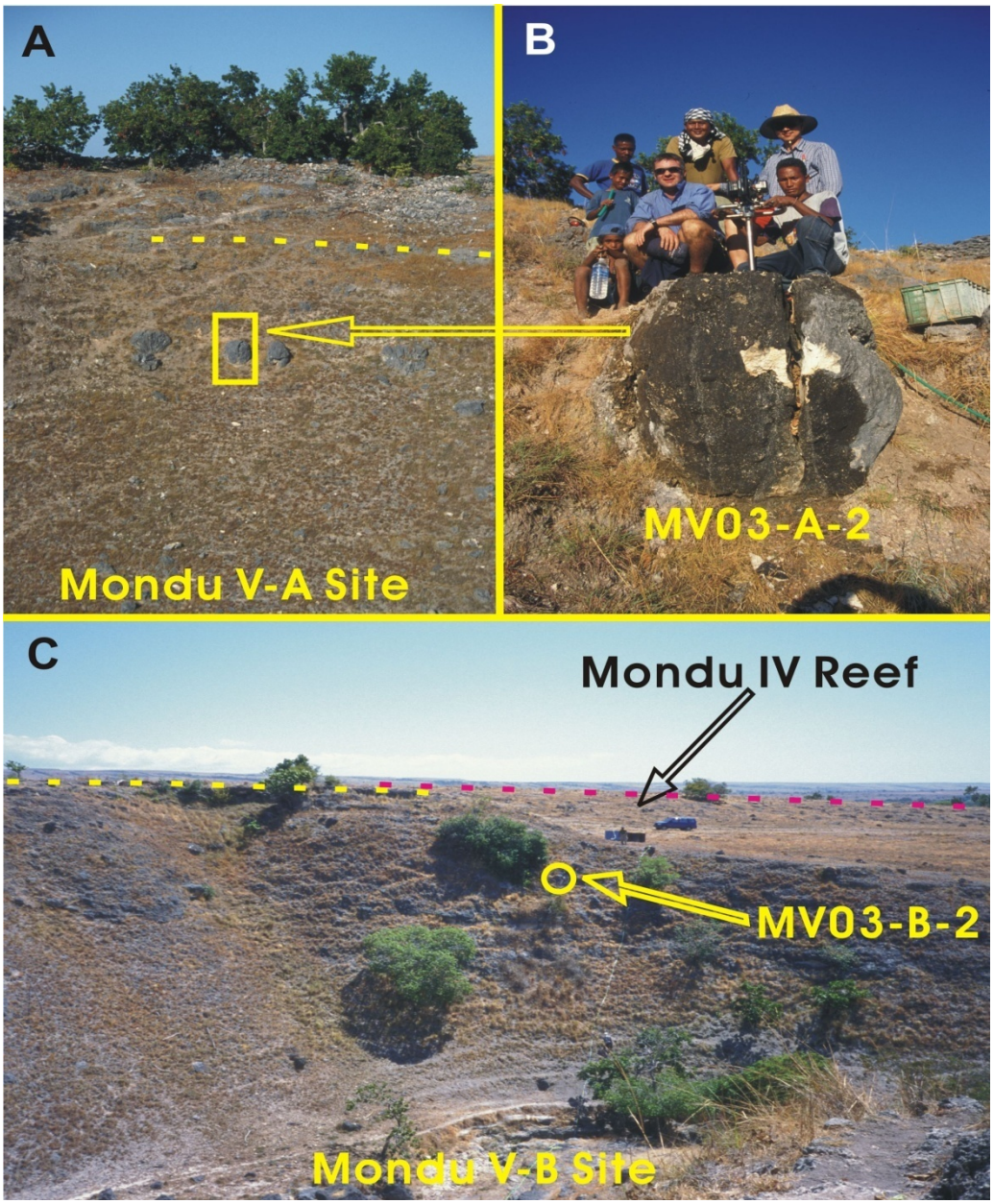

Figure 5.8 Panorama of Mondu V-A, V-B, and IV reefs with important coral heads indicated.

In general, the corals are badly weathered. Actually, they are the worst weathered material among all the studied reefs. Even though the material quality of the reef is poor as a whole, we collected some cores in the west side of the creek. The corals are very white and light-weight, and show no obvious evidence of calcification but might be a result of material dissolving.

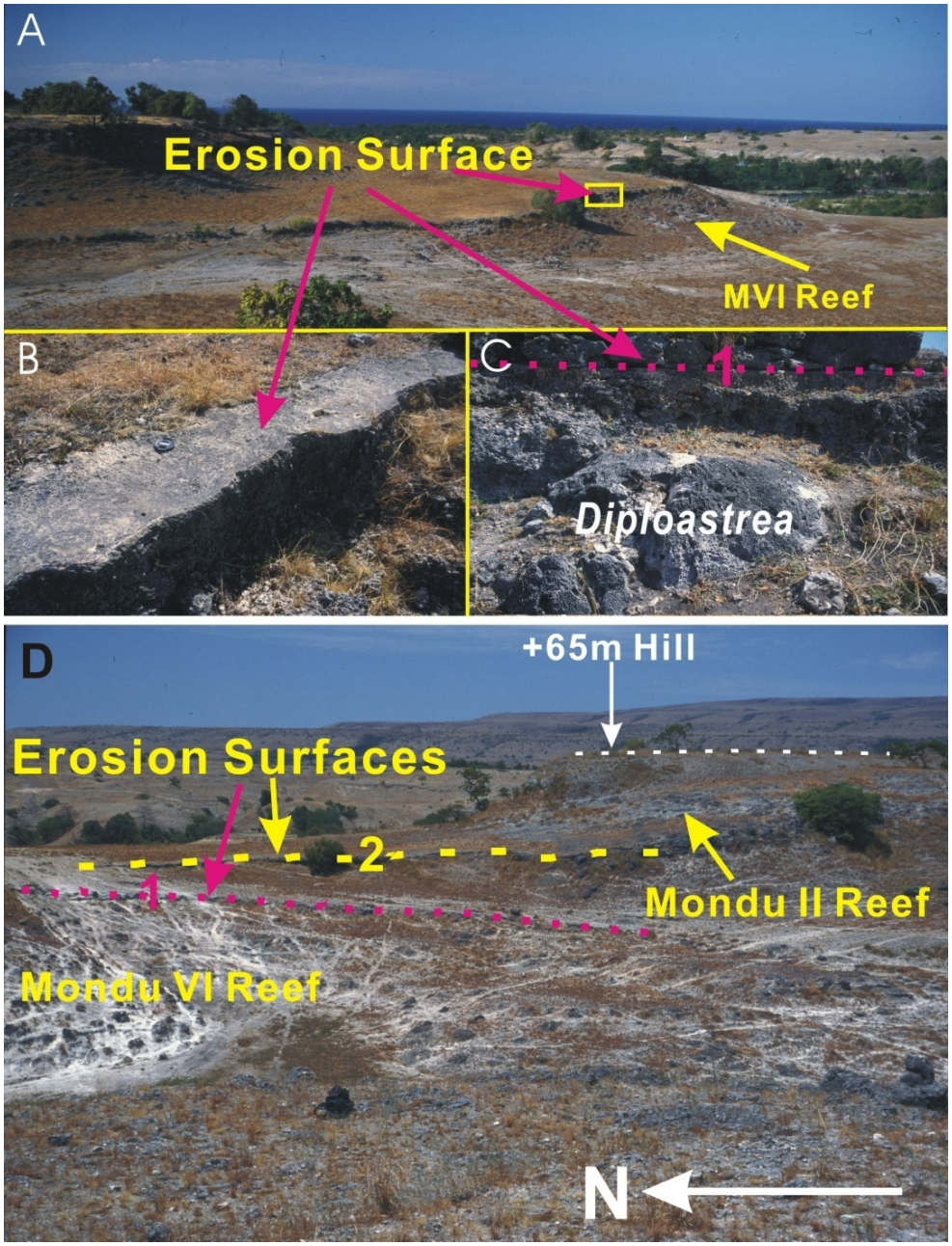

Figure 5.9 Mondu VI reef and the erosion surfaces. Magenta dashed lines illustrate the erosion surface on the top of Mondu VI reef, yellow dashed line indicates the reef base of Mondu II reef, and the white one shows the flat top of the 65m hill.

Apart from the conspicuous weathered quality, another major feature of this reef is the remarkable overlying erosion surface. Figure 5.9A shows the surface on the east site of the +65 m Hill. It is just on the top of some of the corals, and is very solid and smooth. Figure 5.9D also shows the surface (line 1 in magenta) on the west side of the +65 m

Hill. According to our survey, the elevation of the erosion surface beneath the Mondu II reef is about 50 m above sea level in front of the 65 m hill and the hard surface on the top of Mondu VI reef is 44m. This very hard and smooth surface also indicates very long time of exposure and erosion. Considering the sea level change and the local uplift rate, the possible age when the reef developed might be 174 ka when there was a highstand in sea level change [*Thompson and Goldstein*, 2005]. After that period, the reef had undergone exposure and erosion for as long as 40 ka.

5.5 AGE DETERMINATION AND REEF RAISING

5.5.1 Isochron slope and history of reef burial/exposure

The isochron correction model [*Scholz et al.*, 2004] suggested an approach independent of the systematic of α-recoil addition, and assumed a linear relationship between ^{230}Th and ^{234}U. It showed that the true age of a reef or coral can be calculated using the intersection of the arrayed line ("isochron") formed by the data points of the reef corals or subsamples of a coral with the seawater evolution curve in the $^{234}U/^{238}U$ – $^{230}Th/^{238}U$ plot. This model combines uranium uptake and loss, with the latter being proportional to the amount of uptake.

As shown in Chapter 4 of this thesis, multiple sub-sample measurements of U-series isotopic composition in a Mondu raised coral MV03-A-2 provide a unique opportunity to examine this kind of U-Th uptake and loss since it evidently experienced two recognisable stages of post-depositional alteration. The earlier process involved addition of allochthonous dissolved ^{234}U and ^{238}U together with addition of detrital non-radiogenic ^{230}Th, while the later process was clearly connected to loss of ^{234}U and ^{238}U occurring along loss of detrital-bound ^{230}Th. Locally radiogenic ^{230}Th appears to have played an important role in maintaining a constant $^{234}U/^{230}Th$ when percolating groundwater with allochthonous U and a high δ^{234}U value entered the coral at the earlier stage. On the other hand, detritus-bound ^{230}Th was critical to maintain a fixed $^{234}U/^{230}Th$

when percolating meteoric water dissolved coral skeletal U at the later-stage. The results suggest that a mechanism like diffusion or osmosis controlled the addition or loss of dissolved U and detrital Th in the coral by way of a solute concentration gradient. This result shows how the U and Th were uptaken or lost, while the ratio of $^{234}U/^{230}Th$ remained roughly constant, as observed by *Scholz et al.* [2004].

The result for the Sumba coral MV03-A-2 supports the calculation of the correction age by intercepting the array line ("addition line" [*Gallup et al.*, 1994] or loss line) with the seawater evolution curve. Figure 5.2 shows that there seems to be two groups of regression lines which are parallel to one another within each group. The group with older ages has larger slopes than the younger ones and they seem to separate around the last interglacial period or Termination II, while the Termination coral MV03-A-2c has both regression lines (refer to Chapter 4 for details). The detailed study of coral MV03-A-2c demonstrates that the later process (shown by the bold black dashed array line in Figure 5.2) mainly involved U/Th loss from the coral after it was exposed directly to meteoric water a low U content, while the earlier process (represented by the bold grey solid line in Figure 5.2) mainly happened when the coral was buried. The process mainly involved U/Th addition from the percolating groundwater with higher $\delta^{234}U$ value derived from the surrounding reefs.

Therefore, I think the two distinct array lines could be connected to different histories of exposure or burial between reefs: the isochrons with bigger slopes should be connected to reefs which experienced long-term burial, while the isochrons with smaller slopes should be connected to reefs with long-time exposure and no history of burial. This speculation seems to be justified by the stratigraphic relationships of the Mondu reefs. Mondu I corals form an array line perfectly parallel to the meteoric water-involved process of the Termination II coral (Figure 5.2), and stratigraphic observation has demonstrated that Mondu I reef has never been buried and was probably exposed to meteoric water for a long time (Figures 5.6 and 5.3). In contrast, the Mondu V-B and Mondu VII corals form parallel array lines with that of a process involving U addition

from the surrounding reefs of the Termination II coral, and our field surveys showed that they are now underlying other reefs (Figures 5.8 and 5.3). The slightly smaller slopes of Mondu V-B and Mondu VII reefs relative to the Mondu V-A coral's earlier alteration process might even imply a longer history of exposure than that of the Mondu V-A reef. This finding would be helpful in corroborating the ages of the Mondu raised coral reefs.

5.5.2 Sea level curve and uplift rates of Mondu reefs

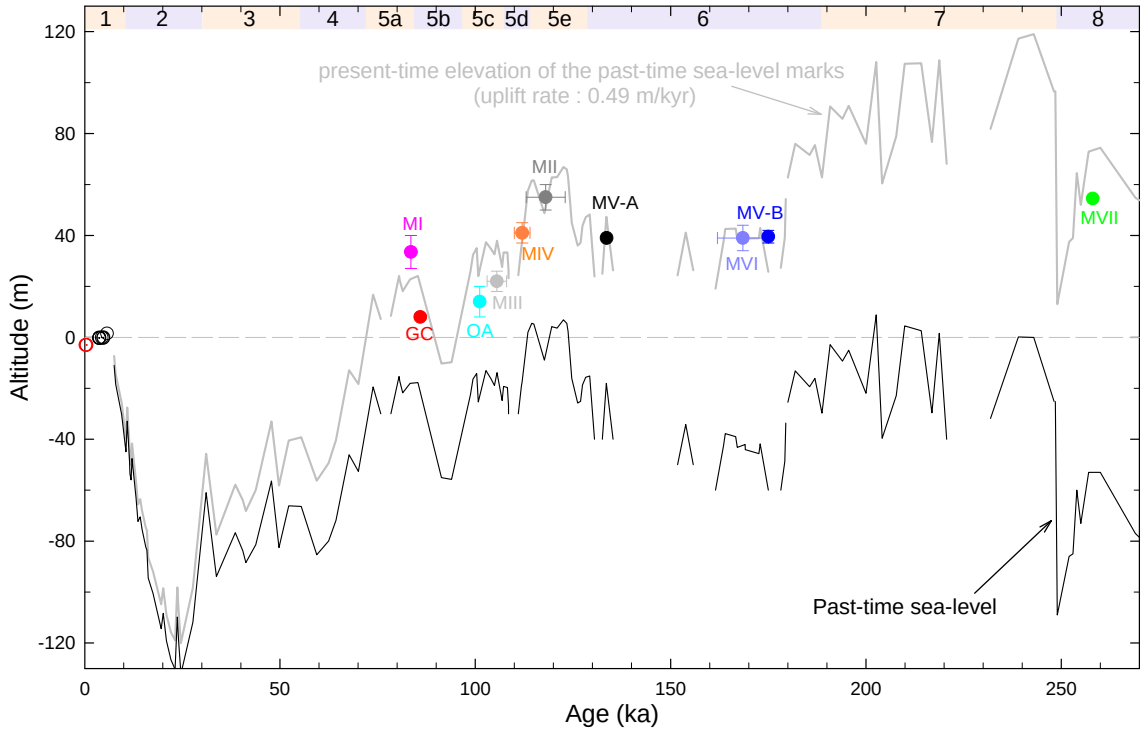

Figure 5.10 Comparison between modern elevation of the Mondu raised reefs (when the result of this study on their ages were used) and the calculated imaginary elevation of the past sea-level marks (grey curve, if a uplift rate of 0.49 m/kyr [*Pirazzoli et al.*, 1991] is applied). The coloured solid dots represent Mondu raised coral reefs with the surveyed elevation and the age results of this study. The upright error bars display the range of the elevation of the corals within one reef and the horizon error bars indicate the possible range of age of one reef. The red and black circles show the altitudes and ages of modern and Holocene corals in Mondu area. The black curve marks the past-time sea-level since 270 ka (the 0-250 ka sea-level data are from Thompson and Goldstein [2005], while 250-270 ka sea-level data are base on Lea et al. [2002]). The dashed grey line denotes the modern sea-level. The main oxygen isotope stages MIS-8 to MIS-1, including the substages of MIS-5, are identified on the top.

Since coral reefs are built up near the sea level (usually -6 to 0 m below the mean sea level), the ups and downs of sea level in the past time would be a key clue for establishment of the soundness of age determination of raised coral reefs. Figure 5.10 shows the recent results of researches on the past-time sea-level curve since 270 ka (black curve), with which we would conveniently find out the history of exposure and burial of reefs. Given an uplift rate, we would easily validate the age of a raised reef if its elevation is known.

Also illustrated in Figure 5.10 is a comparison between the present-time elevations of the Mondu reefs (colour dots or circles with error bars for both elevations and ages) and the elevations of the imaginary marks of the past-time sea-level (grey curve) if a uplift rate of 0.49 m/kyr [*Pirazzoli et al.*, 1991] was applied. The final ages which are described further in details in next section are applied here to more clearly illustrate the stratigraphic relationships and histories of burial/exposure of the Mondu reefs, and to help arguing on the soundness of age determination of this study.

It shows very good consistency between the elevations of the raised reefs and the past-time sea level curve if an uplift rate of 0.49 m/kyr was applied, corroborating the age determination of the Mondu raised reefs in this study. It supports a constant uplift rate of 0.49 m/kyr of the Mondu reefs since 258 ka, consistent with the findings of Pirazzoli et al. in the nearby Cape Laudi of 10 km away [*Pirazzoli et al.*, 1991]. Our results seem also to show a slightly lower rate in 5c and higher rate in 5a/5b and both seem to offset with each other very well and seem to have not affected the long-term rate of uplift. The fluctuation of uplift rate has also be reported by Bard et al. for the lower terraces in Cape Laudi [*Bard et al.*, 1996].

5.5.3 Analysis of ages of the reefs

Mondu I reef

One of the corals in reef Mondu I produced the only age value among all the measured

samples, which is thought to be reliable with an initial $\delta^{234}U$ value of 139.7‰ (Table 5.3, from a *Porites* coral MI6). Even though it might be slightly younger than its true age (beneath the seawater evolution curve), both the measured age of 84.1 ka of this coral and the corrected isochron age of 83.5 ka of Mondu I reef correspond to the highstand of MIS 5a. Notwithstanding the surveyed elevation of this reef is higher than the elevation of the coeval imaginary marks with an uplift rate of 0.49 m/kyr, I think the Isochron correction age of 83.5 ka reflects the true age of the reef Mondu I and it built up during MIS 5a. The main reasons are as followings:

- The initial $\delta^{234}U$ value of one of the corals is within the range of the reliable;

- The correlation coefficient r^2 of the array line is strikingly 0.99 for all the 6 ICP-MS data points on the $^{234}U/^{238}U$ – $^{230}Th/^{238}U$ plot; the only exception is measured by TIMS, and the sample is from the same coral deriving a reliable age of 84.1 ka, therefore it does not represent a different age but a possible discrepancy of diagenesis or measurement error between different instrumental methods or laboratory differential;

- Both of field observation (Figure 5.6) and the gentle slope of the MI reef array line which is parallel to the late meteoric water involved process for the Termination II coral (Figure 5.2, the bold dashed pink line and the parallel bold dashed black line) demonstrate a non-buried history of this coral reef, which is consistent with what the sea level curve has suggested (Figure 5.10).

- This age determination is consistent with the stratigraphic relationships: it is very possible that this reef is developed on the top of Mondu III reef, and even Oasis reef which built up during 5c suggested by the analysis of stratigraphy.

The possible reasons for the higher elevation of this reef are either a higher sea level during that time or a higher rate of uplift during that time which is likely that it does not affect the average uplift rate and the higher rate of uplift might be offset by lower uplift

rate immediately before or after this period. The lower elevation of reef Oasis might imply a lower rate of uplift during 5c. The fluctuation of the uplift rate has also be reported by Bard et al. [*Bard et al.*, 1996] for the Cape Laudi.

Mondu V-B and Mondu VI reefs

Even though no age could be directly achieved for Mondu VI reef by the U-series method and the model correction, the stratigraphic analysis basically supports that the age of the reef is an early sea-level highstand during MIS 6 around 174 ka, which means it should be the same reef as Mondu V-B in the further south.

5 of the 6 Mondu V-B corals produce an Isochron correction age of 175 ka with a correlation coefficient r^2 of 0.94 (Figure 5.2), which points to a sea-level highstand during early MIS 6 (Figure 5.10). It is worth to mention that even all the Open-System model correction ages of the 5 corals fall in the same sea-level highstand (Table 5.3). Figure 5.10 also shows the elevation of this raised reef is consilient with the sea-level curve with a locally constant uplift rate of 0.49 m/kyr. Furthermore, the isochron slope of coral U-Th data agrees with that of the earlier diagenetic process involving groundwater with high U and $\delta^{234}U$ sourced from the surrounding reefs, suggestive of history of burial by other younger reef(s). Stratigraphic analysis has supported that this Mondu V-B reef has been at least partly covered by Mondu IV reef in the north (Figure 5.8) and totally covered by Mondu II reef in the south (as Mondu VI reef there, Figures 5.9 and 5.3). It is very possible that this reef is covered by Mondu V-A reef somewhere between the 60 m hill and the 65m hill. The very hard erosion surface above Mondu VI (Figure 5.9B and C) and its weathered material are also consistent with a very long time of exposure which is as shown as the long-term of sea-level lowstand during the glacial of MIS 6 (Figure 5.10). Therefore, all those evidences indicate that the Isochron correction age of 175 ka is reasonable for Mondu V-B and VI reefs.

A long *Porites* core of MV03-B-2b from reef Mondu V-B gives a conventional U-series age of 99 ka (Table 5.3). Since it has a marginal $\delta^{234}U$ value of 161.1‰, its true age

might be younger based on the observation of Gallup et al. [1994] and the possible age should be less than 95 ka which corresponds to late 5c or 5a. Given its elevation of 37.5 m and it grew on the seaward edge of reef Mondu V-B, its most possible age should be MIS 5a, the same as reef Mondu I since the sea-level in late 5c (< 95 ka) was too low to reach that point according the sea-level curve [*Thompson and Goldstein*, 2005] when a higher rate of uplift is excluded during 5c which is confirmed by the elevation of reef Oasis (see below). Figure 5.2 also shows that this coral is arrayed with the other corals of Mondu I reef. So I date this long core for now as 83.5 ka (Table 5.3).

Mondu VII reef

Even though the Mondu VII reef's Isochron correction age was given by only 3 corals, its model age of 258.1 ka seems to be well consistent with our analysis of stratigraphic relationship and history of burial. It is located in the most south of the study area and should be a very old reef given its low altitude (Figure 5.3). The corrected age and elevation is accordant with the sea level curve with the local uplift rate of 0.49 m/kyr, indicative of a highstand during late MIS 8 (Figure 5.10). The sea level curve also demonstrates that this reef would have been exposed for erosion after it built up during the end of the glacial MIS 8, which explains the erosion surface on the top of the reef. Field observation indicated that this reef is buried by unknown reef(s) or sediments, which is in agreement with the fact that the reef should be burial by reefs or sediments after the sea level raised again and maintained at a much higher level during the whole period of interglacial of MIS 7 according to the sea-level curve (Figure 5.10). The steep slope of isochron for this reef (Figure 5.2) also reflects a history of burial of this reef or by some younger reefs or sediments.

Mondu V-A reef

A Mondu V-A *Porites* coral gave a conventional ^{230}Th age of 136.8 ka for the most pristine sub-sample with a marginal initial δ^{234}U value of 158.9‰, which implies that the true age of the coral is slightly younger. According to the observation of Gallup et al.

[1994], the true age of coral MV03-A-2 might be between 133 ka and 134 ka (see pp. 56-57 in Chapter 4 for details). Further analysis of multiple sub-sample measurements demonstrated that the coral experienced two distinct processes of U-series diagenetic alteration and two models derived from each process gave essentially the same model correction age of 133.6 ka (see Chapter 4 for dating of this coral).

All the achieved U-series ages, including the conventional ^{230}Th age, the experiential age and the correction ages of different models, confirmed that this coral was growing during the termination of the penultimate glacial period (Termination II, 140 ka ~ 128 ka) [*Martinson et al.*, 1987; *Muhs*, 2002; *Brauer et al.*, 2007]. During Termination II, sea level was believed to rise rapidly between the glacial ~ -120 m, [*Lea et al.*, 2002; *Cutler et al.*, 2003; *Risebrobakken et al.*, 2006] and interglacial ~ +5 m [*Stirling et al.*, 1995] positions. However, recent research suggests that Termination II did not consist of a monotonic sea-level rise as occurred during Termination I [*Fairbanks*, 1989; *Bard et al.*, 1990] but instead included an interlude of significant sea-level fall [*Esat et al.*, 1999; *Gallup et al.*, 2002; *Antonioli et al.*, 2004; *Siddall et al.*, 2006; *Andrews et al.*, 2007], as shown by the Thompson and Goldstein's sea level curve [2005] in Figure 5.10. The sea level had reached an early highstand lasting several millennia around 134 ka, followed by a sharp drop in sea level and still-stand of several millennia around 131 ka, before the final sea-level rise to the MIS 5e interglacial starting at 128 ka.

Our stratigraphic investigation strongly supports those achieved U-series ages of the Mondu V-A reef and the ups and downs of sea-level during the Termination II. The loose erosion surface 5 m above on the reef (Figure 5.8A) demonstrates only a short period of exposure after its burial, while a sporadic distribution of corals in this reef might imply a short period of stable sea level, which are both consistent with a short highstand during Termination II following a dramatic sea-level drop. The observation that Mondu II reef developed on the erosion surface of the Mondu V-A further confirms the age of this TII reef. The two slopes of the U-Th data in Figure 5.2 for the single colony exactly reflect the history of the coral which was buried firstly by younger reef

(the last interglacial maximum reef) and then fully exposed to meteoric water owing to a large crack cutting the coral (see details in Chapter 4).

Goat Site Reef

Seven of the Goat Site reef corals form an array which gives out an isochron model age of 85.9 ka. The GC 6c was excluded because of the same reason as the MI6D that it is also a TIMS result of measurement, while the GC13-D-6 give a strange data point and the reason might be its complicated diagenesis.

The 85.9 ka of age corresponds to MIS 5b when the sea level was much lower than today, consistent with the low elevation of the Goat Site reef if an uplift rate slightly higher than a local long-term rate of 0.49 m/kyr is applied (Figure 5.10). But this higher rate seems still not enough to make the MIS 5b reef covered by a MIS 5a reef which is the only reef possibly able to cover the MIS 5b reef, as shown by the sea level curve, (Figure 5.10) since the sea level gap between them is up to more than 30 m. Instead, our topographic survey demonstrated that the MIS 5a reef of Mondu I developed much higher (20 m higher) in further south on top of other reef(s) (Figures 5.1 and 5.3). Field observation found that all of the GC corals seem to cover the foot of an ancient marine notch (the cliff in Figure 5.5). This demonstrates that, even though the reef is exposed to meteoric water since it formed, it has also been very closely connected with the percolating groundwater from the cliff. The isochron slope of this reef (red line in Figure 5.2) seems to exactly reflect this kind of situation: it is between the two main groups and a little more close to the “meteoric water” array lines. Therefore, all the results of analysis on stratigraphic relationships, sea-level’s up-and-down, local uplift rate, and the history of burial and exposure support an age of MIS 5b for the Goat Site reef.

Mondu IV reef

Only one age has been obtained from the U-Th measurement. Fortunately, it has a

marginal initial $\delta^{234}U$ value of 162.9‰ which means the true age of this reef is only slightly younger than its conventional U-series age of 121.3 ka. And the range of its possible age could be achieved owe to the slightly changed initial $\delta^{234}U$ since we can constrain the range of age by applying the two slope values of the two group array lines. If this reef did not buried and the corals in the reef would form an array parallel the array line like the Mondu V-A coral later evolution line or the one like the Mondu I reef, both give out a latest age of this reef as 110 ka, or if this reef was buried for long time, the array line would parallel the array line of the Mondu V-A earlier-stage process evolution line and it gives out a oldest age of 118 ka. Therefore, the age of Mondu IV reef would be within the range of 110-118 ka. Since field observation showed that the reef is on the top of the Mondu V-B and no reef covers it, the age range of this coral should be the late half: 110-114 ka. This age and elevation are also well consistent with the published sea level curve when an uplift rate of 0.49 m/kyr is applied (Figure 5.10).

Oasis reef

No upper covering reef was found and all the corals in this reef are directly exposed at Oasis site. But at Mondu I site, Mondu I reef developed on the top of a cliff which is based on a 20 m platform there, suggest that the Oasis reef is older than Mondu I reef. The sea level curve suggests that the possible age of the reef is 5c. Even though the U-series measurement gives a scattering data distribution, the array line of the Oasis reef should follow the slope of the Mondu I array line since this reef is not covered. Three of the corals from the Oasis reef form an array with a similar slope as Mondu I corals, and it gives an age of 101.1 ka.

Mondu III and Mondu I West reefs

Stratigraphic analysis indicates that Mondu III and Mondu I West should be coeval coral reefs and the Mondu I reef directly covers them, suggestive of an older age than the Mondu I (MIS 5a) reef for these reefs. And, the cliff (18 ~ 26 m) between Oasis platform (erosion surface, 21 m) and the Mondu I reef (27 ~ 40 m) should be the Mondu

III and Mondu I west reef. Therefore, the possible age for them is 5c, which is 103 ~ 108 ka.

Mondu II reef

The Mondu II reef and the extensive terrace platform at 60 ~ 65 m above the sea level represent an obvious feature of the Mondu area topography. The reef has never been covered by any other reefs. Based on the present-time elevation of imaginary past-time sea-level mark curve with a uplift rate of 0.49 m/kyr (Figure 5.10), the only possible age for this reef is 113 ~ 123 ka, corresponding to MIS 5e. Since all the corals of this reef give highly raised $^{234}U/^{238}U$ and $^{230}Th/^{238}U$ ratios (Figure 5.2), and only 2 or 3 of them form array lines, it is difficult to achieve a precise isochron correction age. Even though 3 of them give an isochron age of 133 ka, it is not possible since the elevation of the coral is too high for this age, and it developed on a loose erosion surface of Mondu V-A reef and Mondu VI reef (Figures 5.2), MIS 5e is the most possible age for this reef.

Table 5.4 summarizes the results of this study on the elevation and age for the Mondu raised coral reefs.

Table 5.4

Summary of reef elevations, ages, and Marine Isotope Stages (MIS) they belong to.

Reefs	Elevation above sea level (m)	Thickness (m)	Average Elevation (m)	Age (ka)	MIS
Holocene	-2~2			**1 ~ 6**	**1**
Mondu I	27~40	13	32	**83.5**	**5a**
Goat Site	7~8			**85.9**	**5b**
Mondu III	19-26	7	22	**103 ~ 108**	**5c**
Mondu I west	18-26	8	22	**103 ~ 108**	**5c**
Oasis	8~20	12	14	**101.1**	**Late 5c**
Mondu IV	37~45	8	41	**110 ~ 114**	**5d**
Mondu II	50~60	10	55	**113 ~ 123**	**5e**
Mondu V-A	39	0	39	**133.6**	**TII**
Mondu V-B	37~42	5	40	**175**	**Early 6**
Mondu VI	34~44	10	39	**162 ~ 175**	**Early 6**
Mondu VII	54			**258.1**	**Late 8**

5.6 CONCLUSIONS

A wealth of fossil *Porites* coral cores have been drilled from the Mondu raised coral reefs in Sumba, Indonesia. To understand the reef environments of the corals, and establish guidelines for further exploration of the long, high-quality cores, the ages of these corals have been determined by combining stratigraphic analysis and U-series age model corrections. The ages were cross-checked using detailed topographic surveys and field observations, which provide new insights into the distribution, elevation, and stratigraphic relationships of the raised reefs. Fifty-four coral samples from the raised reefs have been measured for U-series isotopic composition, but almost all the results did not give reliable conventional ^{230}Th ages. The open-system model [*Thompson et al.*, 2003] was first applied, but did not produce consistent ages, indicating that the Mondu raised corals did not experience diagenetic processes involving the mechanism of coupled addition of ^{234}Th and ^{230}Th through α-recoil. However, the isochron model [*Scholz et al.*, 2004] could be applied to the Mondu raised reefs and the model ages are proven to be consistent with the stratigraphic relationships and features of the reefs.

The ^{234}U/^{238}U – ^{230}Th/^{238}U plot for the corals displays two distinct groups composed of parallel arrays of lines, with only a couple data points excepted. The array lines associated with the older corals have much larger slopes than the array lines associated with the younger corals. The stratigraphic analysis demonstrates that the slopes of the array lines reflect the burial/exposure history of the reefs: the reefs with smaller isochron slopes have experienced no history of burial and the reefs with bigger slopes have been buried by younger reef(s). This finding has served very well to help determine the ages of reefs whose ages could not be achieved by the Isochron correction model along.

The results support a constant uplift rate of 0.49 m/kyr for the Mondu raised reefs since ~260 ka, although the rate may be higher during MIS 5a/5b and lower during 5c. This

study demonstrates that some very high-quality *Porites* cores have been retrieved for high-resolution paleoclimate records (such as that from the early highstand during Termination II). Other promising time-windows for paleoclimate records from the Mondu reefs might include the interstadials and stadials of MIS 5, highstands in glacial MIS 6, and even a late highstand during glacial MIS 8.

CHAPTER 6

CLIMATE AND OCEANOGRAPHY OF THE INDO-PACIFIC WARM POOL RECORDED BY A MODERN *PORITES* CORAL FROM SUMBA, INDONESIA

ABSTRACT

This study demonstrates that modern corals from Sumba are excellent recorders of climate and oceanography in the Indo-Pacific Warm Pool. High-resolution (fortnightly) time series, stacked annual climatology, and seasonal means have been characterised for modern coral $\delta^{18}O$ and $\delta^{13}C$. Detailed correlation and spectral analysis of these features with local instrumental records and main climate system indexes have been conducted, and the results demonstrate that the ENSO, Asian-Australian monsoon, and even remote equatorial Indian Ocean forcing all have a strong influence on the local climate and oceanography. The high-resolution coral $\delta^{18}O$ record from Sumba shed light on the key climate signals to improve our understanding the climate and oceanography in this area. The Sumba coral $\delta^{18}O$ record shows the dominant control of ENSO in austral winter whereby the interannual variability of the winter $\delta^{18}O$ serves as a good index for ENSO events. In austral summer and autumn (November through May), the coral $\delta^{18}O$ is overwhelmingly controlled by the tropical Indian Ocean winds and the monsoon.

The high-resolution Sumba modern *Porites* coral $\delta^{18}O$ provides evidence for the routine penetration of the South Java Current (SJC) in austral summer and remote forced equatorial Indian Ocean Kelvin wave in autumn into the Savu Sea, which results in distinct freshening of the surface ocean during the austral autumn. By sensitively recording variability of sea surface temperature and salinity in this important exit of the Indonesian Throughflow (ITF), the Sumba coral $\delta^{18}O$ revealed active oceanic current activity in Sumba Strait. In austral winter, westward currents generally flow in the Sumba Strait and the ITF brings Pacific source-water with moderate salinity. In summer, the more saline SJC enters the Savu Sea from the west until around March. After March, two causes gradually lower the seawater salinity: the gradual weakening of the eastward SJC owing to the weakening of northwest monsoon winds, and the arrival of a remotely forced Kelvin wave with very warm and fresh water during April-July. Input of Indian Ocean water into the Savu Sea by the summer SJC and autumn Kelvin wave could have

significantly influenced the transport of the Indonesian Throughflow.

Detailed correlations between annual skeletal density banding and the high-resolution coral $\delta^{13}C$ record show that the low skeletal density band coincides with peak summer monsoonal rainfall and maximum depletion in skeletal $\delta^{13}C$. This correlation was attributed to the large input of terrigenous nutrients linked to peak summer monsoonal rainfall. This relationship could be applied to explore local monsoon variability in an economical and more efficient way by measuring the coral density.

6.1 INTRODUCTION

The Indo-Pacific Warm Pool (IPWP) - Indonesian Maritime Continent region is a key area for global climate system as a major source of moisture and latent heat for the global atmosphere and plays a fundamental role in driving the globally important meridional Hadley and zonal Walker circulations [*Keenan et al.*, 2000]. Studies have indicates that changes of sea surface temperature and convection in this tropical Indo-Pacific region contribute to the interannual, decadal, even millennial-scale climate variability observed in extra-tropical regions [*Cane*, 1998; *Cane and Clement*, 1999; *Hoerling et al.*, 2001; *Stott et al.*, 2002; *Visser et al.*, 2003]. Important tropical climate systems with global impact, such as the El Niño-Southern Oscillation (ENSO), Asian-Australian Monsoon and Indian Ocean Dipole (IOD), strongly interplay within this region. The Indonesian maritime continent is also the only tropical intersection between major oceans for water mass and energy exchange. The Indonesian Throughflow (ITF) brings huge amount of cool, low-salinity water into the Indian Ocean and alters the meridional overturning circulation of the Indian Ocean [*Gordon*, 2005]. The oceanic heat and freshwater fluxes into the Indian Ocean affect atmosphere-ocean coupling with potential impacts on the ENSO and monsoon phenomena [*Webster et al.*, 1998] and their variabilities are believed to affect climate in interannual and longer time scales [*Schott and McCreary*, 2001].

The ITF has been shown strong variability in an extensive range of time scales. Remote forcing on interannual variability of the ITF from the tropical Pacific associated with the ENSO has long been recognised: a weakened ITF linked with El Niño and an intensified ITF linked with La Niña [*Clarke and Liu*, 1994; *Bray et al.*, 1996; *Meyers*, 1996; *England and Huang*, 2005; *Susanto and Gordon*, 2005]. The annual and semiannual variations in transport have been related to the monsoon winds [*Meyers et al.*, 1995] and the equatorial Indian and Pacific winds [*Masumoto and Yamagata*, 1993; 1996]. Intraseasonal variability [*Bray et al.*, 1997; *Qiu et al.*, 1999; *Chong et al.*, 2000;

Potemra et al., 2002; *Syamsudin et al.*, 2004] has been attributed to the remote Kelvin waves forced in the tropical Indian Ocean. The variability of the ITF has been complicated by the overlapped time scale of different forcings and most of the studies were based on short-term (several months to several years) observation or modelling, the only continuous observation is the decadal-long time series of Meyers [[*Meyers*, 1996]. Detailed researches on individual passage and longer time series are needed to further understand the forcing and mechanism for the ITF variability and then the impact of the ITF on regional and global climate/oceanography and the interaction of the ENSO, IOD and the Asian-Australian monsoon systems.

More than 40% of the ITF flows into the Indian Ocean via the Savu Sea [*Gordon*, 2005], which is located in the south-central part of the Indonesian maritime continent (Figure 3.12). Strong annual variability (up to 12 Sv in 1996) in transport through Ombai Strait [*Molcard et al.*, 2001a] which is the eastern control entrance for the ITF passing the Savu Sea. Recent oceanic observation and numerical model have shown that there can be up to a 10 Sv imbalance [*Potemra et al.*, 2003] between the inflow and the outflow transport in the Savu Sea at times and most of the variability in estimated convergence is controlled by the flow through the Sumba Strait [*Potemra et al.*, 2003] which is the western control exit for the ITF passing the Savu Sea, indicative of the importance of understanding the inflow and outflow in this Strait. Despite the importance of understanding the climate and oceanography in the Sumba Strait, only one attempt, to date, has been reported. In December 1995 to April 1998 a pair of sub-surface pressure gauges was deployed in the western edge of the Sumba Strait and concurrent Acoustic Doppler current profiler (ADCP) survey across the strait was employed as part of the three year Shallow Pressure Gauge Array (SPGA) study. Pressure, temperature and salinity data were recorded and a series of encouraging achievement have been reported [*Chong et al.*, 2000; *Hautala et al.*, 2001; *Potemra et al.*, 2002; *Potemra et al.*, 2003; *Sprintall et al.*, 2003]. Here we report 37 years of oxygen and carbon stable isotope composition records during 1962 to 1998 from a modern *Porites* coral which grew just in the southern side of the strait within the Savu Sea near the shallow sill (about 900 m)

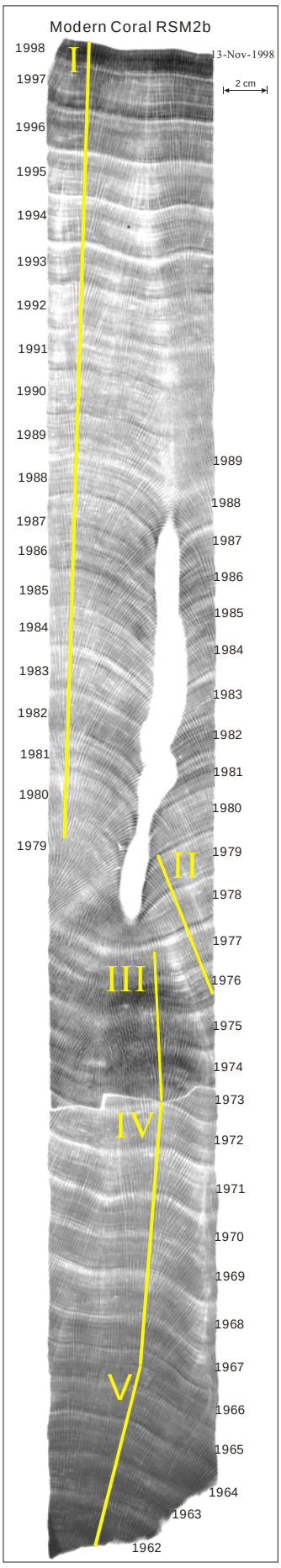

[*Hautala et al.*, 2001] of the strait. The $\delta^{18}O$ and $\delta^{13}C$ records reconstruct the climate and oceanography in Sumba Strait with seasonal, interannual, decadal variability and long-term trends, which reflect strong impacts of the ENSO, IOD, and the Asian-Australian monsoon systems. The high resolution records enable us disentangle the complicated interaction of the ENSO, IOD, and monsoon, and show a 37-year historical record of routine penetration of the coastal Kelvin wave remotely forced in the tropical Indian Ocean, implying strong impacts of the tropical Indian Ocean winds and local monsoonal winds on the ITF transport through the Sumba Strait and the Savu Sea.

Figure 6.1 (right) X-ray positive print of modern coral RSM2b. Numbers show the years of coral growth. Yellow lines and Roman numbers indicate sub-sampling transects.

6.2 MATERIALS AND METHODS

6.2.1 Modern coral sampling

The *Porites sp.* coral core RSM2b used in this study was collected from a patch reef (9°27'30.7"S, 120°04'51.4"E) about 500 m off shore west of Mondu River (Fig.4.1, River Site) on 13 November 1998. This core (68 cm in length and 7.5 cm in diameter) was drilled from a big living colony (2.5 m in height from top to coral bottom) in 3 m water depth using a large RSES water-driven drill. No calcite and secondary aragonite over-growths were found by examination under UV light and thin-section observation,

indicative of excellent preservation for climate reconstruction.

The coral core was slabbed, ledged, and sub-sampled for isotopic analysis following a procedure developed by [*Gagan et al.*, 1994; *Gagan et al.*, 1998]. X-ray photographs of the coral slabs (shown in Fig.6.1) were taken and used to develop a chronology and as a guide for sub-sampling transects along the axis of maximum growth. Sub-samples were collected continuously at intervals of 0.4 mm, which is or close to weekly resolution.

6.2.2 Isotopic analysis

Oxygen and carbon isotope analyses were obtained by reacting ~200 μg aragonite samples with two drops of 103% H_3PO_4 at 90°C for 12 minutes in an automated individual-carbonate reaction (Kiel) device coupled with a Finnigan MAT-251 mass spectrometer. The isotope ratios are reported in standard delta notation relative to Vienna Peedee Belemnite (VPDB) and calibrated via the NBS-19 calcite standard ($\delta^{18}O$ = -2.20‰, $\delta^{13}C$ = 1.95‰) and the NBS-18 calcite standard ($\delta^{18}O$ = -23.0‰, $\delta^{13}C$ = -5.0‰). 238 NBS-19 and 11 NBS-18 were analyzed during the measurement of 1087 RSM2b modern coral sub-samples. The standard deviations ($\pm 2\sigma$) were 0.07‰ ($\delta^{18}O$) and 0.03‰ ($\delta^{13}C$) for NBS-19, and 0.08‰ ($\delta^{18}O$) and 0.07‰ ($\delta^{13}C$) for NBS-18.

58 samples from the top 10 years of the coral were analysed by Mr. Bambang Suwargadi (LIPI, Bangdung, Indonesia) who visited our laboratory in November 2000. 4 years later 29 of them were repeated during my PhD and reproducibility ($\pm 2\sigma$, $n = 29$) is $\pm$0.07‰ for $\delta^{18}O$ and 0.10‰ for $\delta^{13}C$, showing good reproducibility in this laboratory even 4 years between the 2 time measurements. Some coral sub-samples were measured 2 or 3 times for better reliability, especially the samples during the austral winters, and average values were calculated.

For most of the $\delta^{18}O$ and $\delta^{13}C$ records, every second sub-sample was measured, which equals almost fortnightly. But for periods when skeletal isotopic composition changed rapidly, such as during austral winters, neighboring sub-samples were added, resulting

in weekly resolution. The annual extensions for this coral varied between 15.6 and 20.8 mm, with an average annual extension of 18.5 mm (excluding the year of 1975 of distorted growth). The sampling frequency of isotope analysis varied from 21 to 32 samples per year (excluding 1975), and the average sampling frequency was 26.8 samples per year, approximately equal to fortnightly resolution.

6.2.3 Chronology

The RSM2b core spans 37 years and 7 months from April 1962 to 13 November 1998 (Figure 6.1). The years shown in Figure 6.1 were assigned by cross-checking the annual density bands counted from the X-ray positive image against the annual $\delta^{18}O$ cycles. A detailed chronology was established by assigning the annual arrival-time of the winter SST minimum in Sumba to each coral $\delta^{18}O$ annual maximum, and then allocating equal time spans to the data points between adjacent $\delta^{18}O$ maxima using linear interpolation by *Analyseries* [*Paillard et al.*, 1996]. Analysis of SST records [IGOSS, *Reynolds et al.*, 2002] for 1982 to 2005 indicates that winter SST minima at Sumba ($1^\circ \times 1^\circ$ grid centred at 120.5° E, 9.5° S) arrive near 8 August (± 32 day, 2σ, $n = 24$). For the modern coral isotope records, 26 equal intervals were assigned between two neighbouring SST winter minima, so resolution of the chronology is similar to the measurement resolution.

6.3 RESULTS AND DISCUSSION

6.3.1 Reproducibility of coral records

6.3.1.1 Different axes of growth in coral RSM2b

In order to check the consistency of the isotopic composition of different axes of growth, overlapping sections of sub-sampling transects II and III were measured, which span from winter of 1976 to winter of 1977 (Figure 6.2).

The two $\delta^{18}O$ records during this one year period impressively show the same trend of

change (point A to E in transect II and A' to E' in transect III). Both records even show small changes in mid-summer (increase in $\delta^{18}O$ value at points C and D in transect II and at C' and D' in transect III). Time-equivalent points of most of the two records have $\delta^{18}O$ values within the standard deviation of measurement excluding points around winter of 1976 (E and E' in Figure6.2), where smoothing of the record at E in Transect II happened because the cut depth had to be increased for the end part of this transect duo to an accident during ledge milling. Differences between the time-equivalent points E and E' are greater than the standard deviation. The $\delta^{18}O$ and $\delta^{13}C$ records of Transect III were applied in this research because the smoothing in this part of Transect III makes the record unreliable. Also, the distortion in growth direction of Transect III (Figure 6.1) starts around the winter of 1976 and might has some effect on the data of $\delta^{18}O$ and $\delta^{13}C$ records. Figure 6.2 shows this complex growth does have effect on the $\delta^{18}O$ and $\delta^{13}C$ records, especially for period around 1975.

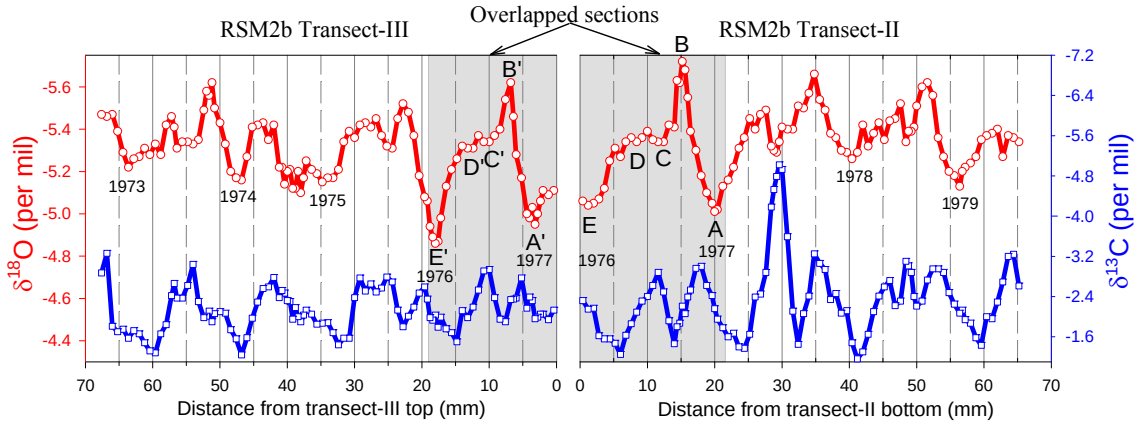

Figure 6.2 Comparison of $\delta^{18}O$ and $\delta^{13}C$ records for overlapping sections on sampling transects II and III for coral RSM2b. Shaded parts are overlapped sections spanning from winter 1976 to winter 1977.

6.3.1.2 Different corals in Sumba

In order to evaluate the representativeness of the single-core reconstruction from RSM2b for the local climate and oceanography, stable isotope records of another coral SU1 from the same site (several hundred metres apart) is applied to compare the

reproducibility. Coral SU1 is a very small *Poretis* colony with dimension of about 30 cm by 30 cm. Heather Scott-Gagan carried out all the sample preparation and measurement of $\delta^{18}O$ and $\delta^{13}C$ for coral SU1. But samples for both corals were prepared and measured according to the same procedure and methodology in the same laboratory at ANU. Since the difference of their average extension rate (18.6 mm for RSM2b and 14 mm for SU1 during the same growth periods 1985-1996), the sub-sampling step for SU1 is 0.3 mm, while RSM2b is 0.4 mm. The difference in sub-sampling steps guarantees that both coral were sub-sampled in weekly resolution and measured in fortnightly resolution.

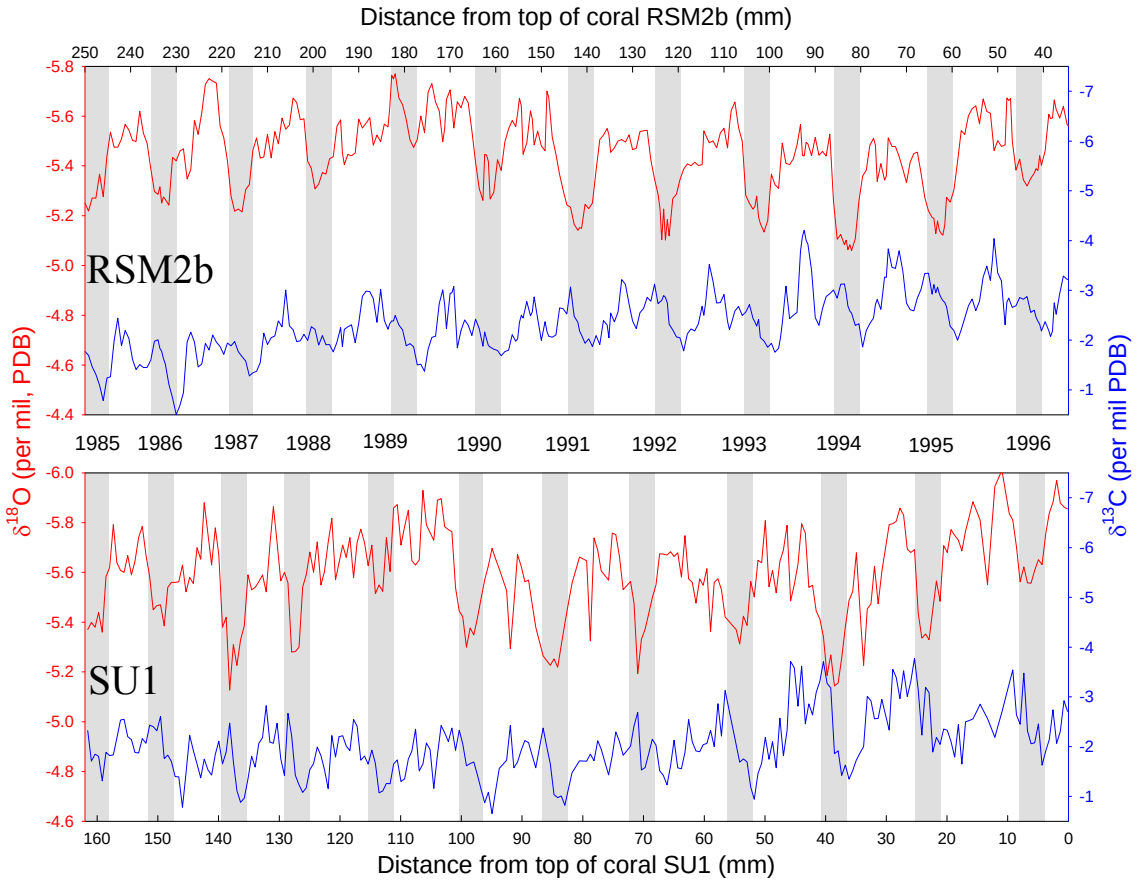

Figure 6.3 Comparison of $\delta^{18}O/\delta^{13}C$ records of Sumba coral RSM2b (upper panel) and SU1 (lower panel). Red curves are $\delta^{18}O$ and blue curves are $\delta^{13}C$. Please note that all the axes are reversed and the ranges of $\delta^{18}O/\delta^{13}C$ axes for the two panels are the same for convenience of comparison.

Figure 6.3 compares the $\delta^{18}O$ and $\delta^{13}C$ records between these two corals. Both the $\delta^{18}O$

and $\delta^{13}C$ records of RSM2b are well replicated by records of SU1. Two coral $\delta^{18}Os$ recorded ENSO events very well, such as heavier values in winter for El Niños in 1991, 1992, 1994, and 1997, obvious lighter value in winter for La Niñas in 1989 and 1996. Both records have lighter values in summers of 1990 and 1996. They also both recorded evident elevated summer $\delta^{18}O$ values during 1991 to 1995. They have similar ranges of variation (0.71‰ for RSM2b and 0.63‰ for SU1) (Table 6.1). For $\delta^{13}C$ records, both have clear annual cycles and reach their annual maximum $\delta^{13}C$ around October. The ranges of variation are very close (2.38‰ and 2.45‰, respectively). Two records both have a trend of decrease from 1985 to 1996, especially, they both recorded obviously decreased values in the last three years 1994 to 1996.

There also some difference between the two coral. The obvious difference between $\delta^{18}Os$ is the small shift of 0.15‰ for their average values (Table 6.1: -5.44‰ for RSM2b and -5.59‰ for SU1). Even though $\delta^{13}C$ also have a shift of 0.33, the percentage of the shift in the range of variation is remarkably smaller than $\delta^{18}O$ (14%, 14% for $\delta^{13}C$ and 21%, 23% for $\delta^{18}O$).

Table 6.1
Comparison between isotopic records for corals RSM2b and SU1 (1985-1996)

Coral		**RSM2b**	**SU1**
Mean (‰)	$\delta^{18}O$	-5.44	-5.59
	$\delta^{13}C$	-2.37	-2.04
Range of variation (‰) (2 * 2σ)	$\delta^{18}O$	0.63	0.71
	$\delta^{13}C$	2.38	2.45
Shift between means (‰)	$\delta^{18}O$	0.15	
	$\delta^{13}C$	0.33	
Percentage (%) of shift in the range of variation	$\delta^{18}O$	23	21
	$\delta^{13}C$	14	14

In general, the $\delta^{13}C$ and $\delta^{18}O$ records of Sumba coral RSM2b could be well replicated by coral SU1, even though SU1 is a very small colony and the extension rate is not as

stable as that of RSM2b.

6.3.2 Seasonality of Sumba coral $\delta^{18}O$

Sumba *Porites* coral $\delta^{18}O$ record shows strong seasonality (Figure 6.4, upper panel). For some year, the seasonality were in a great magnitude, for example, in 1976, the value of coral $\delta^{18}O$ increased 0.65‰ from middle April to early August, and then dropped 0.72‰ until early May 1977; in some year, however, the seasonal cycle was not remarkable, such as that in 1989-1990 cycle.

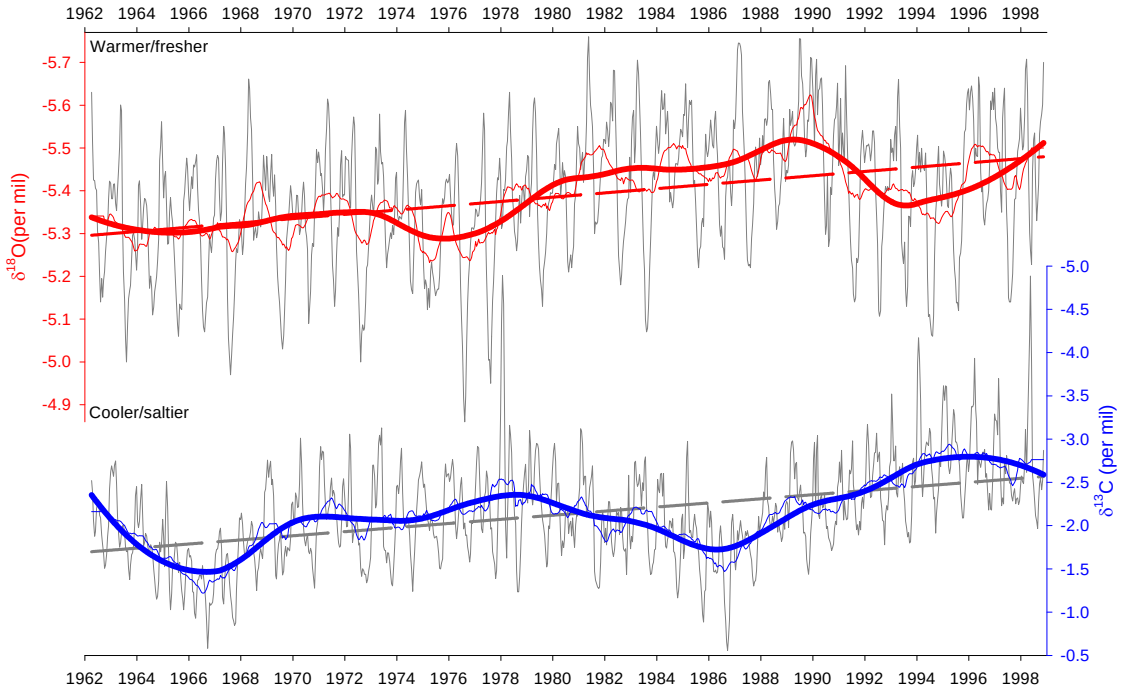

Figure 6.4 Time series of skeletal $\delta^{18}O$ (upper panel) and $\delta^{13}C$ records (lower panel) of modern coral RSM2b. Grey curves represent fortnightly records and black lines represent linear regression to highlight long-term trends. Heavy lines are 10-year Loess (smoothing technique with tricube weighing and polynomical regression) smoothed series to present decadal variability. Thin lines show interannual variability by removing the seasonal cycles using 1-year running average smoothing (red for $\delta^{18}O$, blue for $\delta^{13}C$).

Figure 6.5 presents the coral $\delta^{18}O$ climatology during 1962 to 1998 (red curve with empty circles). The highest $\delta^{18}O$ occurred in winter and the mean of the winter highest was -5.16‰. Coral $\delta^{18}O$ stays around its highest in winter for only a short time, and

then it rapidly drops to summer low level of value and maintains below -5.40‰ for up to 7 months. During the whole summer and autumn, the coral $\delta^{18}O$ keeps decreasing until reach its annual lowest in early May, which is -5.52‰. It is noteworthy that there is a remarkable "hunch" during autumn (Late march through May) because of the extraordinary decrease of coral $\delta^{18}O$. The scale of the "hunch" is 0.06‰ in terms of departure from the mean $\delta^{18}O$ in early March. The average difference between the winter high in early August and summer low in late April is 0.36‰, while the average difference between the winter high and the summer is close to 0.3‰.

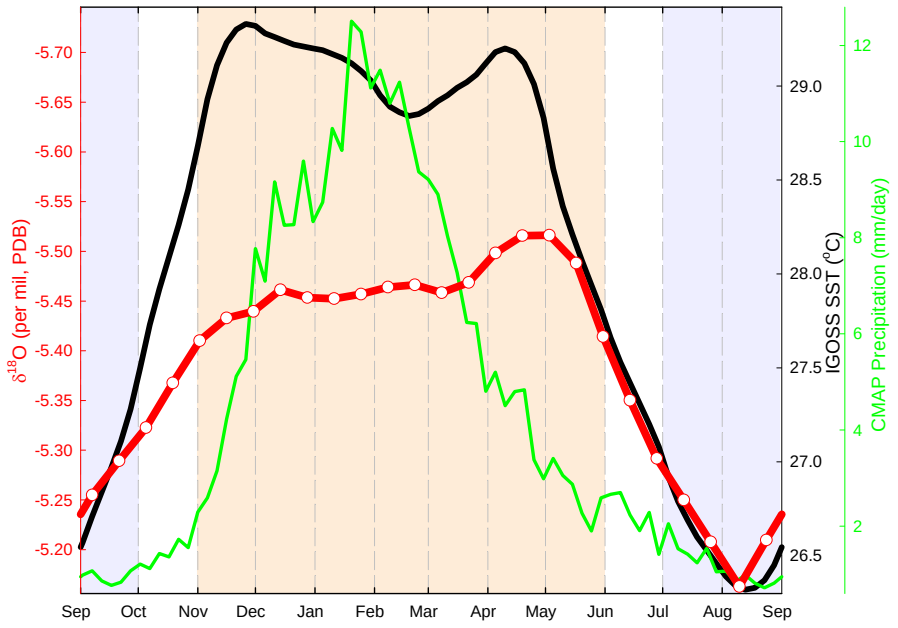

Figure 6.5 Annual climatology of Sumba coral $\delta^{18}O$ (red curve with circles) and comparison with annual climatology of sea surface temperature (SST, black curve) and rainfall (green curve). SST data are from IGOSS [*Reynolds et al.*, 2002] and rainfall data are from CMAP ([*Xie and Arkin*, 1997]. Grey shaded areas represent the austral winter (July to September) and light red shaded area represents prolonged summer (November to May). The vertical scale for $\delta^{18}O$ is adjusted to show the same temperature sensitivity with the SST scale (-0.189‰/℃).

In Figure 6.5, $\delta^{18}O$ is scaled to have the same temperature sensitivity with the SST (-0.189 ‰/^{o}C), which is the average slope of coral $\delta^{18}O$-SST equations from literature around the Indo-Pacific Warm Pool [*Abram*, 2004]). It shows that the 3.1^{o}C seasonal

range in SST would have been expected to result in about a 0.6‰ $\delta^{18}O$ range. Since the observed seasonal cycle of coral $\delta^{18}O$ is only about 0.3-0.36‰, sea water $\delta^{18}O$ must be changing through the seasons in response to changes in salinity around Sumba. Recent data of an assimilation experiment (SODA) shows the seasonal difference in SSS around Sumba is up to 0.4‰ between austral autumn and summer. The average difference of SSS between summer and winter is also up to 0.2‰ (Figure 3.3, [*Carton et al.*, 2005]). Direct measurements of SSS from May 1999 to December 2005 in the Sumba Strait demonstrated that the SSS difference between summer and autumn could be up to 1.5‰, such as the change from 34.2‰ in March to 32.7‰ in May 1996 [*Sprintall et al.*, 2003]. Therefore, salinity variability would play a key role in the Sumba coral $\delta^{18}O$ record.

Figure 6.5 shows that, even though the impressive consistency in changes of the curves between the $\delta^{18}O$ climatology and the SST climatology, minor but arrestive inconsistency of these two curves occurs during the austral summer and autumn time. There are double peaks for SST, while coral $\delta^{18}O$ keeps decreases all the summer and autumn and has a remarkable peak (the "hunch") in autumn.

The relative change in coral $\delta^{18}O$ depends mainly on environmental variations in sea surface temperature (SST) and sea surface salinity (SSS). So, the obvious inconsistency between the Sumba coral $\delta^{18}O$ and SST in summer should result from variations in sea surface salinity. Local rainfall is a reasonable candidate for the source of change in SSS. Analysis of the timing of uncoupling of SST and coral $\delta^{18}O$ and the change in rainfall could help to decide if it is the case. The uncoupling begins in early November when SST continues to rapidly increase while the decrease in coral $\delta^{18}O$ evidently slowed, coincident with the start of rapid increase of rainfall; the uncoupling of the trends of change ends in the middle of February when rainfall begins to decrease rapidly. This indicates that the local rainfall might be connected with the coral $\delta^{18}O$ signal in summer (November through February). On the other hand, it is also possible that it is not be the case either, since the salinity change could result from direct input of water with distinct

salinity during summer. In contrast, the autumn "hunch" in coral $\delta^{18}O$ has nothing to do with the local rainfall because during this time the local rainfall has decreased rapidly 3 months ago and it is impossible that the lagging of the impact of local rainfall resulting from lagged run-off effects after 3 month (our $\delta^{13}C$ average climatology shows that the impact of local rainfall is only 1 month and that includes the impact of both the inflow of its run-off and the lasting turbidity in sea water after the run-off). The raise in SST in autumn cannot be the reason either, because the former raise in summer in SST does not bring so high change in coral $\delta^{18}O$ even plus the positive effect of rainfall during the same time. Therefore, the "hunch" in autumn should result from an inflow of a huge amount of fresh water in autumn. The Sumba coral $\delta^{18}O$ "hunch" coincides with the distinct freshening of sea water in March to May in Savu Sea recorded by instrumental measurement during December 1995 to May 1999 [*Sprintall et al.*, 2003]. Since local SST records a SST peak in the same time, the inflow of outside source should be low-salinity and warm. So the Sumba coral $\delta^{18}O$ annual climatology clearly records an input of a huge amount of low-salinity water of outside source in autumn. In late part of this chapter, analysis on interannual variability of the Sumba coral $\delta^{18}O$ shows that the important source of this fresh water is from the Indian Ocean, not other Indonesian inner seas or the Pacific Ocean.

6.3.3 Interannual variability of coral $\delta^{18}O$ record

6.3.3.1 Substantial interannual variability

Interannual variability of the Sumba modern coral $\delta^{18}O$ record has been shown in Figure 6.1 after the seasonal cycles were removed (the thin red line). Even though the annual change of $\delta^{18}O$ was relatively small during 1962 to 1967, most of the time (1967 to 1998) strong interannual variability is a remarkable character of this coral record. The difference in 1-year running averages between 1967 and 1968 is up to 0.16‰, and that is very nomal for most of the interannual variability during 1967 to 1998. The biggest interannual variability of this $\delta^{18}O$ record occurred during 1989 to 1994, which is 0.3‰

of difference in annual average, and most of the change (0.25‰) happened in less than 2 years (1989 November to 1991 October).

Winter δ^{18}Os in July to September show much greater interannual variability than the annual averages, as shown as remarkable up-and-down in the blue curve in Figure 6.6. The dramatic decrease of winter mean δ^{18}O in some years is among the most conspicuous, such as that in 1968, 1973, 1978, 1984, 1989, 1996, and 1998, the decrease of winter mean δ^{18}O is around 0.25‰ compared with the previous winter. And in 1989, the seasonal cycle disappeared as a result of the vanished winter peak, bringing on a huge difference (0.42‰) of winter mean δ^{18}O in 2 years between 1989 and 1991. In contrast, the winter mean δ^{18}O increased a lot in 1969, 1972, 1976, 1982-1983, 1990-1995, and 1997.

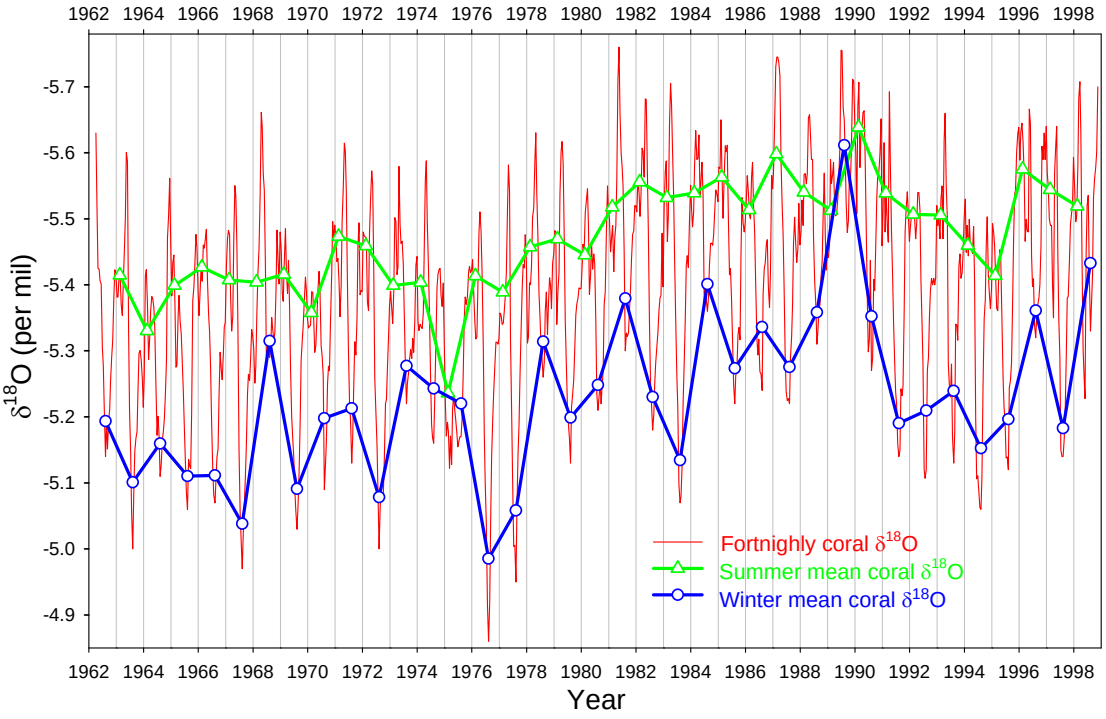

Figure 6.6 Substantial interannual variability of the Sumba modern coral δ^{18}O record. Red line represents the fortnightly δ^{18}O record. Blue line shows the winter mean δ^{18}O during July to September and the green line the summer mean δ^{18}O during November to May. Note that part of the 1975 summer record has been lost because of the wobbly growth of coral during that time (refer to Figure 6.1), so the 1975 summer mean δ^{18}O is not a real record of the climate and oceanography during that time.

Even if the interannual variability in summer mean $\delta^{18}O$ (November to May) is not as dramatic as that of winter mean $\delta^{18}O$, some of the changes are still noticeable (green curve in Figure 6.6). One of them is the lasting increase of mean summer $\delta^{18}O$ during 1991 to 1995, which presents a total increase of 0.22‰ in mean summer $\delta^{18}O$. Another one is the obvious increase of mean summer $\delta^{18}O$ compared with the previous summer in 1964, 1970, 1973, 1977, 1980, 1986, and 1988.

Since the strong interannual variability in winter and summer, the seasonality of the modern coral $\delta^{18}O$ record, accordingly, also has strong interannual variability. In 1976 and 1983, the difference of $\delta^{18}O$ between winter and summer was more than 0.4‰; and in 1963, 1966, 1967, 1969, 1972, 1977, 1982, 1987, 1991, 1992, 1994, and 1997, the seasonal differences were all exceeded 0.3‰. In contrast, in 1998 and 1968, the seasonal changes of $\delta^{18}O$ were less than 0.1‰; and in 1964,1970, 1973, 1974, 1978, 1981, 1984, 1986, and 1988, all the seasonal changes were less than 0.2‰. Extremely, in 1989, the seasonality disappeared, even reversed, the winter mean $\delta^{18}O$ is 0.1‰ lower than that in summer.

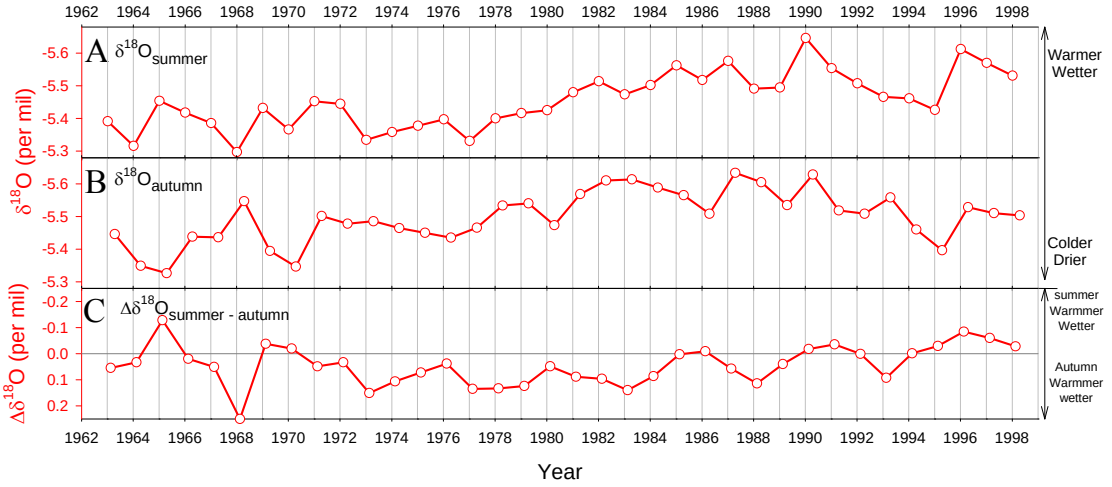

Figure 6.7 Interannual variability of seasonal $\delta^{18}O$ for Sumba coral RSM2b. The summer includes December through February and the autumn refers to March to May.

Figure 6.7 shows the interannual variability of seasonal summer coral $\delta^{18}O$. Both the summer (December through February) and autumn (March to May, the "hunch" in the $\delta^{18}O$ annual climatology) show noticeable interannual variability in 1960s and 1990 and minor interannual variability during 1970s and early 1980s, even the autumn shows stronger variability. The difference between summer and autumn presents strong interannual change only during 1960s, but a strong 5-year periodicity during 1980s and 1990s.

6.3.3.2 Local SST, rainfall and the interannual variability of coral $\delta^{18}O$

The $\delta^{18}O$ record of Sumba modern coral RSM2b is strongly correlated with the local sea surface temperature (r = 0.75, see Figure 6.8A). After seasonality is removed, the correlation decreases but still relatively high (r = 0.50, Figure 6.8B).

However, the correlation is different in summer and winter. Even though the change of winter mean $\delta^{18}O$ is strongly correlated with that of winter mean SST (R = 0.71), the variabilities of $\delta^{18}O$ and local SST among summers only have weak correlation (R = 0.10) (Figure 6.8C and D).

The annual mean $\delta^{18}O$ is also related with local rainfall (R = 0.37, Figure 6.7D), but this correlation only results from the winter (R = 0.61, Figure 6.6C), because summer mean $\delta^{18}O$ is not correlated with the local summer rainfall (R < 0.01).

Figure 6.9 shows the correlation between seasonal coral $\delta^{18}O$ and the local SST and rainfall. Interestingly, the correlation of coral $\delta^{18}O$ with local SST and rainfall reverses in summer and autumn even though the correlations are relatively low (R = 0.20 with rainfall in summer, R = 0.22 with SST in autumn). However, the difference of coral $\delta^{18}O$ between summer and autumn is obviously related with both the differences of local SST and rainfall between early and autumn.

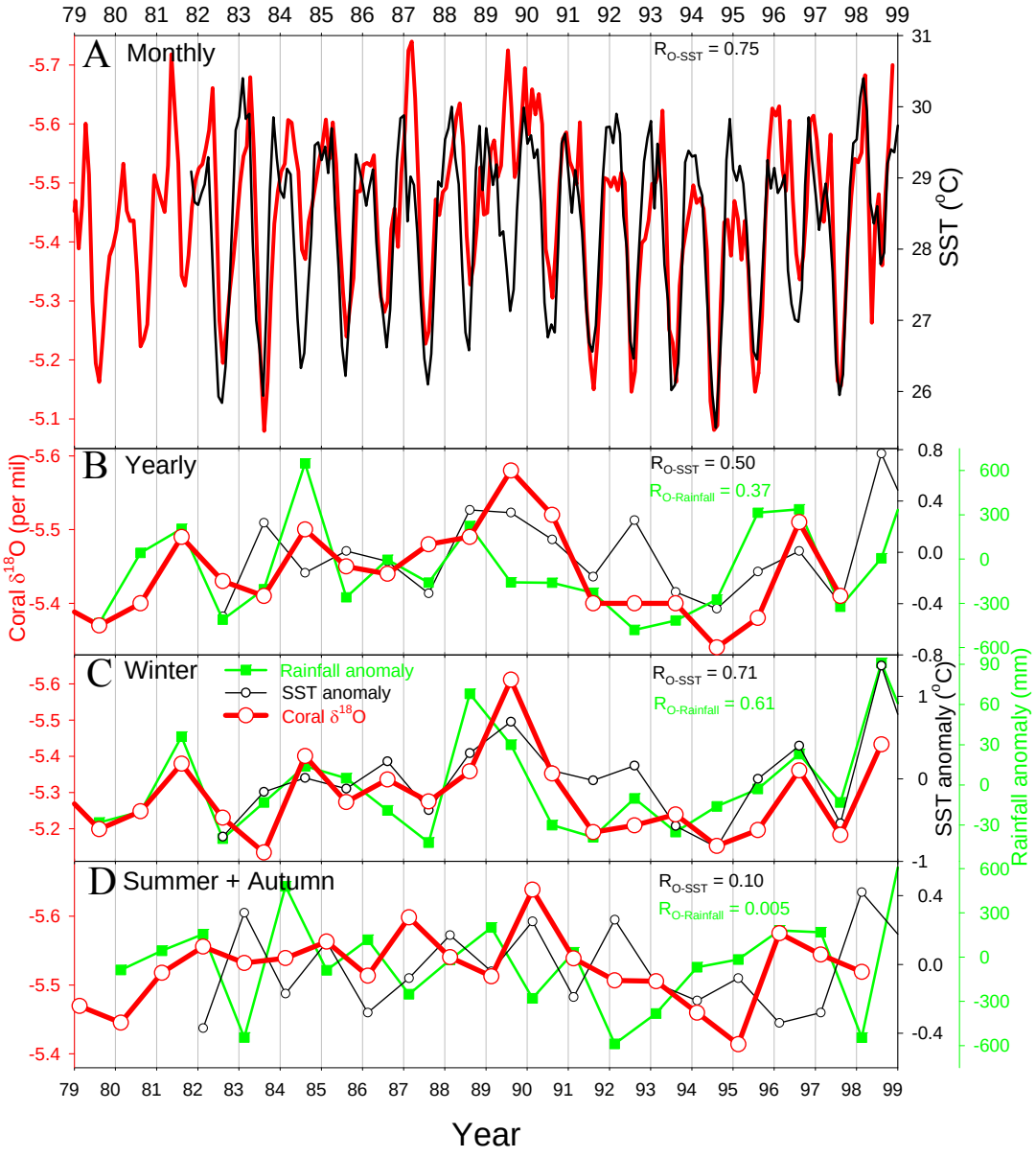

Figure 6.8 Comparison of interannual variabilities between Sumba modern coral $\delta^{18}O$ record and local sea surface temperature and rainfall. (A): Sumba modern coral $\delta^{18}O$ record and local SST record. The coral $\delta^{18}O$ (red curve) is resampled as monthly record for correlation based on the fortnightly coral $\delta^{18}O$ data. The black curve represents local sea surface temperature record (1 by 1 grid centred at 120.5°E and 9.5°S including the study area) from the NOAA optimum interpolation monthly SST data set [*Reynolds et al.*, 2002]. (B) through (D): comparison of winter (July to September), summer and autumn (November to May), and yearly (January to December) records of coral mean $\delta^{18}O$, SST anomaly, and rainfall anomaly. The rainfall records are calculated from the NOAA CMAP precipitation data set version 1 in 2 by 2 grids centred at 121.25°E 8.75°S [*Xie and Arkin*, 1997] including the research area.

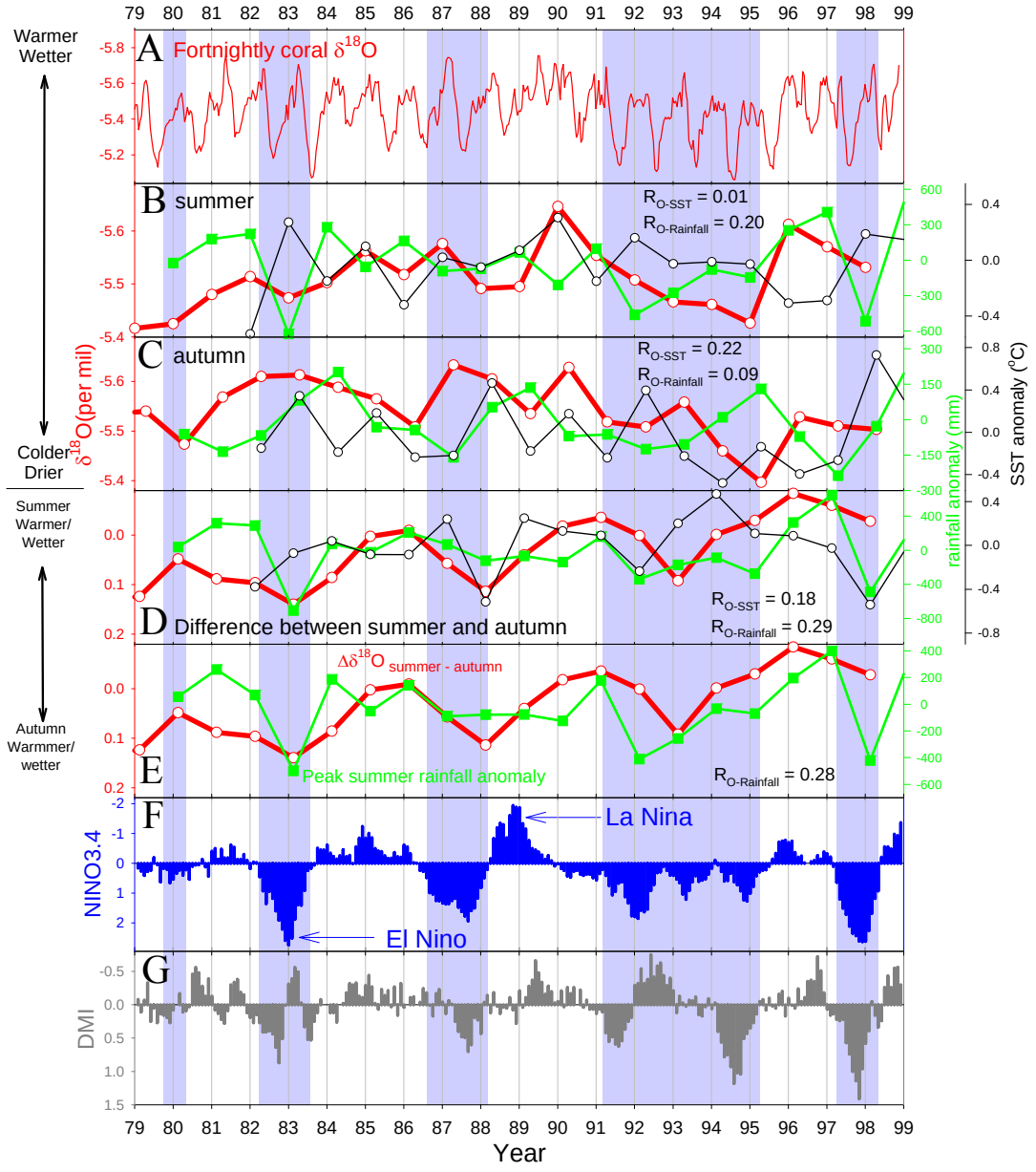

Figure 6.9 Comparison of Seasonal summer $\delta^{18}O$ of coral RSM2b with SST, rainfall, NINO3.4 index, DMI during 1979-1988. The sources of SST and local rainfall are the same as that in Figure 6.8. NINO3.4 index is from the LDEO (Lamont-Doherty Earth Observatory) data set "Extended Nino indices" at http://iridl.ldeo.columbia.edu/SOURCES/.Indices/.nino/.EXTENDED/.NINO34/ [*Kaplan et al.*, 1998], and the DMI (Indian Ocean Dipole Mode Index is from http://iprc.soest.hawaii.edu/%7Esaji/dmi.txt [*Saji et al.*, 1999]. The summer includes December through February and the autumn refers to March to May.

Furthermore, it is correlated with the peak summer rainfall (R = 0.28). This result of correlation between seasonal characteristics of the summer coral $\delta^{18}O$ supports that there is a huge amount of input of outside source water in autumn and that is the reason

why the correlation reversed in early and autumn (Figure 6.9B and C). The obviously increased correlation between the relative decreases of $\delta^{18}O$ from summer to autumn and the rainfall during peak rainfall time (December to February) suggests that the autumn "hunch" in $\delta^{18}O$ is related to rainfall. Since the result also shows that it is not related to the local rainfall, an input of water from outside rainfall source should be a candidate of its cause on the ground that the outside rainfall is related to the local rainfall during the summer peak wet season. Since the whole area around Indonesian maritime continent experiences the north-west monsoon peak season almost in the same time during December through February and the interannual variability in rainfall should be strongly related, the source of the input fresh water from rainfall could be the whole area.

6.3.4 Long-term and decadal variability of coral $\delta^{18}O$

6.3.4.1 Long-term trend and the 1976 shift

Long-term trend towards lower $\delta^{18}O$ values is superimposed on strong seasonal cycles and interannual variability of the 37-year $\delta^{18}O$ record of Sumba modern coral (Figure 6.4). The difference in $\delta^{18}O$ between 1962 and 1998 is 0.18‰. Instrumental record of sea surface temperature (SST) around Sumba from the NOAA NCDC extended reconstructed SST (ESSST) data set Version 2 [*Smith and Reynolds*, 2004], as shown in Figure 6.10, indicates that SST had the same trend and increased by 0.62℃ during the same period of time.

But this temperature increase is not enough to account for all the range of change in $\delta^{18}O$. According to a $\delta^{18}O$-SST dependence of -0.189‰ per ℃, which is a mean of eight published $\delta^{18}O$-SST calibrations for *Porites* sp. from sites where $\delta^{18}O_w$ variations are negligible or have been incorporated in the calibration [see Chapter 3, cited from *Abram*, 2004], the SST increase only accounts for 64% of the whole range (that is 0.12‰ in 0.18‰). The coral record thus implies a freshening of 0.24‰ in salinity during this period based on an average relationship of 0.27‰ $\delta^{18}O$ per 1‰ salinity

[*Fairbanks et al.*, 1997]. This freshening of sea water is associated with the additional decrease of 0.07‰, which is 36% of the whole decrease in $\delta^{18}O$ during this time. Figure 6.10 shows that the freshening mainly happened during the 1980s. Freshening of 1980s in comparison with 1990 in the Indonesian-Australian Basin has also be reported from a recent study of the freshwater content of Indonesian-Australian basin [*Phillips et al.*, 2005].

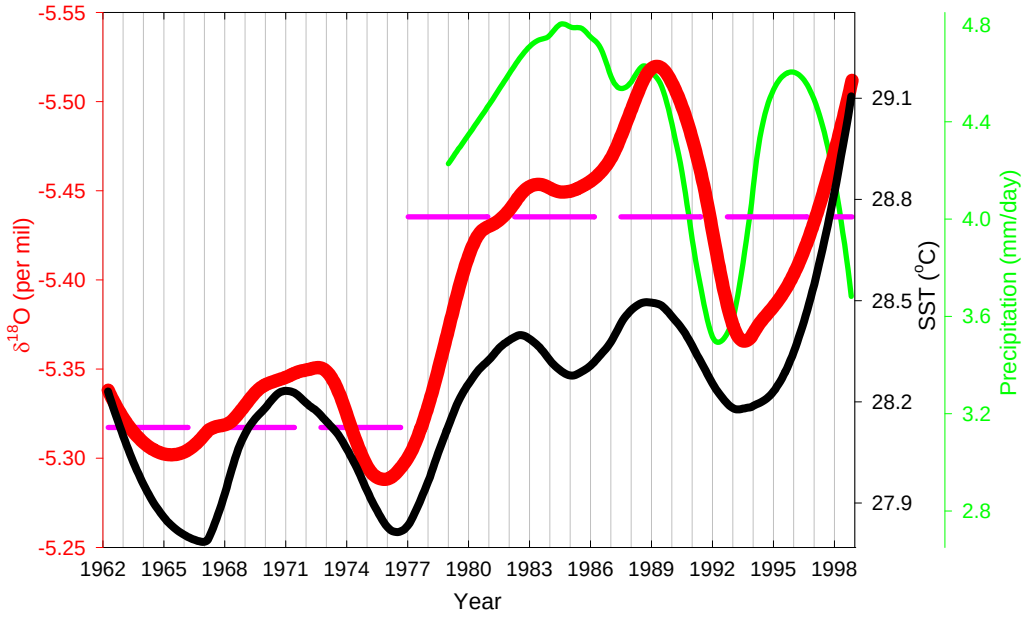

Fig. 6.10 Comparison of long-term trends and decadal variability between coral RSM2b skeletal $\delta^{18}O$ (red lines) and instrumental records of SST (ERSST from the US national Climate Data Center, black lines) [*Smith and Reynolds*, 2004] and rainfall (NOAA CMAP, green lines) [*Xie and Arkin*, 1997] around Sumba, Indonesia. Heavy curves represent 10-year smoothing to highlight decadal variability. Dashed pink lines represent $\delta^{18}O$ means of 1962-1976 and 1977-1998, showing the 1976 climate shift in Sumba. Vertical scale for $\delta^{18}O$ is adjusted to show the same temperature sensitivity with the SST scale (-0.189‰/℃).

Figure 6.4 indicates that most of the Sumba coral $\delta^{18}O$ long-term trend occurred in the 1976 climate shift, which is characterized by a sharp rise in Pacific equatorial temperatures and has been identified as a change in the background state of the El Niño Southern Oscillation [*Trenberth*, 1990; *Graham*, 1995; *Trenberth and Hoar*, 1996; *Rajagopalan et al.*, 1997; *Guilderson and Schrag*, 1998; *Giese et al.*, 2002; *McPhaden and Zhang*, 2002; *Vecchi et al.*, 2006; *Wainwright et al.*, 2008]. The dashed pink lines in

Figure 6.10 show that the difference between the mean $\delta^{18}O$ of 1977-1998 and the mean $\delta^{18}O$ of 1962-1976 is up to 0.12‰, which is significant for a change of average climate.

Nearly two-thirds of the Sumba coral $\delta^{18}O$ trend resulted from the 0.6℃ increase in sea surface temperature. The 0.6℃ increase of SST in the study area is the same as increase of the average global surface air temperature during the same time ([*Jones and Mann*, 2004]. It also coincided with the 0.6℃ SST increase in the eastern part of the Indo-Pacific Warm Pool in central Pacific [*Urban et al.*, 2000]. Even though individual El Niño events make SST cooler in Sumba and more El Niño has happened since 1976, the long-term trend of Sumba SST seems more likely affected by the background climate which has been regarded as a result of increased anthropogenic activity [*Jones and Mann*, 2004; *Meehl et al.*, 2004]; the SST long-term trend in Savu Sea is likely related to the SST background trend in the Pacific which is one of the source area of inflow around Sumba through the Indonesian Throughflow. In the following parts of this chapter, our coral $\delta^{18}O$ record would show that the Indian Ocean input into the Savu Sea would have dominant influence on the SST and salinity due to remarkable inflow of very warm, low-salinity South Java Current (SJC) during November through May. So it is possible that increased input of the SJC could also contribute to the long-term trend of SST increase.

6.3.4.2 Strong decadal variability and salinity reconstruction

The same impressing as the long-term trend in the Sumba coral $\delta^{18}O$ record is the remarkable decadal variability, as shown as change in the heavy curves in Figures 6.4 and 6.10. Remarkable increase of $\delta^{18}O$ in 1970s and 1990s and decrease of a period up to 10 years in 1980s are 3 periods of major decadal variability. The dramatic increase of $\delta^{18}O$ in 1991 to 1995 is one of the most conspicuous multiannual variability of Sumba coral $\delta^{18}O$ record (Figure 6.4). The increases in $\delta^{18}O$ are 0.06‰ during 1972 to 1975, and 0.15‰ during 1989 to 1993 in the curve of decadal variability. The difference in $\delta^{18}O$ between 1975 and 1989 is up to 0.23‰.

By comparison of $\delta^{18}O$ and SST records, Figure 6.10 shows that changes in SST control most of the variability of Sumba $\delta^{18}O$ record: all the cooling of SST in mid-1960, mid-1970, mid-1990, even minor mid-1980 cooling had been reflected by the Sumba $\delta^{18}O$ record. However, uncoupling of the $\delta^{18}O$ and SST curves since the late 1970s until early 1990s indicates that, even though the increase of $\delta^{18}O$ during 1970s was more likely resulted mainly from SST cooling, freshening in salinity would play a much more important role in decreasing coral $\delta^{18}O$ during 1975 and 1992.

The mid-1970s $\delta^{18}O$ increase seems to be mainly connected with the SST decrease. According to the $\delta^{18}O$-SST dependence of -0.189‰ per ℃, the cooling in Sumba could be up to 0.3℃, the same as reflected by the instrumental ERSST records [*Smith and Reynolds*, 2004]. A 1970s SST cooling has also been recorded by a central tropical Pacific coral with the same amplitude of roughly 0.3℃ [*Cobb and Charles*, 2001]. And 1970s air temperature cooling has also been recorded in many places. This could be another example of the strong influence of global background climate on the Savu Sea. Freshening of sea water became a more important factor in affecting the coral $\delta^{18}O$ decadal variability in Sumba during late 1970s and the whole 1980s. From early 1990s, both cooling in SST and saltier surface water contribute to the remarkable increase in coral $\delta^{18}O$. The instrumental record indicates that the cooling during this period of time was about 0.3℃, which equals 0.06‰ of increase in $\delta^{18}O$. So the extra increase of 0.09‰ in $\delta^{18}O$ could be explained as increase of 0.3‰ in salinity in the early half of 1990s. Even the impressive increase of Sumba coral $\delta^{18}O$ in the early half of 1990s seems to be associated with the unprecedented 1990-1995 El Niño event, our result of coral $\delta^{18}O$ analysis in the following part of this chapter supports that the decrease in the input of warm, low-salinity water from the SJC during this time might be the main reason for the coral $\delta^{18}O$ increase. The eruption of the volcano Pinatubo in June 1991 could also contributed the cooling of early half of 1990s [*Gagan and Chivas*, 1995].

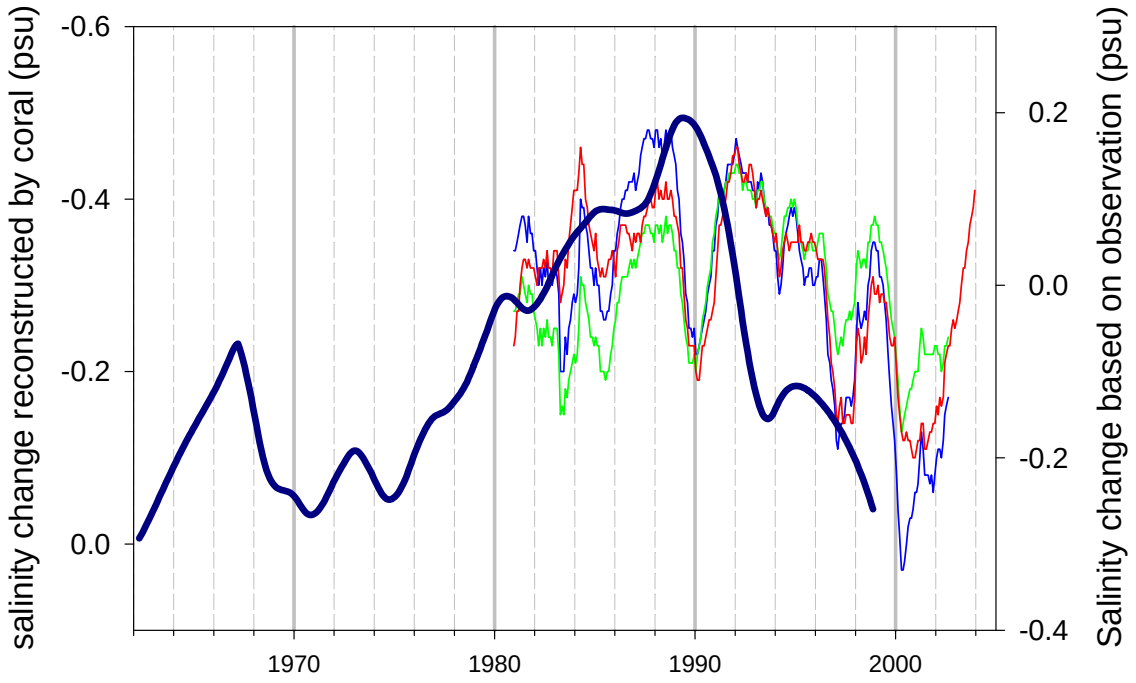

Figure 6.11 Variability of the sea surface salinity (dark blue curve) in the Savu Sea during 1962 to 1998 reconstructed from the Sumba coral $\Delta\delta^{18}O$ by removing the SST effect. Reconstruction is based on the coral $\delta^{18}O$ and the SST curves in Figure 6.10 using the $\delta^{18}O$-SST dependence of -0.189‰/°C and the $\delta^{18}O$-SSS dependence of 0.273‰/psu [*Fairbanks et al.*, 1997]. Also illustrated are the predicted salinity changes of the upper 180 m in the Australian-Indonesian Basin from NCEP (red thin line), ERA (blue) and ERA corrected (green) P-E data reanalysis [*Phillips et al.*, 2005]. The data were kindly provided by H. Phillips and S. Wijffels. Note that even though their records are high-resolution data with strong interannual variability, and the interannual variability of the Sumba coral reconstructed SSS record has been suppressed, both indicate the same decadal variability (and amplitude) in the overlapped periods.

Based on the uncoupling of the curves of SST and $\delta^{18}O$ in Figure 6.10, the history of variability in the sea surface salinity in the Sumba Strait during 1962 to 1998 could be reconstructed by removing the temperature effect (using the $\delta^{18}O$-SST dependence of -0.189‰/°C and the $\delta^{18}O$-SSS dependence of 0.273‰/psu), as shown in Figure 6.11. The reconstructed salinity curve shows a strong freshening happened during mid-1970s to 1989 and the change range was more than 0.4 psu. The same range of increase in salinity happened during 1990 to 1998 but this change is much quicker. In 1998, the salinity is almost the same as that in mid-1970s. The trend of increased salinity in the

Sumba Strait during 1990 to 1998 is consistent with that in the Australian-Indonesian Basin and the range of change is also comparable (Figure 6.11) [*Phillips et al.*, 2005]. Their result started from 1980 and also showed a freshening trend during 1980 to 1987, consistent with part of this coral reconstructed salinity record in the Savu Sea during 1974 to 1989.

Even though the strong 1989 freshening coincided with a strong rainfall from a La Niña and a negative Indian Ocean Diploe event, there was no significant La Niña event happened in other years during the whole 1980s; in contrast, there are 2 very strong El Niño happened in 1982-1983 and 1987. Then single ENSO event is not the main reason of the freshening in the 1980s. In fact, the rainfall change around the Indonesian maritime continent resulting from the monsoon, ENSO, and IOD have evident influence in the interannual variability of the salinity in the Savu Sea (Figure 6.10, 6.11), but the main reason for the decadal or multidecadal variability of the salinity in the Savu Sea is not the rainfall around the Indonesian maritime continent. Strong freshening of sea water in the central Pacific since 1976 has been recorded by coral $\delta^{18}O$ records and decrease in salinity of 0.6‰ to 0.8‰ have been attributed to more rainfall or the eastward expansion of the warm pool because of more El Niño events since 1976 [*Urban et al.*, 2000; *Cobb and Charles*, 2001]. Since the Indonesian Throughflow (ITF) brings up to 10 Sv (1 Sv = 10^6 m^3 s^{-1}) of tropical Pacific water into the tropical Indian Ocean [*Gordon*, 2005] and 4.5 Sv of the ITF exits into the Indian Ocean by Savu Sea [*Molcard et al.*, 2001b], the decadal change in salinity of the Pacific water could possibly influence the decadal salinity of the Savu Sea. As mentioned above, the following parts of this chapter would show strong input of the warm, low-salinity SJC water into the Savu Sea during November to May. So the freshening of the Savu Sea would also possibly indicate a decadal variation in input of the SJC water. This could be proved by the strong increase of salinity of the Savu Sea in 1991 to 1995 which coincides with the remarkably decreased penetration of the very fresh Kelvin wave forced in the tropical Indian Ocean.

6.3.5 $\delta^{13}C$ record of Sumba modern coral RSM2b

6.3.5.1 Annual cycles of Sumba coral $\delta^{13}C$

$\delta^{13}C$ record of Sumba coral RSM2b has strong annual cycles as shown in Figure 6.4. For most of the years, the heaviest $\delta^{13}C$ value occurs in the late part of a year (around October), and two peaks of lighter $\delta^{13}C$ values in the early part and the middle of a year, respectively. Figure 6.12 presents the climatology of the Sumba $\delta^{13}C$ from 1962 to 1998. The $\delta^{13}C$ mean reaches its annual maximum of -1.62‰ in early October, but drops rapidly until late February to its annual minimum of -2.61‰. There is a minor decrease in May and June during its increase to the next annual maximum in October. The average range of annual change is almost 1‰, and the difference between the secondary minimum in June and the annual maximum in October is also up to 0.65‰.

In contrast with coral $\delta^{18}O$, coral $\delta^{13}C$ records are usually irregular and difficult to explain. The reason is that coral $\delta^{13}C$ generally has a complicated relationship with environmental and physiological variables. Potential influences mainly include $\delta^{13}C$ of reef dissolved inorganic carbon (DIC) [*Swart et al.*, 1996], light related photosynthetic modulation of the isotopic composition of the coral internal DIC pool [*Weber and Woodhead*, 1970; *Fairbanks and Dodge*, 1979; *Swart*, 1983; *McConnaughey*, 1989; *Wellington and Dunbar*, 1995; *Swart et al.*, 1996], symbiotic relationship between corals and zooxanthellae [*Porter et al.*, 1989; *Carriquiry et al.*, 1994; *Allison et al.*, 1996], heterotrophic vs autotrophic feeding [*Carriquiry et al.*, 1994; *Swart et al.*, 1996; *Felis et al.*, 1998], coral spawning [*Gagan et al.*, 1994; *Gagan et al.*, 1996], colony topography [*Cohen and Hart*, 1997], and kinetic effects associated with the rate of coral growth/calcification [*McConnaughey*, 1989; *de Villiers et al.*, 1995; *Allison et al.*, 1996; *Cohen and Hart*, 1997; *McConnaughey*, 2003].

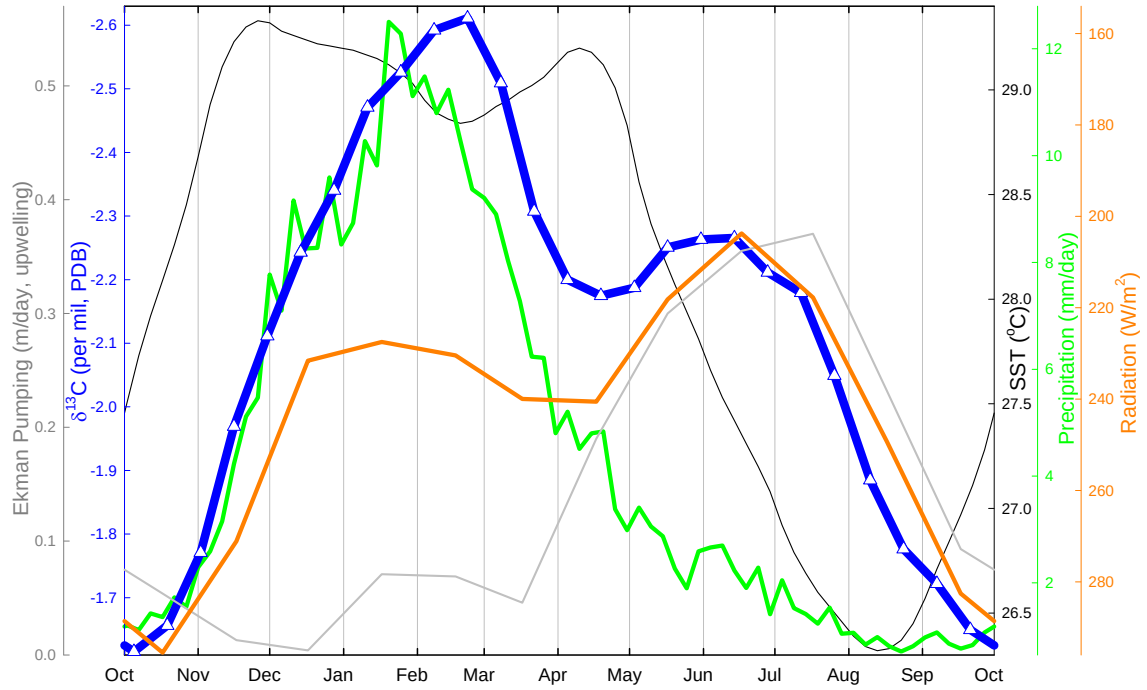

Figure 6.12 Annual climatology of coral $\delta^{13}C$ (blue curve with triangles) and comparison with annual climatology of sea surface temperature (SST, black), rainfall (green), incoming short-wave radiation (orange), and Ekman pumping in the Savu Sea (grey). SST data are from IGOSS [*Reynolds et al.*, 2002], rainfall data are from CMAP ([*Xie and Arkin*, 1997]. Radiation data is from *Atlas of Surface marine data 1994* [*da Silva et al.*, 1994]. Ekman pumping data is from Potemra *et al.* [*Potemra et al.*, 2003].

Even though this complication, the Sumba $\delta^{13}C$ mean climatology seems to have a relatively simple and straightforward relationship with light and nutrient availability. Figure 6.12 puts together major environmental variables and compares them with the Sumba coral $\delta^{13}C$. Unlike Sumba $\delta^{18}O$ mean climatology, Sumba $\delta^{13}C$ mean climatology has no correlation with the sea surface temperature mean climatology. Instead, it strongly correlated with local incoming short wave radiation and rainfall mean climatology. The strong correlation between the coral $\delta^{13}C$ and local incoming short-wave radiation lies in that they have almost the same timing of up and down with mean climatology curves (Figure 6.12). When radiation reaches its annual maximum, the coral skeleton is the most depleted in ^{13}C in October; when radiation experiences annual lowest in June, the coral produces skeleton with the secondary minimum in $\delta^{13}C$ the same time. During that time, the ranges of change for them are also comparable.

However, during the whole wet season from late October through next May, their ranges of change are no longer comparable even though the timings of their changes are still strongly correlated. During that time, instead, the coral $\delta^{13}C$ strongly correlated with local rainfall. It is exactly synchronous for decrease of $\delta^{13}C$ and the increase of local rainfall from middle October through middle January. Noticeably, there are two small but evident inconsistencies between the two correlations. One is an inconsistency of timing: a lagging about 1 month occurs for the arrival of the annual lightest $\delta^{13}C$ in late February and the following increase of $\delta^{13}C$ behind the arrival of annual rainfall maximum in Late January and the following decrease of rainfall until early April; Another one is an inconsistency in range of change between the decrease of radiation and the coral $\delta^{13}C$ from middle April to middle June. Both the inconsistencies help us to attribute the annual $\delta^{13}C$ change to local light and nutrient availability.

The control of light on coral $\delta^{13}C$ has been observed by many previous researches [*Weber and Woodhead*, 1970; *Erez*, 1978; *Fairbanks and Dodge*, 1979; *Swart*, 1983; *McConnaughey*, 1989; *Wellington and Dunbar*, 1995; *Swart et al.*, 1996] and the following mode has been generally believed that coral calcification takes place from an internal inorganic carbon pool [*Erez*, 1978; *Swart*, 1983; *McConnaughey*, 1989]. This pool is composed of carbon derived from the ambient seawater and respiration and modified by fractionation during CO_2 uptake by photosynthesis. The zooxanthellae photosynthesis preferentially fixes ^{12}C and leave behind ^{13}C, increases in the rate of photosynthesis therefore enrich carbon isotope ratio of the skeleton. The incoming short-wave radiation is highly correlated with incoming photosynthetically active radiation and the change of availability in incoming short-wave radiation would change the photosynthetic activity of Sumba coral's endosymbiotic zooxanthellae, and then change $\delta^{13}C$ of Sumba coral skeleton.

But our result indicates that the correlation between light availability and the skeletal $\delta^{13}C$ in this Sumba coral works very well only when the local rainfall is at a low lever (less than 2 mm/day during Mid-June to mid-October, averagely). The decrease of

radiation raised from increased cloud cover during wet season is not enough to explain all the range of the increase in the coral $\delta^{13}C$, because of the following two reasons: one is the range of the change is not enough; another one is the timing of the maximum cloudiness which is one month before the lightest $\delta^{13}C$. Turbidity resulting from land run-off during or after rainfall might also be a possible reason for the decrease of coral $\delta^{13}C$ because it could dramatically decrease the light availability for the symbiotic algae and it could meet both the above-mentioned condition in range and timing of change. This modern coral grew under strong influence of flood plumes of the local main river, the Mondu River. Even though the coral site is 3 km northwest from mouth of the river and 500 m offshore, it was still within the huge flood plumes of the river in summers because of the northwest direction of the water outflow and strong rainfall in summer (the mean summer peak rainfall from 1979 to 2005 is up to 925 mm in December, January and February). Long time of winter dry-season and focused summer strong rainfall makes the outflow in summer extremely turbid and brings huge amount of terrigenous particulate inorganic and organic matter into the sea. However, our result does not support the scenario that decreased light resulting from the turbidity is the major cause for the extremely low value in the Sumba coral $\delta^{13}C$ during the peak time of summer rainfall even though it could be a minor cause or one of the triggers for this change, since if decreased light was the main reason, that means the only major source of energy input for coral decreased dramatically, and then the growth of the coral should had been inhibited during that time. Our result of density analysis, however, shows that the growth of the coral during that time was enhanced, instead of inhibited (see next section 6.3.4.2). As rainfall reaches its annual peak, coral RSM2b grew more quickly as shown by a greater rate of extension and a gradually decreased skeletal density until a substantially low density band formed in the same time when the coral $\delta^{13}C$ reached its annual minimum during late February to early March. The occurrence of this dramatically increased rate of extension means that there was remarkable increase of energy input other than solar light during that time. We propose that the increased feeding of coral host (polyp) on terrigenous nutrients is the major cause of formation of the light skeletal $\delta^{13}C$ peak during summer wet season in the Sumba coral RSM2b.

We think increased feeding of the Sumba *Porites* coral resulted from the impaired zooxanthellae photosynthetic activity and the reinforced input of terrigenous nutrients during summer wet season. Even though the symbiotic algae could provide their coral host with up to 100% of its daily metabolic energy requirements [*Muscatine et al.*, 1981] and in most circumstance they provide most part of them [*Grottoli et al.*, 2006], researches have demonstrate that their photosynthetic activity could decrease even totally lose under some environmental stresses, such as elevated temperature and light [*Porter et al.*, 1989; *Jokiel and Coles*, 1990; *Fitt et al.*, 2000]. In Sumba, at least 3 factors could impair the photosynthetic activity of the symbiotic algae during summer time. (1) Elevated temperature, which could be the main cause for formation of the "stress band" during October and November (see next section 6.3.4.2); (2) decrease in light availability because of increase in turbidity or (3) increase of cloudiness during rainfall peak time in December through next March. The decrease of the rate of zooxanthellae photosynthetic activity could results in decrease in intake of ^{12}C from the coral inner DIC pool and increase of precipitation of ^{12}C in coral skeleton [*Swart*, 1983; *McConnaughey*, 1989]. We think the decreased light input could only be a minor contributor for the light coral $\delta^{13}C$ during December to March in Sumba. Most importantly, it could trigger the stress response of coral animal to increase the feeding of terrigenous nutrients to meet their daily metabolic energy requirements. Our density analysis demonstrates that increased rate of growth of coral RSM2b coincided with the rainfall-derived terrigenous nutrient boom, showing strong connection between active metabolism with increased input of nutrients. Most recently, Grottoli *et al* [*Grottoli et al.*, 2006] have found that some coral species could meet more than 100% of their daily metabolic energy requirements by markedly increasing their feeding rates and CHAR (per cent contribution of heterotrophicaaly acquired carbon to daily animal respiration) when coral loss its photosynthetic energy input from the symbiotic zooxanthellae. *Porites* colonies can switch from autotrophy to heterotropy depending on food availability and this plays an important role in interannual skeletal $\delta^{13}C$ variability [*Felis et al.*, 1998]. Anthony [*Anthony*, 1999; 2000] found that coral from the inshore GBR have a greater capacity to feed on suspended sediment than the same species

living in the midshelf, suggesting a heterotrophic adaptation to the turbid coastal conditions. Risk *et al.* [*Risk et al.*, 1994] also discovered that the coral $\delta^{13}C$ trend across the GBR shelf may result from shifting levels of autotrophy with changes in water turbidity. So it is reasonable to speculate that the increased availability of terrigenous nutrients and the decreased photosynthetic activity could dramatically change the proportions of heterotrophic to autotrophic feeding of the Sumba coastal coral. And that dramatic change should in turn result in severe depleting in ^{13}C in coral skeleton in the peak wet season because C_3 plant-dominated, land-derived organic matters are characteristically depleted in ^{13}C (typically around -26‰ in $\delta^{13}C$) relative to marine organic matters (typically around -15‰ in $\delta^{13}C$) [*O'Leary*, 1981; *Gagan et al.*, 1987; *Goni et al.*, 1997].

The one month lagging of carbon $\delta^{13}C$ behind the rainfall contributes to the speculation in that river runoff may continue a short time after the rainfall peak, and importantly, the turbidity would last a longer time (up to 1 month at first and then the lagging decrease to half a month in March, see Figure 6.12) after the rainfall peak, so the land nutrients and terrigenous carbon in food chain could last for some time in Sumba coastal reef environment, such as one month. Even though we attribute the main reason for the secondary minimum of coral $\delta^{13}C$ during mid-April through mid-July to local radiation minimum, the inconsistency in the early part of this peak should partly be attributed to the remained level of rainfall (more than 2 mm/day) during that time and input of terrigenous nutrients made the coral $\delta^{13}C$ more depleted than radiation should be.

Figure 6.12 also shows the comparison between the coral $\delta^{13}C$ and Ekman pumping mean climotology in Savu Sea [*Potemra et al.*, 2003]. It shows that the monsoonal wind-driven Ekman up-welling might not be the major cause of the depleted peak of the coral $\delta^{13}C$ mean climatology during May and June, but we could not exclude minor contribution of upwelling prevailing during May to July. Rosenfield *et al.* provided direct evidence that coral could digest the sediment's organic fraction [*Rosenfeld et al.*, 1999]. The monsoonal wind-driven upwelling re-suspends the bottom terrigenous

matter and reduces the water clarity. It could have the same effect on coral $\delta^{13}C$ as that of rainfall peak on the Sumba coral if the upwelling is strong enough in some year, such as that in June 1998. The extraordinarily light value of the Sumba coral $\delta^{13}C$ in June 1998 might result from a strong upwelling, because there was no strong rainfall at that time, instead, it coincided with an dramatic SST decrease as shown by the heavy $\delta^{18}O$ (refer to Figure 6.4).

6.3.5.2 Sumba coral density rhythms and its correlation with $\delta^{13}C$ record

Sumba modern coral RSM2b shows very clear density banding; especially a sound annual lowest-density band in early part of a year makes it very easy to distinguish annual cycles from an X-ray photo of coral skeleton (Figure 6.1). In the upmost section which is the straightest part of this coral parallel with coral growth axis, these lowest-density bands formed in January to April (mean for 1988 to 1998 is March 3, $\pm$35 day, 2σ, n=11), coincident with the late austral summer wet seasons, just after the annual rainfall maxima (Figure 6.13). Furthermore, the annual highest density bands appear immediately after the annual lowest density bands, i.e., both the lowest and highest density banding formed during late austral summer wet seasons. This observation is different with some Panama *Porites* modern corals in which the low density bands formed during annual dry seasons resulted from the higher rates of photosynthesis and greater extension rates triggered by decreased cloud cover [*Linsley et al.*, 1994]. This difference may imply the unique of density banding of this Sumba coral.

By careful observation, it could be found that, typically, there are 5 bands occur in every year even some more fine bands could be identified in some years, as shown in Figure 6.14A and B. Band I is the above-mentioned lowest-density band, and band II is the highest-density band. Band III is a low-density band and then band IV is another high-density band. Band V is a low-density band and gradually changes to the lowest-density band (band I) of next year.

This density rhythm pattern in this sumba modern coral is very special. Barnes and

Lough have noticed that almost all the published papers on coral density banding describe the annual pattern as one band of higher density and one of lower density [*Barnes and Lough*, 1989], even in corals with 12 or more fine bands which group together to form this kind of annual band couplet [*Buddemeier*, 1974; *Barnes and Lough*, 1989]. So the Sumba modern coral is very rare in that it has 2 dense bands and 2 less dense bands (the exceptional low-density band is an extreme case of less dense band) in a certain year. Part of the reason of the recognition of this fine pattern is its unusual rate of growth, in many years it is around 20 mm/year.

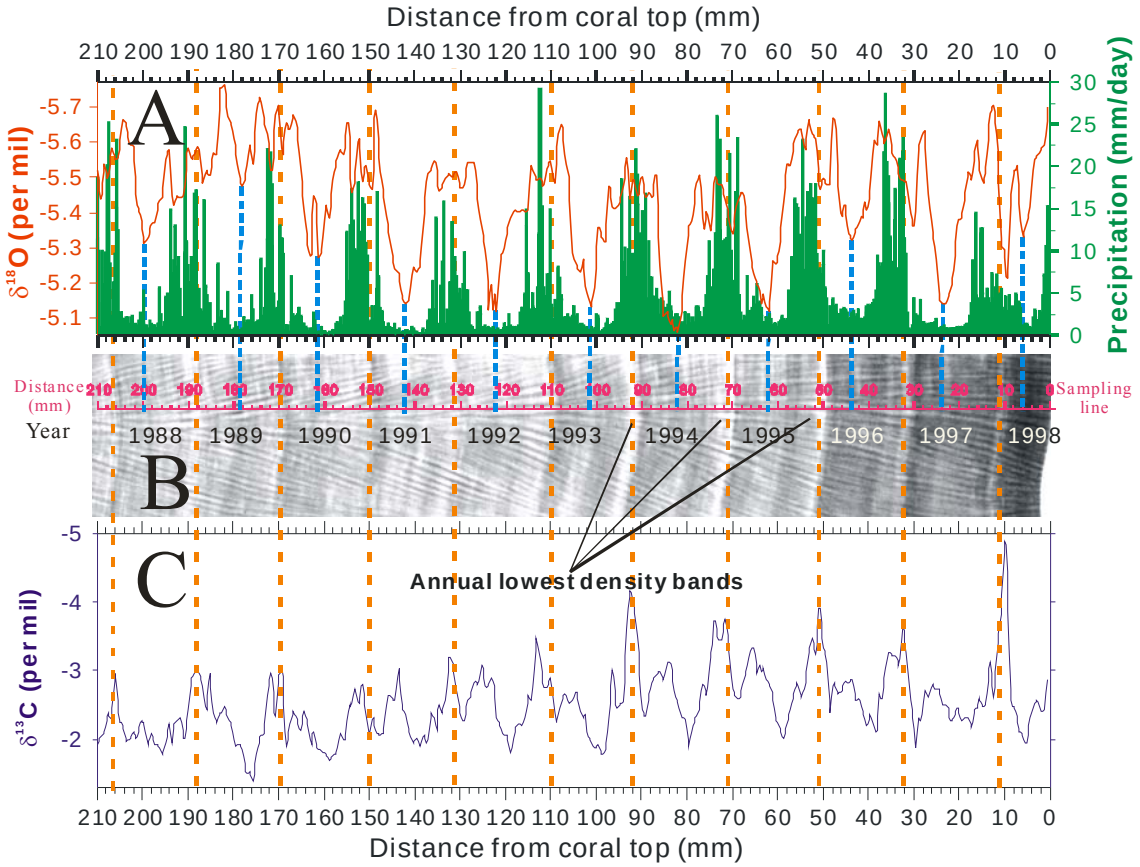

Figure 6.13 Modern *Porites* coral RSM2b density banding compared with $\delta^{18}O/\delta^{13}C$ records and the rainfall. Orange lines go through the annual lowest density bands on the sampling transect and the blue lines correspond with the annual maximum of coral $\delta^{18}O$.

Figure 6.13C shows that the lowest-density bands correlate very well with one of the peaks of the annual minimum of coral $\delta^{13}C$. They correspond to or immediately after these peaks which are located in the early part of a year related with summer rainfall

peak (see the previous section about annual cycles of $\delta^{13}C$). In fact, all the 5 bands are corresponding to different stages of the annual $\delta^{13}C$ cycle. Figure 6.14B and C show a detailed example for this correspondence and Figure 6.15 shows a summary of correlation between Sumba coral density rhythms and coral mean climatology.

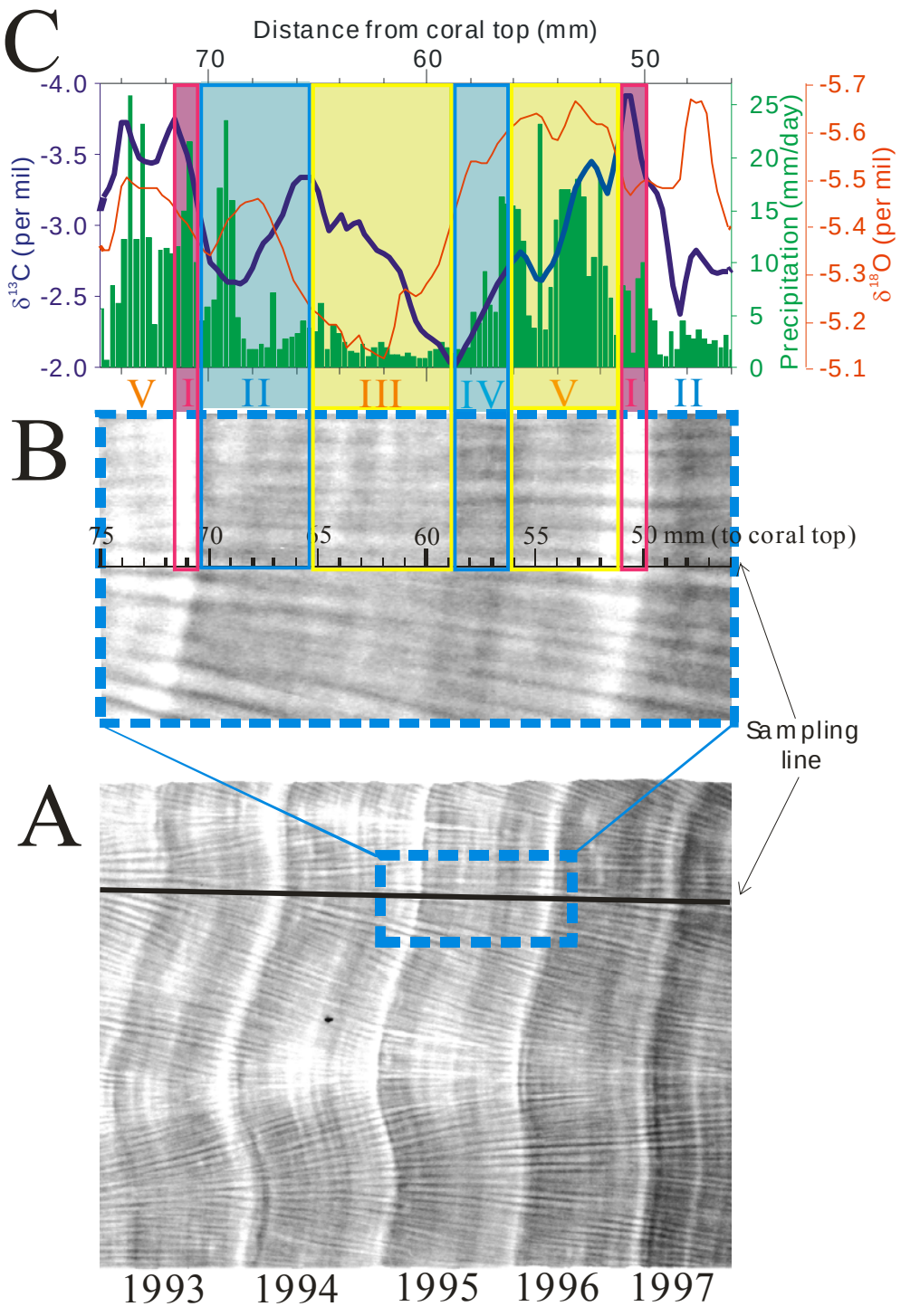

Figure 6.14 Detailed comparison of density rhythm with d13C/d18O records and rainfall. A: X-ray image of coral section 1993-1997. B: enlarged X-ray image of coral density banding in 1995.

The lowest-density band I corresponds to annual minimum $\delta^{13}C$ peak or immediate after it in late February and early March. The highest-density band responds to period after that until the secondary minimum $\delta^{13}C$ peak which is related to the annual radiation minimum (see the previous section). The low-density band III centred at the mid-winter, coinciding with lower annual SST and heavier $\delta^{18}O$. It also coincides with the increase of coral $\delta^{13}C$ from its annual secondary minimum to its annual maximum. The second high-density band (band IV) corresponds to the early part of coral $\delta^{13}C$ decrease companying the increase of summer rainfall but stops when $\delta^{13}C$ reaches some value at low level in late November. From this point the skeletal density starts to decrease gradually and the low-density band V starts. The skeletal density decrease to a very low level in mid-February coinciding with the coral $\delta^{13}C$ and that is the next lowest-density band.

Like coral $\delta^{13}C$, coral growth (skeletal density, linear extension rate, and calcification rate) varies with different marine environments (mainly including temperature, light, nutrient availability, water turbidity, sedimentation, and hydraulic energy. See reviews in [see reviews in *Lough and Barnes*, 1997; *Lough and Barnes*, 2000]. Even though extensive research has been conducted since the discovery of annual density banding patterns in massive coral skeletons by Knutson et al. [see reviews in *Knutson et al.*, 1972], the conclusions have not always been in agreement. It seems likely that the sensitivity of corals to their environment varies with species and location [*Lough and Barnes*, 1997], and extension, density and calcification do not necessarily increase or decrease in concert in response to the changes in environmental conditions [*Dodge and Brass*, 1984]. However, many studies have shown that, at least for *Porites*, extension rate is inversely related to average skeletal density [*Lough and Barnes*, 1992; *Scoffin et al.*, 1992; *Lough and Barnes*, 2000], and is directed linked with calcification rate [*Dodge and Brass*, 1984; *Grigg*, 1997; *Lough and Barnes*, 2000]. Therefore, in this study we assume that the denser bands of the Sumba *Poretis* coral represent lower extension rate and are linked with lower calcification rate, i.e. lower coral growth; while less dense banding including the lowest-density band represent higher extension rate

and higher calcification rate, i.e. higher coral growth.

The unique complicated density pattern of Sumba coral provide an opportunity to further evaluate the environmental influence on coral growth, and the correlation between coral $\delta^{13}C$ and density banding could allow use of both characteristics to extract environmental information from Sumba fossil corals.

Just like the analysis of coral $\delta^{13}C$, in order to simplify comparison and find the major cause, annual mean climatologies of various environmental variables were applied and compared, as shown in Figure 6.15. Unlike the Sumba coral $\delta^{13}C$ climatology, which is basically controlled by the local radiation and the radiation control is sharply interrupted by strong rainfall in summer, the Sumba coral density banding seems to be mainly controlled by local sea surface temperature and this SST control is also intensively interrupted by local strong summer rainfall.

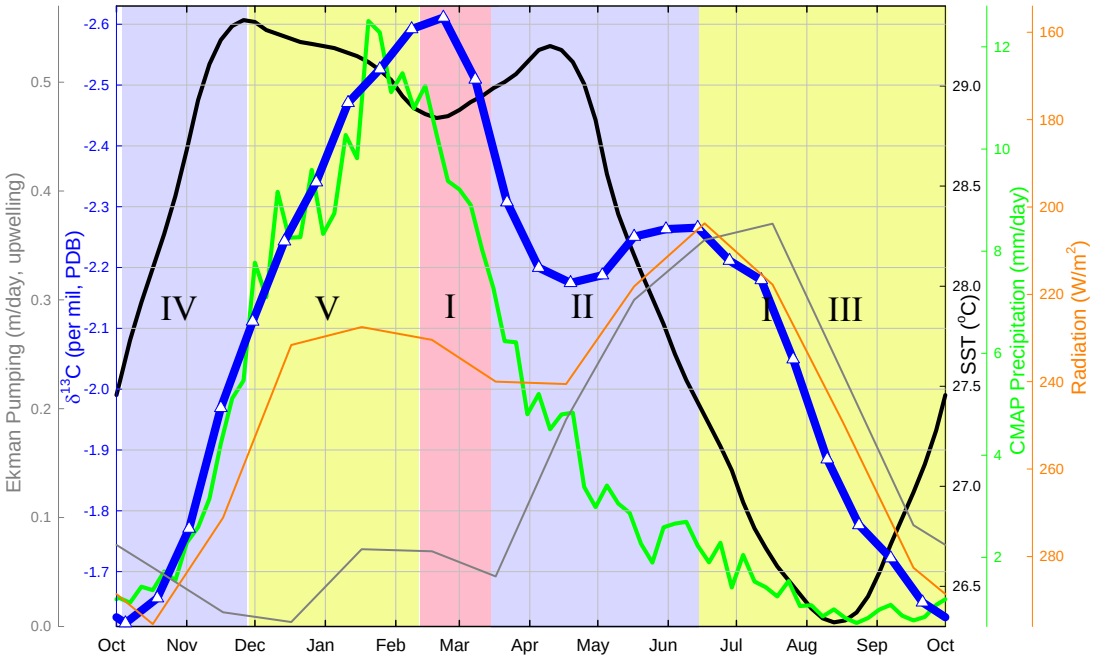

Figure 6.15 Summary of relationship between coral RSM2b's density banding and annual climatology of various environmental variables. Shaded areas are different density bands: pink areas are the lowest-density bands, yellow areas are low-density bands, and light blue areas are high-density bands. I: the lowest-density band; II: the highest-density band; III: the winter low-density band; IV: V: the wet season low-density band. Other legend and sources of data is the same as in Figure 6.12.

During late March through November, the SST control is very evident. From middle June to early October, the coral seemed to have a optimum temperature environment (26.3 to 27.5℃ averagely) and coral had a fast extension rate and secreted a low-density band (band III). Late March through early June and October through November, the mean SST is over 27.5℃, the coral seemed stressed and experienced low extension rates and slow growth rates and produced two high-density bands (bands II and IV). Influence of temperature on coral extension and calcification rates has been clearly demonstrated by co-variation of extension and calcification with latitude in Hawaiian Archipelago [*Grigg*, 1997] and the Australian Great Barrier Reef (GBR) [*Lough and Barnes*, 2000].

Since corals are believed to generally live in temperature environment close (within 1 and 2℃) to their upper lethal limit during summer months [*Jokiel and Coles*, 1990], they should be extremely sensitive to any increase in ambient temperature in summer time when the temperature has been in a high level. Jokiel and Coles' study indicated the sublethal effects of expose to temperatures only 1 or 2℃ higher than the ambient mean on coral in Hawaii [*Jokiel and Coles*, 1977]. Glynn and D'Croz [*Glynn and D'Croz*, 1990] provided definite data showing steady decrease in densities of symbiotic dinoflagellates in proportion to the increase in temperature from 28, to 30 and then 32℃. Recent study in the Bahamas [*Fitt et al.*, 2000] has clearly shown seasonal cycles in their tissue biomass and the symbiotic dinoflagellates: densities of zooxanthellae were highest during the coldest part of the year, generally preceding peaks in coral tissue biomass in the spring; both coral tissue biomass and symbiotic dinoflagellates densities declined through the summer and reached low level during the autumn or fall. They speculated that the reductions in coral tissue biomass from the spring highs through the autumn-fall lows involves seawater temperatures and their effect on increasing respiratory metabolism and decreasing energy reserves in the coral tissue, and contributed the decrease in densities of symbiotic dinoflagellates with increase in

temperature to decreased growth rate of the symbiotic algae and the heat stress. Therefore, the Sumba coral's skeletal density rhythm during late March to November (Band II, III and IV) reflects coral animal's growth changes which were controlled mainly by ambient seawater temperature through modulating coral respiration and the consumption of energy reserves, and changing the input of photosynthetic energy from symbiotic dinoflagellates.However, the seawater control on skeleton growth was interrupted when summer rainfall peak arrived. From Figure 6.15, this interruption occurred when the local rainfall was averagely above ~6 mm/day in late November, almost half on the way to local annual maximum mean (12 mm/day). During December through early March, a special low-density band occurred, especially, a very low-density band was secreted coinciding with the sharp peak of annual coral $\delta^{13}C$ minimum during late February and early March. Obviously, this period of rapid coral growth is not controlled by the local seawater temperature because the temperature remains at a high level. We attribute this rapid growth of coral to largely increased input of terrigenous nutrients during that time. Two reasons make us to attribute to "terrigenous" input: (1) largely increased availability of terrigenous nutrients during Sumba summer rainfall peak (details see the preceding Section 6.3.4.1); (2) sharply depleted $\delta^{13}C$ value during this time compared with the secondary lightest $\delta^{13}C$ from decrease in light availability in May and June because C_3-plant-dominated terrigenous organic matters are much depleted in ^{13}C than local marine materials [*O'Leary*, 1981; *Gagan et al.*, 1987; *Goni et al.*, 1997]. Four more reasons make us to speculate the intake of extra nutrients during that time: (1) occurrence of the low-density band V and the lowest-density band I indicates rapid coral growth; (2) high level of seawater temperature requires more energy for coral polyp to meet increased respiratory metabolism, while use of inner energy reserves and decreased input of photosynthetic energy from the symbiotic algae could no longer meet this requirement indicated by formation of two high-density bands (Bands II and IV) at similar even lower seawater temperatures; (3) proven capability of coral animals to markedly increase their feeding rates and percentage of contribution of heterotrophically acquired carbon to daily animal respiration [*Risk et al.*, 1994; *Felis et al.*, 1998; *Anthony*, 2000; *Grottoli et al.*,

2006]; (4) confirmed less susceptibility of coral host for thermal stress than their symbiotic algae [*Fitt et al.*, 2001], which could keep coral hosts' vitality for even stronger feeding when their symbiotic zooxanthellae have remarkably lost their activity and their photosynthetic energy input have evidently decreased.

So, during austral summer rainfall peak, the availabililty of terrigenous nutrients would have controlled the occurrence and intensity of the unique low-density band in Sumba corals. Since the input peak of terrigenous nutrients is connected with the summer rainfall especially the rainfall peak in December to Early March, we could apply the coral density band during that time to evaluate local rainfall in Sumba. In fact, by observing the X-ray photograph of the Sumba coral (Figure 6.1) and comparing it with the summer rainfall (Figure 6.8D), we could find some very good correlations. In 1984 there was a very wide and evident low-density band, correspondingly, 1984 summer had the strongest summer rainfall in all the instrumental record from 1979 to 1999. 1989 had the secondary highest rainfall during the instrumental record, and also had a very wide low-density band in summer time. During 1990 to 1993, the summer especially the autumn rainfall is low (Figure 6.9C) and all of them had faint density bands during December to March; in contrast, in 1994, 1995 and 1996 the rainfall increased a lot and they had very bright low-density bands during summer.

The control of rainfall on summer time density band could be best demonstrated by the 1997 banding. Even though in summer during December 1996 to February 1997 there was strong rainfall due to La Niña and there was a low-density band, it did not fully develop. Instead, there was a remarkable high-density band developed immediately after that low-density band, because a strong El Niño suddenly happened in March 1997 (Figure 6.9) and immediately brought down the rainfall from early March (Figure 6.13A). We think that the abnormally low rainfall during the remaining 1997 summer time until May made the temperature as the main control factor again on coral growth because there were no enough extra nutrients to meet the elevated requirements for energy at this high level of summer temperature.

Given the good correlation between summer rainfall and the summer lowest-density band, we could use this unique band to detect changes in rainfall before the instrumental record. Figure 6.1 shows a very bright low-density band during 1978 summer time which is the most conspicuous low-density band of the whole coral record. Interestingly, an abnormally low $\delta^{13}C$ value peak coincides with this brightest low density band and this low $\delta^{13}C$ is also the most conspicuous peak in the whole coral $\delta^{13}C$ record (Figure 5.4). The most possible cause is that in 1978 there was a very strong summer rainfall or land runoff, even though a strong upwelling could also have the same effect because a coincident sudden increase in coral skeletal $\delta^{18}O$ (Figure 6.13) showing a possible decrease in seawater temperature in the mean time. Two reasons, however, make the strong rainfall be more preferred than a strong upwelling: (1) it happened during a northwestern monsoon season peak time (January) and a huge input of runoff from heavy rainfall could remarkably decrease the sea water temperature in the vicinity of the Mondu River mouth. The coincidence of the timing of the summer minimum in sea surface temperature climatology (late February) with the minimum in coral $\delta^{13}C$ climatology (also in late February) supports that the heavy input of runoff could remarkably decrease the SST (averagely up to 0.5℃). (2) In the Savu Sea, strong upwelling happens when southeast monsoonal wind prevails during Late May to July [*Potemra et al.*, 2003] as shown in Figure 6.9. The coincident $\delta^{18}O$ increase also provides another possibility: the suddenly increased seawater salinity, since slight elevation of salinity might impart increased resistance to other physical stresses [*Coles and Jokiel*, 1978] such as high level of summer seawater temperature in Sumba. But it seems not to be the case for our coral records because it is hard to explain a salinity increase in January in this area. Other obvious low-density bands before instrumental record include that in summers of 1976, 1972, and 1971 (Figure 6.1), which could also be linked to high level of summer rainfall since during all of these three years strong La Niña occurred during summers (refer to Nino 3.4 Index and Southern Oscillation Index in Figure 6.20).

6.3.5.3 Interannual variability of Sumba coral $\delta^{13}C$ record

Even the high resolution fortnighly Sumba coral $\delta^{13}C$ record shows strong interannual variability (Figure 6.4), curve of annual mean (January to December) of the $\delta^{13}C$ is much smoother (Figure 6.16A). The change of the annual mean $\delta^{13}C$ looks like to be controlled by the same factors that control the decadal variability of the coral $\delta^{13}C$ because this annual mean curve resembles the decadal variability curve very much (the blue heavy curve in Figure 6.4).

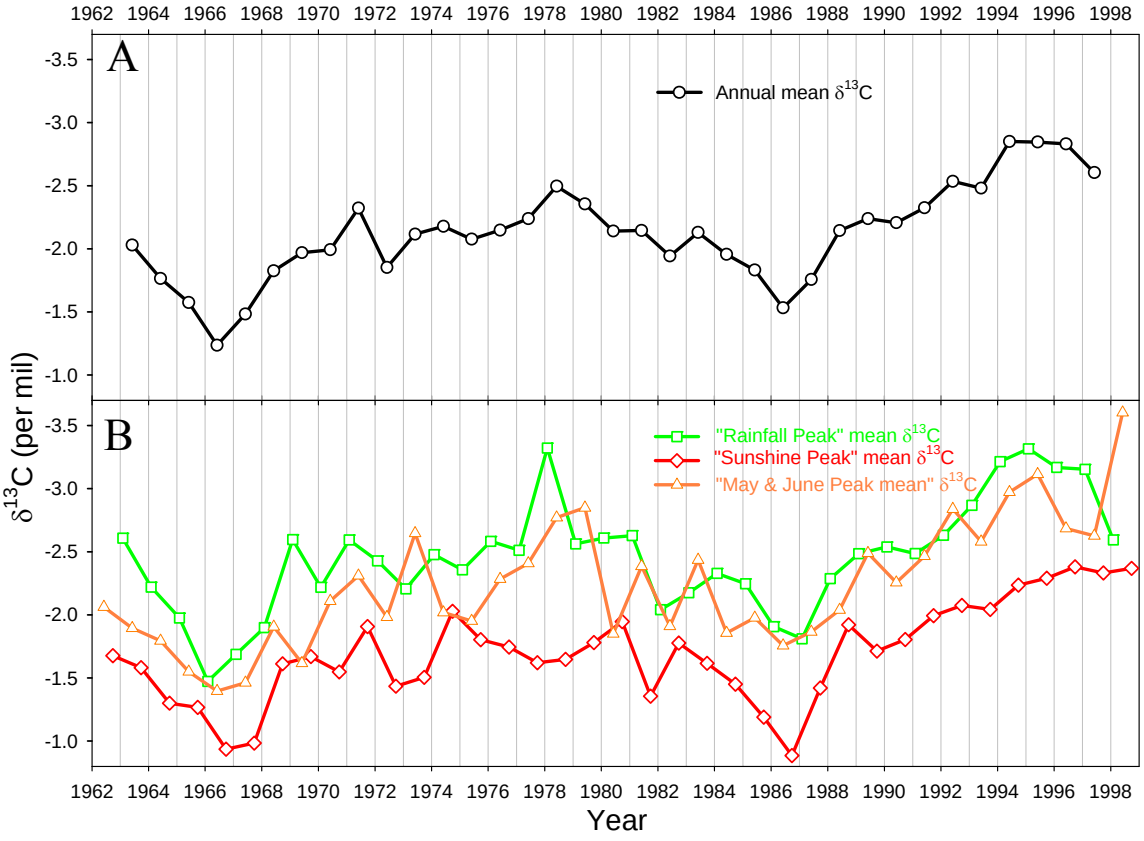

Figure 6.16 Interannual variability of coral $\delta^{13}C$ record. A: annual mean $\delta^{13}C$. B: sub-annual components of coral $\delta^{13}C$.

Under the smooth change of annual mean is the remarkable interannual variability of sub-annual components of the coral $\delta^{13}C$ record. The climatology of this $\delta^{13}C$ record

shows there are 3 typical sub-annual components: (1) an annual maximum which is linked to the annual maximum of radiation during late August to October ("Sunshine Peak"); (2) an annual minimum connected with summer peak rainfall during December to March ("Rainfall Peak"); (3) the secondary annual minimum which is coincided with the annual radiation minimum and also influenced by the autumn rainfall during May and June (name as "May & June Peak"). Figure 6.16B shows interannual variability of the 3 sub-annual components of the coral $\delta^{13}C$. Among the 3 components, interannual variation of the "Sunshine Peak" is relatively smooth, and the "May & June Peak" showsthe strongest interannual variability.

Figure 6.17 presents the interannual variability of relative difference of the 3 sub-annual components. The difference between the "Sunshine Peak" and the "May & June Peak" shows the biggest interannual variability. The difference between the "Sunshine Peak" and the "Rainfall Peak" shows obvious correlation (R = 0.39) with the summer peak rainfall (December to February), further confirming the connection between them.

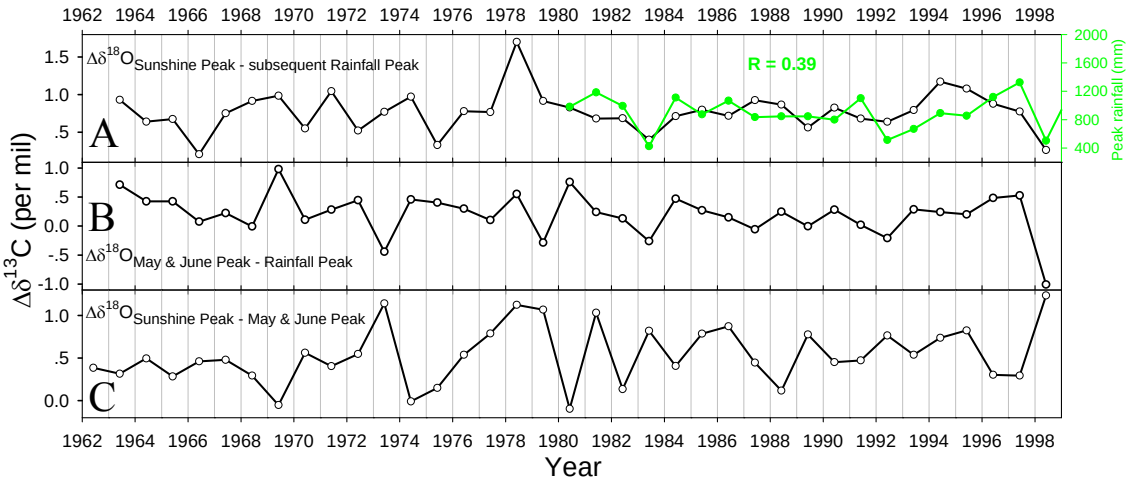

Figure 6.17 The relative variation of sub-annual components of coral $\delta^{13}C$ record. Panel A is the "Rainfall Peak" and its correlation with the rainfall during peak wet season.

Figure 6.18 shows detailed comparison between the $\delta^{13}C$ and the $\delta^{18}O$ of this Sumba coral.

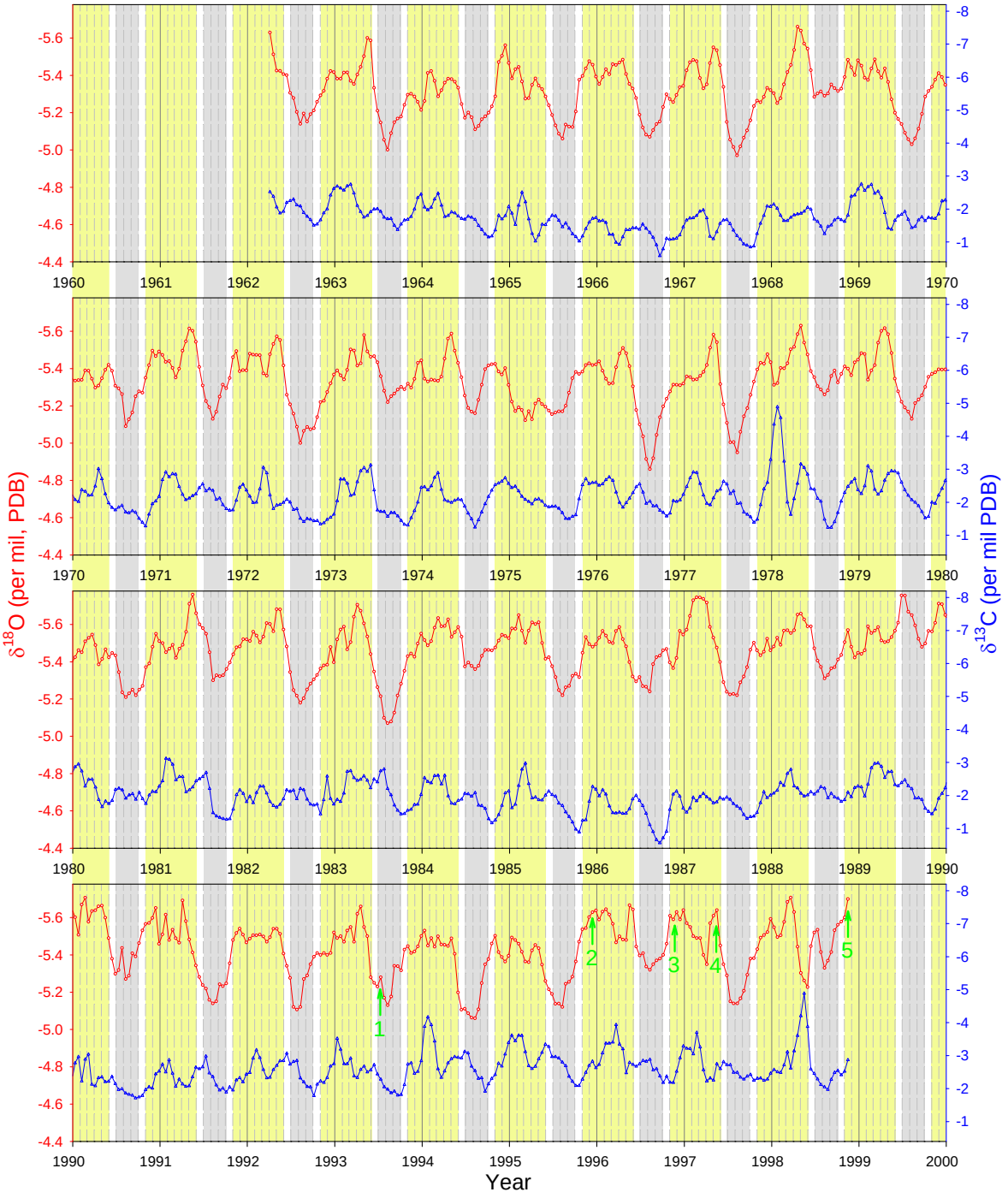

Figure 6.18 Detailed comparison between $\delta^{13}C$ and $\delta^{18}O$ records of the Sumba coral RSM2b. Grey shaded areas represent winter (July to September) and Yellow shaded areas represent summer season (November to May). Numbered green arrows indicated Kelvin wave events recognised by Syamsudin et al. during 1993 to 1998 [*Syamsudin et al.*, 2004]

6.3.5.4 Decadal variability and long-term trend of the coral $\delta^{13}C$ record

Decadal variability

Just as demonstrated above, substantial decadal variability of the coral $\delta^{13}C$ controls its interannual variability. And Figure 6.4 shows, compared with its $\delta^{18}O$ record, Sumba coral RSM2b has much stronger $\delta^{13}C$ decadal variability relative to their seasonal cycles. The most remarkable decadal variation is two periods of much heavier values of $\delta^{13}C$: one was during 1960s which peaked in 1966, the other was much prolonged during the whole 1980s and early 1990 which peaked in1986.

Figure 6.19 compares the decadal variabilities among the $\delta^{13}C$, $\delta^{18}O$, and sea surface temperature. The influence of seawater temperature seems to be one of the evident factors for decadal variability and long-term trend of the Sumba $\delta^{13}C$ record. In this coral $\delta^{13}C$ record, every obvious decrease\increase in seawater temperature was companied by increase\decrease in coral $\delta^{13}C$ or decrease\increase in rate of changes of $\delta^{13}C$ which resulted by other factors. It is obvious that the heavier $\delta^{13}C$ during 1960s is strongly linked to the decreased seawater temperature, and decreased temperature in mid-1970s and mid-1980 contributed to the heavier $\delta^{13}C$ during those times. Also, decreasing temperature during in 1990-1993 obviously lowered the rate of decrease in $\delta^{13}C$. We speculate that the reason why the seawater temperature affects the decadal variation of Sumba coral $\delta^{13}C$ is that the elevated ambient temperature decreases the ratio of photosynthesis vs respiration by increasing the rate of respiration and/or decreasing the photosynthesis in the zooxanthellae and coral tissures [*Jokiel and Coles*, 1977; 1990; *Fitt et al.*, 2000; *Fitt et al.*, 2001] and the deceased photosynthesis vs respiration ratio would then produce skeleton with depleted $\delta^{13}C$ [*Swart*, 1983; *Swart et al.*, 1996].

The other recognizable factor impacting the decadal variability of the Sumba coral $\delta^{13}C$ seems to be the decadal variation in seawater salinity. Sumba coral $\delta^{18}O$ record has shown an obvious freshening during the whole 1980s and an evident increase in salinity in the following four years of 1992 to 1995. The former coincides with the prolonged

period of heavier coral $\delta^{13}C$ and the latter is in the same time when the $\delta^{13}C$ is obviously depleted, indicating that in decadal time scale, the slight freshening of ambient seawater could possibly make the coral deposit heavier skeletal $\delta^{13}C$ and slight increase in salinity could result in lighter coral skeletal $\delta^{13}C$. The increase in $\delta^{13}C$ during 1996 to 1998 might also result from the freshening of seawater during that time.

Long-term trend

Even though the $\delta^{13}C$ record does not show obvious climate shift in 1976, which is very evident in the $\delta^{18}O$ record, it does has a long-term trend of becoming lighter, just as same as the long-term trend in the $\delta^{18}O$ record (Figure 6.4). In the whole record of 37 years of the Sumba coral RSM2b, there is a decrease in coral $\delta^{13}C$ of 0.87‰, that means -0.024‰ per year. This rate is very close to the high end of the range of published values of the oceanic Suess effects during the past several decades: from -0.007 to -0.026‰ per year [*Druffel and Benavides*, 1986; *Quay et al.*, 1992; *Bacastow et al.*, 1996; *Gruber et al.*, 1999; *Bohm et al.*, 2002; *Kortzinger et al.*, 2003; *Tanaka et al.*, 2003].

The oceanic Suess effect is the decrease of the $\delta^{13}C$ of dissolved inorganic carbon (DIC) as a consequence of CO_2 exchange with the atmosphere in which the addition of anthropogenic CO_2 (resulting from the burning of fossil fuel and changes in land use) has caused a decrease in the $^{13}C/^{12}C$ ratio of atmospheric CO_2 because the anthropogenic CO_2 is depleted in ^{13}C due to the preferential uptake of ^{12}C during photosynthetic utilization of CO_2 by plants. The decrease of the $\delta^{13}C$ in the ambient dissolved inorganic carbon definitely would influence the $\delta^{13}C$ of the coral skeleton.

But, since coral does not secretes skeletal aragonite in equilibrium with the ambient DIC system and various physiological and kinetic factors control the skeletal $\delta^{13}C$, it is hard to say how much the oceanic Suess effect had influenced the long-term trend of the Sumba coral $\delta^{13}C$. Since the trend of -0.024 is almost the upper limit of reported Suess

effect, it is reasonable to speculate that there are other factors affected the Sumba coral $\delta^{13}C$. Seawater temperature is one of the possible candidates because the decadal variation of seawater has strong link with the decadal variability of the coral $\delta^{13}C$. The long-term trend of lighter Sumba coral $\delta^{18}O$ has been attributed mainly to the increase in seawater temperature, and the long-term trend of lighter $\delta^{13}C$ could be also partly attributed to the warming trend of the seawater. If the long-term trend of depleted coral $\delta^{13}C$ is strictly attributed to the increase in temperature, that would mean a decrease in coral $\delta^{13}C$ of 0.87‰ vs. a rise in temperature of 0.61℃, or 1.40‰ decrease in coral $\delta^{13}C$ vs. 1℃ rise in seawater temperature. But, more possibly, both the warming seawater and the oceanic Suess effect could contribute the long-term trend of depleting coral $\delta^{13}C$ in Sumba.

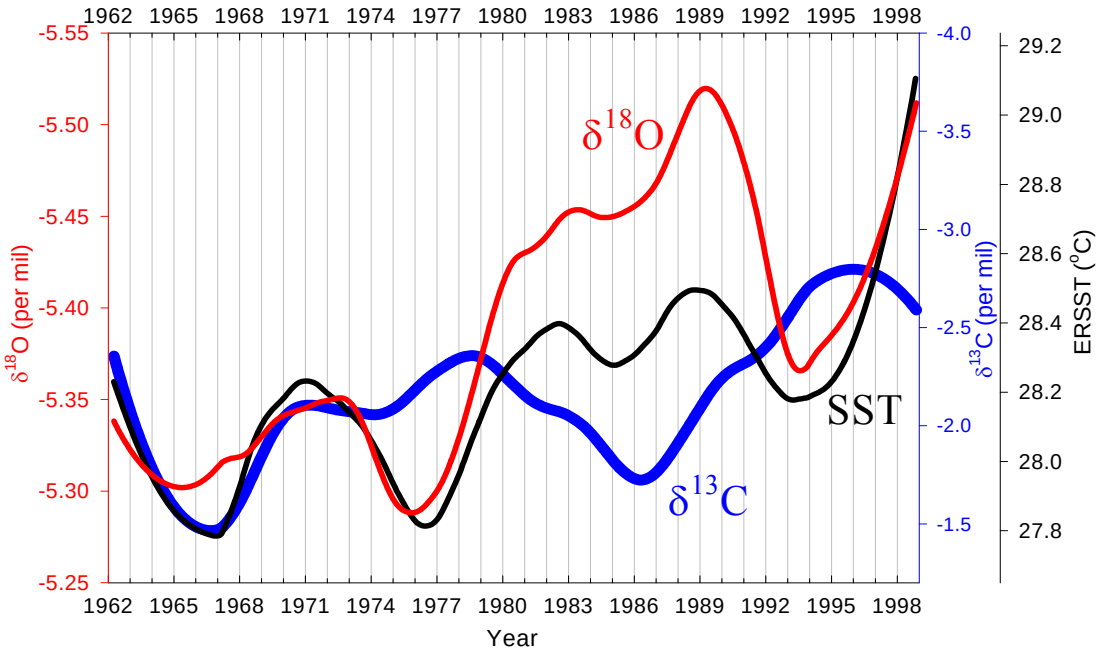

Figure 6.19 Decadal variability of the coral $\delta^{13}C$ (blue curve) and comparison with $\delta^{18}O$ (red) and SST (black).

6.4 SYNTHESIS OF FORCINGS

The climate of the southern sector of the Indonesian maritime continent is influenced by

ENSO, the IOD ocean-atmosphere system and the Asian-Australian monsoon system [*Philander*, 1990; *Webster et al.*, 1998; *Yamagata et al.*, 2004]. These three systems interact and it is thus necessary to evaluate their impacts and evolutions separately on the local climate and oceanography. The previous analysis in this chapter has shown the potential of the Sumba coral $\delta^{18}O$ and $\delta^{13}C$ for this because they have responded to different climate elements in different seasons. This section will synthesize those connections and show how the seasonality of the Sumba coral $\delta^{18}O$ and $\delta^{13}C$ records can be used to make inferences about the individual influence of the three systems.

6.4.1 Spectral analysis of forcings

Firstly, we will present periodicity on interannual variability of the seasonal characteristics of the coral $\delta^{18}O$ and their connections with ENSO, IOD, and the monsoon.

6.4.1.1 Periodicity of coral $\delta^{18}O$ interannual variability

Figure 6.20A illustrates the periodicity of seasonal coral $\delta^{18}O$. Since the Sumba coral $\delta^{18}O$ climatology was shaped mainly by seasonal characteristics in austral winter (July ~ September), summer (November ~ February), and autumn (March ~ May) (Figure 6.5), the periodicities of mean $\delta^{18}O$ in the three seasons, as well as annual means (January ~ December), have been analysed. First, the mean $\delta^{18}O$ for the corresponding season of a year was calculated. Then, $\Delta\delta^{18}O$ was obtained by subtracting the subsequent year's mean. The Blackman-Tukey spectra of those seasonal signals were then obtained for $\Delta\delta^{18}O$ of the whole record by applying the *Analyseries* software [*Paillard et al.*, 1996] using a Bartlett window. $\Delta\delta^{18}O$ was used (rather than $\delta^{18}O$) to focus the analysis on interannual variability and to suppress the decadal signals. Comparison of analyses of $\Delta\delta^{18}O$ and $\delta^{18}O$ has indicated that using $\Delta\delta^{18}O$ could effectively keep periodic characteristics between 2 to 5 years.

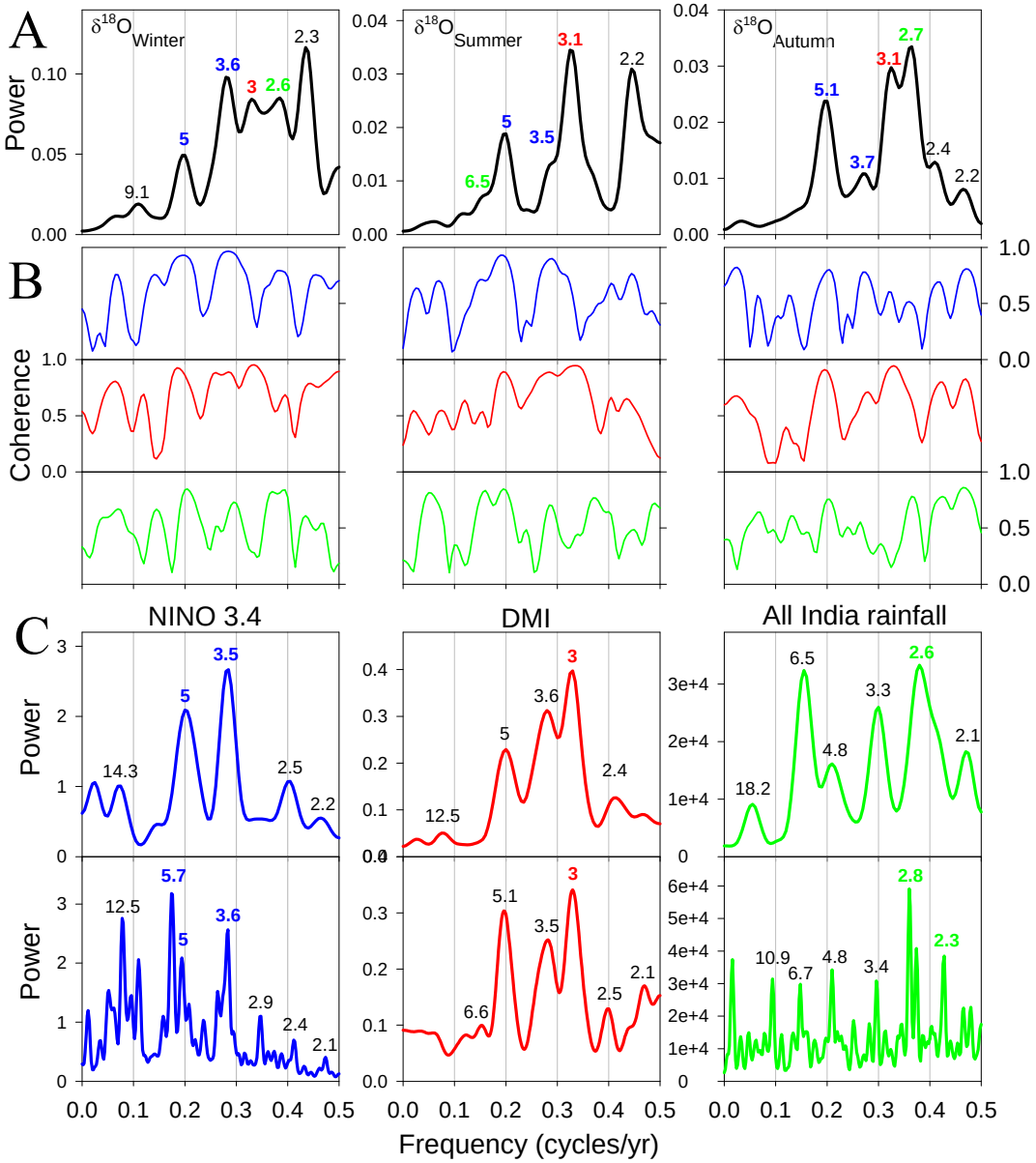

Figure 6.20 Spectral analysis of seasonal characteristics of the coral $\delta^{18}O$ record and their correlation with indices of ENSO, IOD, and the Asian-Australian Monsoon systems. **A:** Blackman-Tukey spectra of seasonal means of $\Delta\delta^{18}O$ of the modern coral RSM2b in austral winter (July to September), summer (November to February), and autumn (March to May) from 1962 to 1998. **C:** Blackman-Tukey spectra of NINO3.4 index (blue curve in left panel), DMI (red in middle panel), and All India summer monsoon rainfall (ISMR, green curve in right panel). The upper panels are for data during 1962~1998, the lowers for all available data. . Annual means of those indices are used for the spectral analysis. Data sources: NINO3.4 index and ISMR from Lamont-Doherty Earth Observatory data sets at http://iridl.ldeo.columbia.edu/SOURCES/.Indices/.nino/.EXTENDED/.NINO34/ [*Kaplan et al.*, 1998] and http://iridl.ldeo.columbia.edu/SOURCES/.Indices/.india/ [*Parthasarathy et al.*, 1995], the DMI from Saji's personal webpage at http://iprc.soest.hawaii.edu/%7Esaji/dmi.txt [*Saji et al.*, 1999]. **B:** Cross-spectra of seasonal coral $\Delta\delta^{18}Os$ with NINO3.4 (blue), DMI (red), and All India summer rainfall (green) during the same time period of 1962 to 1998. Spectral analyses are completed using *Analyseries 2.0* [*Paillard et al.*, 1996] and a Bartlett window is used when generating the Fourier spectra. The bandwidths are 0.0517241. Non-zero coherences are higher than 0.581075. The numbers on the top of the peaks highlight major periodicities as year(s)/cycle.

6.4.1.2 Periodicity of ENSO, monsoon, and equatorial Indian Ocean forcing

The results of the spectral analysis on the annual means of indices characterizing the three climate systems are shown in Figure 6.20C. The upper panels estimate the power spectra for data from 1962–1998 which is the same period for the modern coral record, and with the lower panels for all available data.

Periodicity of ENSO*:* NINO3.4 SST index from the central tropical Pacific was spectrally analysed to represent the periodicity of ENSO. The power spectrum for the NINO3.4 index during 1962–1998 has variance concentrated in the characteristic 3.6 yr and 5 year bands (upper left panel in Figure 6.20C), which is consistent with previous analyses of the NINO3 index for 1960–1998 by Hughen et al. [1999] and analysis of all El Niño events between Little Ice Age and the present by Enfield and Cid [1991]. The spectral peaks around 3.6 and 5 yr are not due to aliasing by using annual means and spectral analysis using annual means of NINO3.4 index in this study could effectively catch the periodic characteristics of ENSO. Since $\Delta\delta^{18}O$ was used to estimate the power spectra for coral records and the low-frequency bands near or above 5 year have been suppressed, only the 3.6 year band was used as a characteristic period for ENSO in this study.

Periodicity of monsoon: Even though early studies considered the monsoon to be a regional physical entity, the trend in modern monsoon studies has been toward an understanding of the 'global' monsoon by studying the dynamic links between regional subsystems [*Meehl*, 1987; *McBride*, 1998; *Webster et al.*, 1998; *Trenberth et al.*, 2000; *Clemens et al.*, 2003; *Chang et al.*, 2004]. The most active Indian, East Asian, and Australian monsoons are now often referred to as one macroscale phenomenon with the tropical convective maximum migrating from over north India in July to Indonesia and northern Australia in January [*Meehl*, 1987; *Hung et al.*, 2004; *Chang et al.*, 2005]. A quasi-biennial variability (2–3 year period centred on 2.6 years, referred to as the tropospheric biennial oscillation – TBO) has been found to be a fundamental characteristic for monsoon rainfall in south Asia, East Asia, Indonesia, and the

Australian subsystem regimes [*Meehl*, 1997; *Webster et al.*, 1998 and references there; *Meehl and Arblaster*, 2002]. Even though the ENSO and IOD also display minor TBO signals, we attribute TBO signals mainly to the monsoon when the TBO is obviously dominating the power spectrum over other peaks in the 2–5 yr band. There is considerable seasonal persistence from the south Asian to Australian monsoon with a strong south Asian or Indian monsoon tending to precede a strong Northern Australian monsoon, and vice versa [*Meehl and Arblaster*, 2002; *Loschnigg et al.*, 2003; *Hung et al.*, 2004]. So, it is reasonable that the All India Summer Monsoon Rainfall dataset has been used for spectral analysis in this study to display the characteristic quasi-biennial variability of the Asian-Australian monsoon in the absence of long-term and complete archives of local rainfall (Figure 6.20C right panels).

Periodicity of IOD and equatorial Indian Ocean forcing*:* The middle panels of Figure 6.20C illustrate the cyclicity of IOD events [*Saji et al.*, 1999; *Webster et al.*, 1999] by estimating the power spectrum of the Dipole Mode Index of SST anomalies in the eastern and western equatorial Indian Ocean [*Saji et al.*, 1999]. Even though controversial theories have been suggested for the forcing of this recently discovered phenomenon [*Baquero-Bernal et al.*, 2002; *Meehl and Arblaster*, 2002; *Yamagata et al.*, 2004; *Yu and Lau*, 2004a], the IOD has been found to be strongly influenced both by ENSO [*Baquero-Bernal et al.*, 2002; *Yu and Lau*, 2004a] and the monsoon [*Loschnigg et al.*, 2003; *Yu and Lau*, 2004a]. The power spectrum of the DMI clearly displays their strong impacts around the 5 and 3.6 yr (for ENSO) and the TBO periods (for monsoon) (Figure 6.20C middle panels). However, the most salient peak in the DMI spectrum is the strong and well-separated peak around the 3-year period, which is not evident in both the ENSO and monsoon spectra.

The result suggests that some unique process within the Indian Ocean might be involved in the formation of IOD events. Recently Wijffels and Meyers [2004] noticed that the equatorial Indian Ocean winds have much more energy at higher frequencies with spectral peaks near 3 yr and 1-2 yr compared to the lower-frequency energy of the

Pacific winds (periods >3.2 yr, ENSO band) and used this to distinguish the impact of these two sources of remote energy on the Indonesian throughflow. Sakova *et al.* [2006] also identified a very clear and well-separated 3-yr period for sea surface height variability over the Sumatra-Java upwelling region and the western tropical Indian Ocean where the zonal equatorial Indian Ocean winds have substantial influence. So this 3 year period might represent the remote equatorial Indian Ocean winds which play a role in the IOD.

Change in periodicity: The spectral analysis using the annual means has also revealed changes in ENSO behaviour, such as spectral shifts from lower amplitudes and longer periods (5.7 yr) to higher amplitudes and shorter periods (3.6 and 5 yrs) in the 1970s, which is consistent with previous results [*Hughen et al.*, 1999; *Kumar et al.*, 1999]. But the 3.6 yr period is still one of the most important characteristics of ENSO variability since 1856. Interestingly, Enfield and Cid [1991] demonstrated that the 3.5 and 5 yr periods did not change since the Little Ice Age, and Rodbell et al. [1999] showed that the modern ENSO periodicity of 3.6 and 5 yrs has been established since 5 ka. Therefore, in this study it is reasonable to use the 3.6 yr period to correlate the ENSO with coral records during the period 1962 to 1998. The quasi-biennial periods (2–2.8 yr) are fundamental for the monsoon so we assume its consistency during this period. There is no historical record for the variability of the IOD, so we have tried to establish the periodicity of the IOD in this study.

Similar results have been obtained from all the analysis of periodicity in the coral records and instrumental data using the Lomb-Scargle periodogram and a Bartlett window applying the *AutoSignal* software, indicating that the results are not biased by different spectral methods.

6.4.1.3 Connections between seasonal coral δ^{18}Os and the climate systems

In this study, we use 3.6, 3.0, and 2.6 yrs/cycle as characteristic periodicities of the ENSO, IOD, and the monsoon systems to explore their impact on the Sumba coral δ^{18}O

record. Figure 6.20A shows those as the major periodicities of the coral $\delta^{18}O$ interannual variability in the 2-5 year time band. The 3.6 yr periodicity dominates the 3 and 2.6 yr periodicities in the winter coral $\delta^{18}O$. The cross spectra in the left panels of Figure 6.20B demonstrate that those 3 periodicities of the coral winter $\delta^{18}O$ have the strongest coherences with ENSO, IOD, and the monsoon, respectively. We think this result indicates that, in winter, ENSO has dominant impact on the Sumba coral $\delta^{18}O$ record, even though the IOD and monsoon still have their obvious signals.

In contrast, the middle panels of Figures 6.20A and B indicate that the IOD overwhelmingly affects the summer coral $\delta^{18}O$, with relatively minor impacts from ENSO and the monsoon. Furthermore, the right panels in Figures 6.20A and B demonstrate the combined strong impact of the IOD and the monsoon on coral $\delta^{18}O$ in autumn, with only minor impacts due to ENSO.

This spectral result reinforces the analysis of the annual climatology and the correlation between rainfall and the seasonal characteristics of coral $\delta^{18}O$. The autumn $\delta^{18}O$ is strongly linked to external sources of fresh water provided by monsoonal rainfall. The fact that the autumn $\delta^{18}O$ has almost equally strong imprints of both the IOD and monsoon strongly implies that the forcing connected to the autumn coral $\delta^{18}O$ is from the Indian Ocean.

6.4.2 Dominating influence of ENSO events in winter

The dramatic interannual variability of the winter coral $\delta^{18}O$ reflects the dominating influence of ENSO events on the winter climate and oceanography in the Sumba Strait. Figure 6.21 shows the comparison between the Sumba $\delta^{18}O$ record and typical ENSO indices.

ENSO events strongly influence the winter coral oxygen isotopic composition. During an El Niño year, the Sumba winter coral $\delta^{18}O$ is enriched in ^{18}O, while during a La Niña, the winter coral $\delta^{18}O$ is depleted in ^{18}O. The winter $\delta^{18}O$ anomaly in a La Niña year

appears bigger than that in an El Nina year. After the long-term trend and most of the decadal variability are removed, Figure 6.22A shows further the strong correlation of the variability of winter coral $\delta^{18}O$ with the ENSO events. All the winters with relatively depleted $\delta^{18}O$ are related to La Niña events. Sumba coral winter $\delta^{18}O$ recorded all the 10 El Niño events during 1962 to 1998 according to the definition of El Niño [*Trenberth*, 1997] when the winter coral was obviously enriched in ^{18}O. An obvious exception happened in 1967, when the winter coral was enriched in ^{18}O but there was no El Niño that year. The reason is that in 1967 there was an Indian Ocean Dipole (Figure 6.22A) and it brought low SST and low rainfall around Sumba. Another minor exception is year 1985, when winter coral was slightly enriched in ^{18}O but it was nothing to do with an El Niño or Indian Ocean Dipole event. The reason is still unsure, but the winter SST in 1985 was low, maybe connected with the mid-1980s' cooling.

Even though there are 2 years that are exceptions, the other 35 winters are strongly influenced by ENSO events. Therefore, the Sumba winter $\delta^{18}O$ record could be a very good index for ENSO events. Given the small change in winter SST which resulted from ENSO events, the winter variability in coral $\delta^{18}O$ amplifies the ENSO events. For example, the difference of winter average SST between 1987 El Niño and subsequent 1989 La Niña was 1℃, equivalent to 42% of average seasonality of SST (2.4℃); while coral $\delta^{18}O$ difference was 0.33‰, equivalent up to 138% of average seasonality of $\delta^{18}O$. Another example is the difference between 1996 La Niña and 1997 El Niño: the SST change was 1℃, 42% of average seasonality of SST, while the coral $\delta^{18}O$ change was 0.18‰, equivalent to 75% of average seasonality of coral $\delta^{18}O$. This amplification of signals further guarantees the Sumba coral winter $\delta^{18}O$ as good index of ENSO events.

As shown in Figure 6.22B, the seasonality anomaly of Sumba $\delta^{18}O$ is also strongly correlated with ENSO events. La Niña years produce negative $\delta^{18}O$ anomalies while positive anomalies occur in El Niño years.

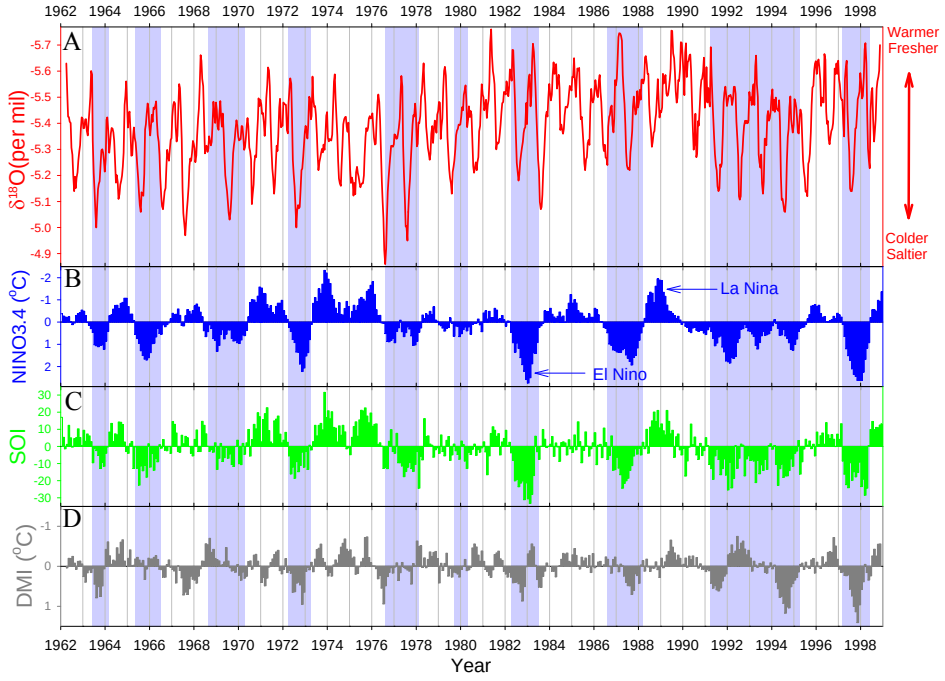

Figure 6.21 Comparison of modern coral RSM2b $\delta^{18}O$ record with monthly ENSO Indices and Indian Ocean Dipole index DMI. SOI is from the Australian Authority of Meterology and the sources of NINO3.4 and DMI is the same as Figure 6.9. Shaded areas represent El Niño years based on the definition of Trenberth [*Trenberth*, 1997].

The fortnightly Sumba coral $\delta^{18}O$ could help to understand how ENSO influence the climate and oceanography around Sumba. The most direct influence is by modulating the local rainfall and air temperature through atmospheric teleconnection (then the local SST by air-sea heat flux) because of the moving of the Indonesian Low. This ocean-atmosphere coupled effect should contribute the local Sumba climate and oceanography without much lagging, which could be evident by comparing the timing of NINO 3.4 and SOI index (Darwin is close to the research area). Remarkable lagging of ENSO signal in the coral $\delta^{18}O$ could help us to understand another mechanism of ENSO influence, i.e. by the Indonesian Throughflow. One of the strongest El Niño started from Aril 1982, reached its peak in January 1983 and ended in July 1983 according to Trenberth's definition [*Trenberth*, 1997], while the coral recorded very strong El Niño signal in August 1983 (Figure 6.21). Since the local SST and rainfall in 1983 winter (Figure 6.8C) had been not as low as that in 1982 winter, the stronger El Niño signal in 1983 should not come from the first mechanism of ENSO's influence.

The stronger El Niño signal should be arisen from the saltier, cooler sea water which was brought to Sumba mostly by the Indonesian Throughflow. Two reasons made the Indonesian Throughflow saltier during or after an El Niño: one is that less low-salinity Pacific water would be transport into the Indonesian seas during an El Niño [*Meyers*, 1996; *Susanto and Gordon*, 2005]; the eastward moving of the Indonesian Low during an El Niño would greatly reduce the rainfall of the Indonesian archipelagos and areas around the South China Sea which are both the source of freshwater of the Indonesian seas [*Gordon*, 2005], and the dramatic reduction of the freshwater flux would then rise the salinity of the Indonesian Throughflow. The cooler SST in western Pacific and temperature in Indonesian archipelagos during an El Niño would also make the Indonesian Throughflow cooler than a normal or La Niña year. The third mechanism of ENSO's influence involves modulating of the IOD, which would be detailed in the following sections, as during ENSO the weakened Pacific trades are often accompanied by easterly wind anomalies along the Indian Ocean equator [*Clarke and Liu*, 1994] and the resulted IOD has similar effect with ENSO.

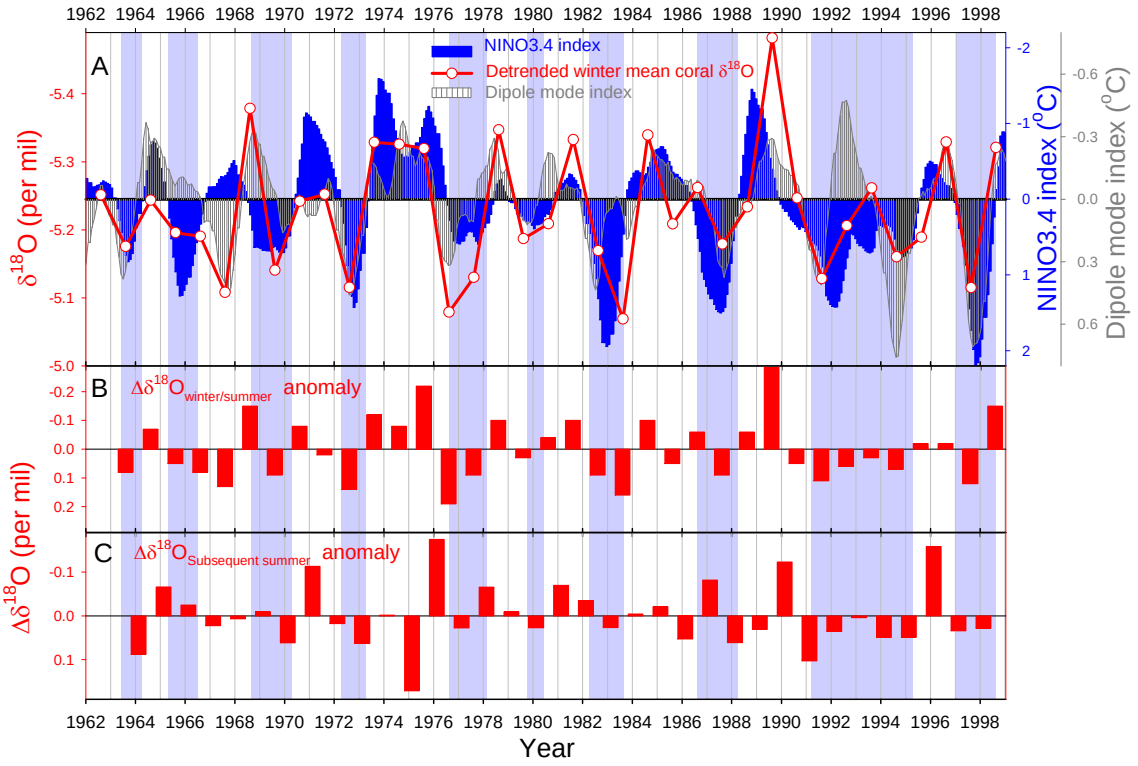

Figure 6.22 The control of ENSO and the signatures of IOD on the Sumba coral $\delta^{18}O$ record.

The correlation between the Sumba summer coral $\delta^{18}O$ and the ENSO events is much weaker, but their connection is still recognizable (Fig. 6.22C): the obviously enriched ^{18}O in the summer following an El Niño event (Figure 6.6). We think the influence of ENSO on the summer climate and oceanography might involve modulation of the IOD, rather than a direct influence, since the summer coral $\delta^{18}O$ points to an overwhelming impact of IOD, and the IOD itself is influenced by ENSO [*Yu and Lau*, 2004b].

6.4.3 Signature of the Indian Ocean Dipole events

Even though ENSO events control the interannual variability of the winter coral $\delta^{18}O$ record, the influence of Indian Ocean Dipole events in winter is still obvious. The most conspicuous example is the peak of remarkably enriched $\delta^{18}O$ in 1967, when there was no El Niño (Figure 6.21). But this peak coincided with a positive departure of Indian Ocean Dipole Mode Index (DMI) [*Saji et al.*, 1999]. In fact, coincidence of enhanced or reduced winter $\delta^{18}O$ superimposed on the ENSO effect is very common in this Sumba coral $\delta^{18}O$ (Figure 6.21 and Figure 6.22). A positive index of DMI would enhance the effect of an El Niño, such as evidently enhanced winter peaks in El Niño years of 1994, 1976, 1979, and 1963; and a positive index of DMI would reduce the effect of a La Niña, as a matter of fact, it happened in all the three years when a positive DMI index coincided with a negative NINO3.4 index in 1976, 1970, 1971. In contrast, a negative DMI index would enhance the effect of a La Niña event on Sumba coral $\delta^{18}O$, such as that in 1989, 1996, 1998, 1968, 1978, 1981, and 1984; also, a negative DMI index would reduce the effect of an El Niño, such as that in 1965 and 1990. Strong correlation suggests that the IOD events could strongly impact the climate and oceanography as far as in the Savu Sea and in some year this influence is even stronger than an ENSO events' influence in this region. Our result support that an positive IOD event bring the same influence in Indonesia maritime continent as that of an El Niño event and a negative IOD event bring the same influence in Indonesia as that of a La Niña event [*Abram et al.*, 2003; *Saji and Yamagata*, 2003].

Not only does IOD have impressive signature in the winter coral $\delta^{18}O$, but also overwhelming influence on the summer coral $\delta^{18}O$, as indicated by the spectral analysis of the seasonal characteristics of this coral $\delta^{18}O$ in Section 6.4.1. As a matter of fact, the overwhelming impact of IOD in summer mainly refers to part of its forcings: some intrinsic processes which have a 3 yr component of periodicity. The following Section 6.4.4 would discuss the forcing in more detail.

6.4.4 Routine penetration of the SJC into Savu Sea

The Sumba Strait is one of the main exits of the Indonesian Throughflow (ITF) into the southeast Indian Ocean [*Potemra et al.*, 2003; *Sprintall et al.*, 2003; *Gordon*, 2005]. While early studies have noticed that the eastward flow of the South Java Current could reduce the transport of the ITF [*Meyers et al.*, 1995], it had not been confirmed if the Indian Ocean water enter into the Indonesian seas through the Sumba Strait for a long time until the recently reported eastward flows in the Ombai Strait [*Molcard et al.*, 2001a] and in the Sumba Strait [*Chong et al.*, 2000; *Hautala et al.*, 2001] measured using current metres in December 1995. Our study area is just on the southern side of the inner part of the Sumba Strait (Figure 3.1), so it should be an ideal site to research the transport of waters between the Indonesian inner seas and the Indian Ocean. The *Porites* corals in this site could provide longer historical record of the transport by reflection of the variability of salinities and sea water temperatures for the different waters.

As mentioned above, the Sumba coral $\delta^{18}O$ has recorded a huge input of fresh water in this area in March to early May, and this water is warm, low-salinity, and strongly related to outside summer monsoonal rainfall. Obviously, there are two possible sources for this water. One is from the Indonesian inner seas mainly through the Ombai Strait in the east of the Savu Sea, and the other one is from Indian Ocean through the Sumba Strait in the west of the Savu Sea. There is no evidence to support this Indonesian inner seas source in the Sumba coral record. In contrast, there are at least three lines of

evidence in the Sumba coral $\delta^{18}O$ record to support an Indian Ocean low-salinity water source.

(1) Spectral analysis (Figure 6.20) indicates that the interannual variability of the autumn coral $\delta^{18}O$ has a very strong periodicity of 3.1 years in addition to the strong monsoonal periodicity of 2.7 years. Even though IOD events are strongly connected to the ENSO events, there were some years when IOD occurred with nothing to do with ENSO events, such as shown by the Sumba coral $\delta^{18}O$ that the strong 1967 winter enriched $\delta^{18}O$ peak occurred in a weak La Niña year rather than a El Niño year. Recent studies have indicated that only about one-third of the IOD events are related to the ENSO forcing [*Yamagata et al.*, 2004; *Behera et al.*, 2006] and modelling experiments support that the IOD is mainly determined by the intrinsic processes within the Indian Ocean basin [*Yamagata et al.*, 2004; *Behera et al.*, 2006]. Our spectral analysis also shows the unique component of 3.1 years in the periodicity of the IOD interannual variability (Figure 6.22A) in addition that the periodicity of IOD shows strong connection with ENSO in the concurrent 5 and 3.6 year components. This 3.1 year component should be a unique marker for some intrinsic processes within the Indian Ocean.

(2) The property of the water of the outside source inflow during autumn recorded by the shallow-water Sumba *Porites* coral $\delta^{18}O$ is very fresh and warm, consistent very well with the published data for the surface layer of the South Java Current which has a very warm, fresh cap (salinities ~33.8) [*Fieux et al.*, 1994; *Bray et al.*, 1997; *Sprintall et al.*, 1999; *Sprintall et al.*, 2000] and is believed to result from the heavy input of strong summer rainfall around Java and Sumatra because it is too fresh to come from the Indonesian inner sea Banda Sea Water (salinities ~34.4) [*Fieux et al.*, 1994; *Sprintall et al.*, 1999]. This current seasonally flows eastward in summer during December to April driven by the prevailing north-westerly monsoonal winds [*Quadfasel and Cresswell*, 1992; *Sprintall et al.*, 1999]. Hautala et al. have observed strong eastward flow in the upper layer of 0 to 150 m during December 1995 in the Sumba Strait using pressure

gauge pairs [*Hautala et al.*, 2001], showing that the warm, fresh water in the upper layer of the South Java Current could inflow into the Savu Sea through the Sumba Strait. Molcard *et al.* also caught a strong north-eastward current in the surface 160 m during the whole December 2005, indicating the SIC could further enter into the Indonesian inner sea the Banda Sea [*Molcard et al.*, 2001a].

(3) Analysis of the interannual variability of the seasonal characteristics of the coral $\delta^{18}O$ demonstrates that the distinct freshening in the Savu Sea in autumn reflected by the coral $\delta^{18}O$ climatology (the "hunch") should result from input of water from the South Java Current rather than the Indonesian inner seas. At first we analyse the case in 1993 when a prolonged El Niño occurred (Figure 6.9F). Even though a negative IOD happened in most part of the 1993 summer, the local rainfall in both early and autumn was in a relatively low level (Figure 6.9B and C) and the rainfall around the Indonesian maritime continent should be also relatively lower compared with a normal or La Niña period. Since in such an El Niño year the ITF from the Pacific should be smaller than a normal year or a La Niña year [*Clarke and Liu*, 1994; *Meyers*, 1996], therefore the inner seas should be much saline. If the water is the main source of the inflow into the Savu Sea in the later summer, the Sumba coral should record a much enriched value of $\delta^{18}O$ in autumn given that the Indonesian inner sea water arrives in the Sumba Strait in around 3 months [*Potemra et al.*, 2003]. But, actually, the Sumba coral recorded a remarkably depleted $\delta^{18}O$ peak in late 1993 summer (Figures 6.9A and C). So, the distinct freshening of water recorded by the coral $\delta^{18}O$ in 1993 autumn shows the occurrence of other source for the very warm and fresh water into the Savu Sea. The only candidate left is the characteristic fresh cap of the South Java Current from the Indian Ocean. Even a negative IOD event in early 1983 a little bit complicated the 1983 case, the 1983 distinct freshening in autumn also supports a SJC source. 1988 autumn should be in a neutral condition for the rainfall around the Indonesian maritime continent (refer to Figure 6.21 the SOI), but still the coral $\delta^{18}O$ recorded a distinct freshening (Figure 6.21A, D and E). It also proves that the source of the autumn "hunch" is from the SJC rather than the Indonesian seas. 1996 could serve as an

example for a La Niña year. The summer monsoon rainfall was very strong in this year (Figure 6.9E). If the source of the autumn "hunch" is the inflow of the Indonesian inner sea water, there should be a huge "hunch" compared with the summer coral $\delta^{18}O$, because in a La Niña year the rainfall around Indonesia (record shows a very high rainfall during the summer rainfall peak time, Figure 6.9B and E) and the ITF both should increase, and the salinity in the Indonesian seas should greatly decrease. But what happened is, the coral recorded no "hunch" at all compared to the summer (Figure 6.9A, D and E). This example indicates that even in a La Niña year when the ITF is believed to be larger than normal and the rainfall around Indonesia is very heavy, the Sumba coral does not record a autumn "hunch" in $\delta^{18}O$, indicating that the "hunch" in the Sumba coral $\delta^{18}O$ did not result from the input of inner Indonesian sea water.

Therefore, the Sumba coral $\delta^{18}O$ record has clearly demonstrated an input of Indian Ocean water into the Savu Sea during the autumn. The high resolution Sumba coral $\delta^{18}O$ record also shows that the SJC could flow into the Savu Sea in other period of summer time (November to May). The periodic eastward flowing during November to May [*Quadfasel and Cresswell*, 1992] has provided the possibility for the penetration of the SJC through the Sumba Strait during the whole summer time. Spectral analysis for the Sumba coral $\delta^{18}O$ has proven that both the interannual variabilities of the property for the Savu Sea water in the whole summer and the summer are mainly controlled by an intrinsic process within the Indian Ocean basin (the 3.1 yr period), strongly implying an important input of Indian Ocean water for the whole summer, not only the autumn. The seasonal characteristics of the coral $\delta^{18}O$ in 1996 and 1997 clearly support that during La Niña (both the 1996 and 1997 summer time were during La Niña conditions as showing in Figure 6.9F) the SJC still flew into the Savu Sea in early part of the summers such as in November 1995 through February 1996 and November and December in 1996. But since the increased pressure difference between the Pacific and the Indian Ocean during a La Niña increases the ITF [*Clarke and Liu*, 1994; *Meyers*, 1996], increased Indonesian sea water into the Savu Sea occurred and decreased the salinity and SST in the Sumba Strait, reflected by dramatic increase in coral $\delta^{18}O$ in

March and April of 1996 and during January to March of 1997 (Figure 6.9A, and for a more detailed presentation, refer to Figure 6.18). These dramatic increases in coral $\delta^{18}O$ could imply westward flows during those times. But in both years, rapid reversals of the direction for the flow in the Sumba Strait have been shown by dramatic depleted $\delta^{18}O$ peak in May 1996 and May 1997. These two examples also show that even heavier rainfall and greater ITF could not make the Indonesian inner sea water fresh enough for the distinct freshening during autumn and some other time in summer. So all the remarkable depleted coral $\delta^{18}O$ peaks could be attributed to input of Indian Ocean water into the Savu Sea. Therefore the Sumba coral $\delta^{18}O$ record shows that during the following years there should be strong penetration of the SJC water through the Sumba Strait and into the Savu Sea during 1962-1998 even before the rainfall record starting in 1980 (Figure 6.21 and 6.18): the autumns (late March to June) of 1981, 1967, 1968, 1971, 1972, 1976, 1977, 1978, 1979, 1981, 1982, 1983, 1987, 1988, 1989, 1991, 1993, 1996, and 1997; the summers of 1965, 1990, 1991, 1996, 1997 (please note: the "summer of a year" in this thesis refers to November and December of the previous year and the January and February of this year). As shown in Figure 6.21, there were also many years when the input from the SJC seems to have happened but was not as strong as the above-mentioned years. So it could be concluded that the inflow of the Indian water into the Savu Sea is very common during summer time and happens in most of years; heavy inflow happens mainly in April and May and the inflow in summer in November and December happens but not as frequently and strongly as in autumn. There are also some years when the inflow did not happen or happened weakly, such as in summers of 1964, 1966, 1969, 1970, 1980, 1984, 1985, 1986, 1992, 1994, 1995.

By comparing this coral $\delta^{18}O$ record with the only available instrumental time series for the surface velocity fluctuation inferred by pressure difference across the strait [*Chong et al.*, 2000] during the period December 1995 to April 1998 (Figure 6.23), we conclude that Sumba coral $\delta^{18}O$ faithfully reflects fluctuations in the direction and source of the surface flows in the Sumba Strait during summer (November to May or June). Not only have the corals recorded the major eastward currents during summer/autumn, it is very

sensitive to major westward currents. Most of the changes in current direction and intensity could be reflected in this high-resolution Sumba coral $\delta^{18}O$ record, not only in summer, but also in winter.

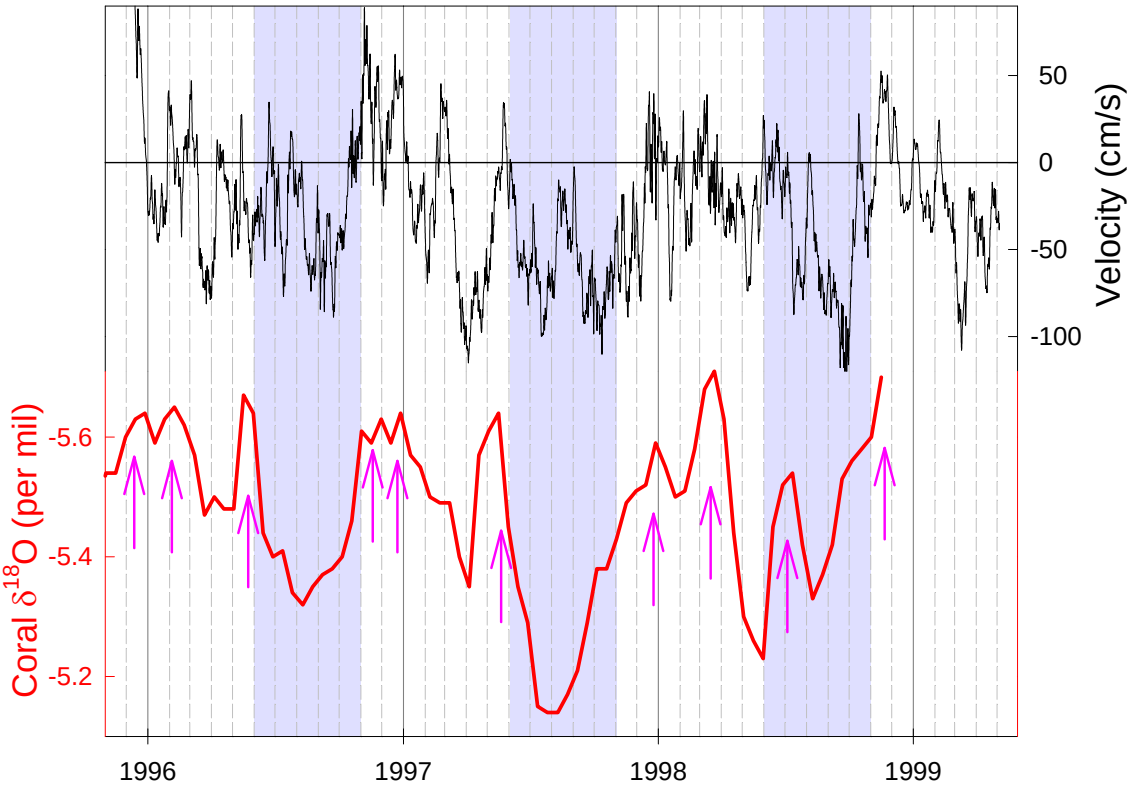

Figure 6.23 High-resolution Sumba coral $\delta^{18}O$ records the oceanic currents entering into or flowing out of the Savu Sea through the Sumba Strait. Shaded areas represent austral winter with lower sea surface temperature during June through October. Lower panel (red curve) is the overlapping part of the fortnightly $\delta^{18}O$ of coral RSM2b until November 1998. Upper panel (black curve) is the cross-strait geostrophic surface velocity (unsmoothed hourly data) for Sumba Strait during December 1995 to May 1999 monitored by the pressure gauge array [*Chong et al.*, 2000]. The velocity data were kindly provided by J. Sprintall. Note the negative values in velocity indicate flow into the Indian Ocean, while the positive values indicate flow of warmer, fresher surface water [*Bray et al.*, 1997; *Sprintall et al.*, 1999] into the Savu Sea. The coral $\delta^{18}O$ would be more depleted in ^{18}O when the ambient surface sea water is warmer and fresher. The pink arrows show some of the major events of eastward flow of the warmer, fresher water into the Savu Sea reflected by the coral $\delta^{18}O$.

The timings and the periods of lasting of the distinctly depleted coral $\delta^{18}O$ peaks suggest that they are mostly likely associated with the semiannual passage of the downwelling coastal Kelvin waves through the Savu Sea. The Kelvin waves are due to

westerly wind forcing in the remote equatorial Indian Ocean during the semiannual April/May and October/November monsoon transition periods [*Clarke and Liu*, 1993; 1994]. Spectral analysis has shown that both the interannual variabilities for late and summer coral $\delta^{18}O$ have a 3.1 yr periodicity linked with the tropical Indian Ocean winds [*Wijffels and Meyers*, 2004]. Recently Syamsudin et al. recognized Kelvin wave activity along the Lesser Sunda Islands during 1993 to 1998 according to the sea surface height anomaly data [*Syamsudin et al.*, 2004, Figure 3a] and our coral $\delta^{18}O$ result is consistent with it very well in that there is no Kelvin wave during the whole 1994 and 1995 and the summer in 1998 (in fact, November and December of 1997), and all the 5 Kelvin waves recognized by them could be found in our coral $\delta^{18}O$ record (numbered green arrows in Figure 6.18). Chong et al. also reported a distinct semiannual frequency for the surface velocity during December 1995 to April 1998 in the Sumba Strait measured by pressure gauges and showed the speed of eastward propagation of this wave from Bali to the Ombai Strait was 2.5 m/s, commensurate with linear wave theory [*Chong et al.*, 2000, Figure 2]. Strong eastward currents in upper 150 m surface water in December 1995 have been unambiguously measured in the Sumba Strait using pressure gauges [*Hautala et al.*, 2001] and in the Ombai Strait using current metres [*Molcard et al.*, 2001a]. Sprintall et al. have detected strong remote forced Indian Ocean Kelvin wave passing through Lombok Strait and intruding into Makassar Strait in May 1997 by a suite of contemporaneous measurements. Wijffels and Meyers' also recently concluded that the Kelvin energy can jump into the Savu Sea based on temperature and sea level analysis since 1983 within the Indonesian seas and southeast Indian Ocean [*Wijffels and Meyers*, 2004]. Even though majority of the incoming Kelvin wave energy is supposed to enter into the Lombok Strait [*Syamsudin et al.*, 2004], our Sumba coral $\delta^{18}O$ record shows that in most of the years during 1962 to 1998 the coastal trapped Kelvin wave continued to propagate eastward along the Lesser Sunda Islands and penetrated through the Sumba Strait, indicative of the remote forced coastal downwelling Kelvin wave entering into the Savu Sea as a routine phenomenon.

The Sumba coral $\delta^{18}O$ seems to show that the penetration of the semiannual Kelvin

wave into the Savu Sea happens much more frequent in austral autumn (March to June) than that in austral summer (November and December). That may be partly because that the eastward Wyrtki Jet in the tropical Indian Ocean associated with the Kelvin wave is weaker during the October/November transition period when the Somali Jet in the Arabian Sea appropriates some of the South Equatorial Current (SEC) [*Wyrtki*, 1973]. More possibly, this penetration still happens during November or December in many of the years, but the intensity is much weaker. Two reasons could make the coral record a weaker penetration than it is in the summer: (1) the penetration only happens in the north side of the Sumba Strait due to a weaker Kelvin wave (it is possible because partly eastward flows in the strait have been observed in March 1997 and March 1998 [*Hautala et al.*, 2001] and the effect on the ambient water of the coral in the south side of the strait is much less both in temperature and salinity; (2) The salinity of the South Java Current in summer is possibly not as low as that in autumn because it is before the summer rainfall peak time (Sprintall et al. observed a obvious freshening of the SJC when a autumn Kelvin wave arrived showing the salinity of the SJC water before the arrival of the autumn Kelvin wave is lower [*Sprintall et al.*, 2000]) and it would not bring on a distinct depleted peak in coral $\delta^{18}O$ as that in autumn. The much weaker monsoon periodicity component (2.7 yr) in the summer coral $\delta^{18}O$'s interannual variability than in the autumn also support that the salinity of the inflow in summer might not be as low as that in autumn. The strong 3.1 yr periodicity strongly suggests that the summer input of the Kelvin wave.

The Kelvin waves during the monsoon transitions appear not to be the only source for the inflow of the Indian Ocean into the Savu Sea during the austral summer time (November to May). These Kelvin wave only last for around one month, but distinct freshening during summers of 1996 and 1997 recorded by the Sumba coral $\delta^{18}O$ were much longer than 1 month, showing input of the SJC during summer time other than the Kelvin wave periods. It is very reasonable that the lasting eastward flowing of the SJC during the northwest monsoon season from November through April could penetrate the Sumba Strait into the Savu Sea when condition is favourable. For example, weak

eastward subsurface flow have been found in the north side of the Sumba Strait during March 1997 and 1998 [*Hautala et al.*, 2001] even though the south side Sumba coral recorded westward Indonesian inner sea water in March 1997 and a distinct freshening possibly resulting from eastward input of SJC in March 1998 when there was no remote forced Kelvin wave [*Chong et al.*, 2000; *Sprintall et al.*, 2000; *Syamsudin et al.*, 2004]. Even though there was no obvious eastward Kelvin wave in November or December 1993 (see this Sumba coral $\delta^{18}O$ record and [*Syamsudin et al.*, 2004], three of five surface drifters deployed in the central Indo-Australian Basin in November moved north-eastward into the Savu Sea in the following 4 months, clearly indicating the occurrence of eastward flowing of the SJC in the austral summer time without the remote forced Kelvin wave. Decrease in rainfall when a positive IOD or El Niño event occurs would reduce the salinity of the SJC and then blur the input signal of the SJC into the Savu Sea in some extent, the enriched coral $\delta^{18}O$ in summers of 1992, 1994, and 1995 demonstrates this possibility.

The Sumba coral $\delta^{18}O$ have shown strong interannual variability for the inflow of the Indian Ocean water into the Savu Sea during the austral summer. Even though the ENSO influences this interannual variability, certain process intrinsic within the Indian Ocean dominantly controls this variability of input. The autumn remote forced Kelvin seems to have remarkable impact for the ITF, even though the Kelvin wave only influences the surface current of the SJC. Model experiences have shown that most of the ITF transport through the outflow straits occurs in the upper 100 m [*Potemra et al.*, 2002; *Potemra et al.*, 2003]. The transport minimum through the Ombai Strait during December 1995 through November 1996 coincides with the intrusion of the Kelvin wave in May [*Molcard et al.*, 2001a]. The eastward transport maximum in the SJC transport climatology [*Meyers et al.*, 1995] coincides with the distinct freshening of the Savu Sea in the Sumba coral $\delta^{18}O$ climatology which has been attributed to the penetration of the autumn Kelvin wave into the Savu Sea during late March to May. Therefore the tropical Indian Ocean wind seems to have significantly influenced the transport through the Savu Sea which is one of most important exits of the ITF.

6.4.5 Strong impact of the Asian-Australian monsoon

The annual climatology analysis of the coral $\delta^{18}O$ has demonstrated an outside source of fresh water. Furthermore, spectral analysis of seasonal $\delta^{18}O$ and the correlation between seasonal rainfall and the seasonal coral $\delta^{18}O$ confirmed the monsoonal rainfall source of the freshwater, indicative of strong impact of monsoon on the autumn coral $\delta^{18}O$ record. In addition, the monsoon also has remarkable signature in the spectrum of winter coral $\delta^{18}O$ record, showing obvious impact of monsoon on winter climate and oceanography in the Sumba Strait.

The Sumba coral $\delta^{13}C$ record has also shown the strong impression of the heavy summer rainfall which contributed to the depleted peak of the annual minimum of the coral $\delta^{13}C$ by bringing along abundant terrigenous nutrients in summer rainfall peak time. The unique density rhythm of the Sumba coral shows that the summer low-density bands is strongly attributed to the strong rainfall and so is the big rate of annual extension of the coral.

In sum, the Sumba coral recorded strong influence of the Asian-Australian monsoon system in this area.

6.5 CONCLUSIONS

This study demonstrates that the Sumba modern corals are excellent recorders of modern climate and oceanography in the Indo-Pacific warm pool. High-resolution (fortnightly) time series, stacked annual climatology, and seasonal means have been characterised for both the modern coral $\delta^{18}O$ and $\delta^{13}C$. Detailed correlation and spectral analysis of these features with local instrumental records, and main climate system indexes such as NINO3.4 index, All India Summer monsoon rainfall, and the Dipole Mode Index have been conducted. Blackman-Tukey spectra of annual and seasonal coral $\delta^{18}O$ and $\delta^{13}C$ characteristics and their cross-spectra with the above-mentioned

climate system indexes have also been carried out. These correlations demonstrate that the ENSO, Asian-Australian monsoon, and remote equatorial Indian Ocean forcing all have strong influence on the local climate and oceanography and the high-resolution coral $\delta^{18}O$ record from Sumba, Indonesia could disassemble the entangled climate system signals in an encouraging scale and helps in understanding the climate and oceanography in this area. The Sumba coral $\delta^{18}O$ record shows the dominating control of ENSO in austral winter and the interannual variability of the winter $\delta^{18}O$ could serve as a good index for ENSO events. In austral summer and autumn (November through May), the coral $\delta^{18}O$ is overwhelmingly controlled by the tropical Indian Ocean forcing agents and the monsoon.

The high-resolution Sumba modern *Porites* coral $\delta^{18}O$ provides evidence for the routine penetration of the South Java Current (SJC) in austral summer and remote forced equatorial Indian Ocean Kelvin wave in autumn into the Savu Sea, which results in distinct freshening of the surface ocean during the austral autumn. By sensitively recording variability of sea surface temperature and salinity in this important exit of the Indonesian Throughflow (ITF), the Sumba coral $\delta^{18}O$ revealed active oceanic current activity in Sumba Strait. In austral winter, westward currents generally flow in the Sumba Strait and the ITF brings Pacific source-water with moderate salinity. In summer, the more saline SJC enters the Savu Sea from the west until around March. After March, two causes gradually lower the seawater salinity: the gradual weakening of the eastward SJC owing to the weakening of northwest monsoon winds, and the arrival of a remotely forced Kelvin wave with very warm and fresh water during April-July. Input of Indian Ocean water into the Savu Sea by the summer SJC and autumn Kelvin wave could have significantly influenced the transport of the Indonesian Throughflow.

The Sumba $\delta^{13}C$ shows clear annual cycles and recorded a distinct depletion in $\delta^{13}C$ during the austral summer time (December to March). Our result shows it results from the large input of terrigenous nutrients linked to local heavy summer monsoonal rainfall. A consistent annual maximum during early October in the coral $\delta^{13}C$ is supposed to be

linked with the maximum of the local incoming short-wave radiation.

Unique density banding in the Sumba modern coral is presented. There are two high-density bands and two low-density bands in a certain year. Detailed study on the banding and correlation with the high-resolution $\delta^{13}C$ record indicate that the unique low-density band in summer resulted from the largely increased availability of terrigenous nutrients connected to the heavy rainfall during the north-west monsoon season. Unlike the coral $\delta^{13}C$, during off-rainfall season the coral density banding is more related to the ambient seawater temperature, rather than the local incoming short-wave radiation.

Long-term trends have been shown in both the coral $\delta^{18}O$ and $\delta^{13}C$ records. The increased global warming has been attributed to the $\delta^{18}O$ trend and both the warming and the oceanic Suess effect have been attributed to the long-term trend of depletion in $\delta^{13}C$. Substantial decadal variability has been found in both the coral $\delta^{18}O$ and $\delta^{13}C$ records, and they are usually linked with the change in background climate and oceanography. Variation in input of warm, low-salinity water from the SJC into the Savu Sea in decadal time scale would also add to the decadal variability of the coral $\delta^{18}O$, such as that in the early 1990s. Large decadal variations in sea surface temperature and salinity in the Savu Sea have been proposed and the variability is supposed up to 0.3℃ and 0.5 ups. Salinity variability in the Savu Sea during 1962 to 1998 has been reconstructed and a remarkable increase in 1974 to 1989 and rapid recover in 1989-1998 has been identified.

The annual climatology of coral $\delta^{18}O$ and $\delta^{13}C$ is a very effective means to simplify and recognize the forcing agents for the variability of the records, especially in an area like Indonesia with entangled multi-systems of climate and oceanography.

CHAPTER 7

CORAL EVIDENCE FOR VARIATION IN MONSOON, ENSO, AND EQUATORIAL INDIAN OCEAN FORCING SINCE THE MID-HOLOCENE

ABSTRACT

High-resolution Holocene coral $\delta^{18}O$ and $\delta^{13}C$ records have been extracted from 4 *Porites* corals in Sumba Strait, Indonesia, where the Asian-Australian monsoon, El Niño-Southern Oscillation (ENSO), and the remote equatorial Indian Ocean forcing have strong impacts on the local climate and oceanography. Both coral $\delta^{18}O$ and $\delta^{13}C$ climatology have been reconstructed, and magnitude and periodicity of the interannual variability of the coral records have been achieved. Strong seasonal variation in the association between the Sumba coral records and the three prevailing climate phenomena has been found, which helps to partly disentangle the three intertwisted climate systems and makes it possible to reveal the variation in the individual climate systems since mid-Holocene. Both the coral $\delta^{18}O$ and $\delta^{13}C$ register a weakening monsoon from 5.7 ka to the present. Fortnightly resolution coral $\delta^{18}O$ records for windows since 5.7 ka illustrate climate scenes distinct from the modern time in the relative intensity and variability of the three climate components in one specific location: at 4.8 ka both the El Niño and summer monsoon were strong and the remote equatorial Indian Ocean forcing was weak; at 3.7 ka ENSO was weak, the monsoon was stronger than at present, a dominant forcing from the remote equatorial Indian Ocean might have caused strong IOD events. These results provide a historical perspective for the understanding of the physical processes and interplay of the three intertwisted climate phenomena.

7.1 INTRODUCTION

The Asian-Australian monsoon is the largest atmospheric circulation system in the world, straddling two continents of the Asian and Australia and two ocean basins of the Indian and Pacific Oceans. Extremes in the interannual variability of the monsoon rainfall result in devastating floods and droughts leading to enormous economic loss and human misery [*Webster et al.*, 1998]. Therefore, understanding of the physical processes responsible for the observed interannual variability of the monsoon is crucial for advancing the capability of predicting the interannual variability. Previous studies have demonstrated that the coupled atmosphere-ocean mode of ENSO in the Pacific basin is one of the most important factors influencing the interannual variability [*Rasmusson and Carpenter*, 1983; *Shukla and Paolino*, 1983; *Holland*, 1986; *Meehl*, 1987; *Webster and Yang*, 1992]. A recently identified coupled atmospheric-ocean mode of the Indian Ocean Dipole (IOD) in the Indian Ocean basin [*Saji et al.*, 1999; *Webster et al.*, 1999] has also been suggested to impact the monsoon in interannual time scale [*Guan and Yamagata*, 2003; *Li et al.*, 2003; *Loschnigg et al.*, 2003; *Saji and Yamagata*, 2003; *Ashok et al.*, 2004].

As a matter of fact, not only the ENSO and IOD influence the monsoon, but also the three climate phenomena interplay with each other, such as the impact of the monsoon to ENSO [*Yasunari*, 1990; *Chung and Nigam*, 1999; *Kirtman and Shukla*, 2000], and the interaction between IOD and ENSO [*Saji et al.*, 1999; *Baquero-Bernal et al.*, 2002; *Behera and Yamagata*, 2003; *Hastenrath*, 2003; *Loschnigg et al.*, 2003; *Yamagata et al.*, 2004; *Yu and Lau*, 2004; *Behera et al.*, 2006]. Owing to the complication of the three intertwisted climate systems, many controversial theories have been argued about the physical processes and their interplays. Part of the reason is that most of the studies of observation or modelling are based on time-limited instrumental records and sporadic historical documents. In order to achieve further understanding for the complicated climate phenomena which are all of global influence, more historical records should be

dug out especially those with high-resolution and under distinctly different climate conditions.

Here we apply fortnightly-resolved coral $\delta^{18}O$ and $\delta^{13}C$ records to reconstruct the intensity and variability of the monsoon, ENSO, and IOD in 4 Holocene periods of 5.7, 4.8, 3.7, and 0 ka. Modern and fossil coral $\delta^{18}O$ has successfully been applied to demonstrate the variability of the ENSO [e.g. *Cole et al.*, 1993; *Dunbar et al.*, 1994; *Fairbanks et al.*, 1997; *Hughen et al.*, 1999a; *Urban et al.*, 2000; *Tudhope et al.*, 2001; *Cobb et al.*, 2003], the monsoon [e.g. *Charles et al.*, 1997; *Sun et al.*, 2005], and the Indian Ocean Dipole[*Abram et al.*, 2003; *Abram et al.*, 2007]. Furthermore, the corals are from the Sumba Strait, Indonesia, especially well situated for exploring the activity of the three climate phenomena because all of the three phenomena prevail there.

The Sumba Strait is located in the pathway of the annual migration of the Asian-Australian monsoon convective centre from over the South Asian subcontinent to over the Australian continent, so this region is subject to seasonally reversing monsoon winds that are from the northeast in austral winter (April through November) and from the northwest in austral summer (December through March) with strong rainfall during the summer monsoon. The Maritime Continent is between the Pacific and the Indian Ocean and is thought of as the intersection of two remote equatorial wave guides of both oceans [*Wijffels and Meyers*, 2004]. The ENSO of the tropical Pacific has been demonstrated to have strong influence in the rainfall and sea surface temperature (SST) of the Indonesian region [*Nicholls*, 1984; *Ropelewski and Halpert*, 1996; *McBride et al.*, 2003], and the IOD has also been shown to impact the rainfall and the SST of this region [*Saji et al.*, 1999; *Abram et al.*, 2003]. Since the Sumba Strait is one of the most important passage of the Indonesian Throughflow [*Gordon*, 2005], the Indonesian Throughflow water that exits the Sumba Strait also carries both ENSO and IOD signals in temperature and salinity which are integrated into the water in the inner Indonesian seas. Recent studies also demonstrate that the coastal Kelvin wave forced by the remote equatorial Indian Ocean winds has penetrated the Sumba Strait [*Hautala et al.*, 2001;

Molcard et al., 2001] and the interannual variability of the Indian Ocean coastal region along the Indonesian archipelago has dominating origin of remote equatorial Indian Ocean forcing and the IOD events [*McClean et al.*, 2005]. Taken together, the Sumba coral should be a very good target for exploring the evolution and interplay of the complicatedly intertwisted monsoon, ENSO, and the equatorial Indian Ocean forcing.

7.2 MATERIALS AND METHODS

7.2.1 Coral sampling and isotopic analysis

A 1.12 m long core (MS7) of 75 mm diameter was collected from a *Porites* at Mutiara Site (9°28.886'S, 120°08.513'E，Figure 5.1) in 1998. The top of the near-spherical colony (1.3 m diameter) was just below the spring low-tide level. Two shorter *Porites* cores of 50 mm diameter were drilled in 1995: coral RS5b from River Site is well exposed on the Holocene reef flat during low tide and coral BS3a from Bridge Site (~200 m seaward of the beach) is exposed in a creek-bed (Figure 5.1). 37 and 11 year-long records for two local modern corals (RSM2b and SU1) are used in this study as baseline coral records of the climate and oceanography (details in Chapter 6).

The cores were slabbed and X-ray photographed as a guide for sub-sampling transects along the axis of maximum growth. Even though this MS7 core is much denser than the modern core RSM2b and the annual density banding is much less clear, annual growth cycles could still be identified by clear fluorescent banding under UV light. Sub-sampling followed the procedure developed by Gagan et al. [1994; 1998] and the interval for every sub-sample is 0.6 mm, which is slightly more than fortnightly resolution.

Oxygen and carbon isotope analyses were obtained by reacting ~200 μg aragonite samples with two drops of 103% H_3PO_4 at 90°C for 12 minutes in an automated individual-carbonate reaction (Kiel) device coupled with a Finnigan MAT-251 mass spectrometer at ANU. The isotope ratios are reported in standard delta notation relative

to Vienna Peedee Belemnite (VPDB) and calibrated via the NBS-19 calcite standard ($\delta^{18}O$ = -2.20‰, $\delta^{13}C$ = 1.95‰) and the NBS-18 calcite standard ($\delta^{18}O$ = -23.0‰, $\delta^{13}C$ = -5.0‰). The analysis precision ($\pm 2\sigma$) were 0.09‰ ($\delta^{18}O$) and 0.04‰ ($\delta^{13}C$) for NBS-19 (n = 238).

For $\delta^{18}O$ and $\delta^{13}C$ measurement of the coral MS7, firstly every second sub-sample was measured, which equals monthly in resolution. Then neighbouring sub-samples were added for periods when skeletal isotopic composition changed rapidly, especially during austral winters, resulting in fortnightly resolution. 1125 sub-samples were measured and 57.5 years of records have been recovered for coral MS7, with average sampling frequency of isotope analysis of 20 samples per year, slightly less than fortnightly resolution.

The sample preparation and isotope measurement for RS5b and BS3a were carried out by Heather Scott-Gagan applying the same procedure and methodology as that of MS7 at the same laboratories at ANU.

7.2.2 Age determination and chronology

3 fossil *Porites* corals were uranium-series dated using thermal ionisation mass spectrometer at the Laboratoire des Sciences du Climat et de l'Environnement, Gif-sur-Yvette Cedex, France by Linda Ayliffe. The results are shown in Table 7.1.

Table 7.1
U-Th dating analysis for Sumba Holocene corals

Sample	U (ppm)	$(230/238)_{act}$	$\delta^{234}U_{(t)}$	$\delta^{234}U_{(initial)}$	$(230/232)_{act}$	Age (cal. yr)
MS7	2.5285	0.0388	148.8	150.4±2.3	373±5	3732±42
RS5b	2.9130	0.0496	149.7	151.8±2.5	2199±23	4791±40
BS3c	2.8430	0.0586	143.4	145.8±2.3	797.±4	5713±46

58 years of $\delta^{18}O$ and $\delta^{13}C$ records have been recovered from the MS7 coral core (3.7 ka by U-Th dating). Two shorter records have been obtained from RS5b and BS3a (4.8 ka

and 5.7 ka by U-Th dating) and span 21 years and 4 years, respectively. The annual cycles were assigned by cross-checking the annual density bands counted from the X-ray positive image or fluorescent banding under UV light against the annual $\delta^{18}O$ cycles.

A detailed chronology was established assuming that the annual arrival-time of the winter SST minimum in the Holocene was the same as today in Sumba, which is supported by the fact that the seasonal minimum of solar radiation occurred at the same time of the year for all the periods of this study (Figure 7.7). Analysis of SST records [IGOSS, *Reynolds et al.*, 2002] for 1982 to 2005 indicates that winter SST minima at Sumba ($1^\circ \times 1^\circ$ grid centred at 120.5° E, 9.5° S) arrive near 8 August ($\pm$32 day, 2σ, n = 24). This annual arrival-time of the winter SST minimum is assigned to each coral $\delta^{18}O$ annual maximum, and then equal time spans are allocated to the data points between adjacent $\delta^{18}O$ maxima by integration interpolation using *Analyseries* [*Paillard et al.*, 1996]. Like the modern records, 26 equal intervals were assigned between two neighbouring winter $\delta^{18}O$ maxima for all the Holocene records. The fortnightly resolution of the chronology is close to the measurement resolution.

7.2.3 Assessment of diagenetic alteration

A full suite of diagenetic screening techniques have been applied to ensure the veracity of the paleoclimate reconstruction from skeletal geochemical records of Holocene coral MS7. The core top is discoloured and the top 10 cm has not been used for any further geochemical analysis. There was no calcite observed under UV light for the whole MS7 core, and X-ray diffraction (XRD) results confirmed that the MS7 core contains no significant calcite. The X-radiograph of the 7-mm thick slab of the core (Figure A.2 in Appendix E), however, revealed that the lowermost part of the core contained a 10-cm section with physical evidence of alteration showing increased skeletal density. Visual inspection of the petrographic thin-sections and scanning electron microscopy (SEM) images (Figure A.3 in Appendix E) confirmed the excellent preservation of most part of

the core and revealed that the physical alteration on the lowermost 10 cm resulted from presence of secondary abiotic aragonite.

A 65 mm by 25 mm petrographic thin-section paralleling the geochemical sub-sampling transection C was employed to assess the diagenetic alteration of the geochemical data in this coral (refer to Appendix E for details). The result of detailed comparison between coral $\delta^{18}O$ and the petrographic images (see Appendix E) indicates that only the first two annual cycles of the $\delta^{18}O$ and $\delta^{13}C$ have undergone diagenetic alteration. The altered part in the first two annual cycles in the Holocene coral MS7 will not be used in the further study. Similar assessment has been conducted for BS3a and RS5b, and the geochemical data used in this study are not diagenetically altered.

Recent researches indicated that secondary aragonite occurred in early marine diagenesis would bring on significant shift toward higher coral $\delta^{18}O$ and $\delta^{13}C$ relative to pristine corals [*Enmar et al.*, 2000; *Muller et al.*, 2001; *Muller et al.*, 2004; *Gallup et al.*, 2006; *Quinn and Taylor*, 2006], where replacement or addition of calcite involving meteoric water would negatively shift those geochemical indices [*Stein et al.*, 1993; *Zhu et al.*, 1994; *Wei et al.*, 1998; *McGregor and Gagan*, 2003]. The result of the diagenesis assessment on the MS7 coral is largely consistent with those observations. The MS7 coral is most possibly restricted in marine environment in the past 3.7 thousand years given the stable uplift of about 0.49 m/kyr in the study area (Chapter 5), and only the basal part of the core experienced progressive addition and replacement of secondary aragonite. Even the amplitude of the change that secondary aragonite brings to coral $\delta^{18}O$ is comparable to those early observations. For example, recent result of Quin and Taylor [*Quinn and Taylor*, 2006] indicated that 20% of secondary aragonite could bring a shift of 0.5‰ higher $\delta^{18}O$ value, and this study displays a 0.25‰ shift in the first winter $\delta^{18}O$ with presence of 10% of secondary aragonite (between C and D in Appendix E, Figure E.4).

Two new findings are noticeable from this study (refer to Appendix E for details). The first one is the clear annual cycles in altered coral $\delta^{18}O$. This result shows that

progressive addition or replacement of secondary aragonite would still have a manifestation of annual cycle. The second one is that even subtle alteration in coral skeleton, such as presence of as low as less than 5% of secondary aragonite, could bring large shifts in interannual variability of coral proxies which have extensive application in recognition of important historical climate events, such as ENSO, and is the base for understanding their vicissitudes by spectral analysis. This result demonstrates that clear annual cycles and small shifts from "normal" values of coral proxy records do not ensure the pristine nature of the corals. Careful diagenesis screening should be performed before reconstructing paleoclimate using coral. And this study shows, even subtle diagenetic alteration in coral could be detected by combination of X-radiograph, petrographic observation, and analysis of interannual variability of coral proxies，and thereby the influence of diagenesis on coral reconstruction of paleoclimate and paleoceanography could be decreased to minimum.

7.3 RESULTS

7.3.1 Time series of Holocene coral $\delta^{18}O$ and $\delta^{13}C$ records

Sumba corals display clear annual cycles both in $\delta^{18}O$ and $\delta^{13}C$ with average rates of annual extension as 18.5 (modern), 16.3 (3.7 ka), 16.2 (4.8 ka), and 14.9 mm/year (5.8 ka), respectively.

There fossil corals show striking similarity in mean $\delta^{18}O$ (-5.0‰), whereas the modern coral value is -5.4‰ (Figure 7.1). $\delta^{13}C$ also show big difference between modern and fossil corals (1.36 to 1.79‰, as shown in Figure 7.2).

For the $\delta^{18}O$ records, two longer records (0 ka and 3.7 ka) exhibit evident long-term trends with different directions: the mean shifts between two ends are 0.18‰ and 0.20‰ respectively. MS7 (3.7 ka coral) shows higher-frequency decadal variability than RSM2b (modern coral), but the amplitudes of the decadal variability is similar (0.15‰).

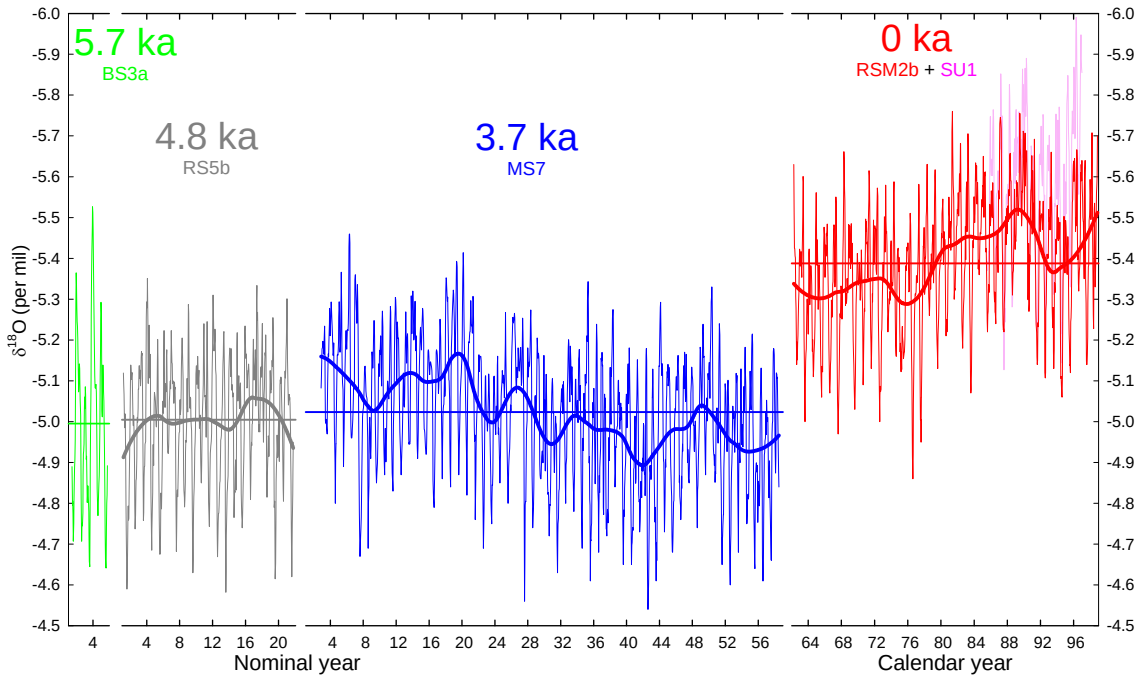

Figure 7.1 Time series of Holocene coral δ^{18}Os. Thin curves are fortnightly records and thin straight lines represent means. Heavy curves present decadal variability using 10-year smoothing with tricube weighing and 2 degree polynomial regression.

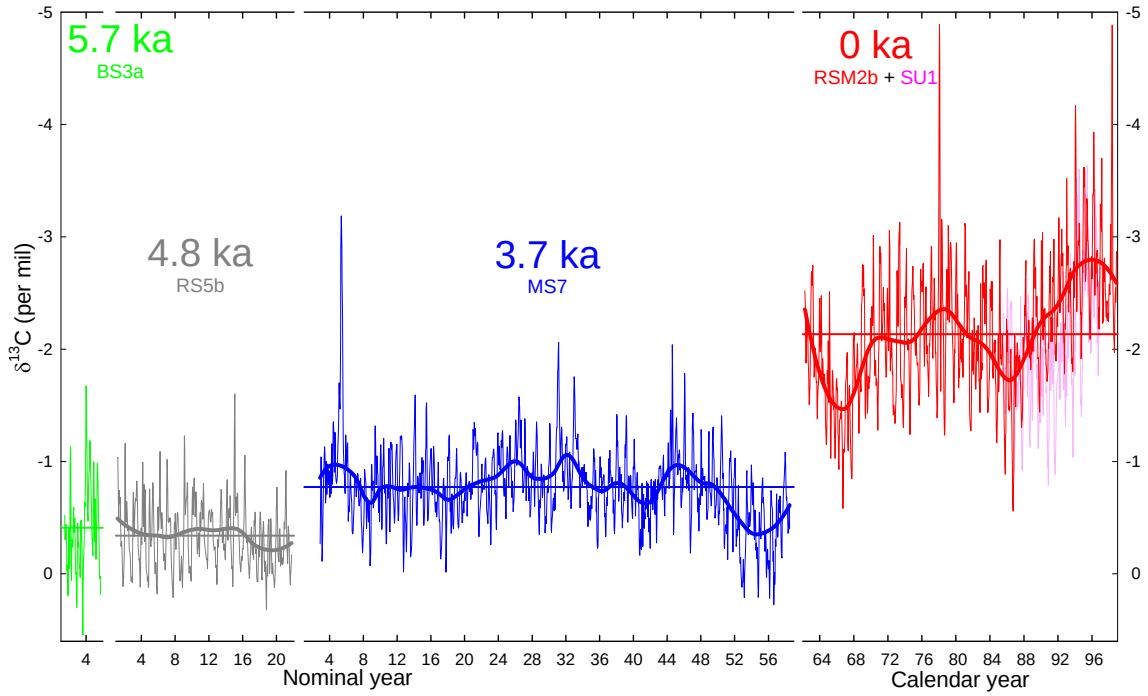

Figure 7.2 Time series of Holocene coral δ^{13}Cs. Thin curves are fortnightly records and thin straight lines represent means. Heavy curves present decadal variability using 10-year smoothing with tricube weighing and 2 degree polynomial regression.

For the $\delta^{13}C$, only the modern coral records remarkable long-term trend (0.87‰ in shift) and substantial decadal variability (more than 1‰), while the 3.7 ka and 4.8 ka corals shows relative stability in terms of decadal variability.

7.3.2 Coral climatology since mid-Holocene

In order to understand the mean climate states and their seasonal and interannual variation in the studied Holocene windows, three longer coral records have been stacked to produce coral climatology (Figures 7.3A and 7.4A). Striking similarity among all the three Holocene corals both in $\delta^{18}O$ and $\delta^{13}C$ climatology demonstrates high quality of all the geochemical data used in this reconstruction study.

$\delta^{18}O$ climatology

As shown in Figure 7.4A, the Sumba Holocene coral $\delta^{18}O$ records show similar seasonality. All three records have a narrow winter trough, a wide summer-autumn platform, and a clear autumn peak during March to May. However, dissimilarities are also evident:

1. There is an extensive summer peak in $\delta^{18}O$ in the 4.8 ka coral record that has the same magnitude as the autumn peak. The 3.7 ka coral record also shows this peak at relatively low magnitude, whereas it disappears in the modern coral record.

2. The modern coral record shows a much smaller autumn peak, relative to the 4.8 ka and 3.7 ka coral records.

3. $\delta^{18}O$ seasonality for the 4.8 ka and 3.7 ka coral records is large, relative to the modern records: 0.40±0.04‰ (2SE) at 4.8 ka, 0.39±0.04‰ (2SE) at 3.7 ka, and 0.35±0.04‰ (2SE) for the modern coral.

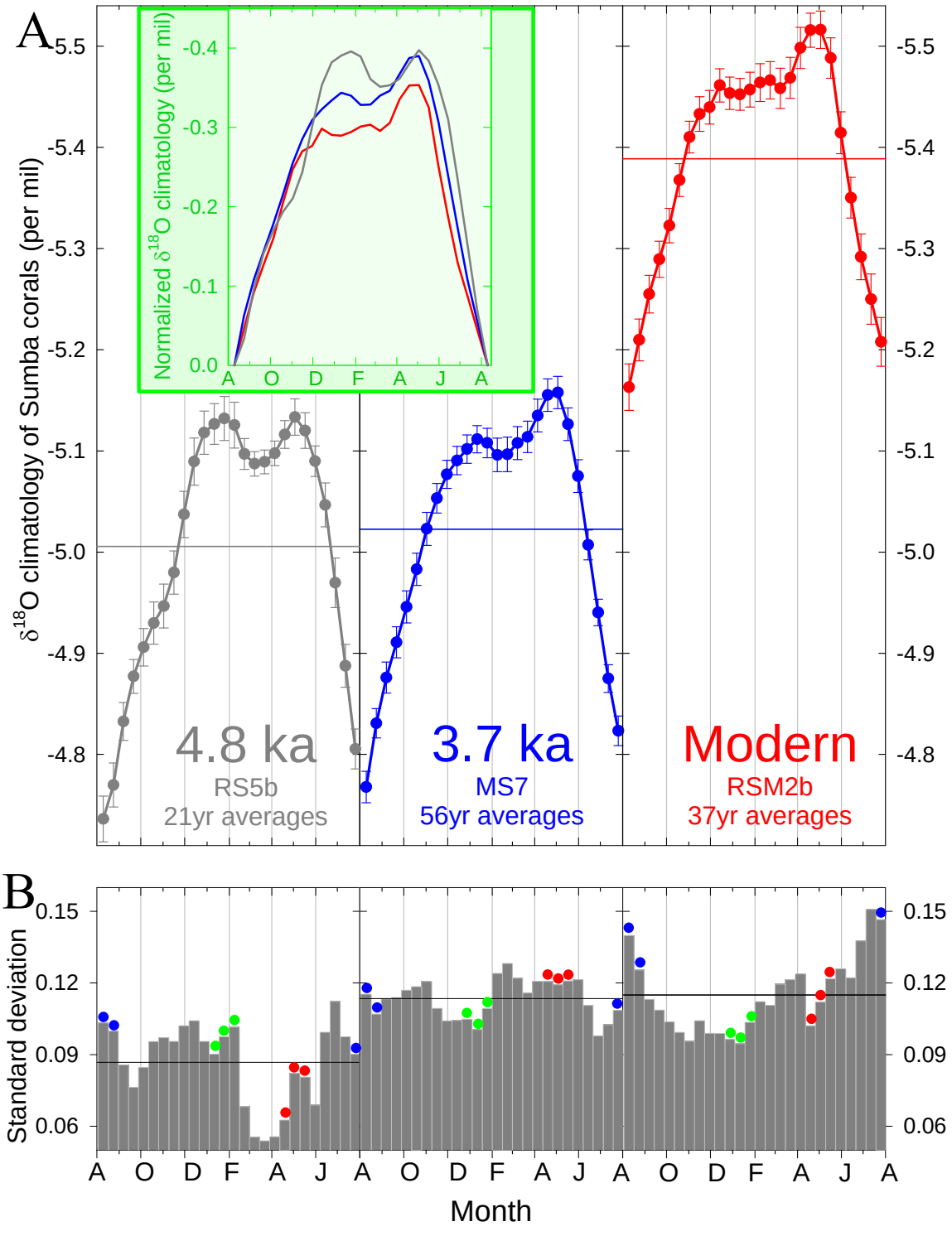

Figure 7.3 **A:** Fortnightly climatology of Holocene coral δ^{18}Os. Error bars represent standard errors of the means for individual data points. Inset is for more direct comparing: the δ^{18}O climatology was normalized relative to the winter maxima. **B:** Standard deviations for individual data points of the stacked climatology of the Holocene coral δ^{18}Os, applied to compare the amplitude of variability in particular data points. Blue, green, and red points mark the amplitude of interannual variability of coral δ^{18}O in peaks and troughs that shape the mean coral climatology in austral winter (Late July to August), summer (around January), and autumn (April to May).

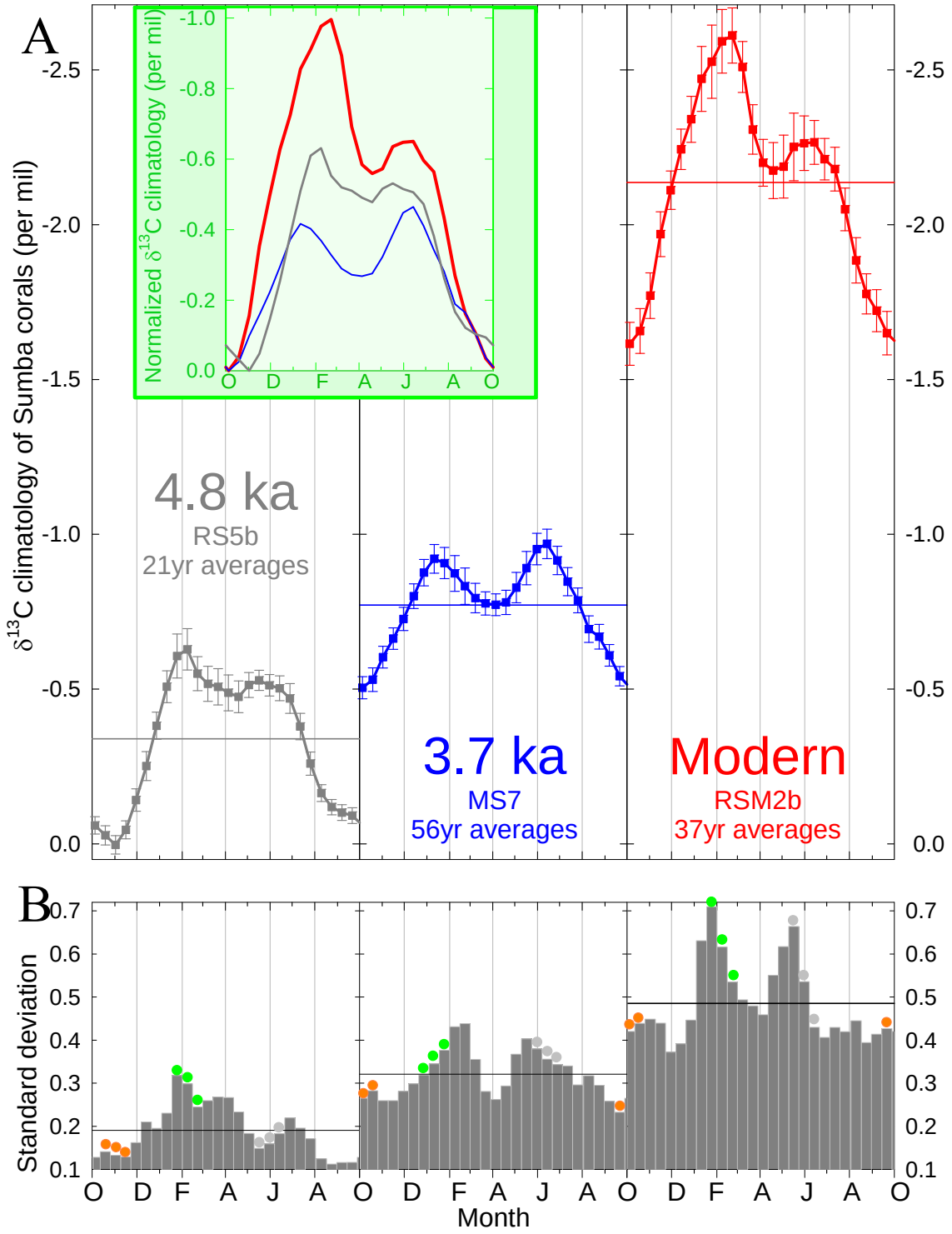

Figure 7.4 **A:** Fortnightly climatology of Holocene coral δ^{13}Cs. Error bars represent standard errors of the means for individual data points. Inset is for more direct comparing: the δ^{13}C climatology was normalized relative to the maxima. **B:** Standard deviations for individual data points of the stacked climatology of the Holocene coral δ^{13}Cs, applied to compare the amplitude of variability in particular data points. Orange, green, and grey points mark the amplitude of variability of coral δ^{13}C in peaks and troughs that shape the mean coral climatology in austral spring (around October), summer (around January to February), and autumn (around May to June).

$\delta^{13}C$ climatology

The similarity of the Holocene $\delta^{13}C$ climatology (Figure 7.4) is surprisingly impressive because $\delta^{13}C$ in corals usually complicated by more environmental factors. The $\delta^{13}C$ climatology for all three Sumba Holocene corals is shaped by a trough in austral spring and two peaks in austral summer and autumn. The coral $\delta^{13}C$ records show some striking differences in the relative magnitudes of the two peaks with the highest summer peak occurring in the modern record, a moderate summer peak for the 4.7 ka record, and a lower summer peak than the autumn peak in the 3.7 ka records. There are significant differences in the amplitudes of the mean seasonality for coral $\delta^{13}C$: 0.63±0.08‰ (2SE) at 4.8 ka, 0.46±0.08‰ (2SE) at 3.7 ka, and 1.00±0.16‰ (2SE) for the modern coral.

7.3.3 Magnitude of $\delta^{18}O$ and $\delta^{13}C$ variability

Figures 7.3B and 7.4B present standard deviations at individual data points of the fortnightly coral $\delta^{18}O$ and $\delta^{13}C$ mean climatology, applied to demonstrate the magnitude of variability of these $\delta^{18}Os$ and $\delta^{13}Cs$. Two aspects of variation in the magnitude of variability should be noticed: one is the evident seasonal difference in the magnitudes of variability within a year for single coral record; another is the difference of seasonal changes among the 3 corals. For example, the variability of $\delta^{18}O$ in autumn is much smaller than that in summer and winter for the 4.8 ka coral RS5B; but the autumn variability for the 3.7 ka coral $\delta^{18}O$ is higher than that in summer and winter; while the modern coral $\delta^{18}O$ has much higher variability in winter than that in summer and autumn. For $\delta^{13}C$ records, even though the summer variability is always higher than spring and autumn for all the 3 records, the 4.8 ka coral apparently has much stronger predominance.

7.3.4 Periodicity of coral $\delta^{18}O$ interannual variability

Figure 7.5A illustrates the periodicity of seasonal and annual coral $\delta^{18}Os$. Since the

Sumba coral $\delta^{18}O$ climatology was shaped mainly by seasonal characteristics in austral winter (July ~ September), summer (November ~ February), and autumn (March ~ May), the periodicities of mean $\delta^{18}Os$ in the three seasons and its annual means (January ~ December) have been analysed. At first the mean $\delta^{18}O$ for the corresponding period of a year were calculated. And then $\Delta\delta^{18}O$ was obtained by subtracting the subsequent year' mean. At last Lomb-Scargle periodogram using a Bartlett window was generated for $\Delta\delta^{18}O$ of the whole record using software *AutoSignal*. Choosing $\Delta\delta^{18}O$ rather than $\delta^{18}O$ is to focus on interannual variability and to suppress the decadal variability. Comparison between using $\Delta\delta^{18}O$ and $\delta^{18}O$ has indicated that using $\Delta\delta^{18}O$ could effectively keep periodic characteristics between 2 to 5 years.

Even though there is minor difference in resolution for the three corals because of the difference of numbers of years for analysis (37, 56, and 21 years for modern, 3.7 ka, and 4.8 ka corals, respectively), the similarities and dissimilarities for the periodicity are distinct both among the seasons and among the corals. We pay special attention to 3 bands of periodicity: spectral peaks near 3.6 yr, 3 yr, and 2.2 - 2.6 yr, since the Sumba coral $\delta^{18}Os$ present significant variation at these periods.

Similarities for three corals: all the three corals demonstrate strong and similar seasonal variation in periodicity. The lower frequencies with spectral peaks near 3.6 yr have much more power in winter than in other seasons, while the higher frequencies in bands of 2.2 - 2.7 yr show more dominant power in summer. The 3 yr period seems to have more power in autumn even though it also has strong power in summer.

Dissimilarities for three corals: 4.8 ka coral shows strong periodicities both in 3.6 yr and the quasi-biennial band of 2.2 ~ 2.8 yr; 3.7 ka coral has preponderant period of 3 yr, while the modern coral $\delta^{18}O$ shows similar concentration of power in the 3 bands of frequencies.

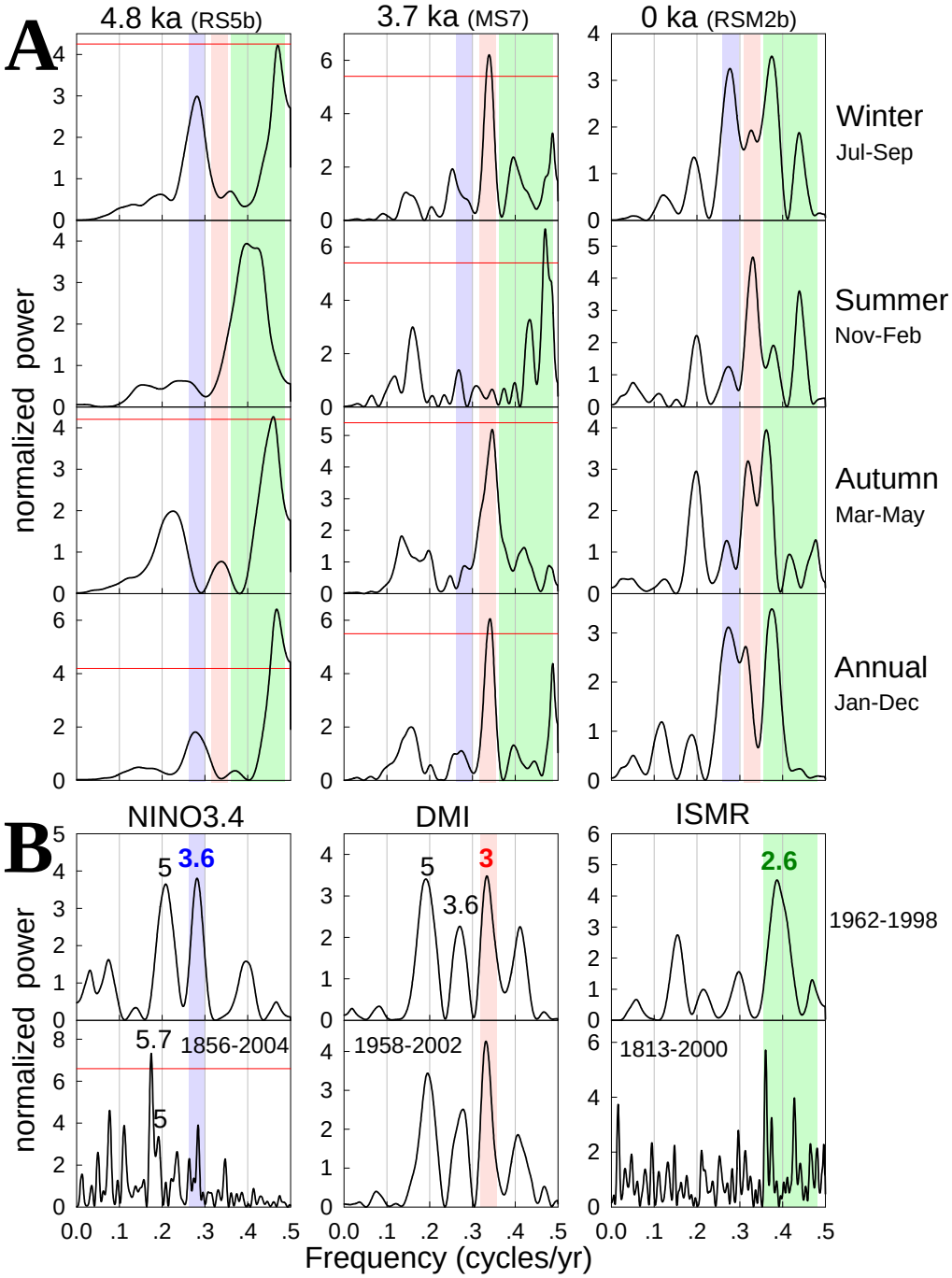

Figure 7.5 Periodicity of seasonal or annual $\delta^{18}O$ means for Holocene corals and the correlation with indices of ENSO, remote equatorial Indian Ocean forcing, and the Asian-Australian monsoon. **A:** Lomb-Scargle periodograms of mean $\Delta\delta^{18}Os$ during winter, summer, autumn, and yearly values for 4.8 ka (left), 3.7 ka (middle), and modern (right) corals. A Bartlett window is used when generating the Fourier spectra. Shaded areas represent characteristic periods of ENSO (blue, 3.6 yr), tropical Indian Ocean forcing (red, 3 yr), and the Asian-Australian monsoon (green, 2.1~2.8 yr). Thin red lines are the 90% significance levels. **B:** Lomb-Scargle periodograms of NINO3.4 index (left), Indian Ocean Dipole Mode Index (DMI, middle), and All India summer monsoon rainfall (ISMR, right). The upper panels are for data during 1962~1998, the lowers for all available data. Data sources: NINO3.4 index and ISMR from http://iridl.ldeo.columbia.edu/SOURCES/.Indices/.nino/.EXTENDED/.NINO34/ [*Kaplan et al.*, 1998] and http://iridl.ldeo.columbia.edu/SOURCES/.Indices/.india/ [*Parthasarathy et al.*, 1995], the DMI from Saji's personal webpage at http://iprc.soest.hawaii.edu/%7Esaji/dmi.txt [*Saji et al.*, 1999].

7.3.5 Periodicity of ENSO, monsoon, and equatorial Indian Ocean forcing

Since the average values for specific period of time in a year were applied to analyse the periodicity of seasonal and annual coral δ^{18}Os, the annual means of indices characterizing the three climate systems were also used to analyse their periodicity to keep consistency in favour of comparing and correlating. The results are shown in Figure 7.5B with the upper panels estimate the power spectra for data from 1962 – 1998 which is the same period for the modern coral record, and with the lower panels for all available data.

Periodicity of ENSO*:* NINO3.4 SST index from the central tropical Pacific was spectrally analysed to represent the periodicity of ENSO. The power spectrum for NINO3.4 index during 1962 – 1998 has variance concentrated in the characteristic 3.6 yr and 5 year bands (upper left panel of Figure 7.5B), which is completely consistent with previous works such as analysis of NINO3 index for 1960 – 1998 by Hughen et al. [1999b] and analysis of all El Niño events between Little Ice Age and the present by Enfield and Cid [1991], indicating that the spectral peaks around 3.6 and 5 yr are not due to aliasing by using annual means and spectral analysis using annual means of NINO3.4 index in this study could effectively catch the periodic characteristics of ENSO. Since $\Delta\delta^{18}$O was used to estimate the power spectra for coral records and the low-frequency bands near or above 5 year have been suppressed, only the 3.6 year band was used to be a characteristic period for ENSO in this study.

Periodicity of monsoon: Even though early studies considered the monsoon to be a regional physical entity, the trend in modern monsoon studies has been toward an understanding of the 'global' monsoon by studying the dynamic links between regional subsystems [*Meehl*, 1987; *McBride*, 1998; *Webster et al.*, 1998; *Trenberth et al.*, 2000; *Clemens et al.*, 2003; *Chang et al.*, 2004], The most active Indian, East Asian, and Australian monsoons are now often referred as one macroscale phenomenon as

Asian-Australian monsoon with the tropical convective maximum undergoing an annual migration from over north India in July to Indonesia and northern Australia in January [*Meehl*, 1987; *Hung et al.*, 2004; *Chang et al.*, 2005]. A quasi-biennial variability (2 – 2.8 year period centred in 2.6 year, referred as tropospheric biennial oscillation – TBO) has been found to be a fundamental characteristic for the Asian-Australian monsoon rainfall in all the India, East Asia, Indonesia, and Australia subsystem regimes [*Meehl*, 1997; *Webster et al.*, 1998 and references there; *Meehl and Arblaster*, 2002]. Even though the ENSO and IOD also display minor TBO signals, we attribute TBO signals mainly to the monsoon when the TBO is obviously dominating the power spectrum over other peaks in 2 – 5 yr bands. There is considerable seasonal persistence from the south Asian to Australian monsoon with a strong south Asian or Indian monsoon tending to precede a strong Northern Australian monsoon and vice versa for weak monsoons [*Meehl and Arblaster*, 2002; *Loschnigg et al.*, 2003; *Hung et al.*, 2004]. So, it is reasonable that All India Summer Monsoon Rainfall dataset has been used for spectral analysis in this study to display the characteristic quasi-biennial variability of the Asian-Australian monsoon in the case of lack of long-term and complete archives of local rainfall (Figure 7.5B right panels).

Periodicity of IOD and equatorial Indian Ocean forcing*:* the middle panels of Figure 7.5B illustrate the cyclicity of the Indian Ocean Dipole events [*Saji et al.*, 1999; *Webster et al.*, 1999] by estimating the power spectrum of the Dipole Mode Index from SST anomaly in the eastern and western equatorial Indian Ocean [*Saji et al.*, 1999]. Even though controversial theories have been suggested for the forcing of this recent discovered phenomenon [*Baquero-Bernal et al.*, 2002; *Meehl and Arblaster*, 2002; *Yamagata et al.*, 2004; *Yu and Lau*, 2004], IOD has been found to be strongly influenced both by ENSO [*Baquero-Bernal et al.*, 2002; *Yu and Lau*, 2004] and monsoon [*Loschnigg et al.*, 2003; *Yu and Lau*, 2004]. The power spectrum of the DMI clearly displays their strong impacts by remarkable peaks around 5 and 3.6 yr (for ENSO) and the TBO periods (for monsoon) (Figure 7.5B middle panels). However, the most salient peak in the DMI spectrum is the strong and well-separated peak around 3-year period

which is not shown in both ENSO and monsoon spectra, implying that some unique process internal within the Indian Ocean might be involved in the formation of the IOD events. Recently Wijffels and Meyers [2004] noticed that the equatorial Indian Ocean winds have much more energy at higher frequencies with spectral peaks near periods of 3 yr and between 1 and 2 yr compared to the lower-frequency energy of the Pacific winds (periods great than 3.2 yr, ENSO band) and used this to distinguish the impact of these two sources of remote energy on the Indonesian throughflow region. Sakova *et al.* [2006] also identified a very clear and well-separated 3 year period for altimeter sea surface height variability over the Sumatra-Java upwelling region and the western tropical Indian Ocean where the zonal equatorial Indian Ocean winds have substantial influence. So this 3 year period might represent the remote equatorial Indian Ocean winds which are likely one of the forcing of IOD.

Change in periodicity: the spectral analysis using the annual means has also caught the changes in ENSO behaviour, such as spectral shifts from lower amplitudes and longer periods (5.7 yr) to higher amplitudes and shorter periods (3.6 and 5 yrs) in the 1970s, which is consistent with previous results ([*Hughen et al.*, 1999b; *Kumar et al.*, 1999]. But the 3.6 yr period is still one of the most important characteristics among the interannual variability of ENSO since 1856, especially in the frequency band of 2 – 5 yr which is the focus in this study. Enfield and Cid [1991] proved that the 3.5 and 5 yr periods did not change since the Little Ice Age, and Rodbell et al. showed that the modern ENSO periodicity of 3.6 and 5 yr periods has been established since 5 ka. Therefore, in this study it is reasonable to use the 3.6 yr period to correlate the ENSO with the Holocene coral records. The quasi-biennial periods (2 – 2.8 yr) are fundamental to the monsoon [*Meehl*, 1997; *Webster et al.*, 1998 and references there; *Meehl and Arblaster*, 2002], so we assume its consistency during Holocene. There is no historical record for the variability of IOD and we would try to establish the association between the coral records and the 3 year period in this study.

For all the analysis of periodicity in coral records and the instrumental data, the similar

results have been obtained from Blackman-Tukey spectra using software ***Analyseries*** provided by Paillard [*Paillard et al.*, 1996], indicating that the achieved periodicities are not biased by different spectral methods.

7.4 DISCUSSION

7.4.1 Seasonal variation in the association between Sumba coral records and major climate phenomena

Strong seasonal variation in the association between Sumba coral records and the three climate phenomena of ENSO, monsoon, and equatorial Indian Ocean forcing has been found. This made it possible to partly disentangle the complications of the three intertwisted climate systems.

Winter coral $\delta^{18}O$ and the ENSO

It has long been known that there is a strong seasonal variation in the association between Indonesian rainfall and the ENSO [*Nicholls*, 1981; *Hastenrath*, 1987; *Haylock and McBride*, 2001; *McBride et al.*, 2003], that is, rainfall in the Maritime Continent is strongly related to the ENSO during the dry half of the year (July to November) but has a very weak association with ENSO during the summer-wet season months. The Sumba coral $\delta^{18}O$ records in this study display the same variation.

Winter $\delta^{18}O$ of Sumba modern coral has dramatic interannual variability (Figure 7.6A). Comparison between the winter coral $\delta^{18}O$ and the ENSO index indicates their strong correlation (Figure 7.6A and B). All the winters with relatively depleted $\delta^{18}O$ are corresponding to La Nina events, and all the 10 El Niño events during 1962 to 1998 according to the definition of El Niño [*Trenberth*, 1997] have been recorded with obviously enriched ^{18}O. With only two exceptions in 1967 and 1985, the Sumba winter

δ^{18}Os of 37 years are very good records for ENSO events. The obvious exception in 1967 is related to a positive event of Indian Ocean Dipole (IOD) and the minor exception in 1985 might be connected with the mid-1980s cooling of background temperature. Even though evident signatures of IOD events, the influence of ENSO is dominant by comparison of the winter coral δ^{18}O with NINO3.4 index and DMI (Figure 7.6B). The 1967 IOD event shows off because only a very weak La Niña occurred that year. The ENSO's dominating impact over IOD could be further illustrated by the obviously enriched winter coral δ^{18}O in 1992 which mainly exhibits effect of the strong El Niño not the opposite effect of the strong negative IOD event.

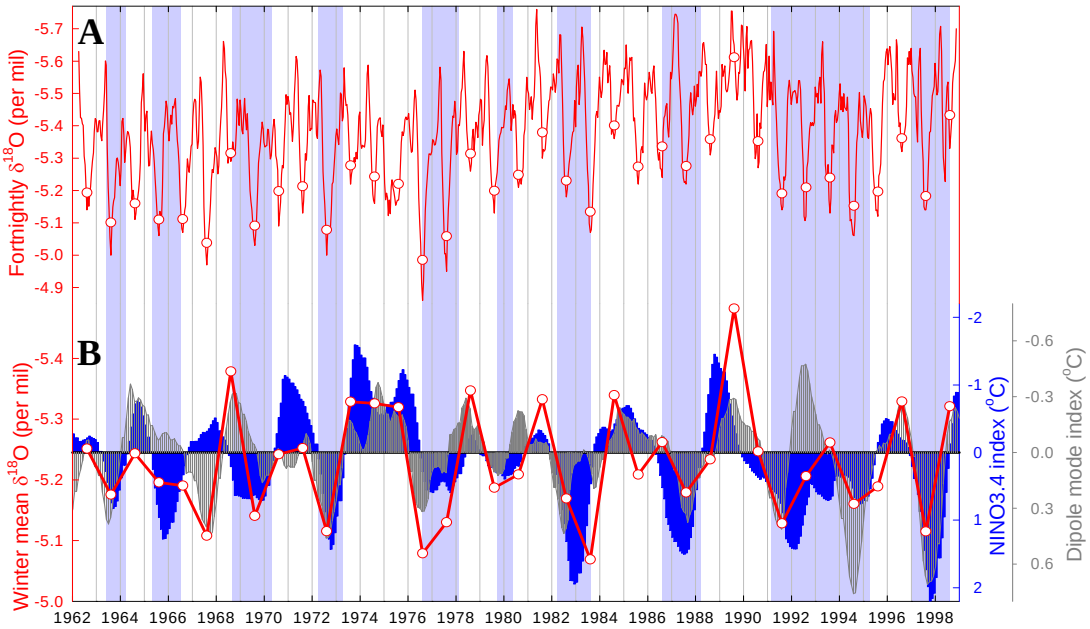

Figure 7.6 The dominant control of ENSO and the signature of IOD on winter δ^{18}O of the modern Sumba coral RSM2b. **A:** Red curve represents the fortnightly coral δ^{18}O with annual maxima in austral winters (around August). Red circles indicate the winter mean δ^{18}Os. Shaded areas represent El Niño years based on the definition of Trenberth [*Trenberth*, 1997]. **B:** Red curve with circles represents the winter averages (July to September) of the detrended coral δ^{18}O (long-term trend and decadal variability removed using the mean of winter average δ^{18}O value of -5.24‰ as the baseline). Blue and grey-shaded bars are 11-month smoothed NINO3.4 and Indian Ocean Dipole Mode Index (DMI). The sources of original monthly NINO3.4 and DMI indices are the same as in Figure 7.5.

No strong correlation could be found between the ENSO index and the coral δ^{18}O means in summer or autumn, indicative of strong seasonal variation in the association

between the Sumba modern coral $\delta^{18}O$ and the ENSO. Spectral analysis of the seasonal modern coral $\delta^{18}Os$ also supports the seasonal variation. The right panels of Figure 7.5A suggest the dominant ENSO period of 3.6 yr over IOD period of 3 yr in winter coral $\delta^{18}O$, but only very low concentrations of power in 3.6 yr compared with in 3 yr and the quaci-diennial periods in summer and autumn $\delta^{18}O$. This seasonal variation seems to occur in Holocene coral $\delta^{18}O$ records. The left panels of Figure 7.5A illustrate a very strong period of 3.6 yr in winter $\delta^{18}O$, but not in summer and autumn $\delta^{18}Os$ for the 4.8 ka coral.

Summer coral $\delta^{13}C$ and the monsoon

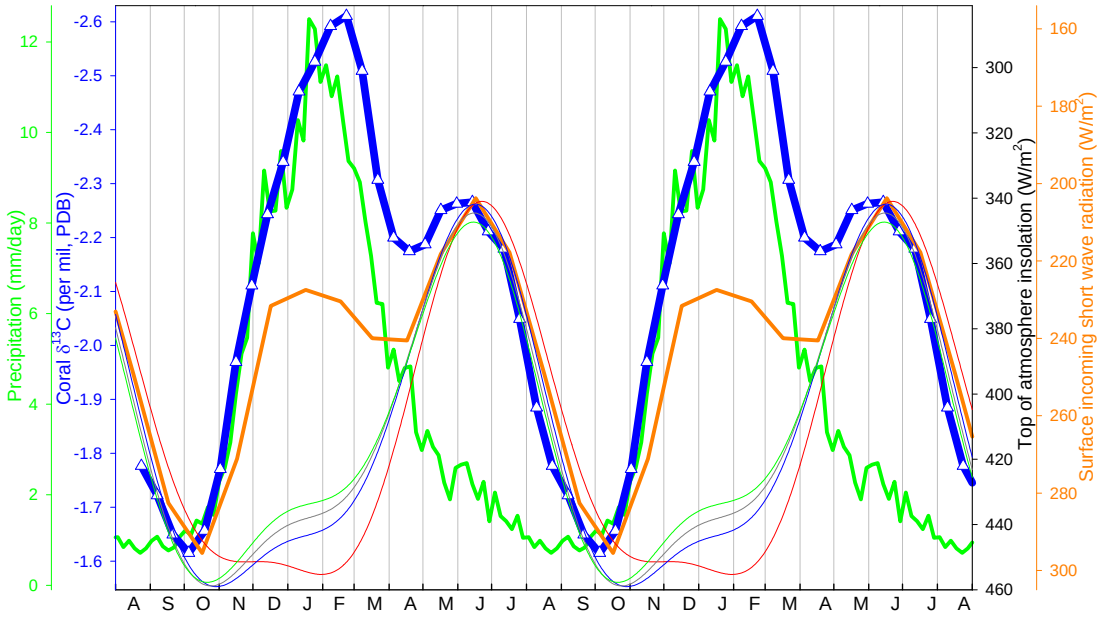

Figure 7.7 Annual climatology of modern coral $\delta^{13}C$ (thick blue curve with triangles) and comparison with annual climatology of rainfall (thick green curve), Surface incoming short-wave radiation (thick orange curve), and top of atmosphere insolation of 0 ka (thin red curve), 3.7 ka (thin blue curve), 4.8 ka (thin grey curve), and 5.7 ka (thin green curve) in the Sumba Strait. Rainfall data are from CMAP ([*Xie and Arkin*, 1997]. Monthly surface incoming short wave Radiation data are from *Atlas of Surface marine data 1994* [*da Silva et al.*, 1994]. Top of atmosphere insolation data are calculated by *AnalySeries* software [*Paillard et al.*, 1996] using the Laskar 2004 solution [*Laskar et al.*, 2004].

The association between summer Sumba modern coral $\delta^{13}C$ and monsoon rainfall peak has been demonstrated in detail in Chapter 6. During the long dry season (April to

November) the coral $\delta^{13}C$ is mainly controlled by the light availability, while during the wet season (December to March) the rainfall overwhelmingly influences the coral $\delta^{13}C$ (as illustrated in Figure 7.7). On the one hand, rainfall reduces the light availability by increased cloud cover and turbidity resulting from run-off through the nearby Mondu River during or after rainfall. On the other hand, rainfall brings a huge amount of terrigenous nutrients by the run-off and increased feeding of the coral host (polyp) on these nutrients is probably the major cause of the light skeletal $\delta^{13}C$ peak during the summer wet season in the Sumba coral RSM2b. In addition, recent human activities may have remarkably increased the land run-off. We think the Sumba modern coral $\delta^{13}C$ may have been affected and that the relative magnitude of the summer $\delta^{13}C$ peak cannot be directly compared with the intensity of the monsoon, while the 3.7 and 4.8 ka records should reflect the relative intensity of the monsoon, assuming human activity during those periods was negligible.

Both the 3.7 ka and 4.8 ka corals strikingly have similar mean climatology as the modern coral in that all of them are shaped by a trough in austral spring and two peaks in summer and late autumn. Since the coral $\delta^{13}C$ between the autumn peak and the spring trough is controlled by light availability and the light availabilities in the same season during the 3 Holocene periods are very similar (the insolation curves in Figure 7.7), it is reasonable to speculate that the summer peaks in other 2 Holocene coral's climatology are also associated with monsoonal rainfall. This seasonal variation in the association with monsoon is also supported by the spectral analysis of seasonal coral $\delta^{13}C$. For example, the 4.8 ka coral summer $\delta^{13}C$ shows dominant monsoonal periodicity of 2.8, 4.8, and 6.7 yr, while spring and autumn $\delta^{13}Cs$ show dominant solar activity periodicity of 11.8 yr (not shown here).

Summer coral $\delta^{18}O$ and the monsoon

Both the 4.8 ka and 3.7 ka corals have a remarkable peak of depleted $\delta^{18}O$ in December to February in their mean climatology (Figure 7.3A). The timing strongly implies a

significant influence of local monsoonal rainfall. The strong influence of monsoon has been further supported by overwhelming periodicity in the quasi-biennial bands shown on the power spectra of the summer $\delta^{18}O$ for both corals (Figure 7.5A). Disappear of the summer peak in the modern coral's mean climatology might be related to the declined intensity of summer monsoon in the present time relative to mid-Holocene, but the monsoon's imprint could still be found from the variability of the modern coral's summer $\delta^{18}O$ which shows evident monsoonal periodicity (Figure 7.5A).

Autumn coral $\delta^{18}O$ and the equatorial Indian Ocean forcing

All the Holocene corals record a distinct freshening of sea water during autumn (March to May) in the coral $\delta^{18}O$ climatology (Figure 7.3A). Chapter 5 has demonstrated the association of the depleted $\delta^{18}O$ peak for the modern coral with the penetration of remote forced tropical Indian Ocean Kelvin wave which brings low-salinity South Java Current water into the Savu Sea. The spectral analysis of the autumn coral $\delta^{18}Os$ for the 3.7 ka and 4.8 ka corals also display the preponderant association between the Sumba coral $\delta^{18}Os$ and the Indian Ocean forcing in autumn over in winter and summer (Figure 7.5A).

7.4.2 Variation in monsoon, ENSO, and equatorial Indian Ocean forcing since mid-Holocene

Since different seasonal coral $\delta^{18}Os$ are dominantly associated with different climate phenomena, the relative activity of the three phenomena could be evaluated by comparing the relative magnitude of the interannual variability of the seasonal coral $\delta^{18}O$ in different Holocene periods. To avoid the effect of different long-term trend and decadal variability among the 3 corals, we compare the relative percentages of the three seasons' magnitude of variability assuming the total variability is one hundred percent in one year's coral $\delta^{18}O$, instead of directly comparison of the absolute values of the standard deviation. Figure 7.8 illustrates the comparison of the relative magnitude of the

interannual variability in seasonal $\delta^{18}O$ and $\delta^{13}C$ of the Holocene Sumba corals.

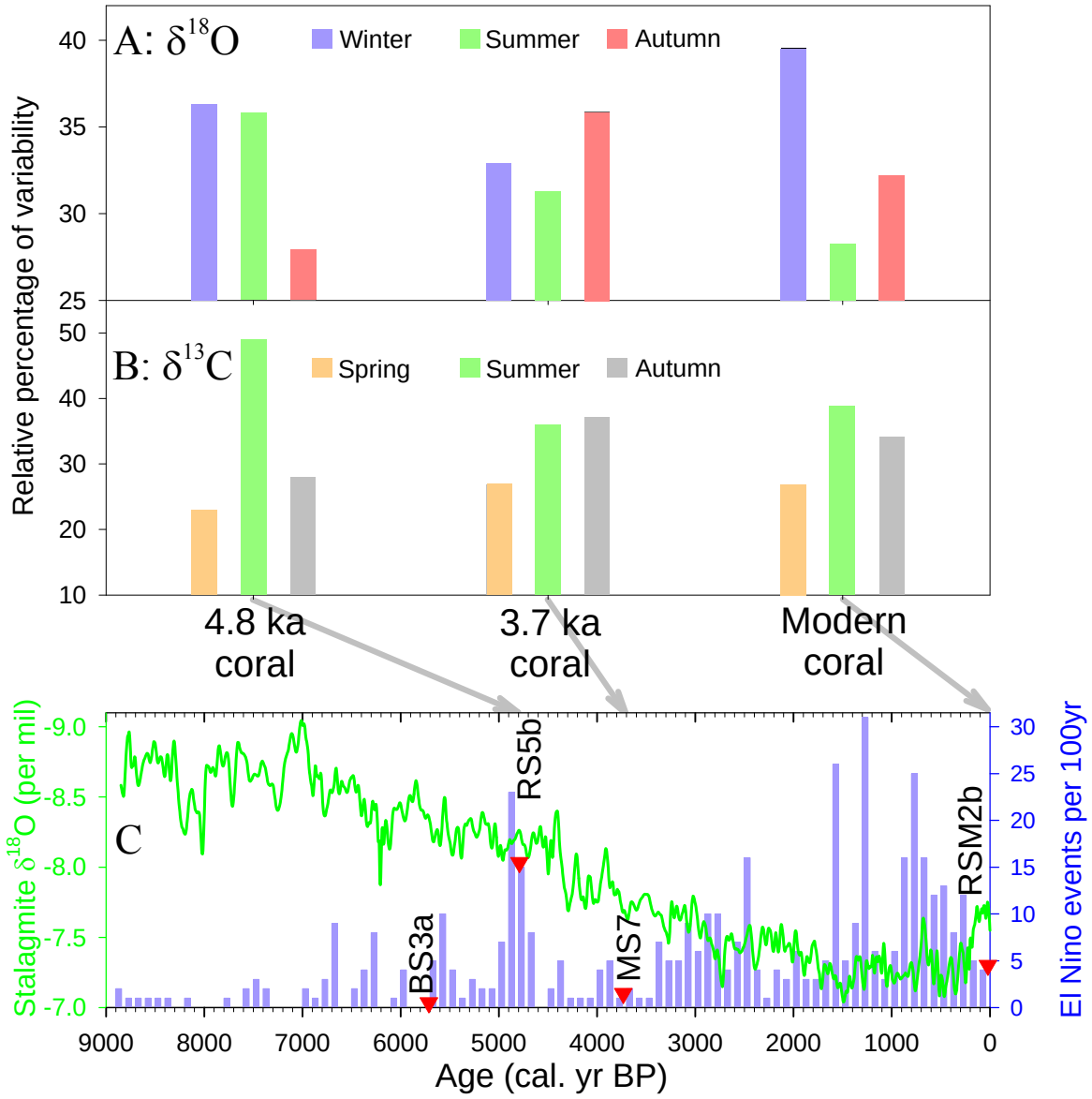

Figure 7.8 **A:** Relative percentage of magnitude of interannual variability for coral $\delta^{18}O$ in winter, summer, and autumn. It strongly implies the relative intensity of interannual variability of ENSO, monsoon, and the equatorial Indian Ocean forcing in the 3 periods of Holocene. **B:** Relative percentage of magnitude of interannual variability for coral $\delta^{13}C$ in spring, summer, and late autumn. The green bars generally display variation in intensity of summer monsoon with part contribution of the human activity in modern time, while the golden and the grey bars are related to the activity of the surface solar radiation maximum and minimum in a year. **C:** Holocene evolution of the Asian summer monsoon and El Niño, as recorded by a Chinese speleothem $\delta^{18}O$ [100-yr smoothed from original data in *Wang et al.*, 2005] (green curve; more depleted $\delta^{18}O$ values correspond to a stronger monsoon) and Peruvian lake sediments [*Moy et al.*, 2002] (blue bars), respectively. Red triangles denote the growth time of the Sumba Holocene corals.

We think they generally suggest the relative intensity of the activity of the ENSO, Asian-Australian monsoon, and the equatorial Indian Ocean forcing since mid-Holocene, but cautions must be taken:

1. One reason is that three integrants are included in the percentage composition, and if both of other two integrants are relatively lower, the remaining one would be much higher in percentage, such as that in modern coral $\delta^{18}O$, the winter magnitude of variability is higher than that in other two Holocene coral, but it does not mean the ENSO has more intensive variability than the other two Holocene times. The high percentage of winter $\delta^{18}O$ variability at modern corral should partly be attributed to the relatively decreased activity for both the monsoon and the Indian Ocean forcing.

2. The second reason is, even though one climate phenomenon is usually dominant in a specific season, other climate phenomena also have minor contribution in the same season; when the dominating climate phenomenon declined, the minor contributor would show up. As an example, in 3.7 ka, the winter coral $\delta^{18}O$ variability was controlled by the Indian Ocean forcing and the ENSO became minor contributor because of the dominant activity of the Indian Ocean forcing at 3.7 ka indicated by the spectral analysis, therefore, much of the percentage of the winter $\delta^{18}O$ variability might be attributed to the Indian Ocean forcing instead of the ENSO.

3. The third reason that cautions should be taken is that, other factors might be responsible for some of the variability amplitude of the seasonal coral records. For instance, all the $\delta^{18}O$ evidences including the mean climatology, the magnitude and periodicity of the summer variability support a weakest monsoon activity in modern time, but the magnitude of summer $\delta^{13}C$ variability of the modern coral has a slightly higher percentage than that in 3.7 ka. We think the increased land run-off resulting from increased human activity in modern time, instead of increased monsoon rainfall, should be responsible for the higher $\delta^{13}C$ variability.

Fortunately, the high-resolution Sumba coral records provide information not only on the magnitude of interannual variability, but also on the mean climatology and the periodicity of the variability for both $\delta^{18}O$ and $\delta^{13}C$. Comprehensive analysis of all the information could provides a more overall understanding for the variation in the three climate phenomena since mid-Holocene.

Variation in the Asian-Australian monsoon

Both the Sumba coral $\delta^{18}O$ and $\delta^{13}C$ record the activity of monsoonal rainfall. It provides a good opportunity to cross-check the variation of the monsoon since mid-Holocene. In summary, the following coral evidences support a weakening monsoon since 5.7 ka:

1. Gradually decreased height of the summer peak in $\delta^{18}O$ mean climatology from 4.8 ka, to 3.7 ka, to 0 ka (Figure 7.3A), indicating declining of the amount of rainfall. The freshening of the water in summer recorded by the Sumba coral $\delta^{18}O$ should result from the monsoonal rainfall which influences the local amount of sea surface precipitation, input of local river, and the salinity of the penetrated Southern Java Current in summer.

2. 3 of the 4 summer peaks are extraordinarily strong in the short 5.7 ka coral $\delta^{18}O$ record in comparison with other Holocene coral records (Figure 7.1), suggesting strongest summer monsoonal rainfall during 5.7 ka in all the periods.

3. Gradually deceased percentage of magnitude of interannual variability in summer $\delta^{18}O$ from the 4.8 ka (36%), to 3.7 ka (31%), to 0 ka (28%) (Figure 7.8A), indicative of decreased activity of summer monsoon.

4. Declined dominance of the monsoonal periodicity in quasi-biennial bands in summer $\delta^{18}O$ from 4.8 ka, to 3.7 ka to modern time (Figure 7.5A).

5. The much higher summer peak relative to the autumn peak in 4.8 ka than in 3.7 ka

(Figure 7.4) reflects stronger local monsoonal rainfall in 4.8 ka than in 3.7 ka, even though the relative intensity of the local monsoon rainfall at those periods in comparison with the modern time could not be judged from the relative magnitude of those peaks in coral $\delta^{13}C$ climatology given strong impact of large land run-off resulting from human activity in the modern time.

6. Remarkably increased relative magnitude of interannual variability in the 4.8 ka coral summer $\delta^{13}C$ (49% to 36% and 39%) in contrast to the almost invariable ratios (near 1.3) of autumn to spring $\delta^{13}C$ in the three corals (Figure 7.8B), proving a remarkably stronger monsoon in 4.8 ka. As mentioned above, the slightly stronger variability of modern coral $\delta^{13}C$ than that of 3.7 ka might result from the increased land run-off owing to increased agricultural activity in modern time, which increased the turbidity of sea water and the input of terrigenous nutrients with depleted $\delta^{13}C$. After deducting the influence of the human activity, the monsoon activity in modern time is more likely weaker than that in 3.7 ka.

Variation in ENSO

Sumba coral winter $\delta^{18}O$ shows obvious variation in average values, magnitude and periodicity of its interannual variability among the 3 Holocene corals. Comprehensive analysis of this variation should reveal the evolution of ENSO in activity and intensity during Holocene owing to the strong association between the Sumba winter coral $\delta^{18}O$ record and the ENSO.

Coral mean climatology has shown that the 4.8 ka coral $\delta^{18}O$ has a remarkable 0.05‰ more enriched winter maximum than the modern one, which accounts for one eighth of the whole seasonality (Figure 7.3A inset). It has been shown that the enriched winter $\delta^{18}O$s of the modern coral mainly result from El Niño events with minor contribution of positive IOD events (Figure 7.6). Also, the power spectrum of the 4.8 ka coral winter $\delta^{18}O$'s interannual variability has demonstrated dominant ENSO variability over IOD (Figure 7.5A), indicative of dominating contribution of El Niño events to the

remarkably enriched 4.8 ka winter coral $\delta^{18}O$ average value. Therefore, the mean climatology shows a significantly stronger ENSO in 4.8 ka than in present time.

The spectral characteristics of winter coral $\delta^{18}Os$ further demonstrate the ENSO's Holocene evolution. Since the winter coral $\delta^{18}O$ manifests the imprint of both ENSO and IOD, comparison of the relative concentration of their characteristic frequencies (3.6 yr and 3 yr) could tell their relative intensity. Figure 7.5A suggests an overwhelming dominance of ENSO in 4.8 ka, an evident dominance of ENSO in present time, and very weak ENSO in 3.7 ka.

Analysis of variability magnitude for the coral winter $\delta^{18}O$ (Figure 7.8A) indicates that in 4.8 ka the ENSO had comparable magnitude of variability with monsoon which has been shown very strong, supporting a very strong ENSO in 4.8 ka. The 3.7 ka winter coral $\delta^{18}O$ shows a weakest variability among the three coral. Given the very strong 3 yr period and very weak 3.6 yr period of the interannual variability, much of the variability magitude should be attributed to IOD, so the amplitude of ENSO variability in 3.7 ka should be much weaker. As mentioned before, the high percentage of variability in the modern coral winter $\delta^{18}O$ does not mean a very strong ENSO activity; the high percentage of winter $\delta^{18}O$ variability should partly be attributed to the low $\delta^{18}O$ variability both in summer and autumn. Furthermore, some part of the variability should be accounted as the contribution of the IOD which has obvious signature in modern winter coral $\delta^{18}O$. Therefore, the percentage of ENSO variability in the three climate phenomena should be very high in 4.8 ka, very low in 3.7 ka, and moderate in modern time.

The variation in ENSO activity could also be reflected by some statistic data on the enriched winter coral $\delta^{18}O$ events. The 2-sigma standard deviation of the detrended coral $\delta^{18}O$ could be well used to diagnose the El Niño events for the Sumba modern coral record, which assigns 13 of the all 37 winters during 1962 to 1998 as El Niño winters, consistent very well with the definition of Trenberth [1997] with only 1 exception in 1967 which is a positive IOD event. By applied to Holocene records, 9 out

of 21 winters for 4.8 ka record, and 17 out of 55 winters for 3.7 ka record, exceed the 2-sigma standard deviation line. Therefore, even if we consider all the enriched winter δ^{18}Os in 3.7 ka as El Niño, the frequencies of enriched δ^{18}O events (9/21 = 0.43, 13/37 = 0.35, 17/57 = 0.3) support a very active ENSO in 4.8 ka, a weak ENSO in modern time, and even weaker ENSO in 3.7 ka. Since it is more likely that a big part of the enriched winter δ^{18}O events correspond to positive IOD in 3.7 ka, the ENSO should be much weaker at that time.

Variation in the equatorial Indian Ocean forcing

Since the equatorial Indian Ocean forcing put more impression on the Sumba coral δ^{18}O in autumn than in winter and summer, the percentage of variability in autumn δ^{18}O for the three corals should reflect the relative intensity of variability in this inner Indian Ocean forcing. Figure 7.8A shows a very weak equatorial Indian Ocean forcing in 4.8 ka, a preponderant intensity of variability in 3.7 ka, and a moderate intensity in modern time. Given that the ENSO was very weak in 3.7 ka and the 3.7 ka coral winter δ^{18}O should record more variability in the equatorial Indian Ocean forcing than the equatorial Pacific forcing, the relative percentage of the Indian Ocean forcing variability would be much bigger than the shown by the 3.7 ka autumn coral δ^{18}O.

The variation of the equatorial Indian Ocean forcing has been further supported by the variation in periodicity of the autumn δ^{18}O for the three corals. The 3-yr period dominates the power spectrum of the 3.7 ka coral autumn δ^{18}O, but shows only a very low concentration in the 4.8 ka coral autumn δ^{18}O spectrum and a comparable concentration with other bands of period in the modern coral autumn spectrum (Figure 7.5A). As shown before, the IOD also has obvious signature on the winter coral δ^{18}O, so the winter coral δ^{18}O also includes information on the periodicity of variability of the equatorial Indian Ocean forcing. Figure 7.5A shows that the power spectra of the winter δ^{18}Os illustrate the same evolution for the Indian Ocean forcing: only a trace of 3-yr period in the 4.8 ka coral, a moderate concentration of the 3-yr period, and even a dominant 3-yr period in the modern coral winter δ^{18}O. The periodograms of the annual

mean δ^{18}Os display the same variation (Figure 7.5A the bottom panels).

Even though there seems to be a slightly higher autumn peak on the mean climatology in 3.7 ka, the difference of the autumn peak among the 3 corals is not statistically significant (Figure 7.3A). The reason is that, the height of the autumn peak lie on not only the amount of the penetrated Southern Java Current (SJC) water driven by the remote equatorial Indian Ocean winds, but also the salinity of the SJC water which is related to the monsoonal rainfall in the source area of the SJC. But the winter maximum on the coral mean climatology might tell us some about the relative intensity of the IOD. We have attributed the evidently enriched winter δ^{18}O maximum in 4.8 ka to remarkably increased El Niño, but the enriched winter δ^{18}O in 3.7 ka relative to modern could not be attributed to El Niño because a weaker ENSO in 3.7 ka has been demonstrated by the coral δ^{18}O. As shown above, positive IOD events also bring enriched coral δ^{18}O, and it seems that the IOD events that have nothing to do with the ENSO even have stronger imprint than other IOD events related with ENSO, such as stronger influence of IOD in 1967, 1968, 1976, 1992, and 1994 (Figure 7.6). Therefore, remarkably stronger Indian Ocean forcing could also bring more enriched winter coral δ^{18}O on the mean climatology even though our evidence shows a slightly less frequent cold events (enriched δ^{18}O) in 3.7 ka (17/57 =0.35) than in modern time (13/37 = 0.30). Taken together, the winter mean coral δ^{18}O might also suggest a stronger intensity of the equatorial Indian Ocean forcing in 3.7 ka than in the present time.

It seems that the decadal variability (periods of 26, 13, 8.7 years), which are the most pronounced periodicity for both the 3.7 ka and the modern coral fortnightly δ^{18}O (Figure 7.1), has a close association with the equatorial Indian Ocean forcing because both the decadal periodicity and the forcing have the same variation through the three Holocene periods: the decadal variability was more frequent (higher variance in period of 8.7 years) in 3.7 ka when the equatorial Indian Ocean forcing is very strong; all the decadal variability were very weak in 4.8 ka when the equatorial Indian Ocean forcing was very weak; while the decadal variability has the same amplitude but is less frequent

(lower variance in the 8.7 yr period in comparison with the 3.7 ka coral) in the modern time when the equatorial Indian Ocean forcing is moderate.

7.5 CONCLUSIONS

4 high-resolution Holocene coral $\delta^{18}O$ and $\delta^{13}C$ records have been extracted from the Sumba Strait, Indonesia, where the Asian-Australian monsoon, ENSO, and the remote equatorial Indian Ocean forcing have strong impacts on the local climate and oceanography. Climatology of these coral records has been reconstructed, and the magnitude and periodicity of the interannual variability of the coral records have been achieved. Strong seasonal variation in the association between the Sumba coral records and the three prevailing climate phenomena has been found, which helps to partly disentangle the three intertwisted climate systems and makes it possible to reveal the variation of the individual climate systems since mid-Holocene.

Both the coral $\delta^{18}O$ and $\delta^{13}C$ record a weakening monsoon since 5.7 ka. The monsoon was very strong in 5.7 ka and 4.8 ka, but evidently weaker in 3.7 ka. The modern time seems to have a weakest monsoon of the four periods of the Holocene. Comprehensive analysis of the coral climatology, the magnitude and periodicity of the interannual variability of the coral $\delta^{18}Os$ indicates a very strong ENSO in 4.8 ka, a very weak ENSO in 3.7 ka, and a moderate intensity of ENSO in the present time. This coral evidence for variation in the Asian-Australian monsoon and ENSO is consistent with previous findings for the evolution of Asian monsoon from a speleothem $\delta^{18}O$ record from Dongge Cave, southern China [*Wang et al.*, 2005b], and Peruvian lake sediment evidence for ENSO evolution [*Moy et al.*, 2002] (Figure 7.8C).

The Sumba coral $\delta^{18}Os$ also record a variation in the equatorial Indian Ocean forcing since mid-Holocene: in comparison with the monsoon and ENSO, the remote equatorial Indian Ocean forcing was very weak in 4.8 ka, very strong in 3.7 ka, and moderate in the modern time. Since the equatorial Indian Ocean forcing might be one of the

important drives for the Indian Dipole Mode (IOD), the IOD events associated with this forcing should have corresponding variation since mid-Holocene.

The Sumba corals provide a historical perspective to understand the evolution and interplay of the three complicatedly intertwisted climate phenomena which are all of global importance. The high-resolution windows illustrate climate scenes distinct from the modern time in the relative intensity and variability of the three climate components in one specific location. For example, the deficit of summer monsoonal rainfall is usually connected with a strong El Niño in most of the Asian-Australian monsoon regions including India, Southeast Asia, and Australia in modern time [*Meehl*, 1987; *Ropelewski and Halpert*, 1996; *Webster et al.*, 1998; *Kumar et al.*, 1999], the Sumba coral records, however, suggest a Holocene period in 4.8 ka when both the El Niño and the summer monsoon were strong. As a contrast, in 3.7 ka, a much weaker El Niño than today occurred in the mean time of a monsoon stronger than today. Similarly, even though the remote equatorial Indian Ocean forcing strongly influences the climate and oceanography of the Indian Ocean coastal areas of the Indonesia in modern time shown by this study and other recent studies [*Sprintall et al.*, 1999; *Sprintall et al.*, 2000; *Hautala et al.*, 2001; *Syamsudin et al.*, 2004; *Wijffels and Meyers*, 2004; *McClean et al.*, 2005; *Sakova et al.*, 2006], the Sumba coral $\delta^{18}O$ displays a overwhelming dominance in 3.7 ka and a very weak activity in 4.8 ka of this remote forcing. Since this forcing might be one of the important drive for the IOD, this study demonstrates that the IOD associated with this forcing could show extraordinarily strong activity in period like 3.7 ka when monsoon was stronger than today and ENSO was much weaker than today. Even though this study shows independent variation of the equatorial Indian Ocean forcing relative to the monsoon's intensity and variability, it also suggests a reversed variation in relationship between the equatorial Indian Ocean forcing (EIOF) and the ENSO: a strong ENSO vs a weak EIOF, a weak ENSO vs a strong EIOF, and a moderate ENSO vs a moderate EIOF. More high-resolution windows of coral $\delta^{18}O$ are needed to further validate these relationships of the equatorial Indian Ocean forcing with the ENSO and with the monsoon.

CHAPTER 8

MEAN CLIMATE, EL NIÑO VARIABILITY, AND MONSOON INTENSITY DURING TERMINATION II

ABSTRACT

A 29-year-long fortnightly resolution $\delta^{18}O$ and $\delta^{13}C$ record was compiled for a 133.6 ka *Porites* coral from an early highstand of the penultimate deglaciation (Termination II) preserved within the Mondu raised reefs of Sumba, Indonesia. The high-resolution isotopic record gave a mean $\delta^{18}O$ value of 4.4‰ at 133.6 ka, which is 0.6‰ higher than the local Holocene coral records, and 1.0−1.2‰ higher than the local modern coral records. Calculations based on the coral $\delta^{18}O$ shows that the mean SST at 133.6 ka was ~2.4°C lower relative to the middle Holocene SST. The seawater $\delta^{18}O$ at 133.6 ka was probably similar to the enriched $\delta^{18}O$ value observed for the mid-Holocene, rather than the depleted modern warm pool $\delta^{18}O$ value.

The high-resolution $\delta^{18}O$ record for the Termination II coral displayed a dramatic 40% decrease in the frequency of strong El Niño events, relative to the modern-day frequency. The $\delta^{18}O$ and $\delta^{13}C$ climatologies both indicate that the Asian-Australian monsoon was more intense at 133.6 ka. The coral $\delta^{18}O$ climatology for 133.6 ka also suggests that freshwater input to the Sumba Strait peaked during October-December. This freshwater flux is interpreted to reflect the incursion of Kelvin waves into the Sumba Strait during the two monsoon transitions (May and November) at 133.6 ka, in contrast to the penetration of only the austral autumn Kelvin wave into the Sumba Strait in mid-Holocene and modern times. The juxtaposition of a stronger monsoon and weaker El Niño during the different background climate state of Termination II (lower SST, higher seawater $\delta^{18}O$) provides a new perspective on the interactions between these climate systems.

8.1 INTRODUCTION

Ocean-atmosphere interactions in the tropical Indo-Pacific Warm Pool are fundamental drivers of the global meridional Hadley and zonal Walker circulations [*Keenan et al.*, 2000]. Recent research indicates that changes in sea surface temperatures and atmospheric convection in this region play important roles in modulating global climate on interannual, decadal, millennial, and even glacial-interglacial time-scales [*Cane*, 1998; *Cane and Clement*, 1999; *Hoerling et al.*, 2001; *Stott et al.*, 2002; *Visser et al.*, 2003]. Knowing the natural bounds of past ocean-atmosphere variability in the Warm Pool region will significantly improve our understanding of the mechanisms of climate variability at different time scales, and enhance our ability to predict the climate in the future.

Massive, long-lived corals are one of the only paleoclimate archives capable of providing high resolution records (weekly to monthly) for periods when climate boundary conditions were different from those of the present day [reviewed by *Druffel*, 1997; *Dunbar and Cole*, 1999; *Gagan et al.*, 2000]. Geochemical records extracted from corals play a pivotal role in the reconstruction of paleoclimate variability on intrannual, interannual and decadal time-scales, and have shed light on the impact of El Niño events on climate variability throughout the tropics [*Cane*, 1986; *Enfield*, 1989; *Philander*, 1990; *Trenberth and Hoar*, 1997; *Cane*, 2005]. Changes in the isotopic composition of coral skeletons also record the variability of monsoonal rainfall in the monsoon prevailing regions [*Charles et al.*, 1997; *Charles et al.*, 2003; *Pfeiffer et al.*, 2004; *Sun et al.*, 2005; *Yu et al.*, 2005; *Chakraborty*, 2006; *D'Arrigo et al.*, 2006; *Morimoto et al.*, 2007]. Knowing the historical variability of El Niño events and monsoon rainfall and their relative intensity during different background climate states could provide new perspectives for understanding the mechanistic links between these two important climate systems. Therefore, coral records will serve to improve the prediction of El Niño and monsoon variability that will probably occur as the mean

climate state changes in the future [*IPCC*, 2007].

Here we report a 29-year-long high resolution record of skeletal $\delta^{18}O$ and $\delta^{13}C$ for a massive *Porites* coral that grew during a sea-level highstand during the penultimate deglaciation (Termination II, 140-128 ka) preserved within the Mondu raised reefs, located southwest of Cape Laundi on the island of Sumba, eastern Indonesia. In this chapter, the fossil coral record will be compared with modern and Holocene coral records from the same site to explore the mean climate state, El Niño variability, and Asian-Australian monsoon intensity at ~133.6 ka during Termination II.

8.1.1 The Termination II coral

The Termination II *Porites* coral gave a conventional ^{230}Th age of 136.8 ka for the most pristine sub-sample with an initial $\delta^{234}U$ value of 158.9‰, which implies that the true age of the coral is slightly younger. Further analysis of multiple sub-sample measurements demonstrated that the coral experienced two distinct processes of U-series diagenetic alteration and two models derived from each process gave essentially the same model correction age of 133.6 ka (see Chapter 4 for dating of this coral).

The U-series dating confirmed that this coral was growing during the termination of the penultimate termination period (Termination II, 140 ka ~ 128 ka) [*Martinson et al.*, 1987; *Muhs*, 2002; *Brauer et al.*, 2007]. During Termination II, sea level was believed to rise rapidly between the glacial ~ -120 m, [*Lea et al.*, 2002; *Cutler et al.*, 2003; *Risebrobakken et al.*, 2006] and interglacial ~ +5 m; [*Stirling et al.*, 1995] positions. However, recent research suggests that Termination II did not consist of a monotonic sea-level rise as occurred during Termination I [*Fairbanks*, 1989; *Bard et al.*, 1990] but instead included an interlude of significant sea-level fall [*Esat et al.*, 1999; *Gallup et al.*, 2002; *Antonioli et al.*, 2004; *Siddall et al.*, 2006], as shown in Figure 8.1. The sea level had reached an early highstand lasting several millennia around 134 ka, followed by a

sharp drop in sea level and still-stand of several millennia around 131 ka, before the final sea-level rise to the MIS 5e interglacial starting at 128 ka.

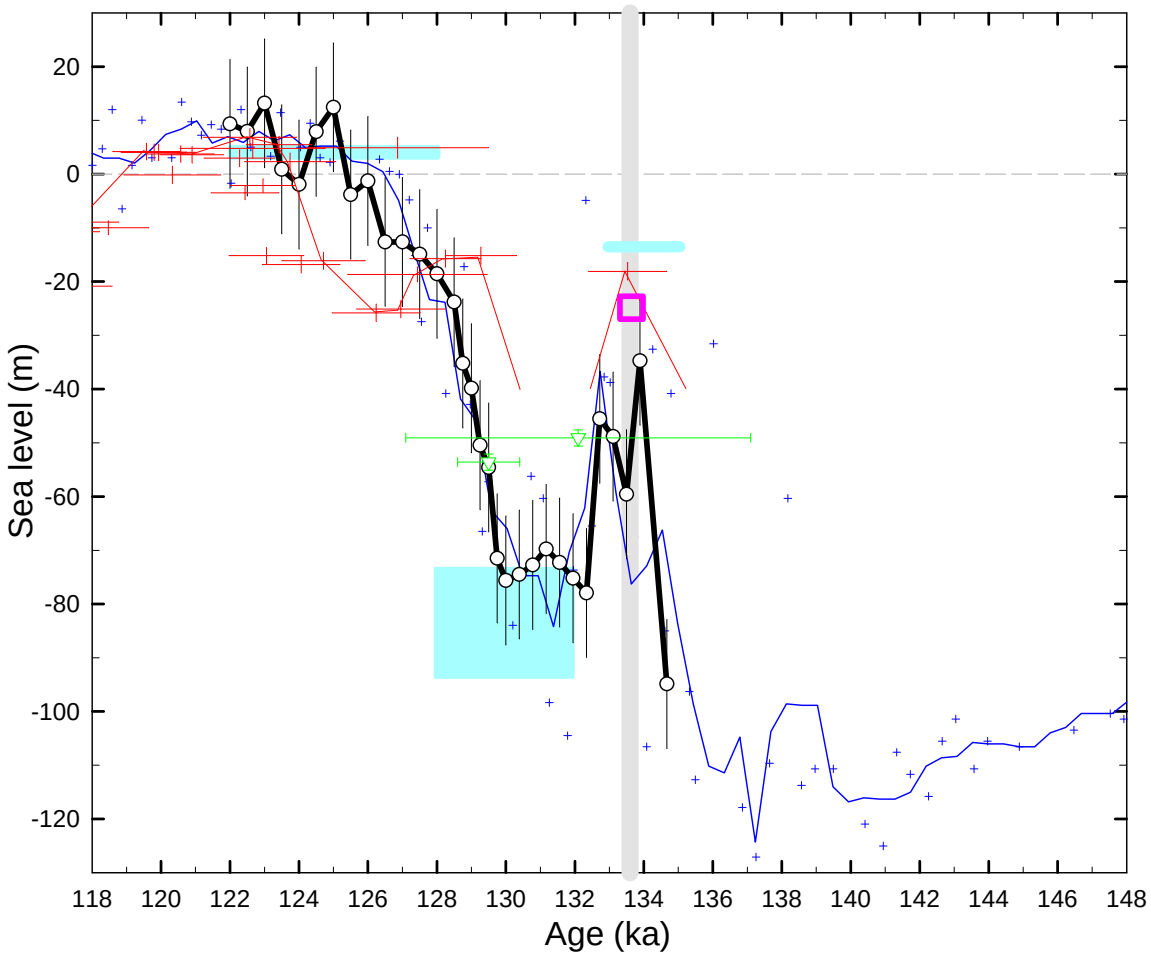

Figure 8.1 Compilation of recent published results on sea level change during Termination II following Siddall *et al.* [2006] and relationship to Sumba fossil coral MV03-A-2 at 133.6 ka. Vertical grey shading denotes the age of the coral and pink square illustrates that the TII coral colony might grow at -8 m to -12 m below the sea level at 133.6 ka if an uplift rate of 0.49 m/kyr is applied [*Pirazzoli et al.*, 1991]. Dashed grey line shows the modern sea level. Black curve with dots is sea-level with error margin (±12 m, thin black lines) from foraminiferal $\delta^{18}O$ in Red Sea sediment core GeoTue KL11 [*Siddall et al.*, 2006]. Cyan blocks represent sea-level estimates from fossil corals at Huon Peninsula, Papua New Guinea [*Esat et al.*, 1999] and western Australia [*Stirling et al.*, 1995]. Red crosses and lines represent open-system U-series ages of corals and sea level [*Thompson and Goldstein*, 2005]. Green triangles with error bars represent times when speleothems in the Bahamas were undergoing a growth phase and sea-level should be below these levels [*Richards et al.*, 1994; *Smart et al.*, 1998]. Blue line is scaling to sea level of the V19-30 benthic $\delta^{18}O$ (Uvigerina) record after Cutler et al. [2003] with 1 ky added to age scale to aid comparison (2-ky running average smoothed from original data which are shown as blue crosses and available at: http://depphi.esc.cam.ac.uk/coredata/wwwcoredata/VEMA/v1930uv.html).

Reconstruction of the climate during Termination II would be highly significant because it involves several distinct periods when the mean climate was different from that at the present time. Not only does it include a period when the climate was slightly warmer (the last interglacial) it also includes a slightly cooler period (the early highstand around 134 ka), and a much colder period (the lowstand at 131 ka). Until now, only three coral records of the last interglacial climate [*Hughen et al.*, 1999; *Tudhope et al.*, 2001] and three coral records of the lowstand (~131 ka) climate of the warm pool have been published [*McCulloch et al.*, 1999; *Tudhope et al.*, 2001]. The new Sumba coral record presented here fills in a gap because it contributes, for the first time, an important climate record for the period of the highstand around 134 ka.

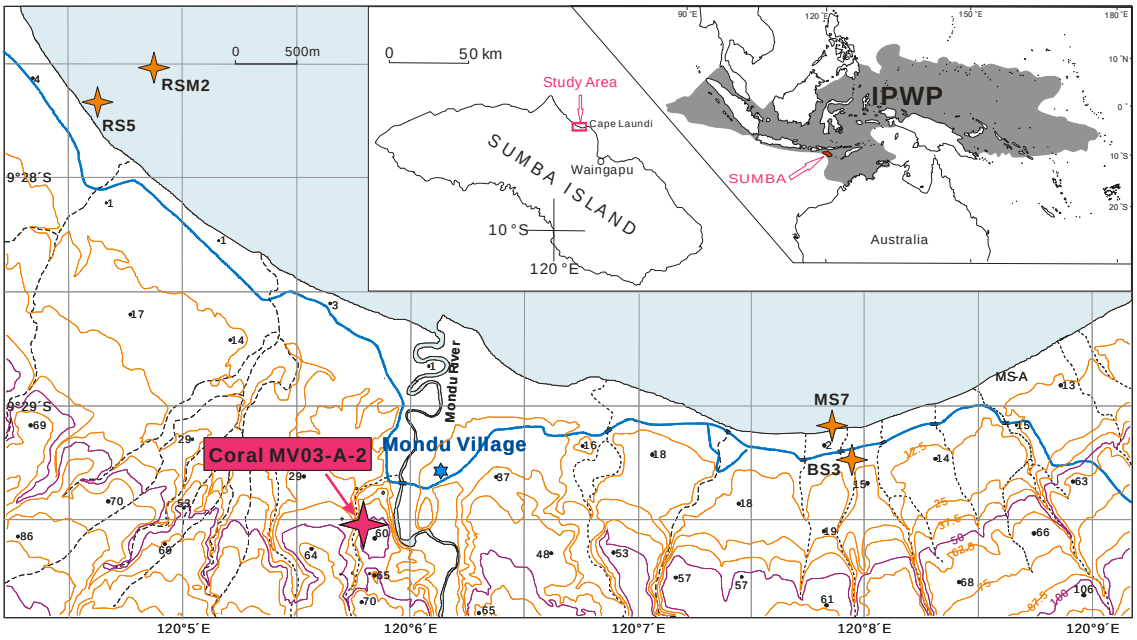

Figure 8.2 Location of *Porites* corals (stars) and physiography of the Mondu raised reefs on the north coast of Sumba, Indonesia. Dark stippling in inset marks the average extent of the Indo-Pacific Warm Pool (IPWP, mean annual SST >28 °C), as defined by Yan et al. [1992].

8.1.2 Climatology and oceanography

The island of Sumba is located in the south-central sector of the Indonesian archipelago (Figure 8.2). The study area is located on the central north coast of the island, facing

Sumba Strait and the western end of the Savu Sea, one of the inner Indonesian seas. As a part of the Indo-Pacific Warm Pool (IPWP, [*Yan et al.*, 1992], the study area has an annual mean sea surface temperature (SST) of 28.2 ^{o}C. The local mean SST is close to or exceeds 29 ^{o}C for six months of the year, and it is only in mid-August SST when the SST drops sharply to below 26.5 ^{o}C (Figure 8.3). Even though most of Indonesia receives high rainfall by world standards, Sumba is relatively dry with a mean annual rainfall of 1655 mm (1979 to 2005), with most of the rainfall concentrated between December and March. The mean rainfall during the peak wet season (January / February) is 15 times as great as the rainfall in August. The long dry season lasts for up to eight months (April-November) with a mean rainfall as low as 22 mm in August (Figure 8.3).

The climatology of the local sea surface salinity is consistent with the low-salinity characteristic of the Indo-Pacific Warm Pool [annual average < 34.2 ppt (part per thousand)]. In spite of that, it still shows small annual variability including freshening during May to July with low SSS of 33.8 ppt in June. Surprisingly, Figure 8.3 shows that the most saline surface water coincides with the summer monsoon peak during December to March, indicative of little effect of local rainfall on sea surface salinity even though the summer monsoon is as strong as 330 mm/month. Similarly, Figure 8.3 suggests that the local incoming surface radiation has little effect on the seasonality of the local sea surface temperature.

The reason that local environmental factors have little impact on the SST and SSS in the study area is that the study area is one of most active passageways for oceanic currents in the world (Figure 8.4) and they control the variability of SST and SSS. The research area is located on the southern side of the inner part of the Sumba Strait, which is one of the most important outflows of the Indonesian Throughflow (ITF) [*Potemra et al.*, 2003; *Sprintall et al.*, 2003; *Gordon*, 2005]. The ITF transports Pacific water into the Indian Ocean via the Indonesia seas and is driven by the Pacific-Indian pressure gradient. The transport varies with the seasonal cycle in wind stress and is at its maximum during May to September when flow is enhanced by the local Ekman response to the southeast

monsoon [*Wyrtki*, 1987]. Thus it is likely that the flow through the Sumba Strait in the austral winter would reflect the uniquely characterized Indonesian Sea Water (ISW) which results from the mixing of Pacific waters with regional rainfall, river runoff, and inflows from marginal seas (such as South China Sea) into the Indonesian seas [*Gordon et al.*, 2003; *Gordon*, 2005].

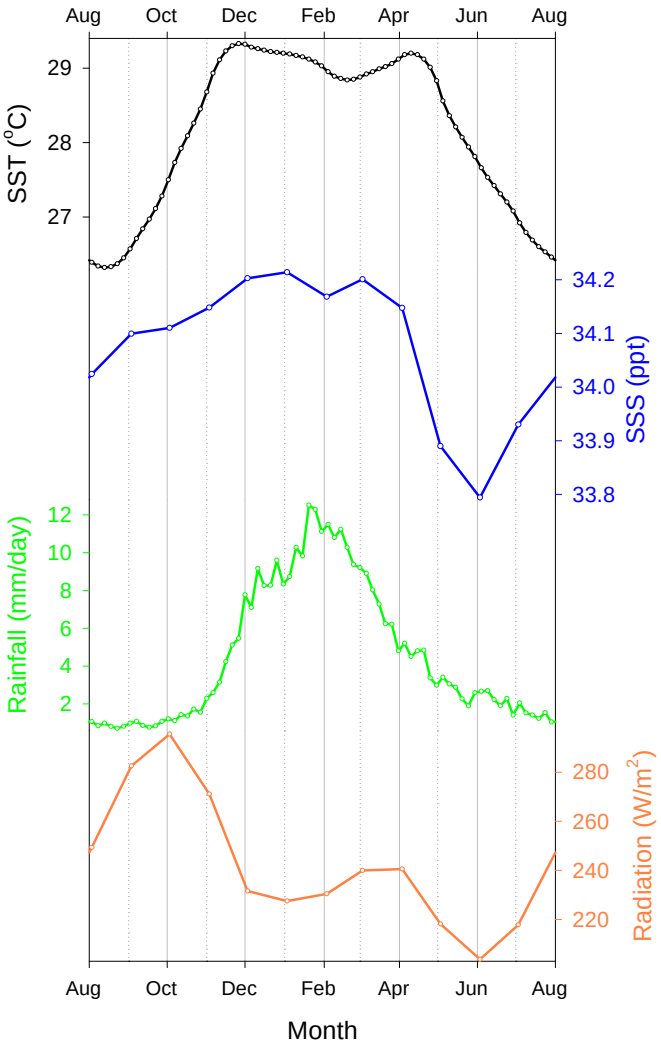

Figure 3.3 The annual climatologies around Sumba, Indonesia. Data sources are as follows: IGOSS sea surface temperature (SST, black curve, 1971-2000 pentad data [*Reynolds et al.*, 2002], http://iridl.ldeo.columbia.edu /SOURCES/.IGOSS/.nmc/), Carton-Giese SODA dataset V1.4.2 sea surface salinity (SSS, parts per thousand, blue curve, 1958-2001 monthly data [*Carton et al.*, 2005], http://iridl.ldeo.columbia.edu/SOURCES/.CARTON-GIESE /SODA/.v1p2/), CMAP rainfall (green curve, 1979-2005 pentad data [*Xie and Arkin*, 1997], http://iridl.ldeo. columbia.edu/SOURCES/.NOAA/.NCEP/.CPC/.Merged_Analysis), and Atlas of Surface Marine Data 1994 incoming short-wave radiation (orange curve, 1945-1993 monthly data [*da Silva et al.*, 1994], http://iridl.ldeo.columbia.edu/SOURCES/.DASILVA/.SMD94 /.climatology/.shortrad/).

It has been shown that the El Niño-Southern Oscillation (ENSO) has a strong influence on rainfall and sea surface temperature in the Indonesia maritime continent on interannual time-scales; during a El Niño event, rainfall is suppressed and ambient SST is cooler than average, with the converse happening during a La Niña event [*Nicholls*, 1981; 1984; *Ropelewski and Halpert*, 1996; *Haylock and McBride*, 2001; *McBride et al.*, 2003]. Therefore, the SST and SSS of Indonesian seawater should strongly reflect ENSO variability on the interannual timescales. Furthermore, the weakened ITF transport of relatively warm, fresh surface water during El Niño events [*Clarke and Liu*, 1994; *Meyers*, 1996; *Potemra et al.*, 1997; *Gordon et al.*, 1999] should also add to the ENSO signal of the ITF.

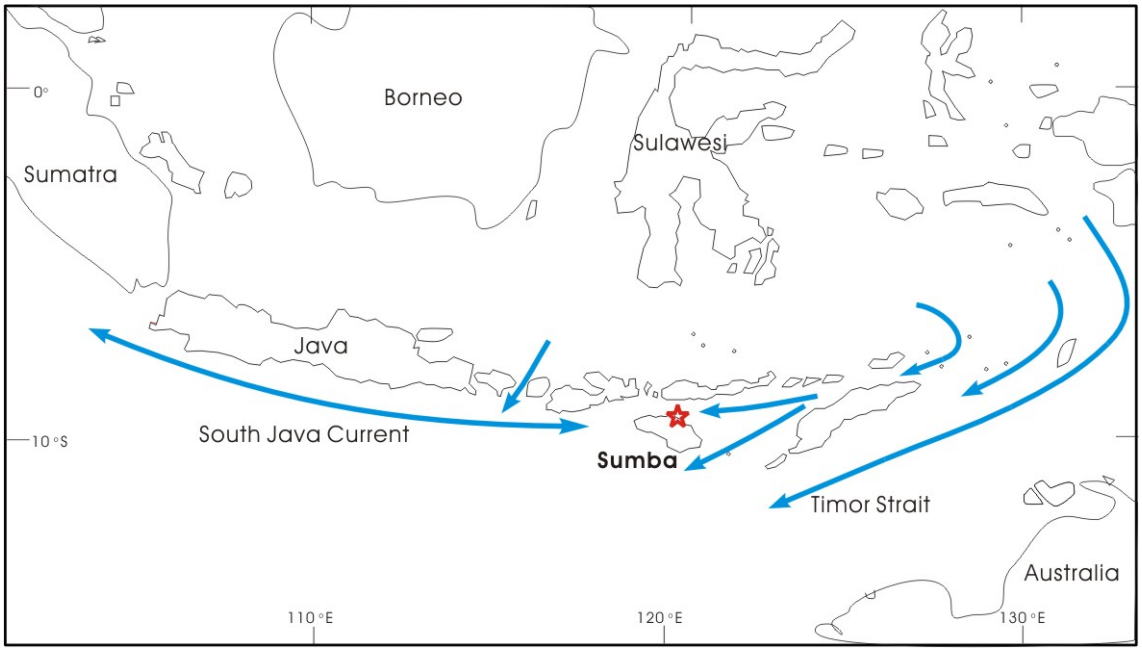

Figure 8.4 Oceanic currents around Sumba, including the South Java Current (SJC, blue double headed arrow) and outflows of the Indonesian Throughflow (ITF, blue arrows). The red star marks the study area on the north coast of Sumba adjacent to the southern side of the Sumba Strait.

The oceanographic setting suggests that SST and SSS in the Sumba Strait could actually reflect the mean climate state of the broader region, including the maritime continent which makes up the central and major part of the Indo-Pacific Warm Pool. The interannual variabililty of the Sumba SST and SSS should be efficient indexes for

recording ENSO events, especially in the winter dry season.

Sumba is also located in the pathway of the annual migration of Asian-Australian monsoon centre of atmospheric convection (Intertropical Convergance Zone, ITCZ). The ITCZ migrates southeastwards from the South Asian subcontinent (July) to Sumatra (November), Java (December), and on to Sumba / north Australia in January / early February [*Meehl*, 1987; *Huang and Mehta*, 2004; *Chang et al.*, 2005]. Heavy rainfall and strong runoff from the Indonesian islands such as Sumatra and Java make the surface salinity near the coast up to 3 psu lower than in the open Indian Ocean [*Wyrtki*, 1973]. The published data demonstrate a very warm, fresh surface layer in the coastal water where the salinity is 33.8 psu and much fresher than the Indonesian Banda Sea Water (salinity is 34.4 psu) [*Fieux et al.*, 1994; *Bray et al.*, 1997; *Sprintall et al.*, 1999; *Sprintall et al.*, 2000]. The reduced salinity gives rise to a cross-shore pressure gradient, driving a south-easterly baroclinic coastal jet along the Java-Sumatra island chain [*Quadfasel and Cresswell*, 1992]. The monsoonal winds, in turn, force an eastward or westward boundary current during the summer and winter, respectively. That is the formation of the semi-annually reversing South Java Current (SJC) (Figure 8.4).

The South Java Current semi-annually reverses to south eastward flow which occurs around May and October-November through the propagation of coastal and equatorial Kelvin waves forced by westerly wind bursts during the monsoon transitions in the equatorial Indian Ocean [*Quadfasel and Cresswell*, 1992; *Sprintall et al.*, 1999]. In summary, the changing monsoon winds and the variations of the freshwater flux from the Indonesian archipelago are responsible for the annual cycle of the flow, while the actual reversals between the seasons are strongly influenced by remote forcing through equatorial and coastal long waves from the central Indian Ocean [*Quadfasel and Cresswell*, 1992].

Even though early studies noted that the eastward flow of the semi-annually reversing SJC could reduce the transport of the ITF [*Meyers et al.*, 1995], it had not been confirmed if the Indian Ocean water enter into the Indonesian seas through the Sumba

Strait. Recently, Molcard et al (2001) reported eastward flows in the Ombai Strait and in the Sumba Strait [*Hautala et al.*, 2001] measured by current metres in December 1995, May 1997, and March 1998. Our analysis demonstrated that a reduction in $\delta^{18}O$ in the modern Sumba *Porites* coral could well record the incursion of the SJC into the Savu Sea around May (see Chapter 6) even though the coral $\delta^{18}O$ climatology does not record a local rainfall signal. However, analysis of the Sumba Holocene corals indicated that the coral $\delta^{18}O$ climatology can also record the local monsoonal signal in January and February along with the arrival of the SJC in May. Therefore the Termination II coral climatology might also contain information about the intensity of monsoon activity at that time.

8.1.3 The Mondu raised reefs

Sumba is situated at the southwest end of a tectonic inflexion where the Sunda Arc passes eastward into the Banda Arc. The island is an exposed part of the outer arc ridge produced by the active subduction of the Indian-Australian plates beneath the Pacific plate [*Fitch and Hamilton*, 1974]. Sumba is separated from Australia by the Java Trench-Timor Trough, and from the volcanic ridge of the Sunda-Banda island-arc to the north by an outer arc basin (the Savu Sea). The collision of the plates and the upheaval of the outer arc ridge result in the uplift of the palaeo-reefs and the formation of the flights of raised coral terraces on the north coast of Sumba. An exceptional 1-million-year-long sequence of coral reef terraces has been reported at Cape Laundi (Figure 8.2) between sea level and an ancient patch reef 475 metres above sea level [*Pirazzoli et al.*, 1991; *Pirazzoli et al.*, 1993]. Using uranium-series and electron spin resonance dating, they deduced a local uplift rate of 0.49 m/kyr which remained almost constant during at least the last million years and, in any case, at least until the last interglacial period. They credited the possibility of dating of the very old fossil corals to the dry local climate, especially the pronounced winter dry season which tends to slow down the processes of diagenesis in fossil corals, leaving some of them almost

unrecrystallized after 600 ka.

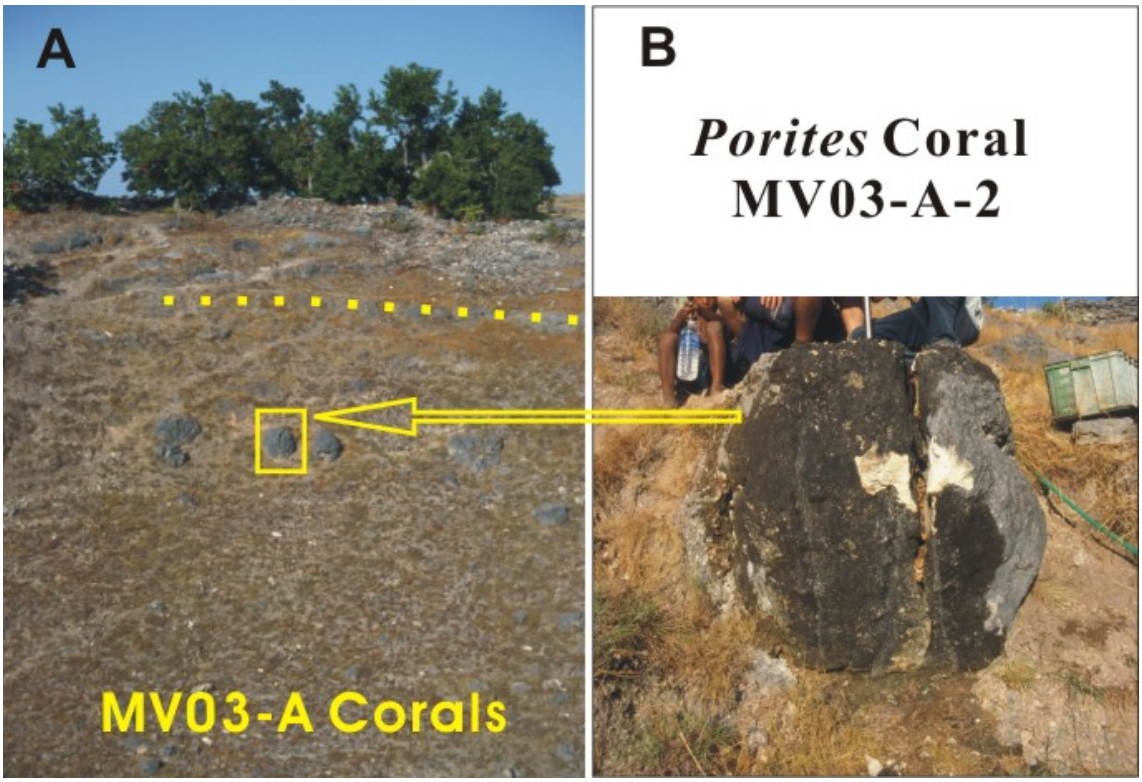

Figure 8.5 (A) Mondu V coral reef. Dotted line marks an erosion surface above the Mondu V coral reef. (**B)** The half exposed large *Porites* coral MV03-A-2 which is still in growth position.

Our research focussed on the area around Mondu village, about 10 km west of Cape Laundi, where extensive paleo-reef terraces are exposed between 0 m and 80 m above mean sea level (Figure 8.2). The Mondu raised reefs better developed than those at Cape Laundi between the same altitudes, possibly because of the gentler underwater slope, better nutrition and greater sedimentary output from Mondu River over the past 150 ka. Three major field investigations in 1995, 1998, and 2003 have been conducted in this area and a wealth of modern and fossil coral cores have been retrieved from the modern and raised reefs. These provide an excellent opportunity for reconstruction of climate and oceanography since MIS 6.

8.2 MATERIALS AND METHODS

8.2.1 Coral sampling

Four large *Porites* corals have been found in the steep wall of a deep valley 1.5 km inland from the sea (Figure 8.5). The corals are 39 m above modern mean sea level and still in their original growth positions. An exceptionally well-preserved coral core, MV03-A-2c, has been retrieved from coral MV03-A-2, which is 1.2 m in diameter and 1.1 m in height.

This 1.1 m long coral core was slabbed, ledged, and sub-sampled for isotopic analysis following a procedure developed by Gagan et al. [1994]. X-ray photographs of 7 mm thick coral slabs (Figure 8.6) were used to help to develop a chronology and as a guide for sub-sampling ledges along the axis of maximum growth. This coral has a relatively rapid skeletal extension rate of 16-20 mm/yr, which is typical for modern and Holocene Sumba *Porites* corals growing in shallow water. The well-preserved middle sections of this core were used to produce the palaeoclimate record and for U-series dating. Vigorous cleaning in a Milli-Q water bath beneath a powerful ultrasonic beam was applied to remove skeletal dissepiments and some surficial diagenesis [*Gagan et al.*, 1994]. Sub-samples were milled every 0.5 mm along 2 mm thick ledges (white tracks in Figure 8.6), which corresponds to a resolution between weekly and fortnightly.

Figure 8.6 X-ray photo of 7 mm slab from the MV03-A-2c core. The white lines with Roman numerals represent the sampling transects. Red circle marks a calcite patch.

8.2.2 Coral preservation

The coral slabs show excellent preservation under natural and UV light with

only one small patch of calcite which has been avoided by the sampling ledges (Figure 8.6). X-ray diffraction analyses yielded 99% aragonite content for typical spots in the middle sections of the core. Inspection of petrographic thin sections confirmed there is no secondary aragonite. There is slight dissolution and traces of calcite overgrowths in some parts of the core, however the smooth septal walls and radial structure of aragonite fibres growing from centres of calcification indicate excellent preservation of this coral skeleton. Figure 8.7 shows the impressive similarity between this fossil coral and a modern *Porites* coral (RSM2b) living on a nearby reef, indicative of extraordinarily good preservation for a very old *Porites* coral that has been exposed to both submarine and subaerial environments for a long time.

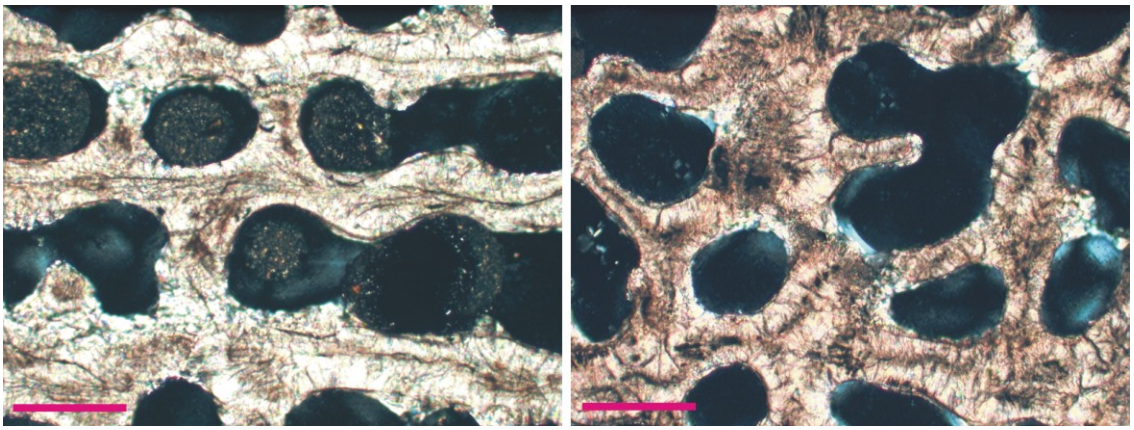

Figure 8.7 Optical microscopic image of petrographic thin-section of fossil coral MV03-A-2c (right) compared with image of a modern *Porites* coral RSM2b (left). Red bar represents 2 mm.

8.2.3 Stable isotope measurements

The coral $\delta^{18}O$ and $\delta^{13}C$ is measured by a Finnigan MAT-251 mass spectrometer coupled with an automated individual-carbonate reaction device (Kiel) at RSES, ANU. Approximately 200 μg aragonite sub-samples were reacted with two drops of 103% H_3PO_4 at 90°C for 12 minutes. CO_2 gas enters the mass spectrometer for isotope

measurements after freezing H_2O from the evolved H_2O-CO_2 gas in a liquid nitrogen trap system. The isotope ratios are reported in standard delta notation relative to Vienna Peedee Belemnite (VPDB) and calibrated via the NBS-19 calcite standard ($\delta^{18}O$ = -2.20‰, $\delta^{13}C$ = +1.95‰) and the NBS-18 calcite standard ($\delta^{18}O$ = -23.0‰, $\delta^{13}C$ = -5.0‰). Analytical precision for repeated measurements (n = 135) of $\delta^{18}O$ and $\delta^{13}C$ in NBS-19 during the fossil coral isotope analysis was 0.05‰ and 0.02‰ (1σ), respectively.

For isotope measurements of the coral MV03-A-2c, every second sub-sample was measured, in the first instance, and then neighbouring sub-samples were measured for periods when skeletal isotopic composition changed rapidly and during the austral winters. 542 sub-samples were measured in core MV03-A-2c (excluding repeated sections between spliced ledges) to produce a 29-year-long record with an average sampling frequency of 19 samples per year. The resolution of the winter $\delta^{18}O$ record was increased to be fortnightly to ensure accurate measurement of the high $\delta^{18}O$ values in the winters, which is important for the accurate reconstruction of El Niño signals.

The isotope data were converted from distance along the sampling transect to time by assigning $\delta^{18}O$ maxima to August 8, which is the average arrival-time of winter SST minima based on analysis of modern SST records [IGOSS, *Reynolds et al.*, 2002]. The data were then linearly interpolating between the annual anchor points using *AnalySeries* [*Paillard et al.*, 1996]. For convenience of comparison with modern and Holocene coral records, 26 equal intervals were assigned between two neighbouring winter $\delta^{18}O$ maxima for the MV03-A-2c, Holocene, and modern coral records. The fortnightly resolution of the chronology is close to the measurement resolution.

8.2.4 U-series age determination

Multiple sub-samples were used to determine the age of fossil coral MV03-A-2 and details about the age determination were given in Chapter 4. The U-series method [*Edwards et al.*, 1986/87] was applied to obtain the U-series isotopic composition and

^{230}Th ages of different sub-samples. Even though a well-preserved sub-sample indicated that the coral would be only slightly younger than the uncorrected age of 136.8 ka, a more reliable age could not be achieved by directly applying any of the recent correction models [*Thompson et al.*, 2003; *Villemant and Feuillet*, 2003; *Scholz et al.*, 2004]. However, coral MV03-A-2 provided an excellent opportunity to explore the diagenetic behaviour of U-series isotopes in corals because it experienced two recognisable stages of post-depositional alteration. Detailed analysis of the U-series isotopes showed that both styles of diagenetic alteration are different from those suggested before, but model correction ages could be achieved from either process and they produced essentially the same age of 133.6 ka. The age determination was also supported with evidence from local stratigraphic analysis combined with the published sea level curve and reef uplift rate.

8.3 RESULTS

8.3.1 Termination II coral $\delta^{18}O$ and $\delta^{13}C$

Figure 8.8 displays the high-resolution records of coral $\delta^{18}O$ and $\delta^{13}C$. Both of them exhibit clear annual cycles which are comparable with the local modern and Holocene records (Chapters 6, 7), suggestive of excellent preservation considering its old age.

The slightly lower $\delta^{18}O$ values in years 6 and 7 probably result from the impact of the small calcite patch, even though it was avoided when sub-sampling and no calcite could be observed on the ledge under UV light. Previous studies have demonstrated the addition of calcite via meteoric water diagenesis would negatively shift coral $\delta^{18}O$ and $\delta^{13}C$ [*Stein et al.*, 1993; *Zhu et al.*, 1994; *Wei et al.*, 1998; *McGregor and Gagan*, 2003]. This Sumba coral result indicates that coral $\delta^{18}O$ is sensitive to even trace amounts of calcite and might be more sensitive than $\delta^{13}C$. It also confirms the pristine condition of

most of the coral $\delta^{18}O$ and $\delta^{13}C$ record for MV03-A-2.

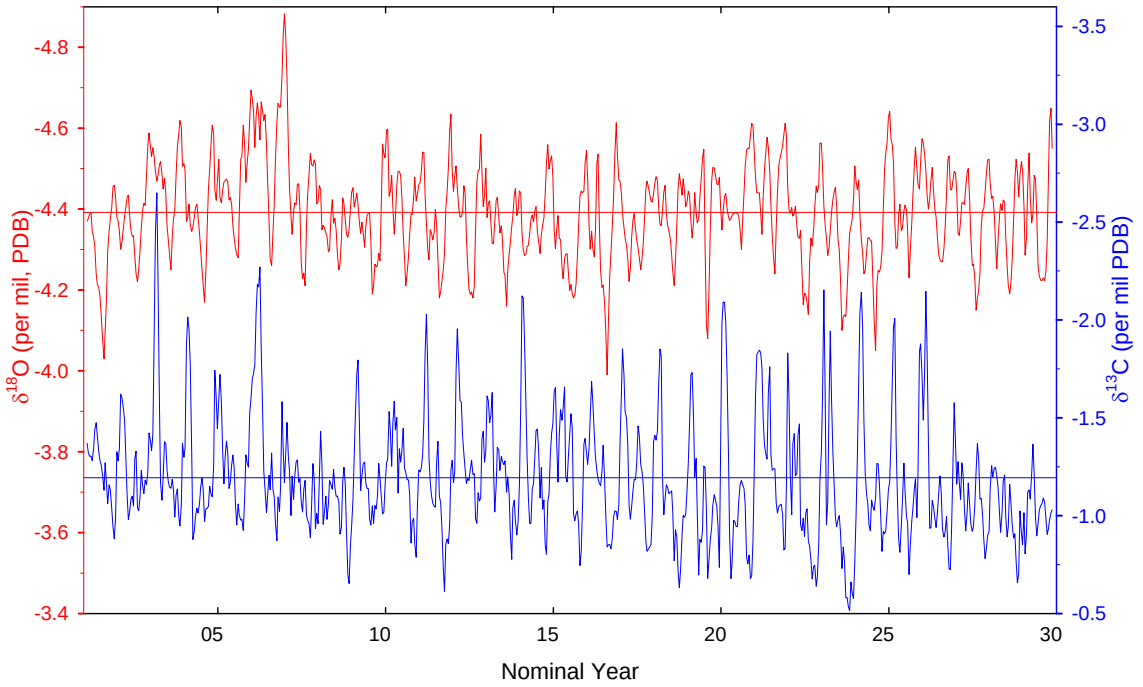

Figure 8.8 High-resolution $\delta^{18}O$ and $\delta^{13}C$ time-series for Sumba *Porites* coral MV03-A-2 which grew at 133.6 ka during an early highstand in Termination II. Curves are fortnightly records and horizontal lines represent mean values (red for $\delta^{18}O$, blue for $\delta^{13}C$).

The MV03-A-2 coral $\delta^{18}O$ record has a mean value of -4.39‰ ± 0.03‰ (2σ standard error), and the 2σ standard deviation is 0.17‰. When the first 6.5 years were excluded due to slight alteration in year 6, the $\delta^{18}O$ has a mean of -4.38‰ ± 0.03‰ (2σ standard error),,and the 2σ standard deviation is 0.15‰. The coral $\delta^{13}C$ has a mean of -1.19‰ ± 0.08‰ (2σ standard error) and the 2σ standard deviation is 0.45‰.

8.3.2 Comparison with modern and Holocene records

Three major features for this Termination II coral records could be easily recognized in comparison with the local modern and Holocene coral records:

1. Higher mean $\delta^{18}O$ during Termination II

Figure 8.9 shows a remarkable difference of 0.6‰ between the mean $\delta^{18}O$ values for the Termination II coral and the Holocene / modern corals from reefs within 2 km of the Termination II coral (Figure 8.2). The replicate corals for the Holocene show a compelling consistent mean value of 5.0‰ (also see Table 8.1). The Termination II coral displays a difference of 1-1.2‰ from the modern coral $\delta^{18}O$, which is much larger than any difference that could be attributed to analytical uncertainties in coral palaeoclimatology.

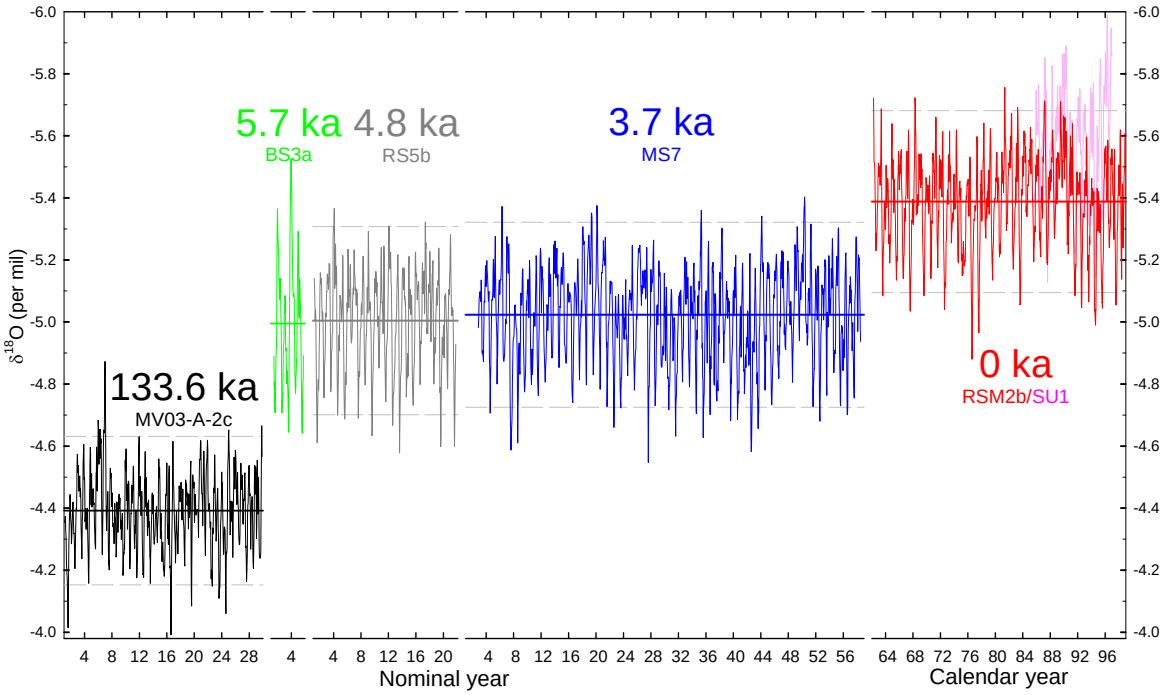

Figure 8.9 Comparison of $\delta^{18}O$ records between the Sumba Termination II coral and local Holocene and modern corals. Various coloured thin curves and straight lines are linear detrended fortnightly records and their means (SU1 and BS3a records are not detrended due to their short range). Grey dashed control lines represent 2σ standard deviations which show the magnitude of variability of the coral records. Note that the winter enriched $\delta^{18}O$ peaks going beyond the lower control lines represent cooler and more saline seawater which usually reflects the impact of an El Niño event (refer to Chapter 6 and 7).

2. *Suppression of cold/saline events in winter during Termination II*

Figure 8.9 demonstrates that there is a dramatic decrease in the frequency of cold and saline events in austral winter. In the 29-year Termination II coral record, there were

only 6 years when the winter $\delta^{18}O$ went beyond the 2σ control line, which means that only 21% of the winters recorded a cold and saline event. In contrast, all the Holocene and modern corals recorded much more frequent cold and saline events. In all cases, more than 30% of the years record cold/saline events; 43% at 4.8 ka (9 events in 21 years), 31% at 3.7 ka (17 events in 57 years), and 35% in modern times (13 events in 37 years) (Table 8.1).

Table 8.1

Comparison of coral $\delta^{18}O$ records and insolation between the Termination II and modern/Holocene

Period	Modern		Holocene			Termination II
Core	RSM2b	SU1*	MS7	RS5b	BS3a*	MV03-2c
Age (ka)	0	0	3.7	4.8	5.7	133.6
$\delta^{18}O$ mean (‰)	**-5.4**	**-5.6**	**-5.0**	**-5.0**	**-5.0**	**-4.4**
Detrended $\delta^{18}O$ range of variability (‰)	0.59		0.60	0.61		0.48
Seasonal range of $\delta^{18}O$ climatology (‰)	0.35		0.39	0.40		0.31
$\delta^{18}O$ change from autumn to winter (‰)	**0.35**		**0.39**	**0.40**		**0.22**
Number of winters included in coral $\delta^{18}O$ records	37	11	55	21	5	29
Number of cold/saline events (beyond 2σ line)	13		17	9		6
Percentage of cold/saline winters (%)	**35**		**31**	**43**		**21**
Insolation seasonality (W/m^2)	114	114	117	114	110	127
Insolation change from autumn to winter (W/m^2)	4	4	16	20	22	45

* No detrended record or average climatology was calculated due to the short length of $\delta^{18}O$ records for SU1 and BS3a corals.

3. Weaker seasonality of $\delta^{18}O$ during Termination II

Figure 8.9 clearly shows the smaller annual amplitude of $\delta^{18}O$ variability for the Termination II coral (20% decreased in variability relative to the modern/Holocene records). Also, the stacked coral $\delta^{18}O$ climatology shows the remarkably weaker seasonality of the Termination II record: the seasonality of the climatology is 11% to 22% weaker relative to the modern/Holocene coral records (Table 8.1). When comparing the magnitude of change from austral autumn (May) to winter (August), the magnitude of change for the TII coral $\delta^{18}O$ is more than 50% greater than the autumn-winter shift in local Holocene and modern $\delta^{18}O$ records (55%, 56%, and 63% respectively, see Figure

8.10 and Table 8.1).

The notable fact is that, even though several recently published coral records have confirmed the control of solar insolation on coral $\delta^{18}O$ seasonality [*Suzuki et al.*, 2001; *Felis et al.*, 2004; *Sun et al.*, 2005; *Ayling et al.*, 2006], the decrease of $\delta^{18}O$ seasonality of Sumba coral records has nothing to do with the change of insolation seasonality because it shows a totally adverse change of large scope of increase (Table 8.1). Figure 8.11 displays the seasonality of the insolation in Sumba since the penultimate deglaciation.

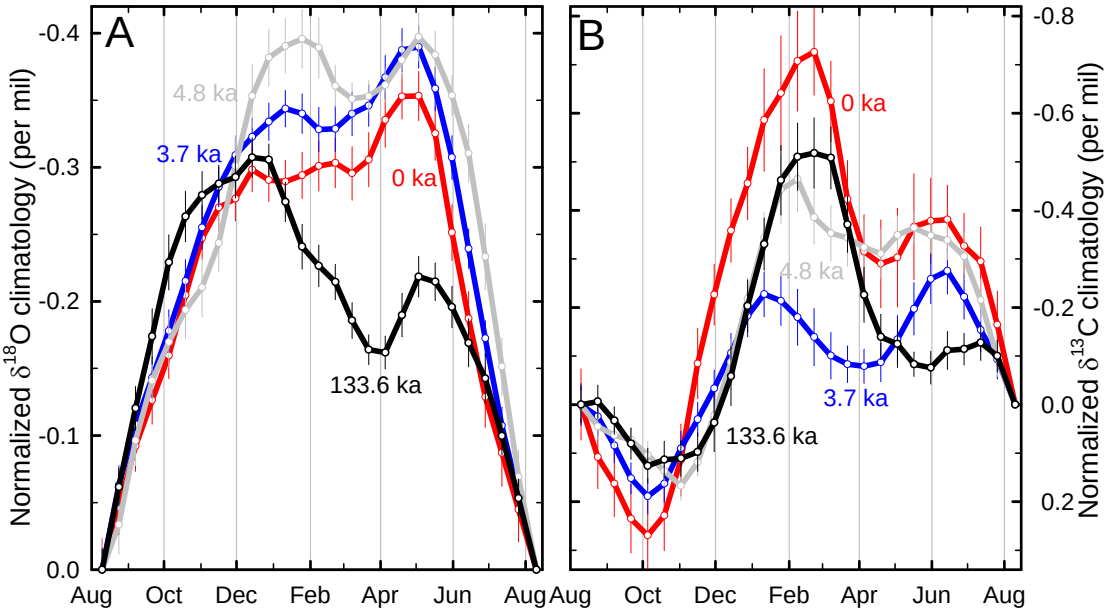

Figure 8.10 Comparison of the stacked climatologies of coral $\delta^{18}O$ (A) and $\delta^{13}C$ (B) for the Termination II, Holocene and modern corals. Black curves with dots are the Termination II records, while red, blue, and grey curves are modern, 3.7 ka, and 4.8 ka records, respectively. Thin vertical bars represent 2σ errors of the stacked records.

4. $\delta^{18}O$ decrease in austral spring during Termination II

Comparison of the coral $\delta^{18}O$ climatologies of the Termination II, Holocene, and modern records shows that the most striking feature of the Termination II record is the

dramatic decrease in $\delta^{18}O$ during austral spring. Even though all the Sumba coral climatologies consist of two distinct stages: a relatively long, low-value stage in November-May (7 months) and a shorter high-value stage in July-September (3 months), the shape of the Termination II climatology is different (Figure 8.10). During Termination II, the low-value stage started in October, one to two months earlier than in the modern/Holocene records. The $\delta^{18}O$ values in October-January were also dramatically lower relative to values in summer and autumn (February to May) in comparison with the modern/Holocene records. During termination II, as much as one third of the $\delta^{18}O$ seasonality is confined to the relatively short period from October to January.

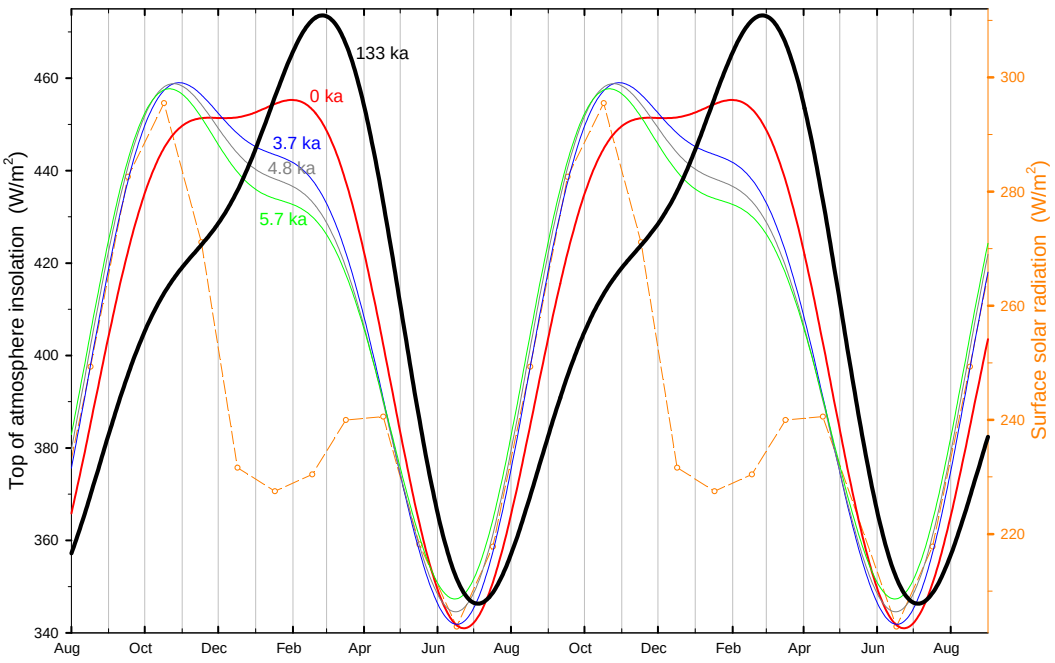

Figure 8.11 Comparison of daily top of atmosphere insolation at 0 ka (red curve), 3.7 ka (blue curve), 4.8 ka (grey curve), and 5.7 ka (green curve) in Sumba Strait. Also shown is modern surface incoming short-wave radiation (dashed orange curve with dots). Monthly surface incoming short wave radiation data are from *Atlas of Surface Marine Data 1994* [*da Silva et al.*, 1994]. Top of atmosphere insolation data are calculated by *AnalySeries* software [*Paillard et al.*, 1996] using the Laskar 2004 solution [*Laskar et al.*, 2004].

8.4 DISCUSSION

8.4.1 SST and seawater $\delta^{18}O$ during Termination II

Even though there are reports that mean $\delta^{18}O$ differs among different coral colonies [*Guilderson and Schrag*, 1999; *Linsley et al.*, 1999], recent studies have shown good replication of skeletal $\delta^{18}O$ records (< ±0.15‰, 2σ) extracted from modern and fossil *Porites* colonies when rigorous coral cleaning and micro-sampling protocols are applied [*Gagan et al.*, 1998; *Cobb et al.*, 2003; *Watanabe et al.*, 2003; *Sun et al.*, 2005]. Therefore, the mean value of $\delta^{18}O$ of massive *Porites* corals from same site has been used to assess the mean climate and sea level [e.g.: *McCulloch et al.*, 1999; *Sun et al.*, 2005]. The Holocene *Porites* corals from Sumba show remarkably consistent mean $\delta^{18}O$ values (-5.0‰) even though their ages differ by up to 2 ka and they are up to 6 km apart. Moreover, the two modern corals only display a difference of 0.15‰ for the same time-period even though coral SU1 is a very young colony of 11 years and located close to shore. Accordingly, the distinct differences between the mean $\delta^{18}O$ values of the Termination, Holocene and modern coral records can be used to determine the mean climate in which the corals grew, and cross-check the age and sea level of the coral growth.

In Chapter 6, it was argued that the rapid-growing low-density band of the Sumba modern coral resulted from the abundant input of terrestrial nutrition which results in much depleted coral $\delta^{13}C$ at the time of low-density band formation. The extremely low $\delta^{13}C$ value in the coral climatology during peak monsoon time (January-March, Figure 8.10B) further confirms the near shore and shallow seawater environment. Furthermore, Pirazzoli *et al.* [1991; 1993] have deduced a local uplift rate of 0.49 m/kyr which remained almost constant during at least the last million years and, in any case, at least until the last interglacial period. Given the current altitude of 39 m above the mean sea level of this fossil coral and a -14 m to -18 m sea level during the early highstand of

Termiantion II [*Esat et al.*, 1999; *Thompson and Goldstein*, 2005], the growth depth of this coral could be -8 m to -12 m. Therefore, deriving a sea surface temperature from this shallow seawater coral should be reasonable.

The difference of 0.4-0.6‰ between Holocene corals and modern corals has been generally found around the Indo-Pacific warm pool [e.g.: *Gagan et al.*, 1998; *Gagan et al.*, 2002; *Sun et al.*, 2005]. Sun et al. [2005] attributed the difference mostly to the differential local seawater $\delta^{18}O$ value since the differences in SST and ice volume between mid-Holocene and the present time are not significant and should only result in less than ~0.1‰ of the ^{18}O enrichment. Our measurement of Sr/Ca ratios for the Sumba coral also shows no significant difference in SST between the mid-Holocene and modern time (see Appendix D). Therefore, we can estimate the mean SST during the early highstand of Termination II using the sea-level curve to place constraints on seawater $\delta^{18}O$ values.

Table 8.2
Summary of difference in sea surface temperature (SST)

Sea-level shift between glacial-interglacial: 125 m $^{\$}$	$\delta^{18}O$ shift owing to sea-level shift *		0.8	1	1.2	1.3
	shift rate of $\delta^{18}O$ (‰/m)		0.0064	0.008	0.0096	0.0104
Sea-level estimate for early highstand of TII: -14 m $^{\#}$	Sea-level composition in $\delta^{18}O$ shift (‰)		0.09	0.11	0.13	0.15
	SST component in 0.6‰ shift in Sumba coral between TII and Holocene	$\delta^{18}O$ (‰)	0.51	0.49	0.47	0.45
		SST (^{o}C)	**2.7**	**2.6**	**2.5**	**2.4**
Sea-level estimate for early highstand of TII: -18 m $^{\wedge}$	Sea-level composition in $\delta^{18}O$ shift (‰)		0.12	0.14	0.17	0.19
	SST component in 0.6‰ shift in Sumba coral between TII and Holocene	$\delta^{18}O$ (‰)	0.48	0.46	0.43	0.41
		SST (^{o}C)	**2.6**	**2.4**	**2.3**	**2.2**

* The shift in $\delta^{18}O$ attributed to ice volume between the LGM and the present is 0.8-1.0‰, 1.2−1.3‰, or 0.8−1.2‰ according to Schrag et al. [1996] , Fairbanks et al. [1989], or Lea et al. [2006], respectively.

$ The sea-level shift between the LGM and the present was 125 m following McCulloch et al. [1999] for convenience of comparison.

The sea level at the early highstand of Termination II was -14 m based on Esat et al. [1999] and Stirling et al. [1995].

^ The sea level at the early highstand of Termination II was -18 m ± 3 m or -18 m ± 1.6m according to Gallup et al. [2002] or Thompson and Goldstein [2005], respectively.

Table 8.2 shows the calculated estimates of the sea surface temperature (SST) using published data for the shift in seawater $\delta^{18}O$ shift between the glacial and interglacial [*Fairbanks*, 1989; *Schrag et al.*, 1996; *Lea et al.*, 2006] and sea-level estimates during the early highstand of Termination II [*Stirling et al.*, 1995; *Esat et al.*, 1999; *Gallup et al.*, 2002; *Thompson and Goldstein*, 2005]. Many authors have confirmed that the SST in mid-Holocene is within 0.5°C of the modern SST and that the $\delta^{18}O$ of surface seawater in the warm pool region is much lower today relative to the early Holocene [e.g.: *Gagan et al.*, 1998]. Therefore, we think that the surface seawater $\delta^{18}O$ value at 133.6 ka is different from that in modern time due to hydrologic processes unrelated to the ice volume shift. Sun et al. [*Sun et al.*, 2005] suggested that the factors of enrichment of ^{18}O in seawater during the middle Holocene include greater advection of moisture towards the Asian landmass, enhanced monsoon wind-induced evaporation and vertical mixing, and/or invigorated advection of ^{18}O-enriched saltier outside seawater into the study area. Therefore, the seawater $\delta^{18}O$ during the early highstand of Termination II is more likely close to the Holocene value, so we have calculated the Termination II SST relative to the middle Holocene.

The result indicates a decrease in SST of ~2.2-2.7°C during Termination II, relative to the average Holocene SST, if the uncertainties in sea level (-14 m or -18 m) and $\delta^{18}O$ shift between glacial-interglacial (0.8−1.0‰ or 1.2−1.3‰) are both included. The 2.2-2.7°C cooling during the early highstand of Termination II implies substantial cooling of the tropical ocean surface when the sea level was only -14 to -18 m lower than today. Even though many studies have suggested a cooling of 1-4°C of the tropical Pacific ocean surface during the last glacial period [*CLIMAP Project Members*, 1976; *Lyle et al.*, 1992; *Pelejero et al.*, 1999; *Crowley*, 2000; *Lea et al.*, 2000; *Lea et al.*, 2006], more extreme cooling of 5-6°C in tropical SST is supported by terrestrial and coral Sr/Ca evidence [*Rind and Peteet*, 1985; *Guilderson et al.*, 1994; *Stute et al.*, 1995; *Thompson et al.*, 1995; *McCulloch et al.*, 1996; *Beck et al.*, 1997; *Guilderson et al.*, 2001]. The coral Sr/Ca results of McCulloch et al. [1999] even suggested a 6-7°C cooling in the warm pool when the sea level during a late lowstand of Termination II

was 60-80 m lower than today. Our result supports a significant shift of SST in the tropical warm pool during glacial-interglacial cycles.

8.4.2 El Niño variability during Termination II

The large SST shift in the Indo-Pacific warm pool at 133.6 ka relative to modern and Holocene provides a good opportunity to examine the El Niño phenomenon under the influence of an altered background climate state [*Cane*, 2005].

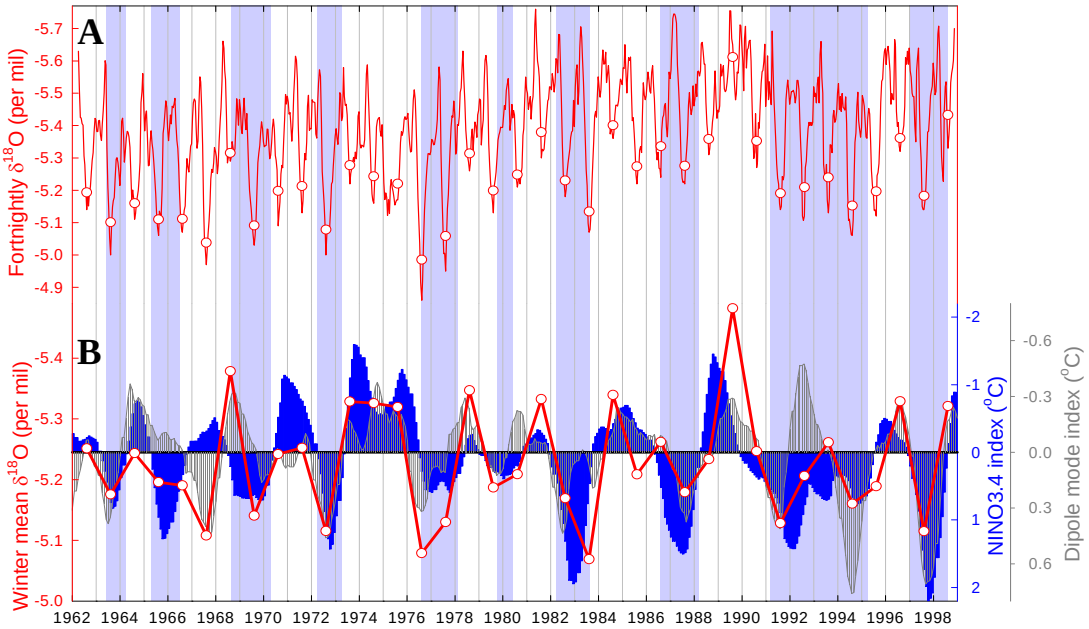

Figure 8.12 The dominant control of ENSO and signature of the IOD on winter $\delta^{18}O$ in modern Sumba coral RSM2b. **(A)** The fortnightly coral $\delta^{18}O$ record with annual maxima in austral winters (around August). White circles indicate the winter mean $\delta^{18}O$ values. Shaded areas mark El Niño years based on the definition of Trenberth (1997). (**B)** Red curve with circles represents the winter averages (July to September) of the detrended coral $\delta^{18}O$ record (long-term trend and decadal variability removed). Blue and grey-shaded bars are 11-month smoothed NINO3.4 and Indian Ocean Dipole Mode Index (DMI). Data sources: NINO3.4 index and ISMR from Lamont-Doherty Earth Observatory data sets at http://iridl.ldeo.columbia.edu/SOURCES/.Indices/.nino/.EXTENDED/.NINO34/ [*Kaplan et al.*, 1998], and the DMI from Saji's personal webpage at http://iprc.soest.hawaii.edu/%7Esaji/dmi.txt [*Saji et al.*, 1999].

A strong correlation between the ^{18}O-enriched winters in the Sumba coral $\delta^{18}O$ and the NINO3.4 index has clearly confirmed a link between the climate of Sumba and El Niño

events (Chapters 6, 7). Figure 8.12 shows that all 10 El Niño events (13 years) from 1962 to 1998, as defined by Trenberth [1997], have been recorded by the Sumba coral as anomalously high $\delta^{18}O$ values during winter. With only two exceptions in the 37 year record (1967, 1985), the Sumba winter $\delta^{18}O$ values are very good recorders of ENSO events. The obvious exception in 1967 is related to a positive Indian Ocean Dipole (IOD) event (refer to Chapter 6) and the minor exception in 1985 might be connected with the mid-1980s cooling of background temperature. Spectral analysis of the seasonal coral $\delta^{18}O$ record confirms that the modern Sumba winter coral $\delta^{18}O$ has a dominant ENSO period of 3.6 years (Chapters 6 and 7).

In order to develop a local index of ENSO activity recorded by Sumba corals, the 2-sigma standard deviation of the detrended coral $\delta^{18}O$ is used to identify El Niño events. Applying this technique to the modern coral record shows that 13 of the 37 winters from 1962 to 1998 are El Niño winters (Figure 8.12), which is consistent with the definition of Trenberth [1997]. Only one exception in 1967 is related to a positive IOD event. Therefore, we could use the number of the cold/saline winters to compare the frequency of El Niño activity among the fossil coral records.

The significant decrease in the number of ^{18}O-enriched winters in the Termination II coral record (Figure 8.9, Table 8.1) indicates a significant decrease in the frequency of El Niño events during the early highstand of Termination II. Overall, the results show a decrease in El Niño activity at 133.6 ka relative to modern time (40% decrease), 3.7 ka (32% decrease), and 4.8 ka (51% decrease).

The Sumba Termination II coral $\delta^{18}O$ climatology also strongly supports a significant decrease in El Niño activity at that time. Since the winter coral $\delta^{18}O$ reflects the impact of El Niño events, the $\delta^{18}O$ shift in the climatology from austral autumn to winter should be proportional to the activity of El Niño if the factors controlling coral $\delta^{18}O$ in autumn are assumed to be constant. In Chapter 6 and 7 it has been argued that the autumn freshening in the Holocene and modern coral records resulted from the penetration of a remotely forced tropical Indian Ocean Kelvin wave into the Savu Sea

during the monsoon transition in autumn, which moves warm and fresh surface water through the Sumba Strait. The magnitudes of this autumn peak in the Termination II, Holocene, and modern coral $\delta^{18}O$ climatologies are similar, suggesting a persistent input of Kelvin waves into the Savu Sea since Termination II. It is noteworthy that the magnitude of the shifts in coral $\delta^{18}O$ from autumn to winter during Termination II, Holocene and modern times exactly reflects the magnitude of the changes in El Niño activity given by the statistics of the winter cool/saline events (Table 8.1 comparing two lines of black bold numbers). The similarity demonstrates that the decrease in the autumn-winter $\delta^{18}O$ shift during Termination II mainly resulted from the decrease in El Niño activity.

8.4.3 Monsoon intensity during Termination II

Until now, most of the features of the Termination II coral $\delta^{18}O$ record have been reasonably explained except the significant depletion in $\delta^{18}O$ during late austral spring and early summer (October to February) relative to the rest of the Termination II $\delta^{18}O$ climatology (Fig. 8.10). At first, it was perplexing. I even suspected that it might result from the addition of small amount of calcite because that would slightly decrease the bulk coral $\delta^{18}O$ value. But when I removed years 1-7 (because years 6-7 shows impact of the calcite patch) and stacked a new climatology, the relatively low $\delta^{18}O$ peak is still there. Furthermore, the low $\delta^{18}O$ anomaly amounts to one-third of the range of the $\delta^{18}O$ climatology and, given that high percentages of calcite contamination would be required to produced such an anomaly, the coral $\delta^{13}C$ climatology should respond too. However, this is not the case (Figure 8.10B). In summary, the relatively low $\delta^{18}O$ values in October-February should not result from slight diagenetic alteration.

The other possibility is that the low $\delta^{18}O$ anomaly is due to strong monsoonal rainfall from October to February during Termination II. The Holocene coral records suggest that monsoonal rainfall could have a small peak in January and a high peak in late January / February even though the modern corals do not record local monsoonal

rainfall (see Chapter 7). But the Asian-Australian monsoon peak migrates, on average, from India in July to north Australia in early February [*Meehl*, 1987; *Huang and Mehta*, 2004; *Chang et al.*, 2005], thus the November-December $\delta^{18}O$ peak in the Termination II record is too early for the local monsoonal rainfall effect. And the Termination II coral $\delta^{13}C$ climatology recorded strong local monsoonal rainfall in January to March, which is consistent with the timing of migration of the Intertropical Convergence Zone (ITCZ). Therefore, the low $\delta^{18}O$ anomaly in October-February during Termination II should not result from local monsoonal rainfall.

However, further analysis of the coral $\delta^{18}O$ climatology shows that there might be a local rainfall peak during January-February which might have been partly masked by the low $\delta^{18}O$ anomaly in October-February. The decrease in the slope of the $\delta^{18}O$ climatology curve during late January-early February relative to the slope during January could be the manifestation of the local rainfall peak. This interpretation is supported by the Termination II coral $\delta^{13}C$ record, which implies a very strong local rainfall (Figure 8.10B). In chapter 6 it was argued that the depleted $\delta^{13}C$ peak in December-March resulted from the large input of terrestrial nutrition brought by the local monsoonal rainfall, and the small depleted $\delta^{13}C$ peak in May-June resulted from the decrease of the incoming radiation. Even though the intensity of the December-March peak is strongly impacted by the location of the coral relative to the Mondu River flood plume, some information on the rainfall could still be retrieved by the relative height of these two peaks. Figure 8.10B indicates a slightly shifted June to July peak which should result from the slight shift of the annual minimum in insolation from June to early July. It also shows a much larger ratio of the height of the two peaks in Termination II $\delta^{13}C$ relative to the Holocene and modern coral records and probably indicates a much stronger local monsoonal rainfall during January and February.

In Chapter 7 we have shown that the local monsoonal rainfall at 4.8 ka is much stronger than at 3.7 ka and the present, so its coral $\delta^{18}O$ climatology shows a higher January-February peak relative to the April-May peak (Figure 8.10A). Analysis of the

January-February peak in the Termination II coral $\delta^{18}O$ climatology seems to show a much higher January-February peak relative to its April-May peak. Therefore, both the Termination II coral $\delta^{18}O$ and $\delta^{13}C$ climatology support an relatively strong local monsoonal rainfall, even stronger than that at 4.8 ka when the local monsoonal rainfall has been argued to be stronger than at 3.7 ka and the present (Chapter 7).

Still, the question remains, what is the source of the relatively warm/fresh water during October-February? The only reasonable explanation is that the warm/fresh water was from the South Java Current (SJC) which must have penetrated further eastward into the Sumba Strait during the early highstand of Termination II. Given that monsoon winds and rainfall/river runoff are the two major forcing agents for the South Java Current [*Quadfasel and Cresswell*, 1992; *Sprintall et al.*, 1999], the intensified monsoon at 133.6 ka would have driven a much stronger SJC at that time. It is reasonable that the increased intensity of the SJC would be sufficient to make it penetrate the Sumba Strait and enter the Savu Sea. Unlike the May-June incursion of the Kelvin wave, the October-December Kelvin wave coincides with the annual rainfall maximum of the source areas of freshwater along the Sumatra-Java-Bali-Sumbawa coastline. Accordingly, the water taken into the Sumba Strait by the October-December Kelvin wave would be much fresher than the May-June Kelvin wave, and the coral $\delta^{18}O$ climatology would therefore record a much depleted $\delta^{18}O$ peak.

The Sumba Termination II coral $\delta^{18}O$ rapidly shifts toward higher values after December, implying that the incursion of the SJC happens only when the remote tropical Indian Ocean Kelvin wave penetrates into the Savu Sea during the monsoon transition between October and December, not during the whole period of October to March when the SJC flows eastward. The October-December Kelvin wave only penetrated through Sumba Strait when the monsoon was extremely strong, while the May-June Kelvin wave can penetrate the Sumba Strait at all times (modern, 3.7 ka, 4.8 ka, and 133.6 ka), which is consistent with the observation of Wyrtki [1973] that the semiannual Kelvin wave sea level signal associated with the October/December

monsoon transition is typically weaker. This observation has also been confirmed by Sprintall et al. [2000].

In summary, the warm/fresh anomaly in the Termination II Sumba coral $\delta^{18}O$ record during October-February should reflect a relatively strong monsoon during the early highstand at 133.6 ka.

8.5 CONCLUSIONS

A 29-year-long fortnightly-resolution $\delta^{18}O$ and $\delta^{13}C$ record was compiled for a 133.6 ka *Porites* coral from an early highstand of the penultimate deglaciation (Termination II) preserved within the Mondu raised reefs of Sumba, Indonesia. The massive coral is located at an altitude of 39 m above the mean sea level. U-series dating of a pristine part of this coral gave a conventional ^{230}Th age of 136.8 ka with an initial $\delta^{234}U$ value of 158.9‰, which suggests that the true age is slightly younger. Multiple analyses of sub-samples in the same coral suggest a model correction age of 133.6 ka, which shows that the coral grew during Termination II. Recent published results show that 133.6 ka coincides with an early highstand during the Termination II.

The high-resolution isotopic record gave a mean $\delta^{18}O$ value of 4.4‰ at 133.6 ka, which is 0.6‰ higher than the local Holocene coral records, and 1.0−1.2‰ higher than the local modern coral records. Calculations based on the coral $\delta^{18}O$ shows that the mean SST at 133.6 ka was ~2.4^{o}C lower relative to the middle Holocene SST. The seawater $\delta^{18}O$ at 133.6 ka was probably similar to the enriched $\delta^{18}O$ value observed for the mid-Holocene, rather than the depleted modern warm pool $\delta^{18}O$ value.

The high-resolution $\delta^{18}O$ record for the Termination II coral disclosed much less frequent El Niño events at 133.6 ka. Comparison between the TII record and Holocene/modern coral records demonstrate a dramatic decrease of 40% of El Niño events than the modern time, a 32% decrease relative to 3.7 ka, and a 51% decrease to 4.8 ka. The smaller seasonality of the TII coral $\delta^{18}O$ has nothing to do with the local

insolation change, it mainly reflects the suppressed ENSO activity during 133.6 ka. The dramatic decrease in austral autumn-winter $\delta^{18}O$ shift mainly derives from the remarkably weaker El Niño.

Both the high-resolution $\delta^{18}O$ climatology and the $\delta^{13}C$ climatology for the Termination II coral suggested an intensified Asian-Australian monsoon operated at 133.6 ka. Comparison with the local Holocene coral records shows that the Termination II monsoon was stronger than the generally accepted strong mid-Holocene monsoon.

A striking warm/fresh anomaly during October-December in the coral $\delta^{18}O$ climatology suggests the routine incursion of Kelvin waves into the Sumba Strait during the two monsoon transition periods (May and November) at 133.6 ka. This is in contrast to the penetration of only the austral autumn Kelvin wave into the Sumba Strait in mid-Holocene and the modern time, which is consistent with an intensified Asian-Australian monsoon during the early highstand of Termination II.

The contrast of a stronger monsoon and weaker El Niño during the different background climate state of Termination II (lower SST, higher seawater $\delta^{18}O$) provides a new perspective on the interactions between these climate systems.

CHAPTER 9

CONCLUSIONS

The Indo-Pacific Warm Pool plays a key role in driving the global atmospheric circulation. Therefore, knowing the history of natural climate variability in this region during different background climate states would provide a better understanding of potential future changes in important climate systems such as the El Niño-Southern Oscillation (ENSO) and the Asian-Australian monsoon, which interact in this area and are of broad political and economic significance. Coral from the island of Sumba are well situated to record this climatic variability because they are strongly impacted by ENSO and in the migration path of the Asian-Australian monsoon convective centre. To this end, this PhD project utilized high-quality *Porites* coral cores from the Mondu raised reefs on the north coast of Sumba, Indonesia, to reconstruct the mean climate conditions, ENSO variability, and monsoon intensity during the Holocene and a sea-level highstand of the penultimate deglaciation (Termination II). The study involved detailed topographic surveys of the Mondu raised reefs, stratigraphic analysis, investigations of coral diagenesis, U-series age determinations and corrections, and the production of high-resolution records of coral $\delta^{18}O$ and $\delta^{13}C$ for palaeoclimate reconstruction. This chapter summarizes the key findings, based on the aims of this study, and provides general suggestions for future work in this area.

9.1 SUMMARY OF KEY FINDINGS

Aim 1: To date the Mondu raised reefs and important corals

- ✧ Stratigraphic relationship and topographic features of the Mondu raised coral reefs have been disclosed by topographic survey and field observation.

- ✧ 54 samples from the raised reefs have been measured for U-series isotopic composition but almost any of them could not give a reliable conventional ^{230}Th age for any of the reefs. However, most corals in a reef array along a straight line in the $^{234}U/^{238}U$ – $^{230}Th/^{238}U$ plot and the isochron model (SCHOLZ et al., 2004) could

be applied to correct the U-series ages of the Mondu raised reefs. This study shows the model ages are consistent very well with the stratigraphic relationships and features.

✧ The assigned ages of the Mondu raised reefs include sub-stages of 5a, 5b, 5c, 5d, and 5e during MIS 5, an early-stage highstand of Termination II, an early-stage highstand of MIS 6, and a late-stage highstand of MIS 8, implying strong potential of the Mondu raised reefs for paleoclimate reconstruction.

✧ Among the raised reefs, the $^{234}U/^{238}U$ – $^{230}Th/^{238}U$ plot displays distinct two groups of array lines and within each group the array lines are parallel to each other, but the group with older ages has larger slopes than the younger ones. Our stratigraphic analysis demonstrates that the slopes of the array lines reflect the burial/exposure history of the reefs, which has helped to determine the ages of some of the reefs.

✧ This study supports a constant uplift rate of 0.49 m/kyr in the area for most of the time since 258 ka even though in MIS 5a the rate might have been slightly higher, and in MIS 5c it might have been lower.

✧ Multiple measurements of U-series isotopes in skeletal sub-samples within a single *Porites* coral were made to explore the diagenetic behaviour of U-series isotopes in fossil corals from the Sumba raised reefs. Detailed analysis of two diagenetic stages and corresponding changes in U-series isotopic composition has revealed two distinct processes of U-series isotope diagenesis in this single coral colony. Both of them are different from those suggested before. The earlier-stage process demonstrates the addition of allochthonous dissolved ^{234}U and ^{238}U together with detrital non-radiogenic ^{230}Th, while the later-stage process clearly shows that loss of ^{234}U and ^{238}U occurred along with detrital-bound ^{230}Th. Locally radiogenic ^{230}Th appears to have played an important role in maintaining a constant $^{234}U/^{230}Th$ as allochthonous U added when percolating groundwater with high $\delta^{234}U$ value entered into the coral, while detritus-bound ^{230}Th was critical to maintain a fixed

$^{234}U/^{230}Th$ when percolating meteoric water dissolved coral skeletal U. The results strongly suggest that a mechanism like diffusion or osmosis controls the addition or loss of dissolved U and detrital Th into or out of the coral by way of a solute concentration gradient. This mechanism explains the constant $^{234}U/^{230}Th$ ratios in either situations of the addition or loss of U. Model correction ages could be determined for both processes and they yield essentially the same age of 133.6 ka. This detailed study agrees with the published isochron model (Scholz et al., 2004) on their way of achieving the isochron age, but provides a further observation and explanation on the way of maintaining the $^{234}U/^{230}Th$ ratio roughly constant as either the addition or loss of U happens.

✧ Stratigraphic analysis demonstrates that this kind of mechanism for U-series isotope diagenetic behaviour could reflect the relative ages of the Mondu raised coral reefs and their history of burial and exposure.

Aim 2: To explore the climatic and oceanographic significance of Sumba coral $\delta^{18}O$ and $\delta^{13}C$

✧ Reproducibility experiences have shown good consistency of the Sumba coral $\delta^{18}O$ and $\delta^{13}C$ between different axes of growth of one single coral colony and different corals from the Mondu modern coral reefs.

✧ This study demonstrates that the Sumba modern corals are excellent recorders of modern climate and oceanography in the Indo-Pacific warm pool. High-resolution (fortnightly) time series, stacked climatology, and seasonal means have been characterised for both the modern coral $\delta^{18}O$ and $\delta^{13}C$. Detailed analysis on correlation of these features with local instrumental records, and main climate system indexes such as NINO3.4 index, All India Summer monsoon rainfall, and the Dipole Mode Index have been conducted. Blackman-Tukey spectra of annual and seasonal coral $\delta^{18}O$ and $\delta^{13}C$ characteristics and their cross-spectra with the

above-mentioned climate system indexes have also been carried out. The strong correlations and spectral connections demonstrate that the ENSO, Asian-Australian monsoon, and remote equatorial Indian Ocean forcing all have strong influence on the local climate and oceanography and the high-resolution coral $\delta^{18}O$ record from Sumba, Indonesia could disassemble the entangled climate system signals of the ENSO, Asian-Australian monsoon, and remote equatorial Indian Ocean forcing agent in an encouraging scale and helps in understanding the climate and oceanography in this area.

✧ The Sumba coral $\delta^{18}O$ record shows the dominant control of ENSO in austral winter and that the interannual variability of the winter $\delta^{18}O$ could serve as a good index for ENSO events. In austral summer (November through February), the coral $\delta^{18}O$ is overwhelmingly controlled by the tropical Indian Ocean forcing, while in autumn (March to May), the monsoon and remote equatorial Indian Ocean forcing both have strong impacts on the Sumba coral $\delta^{18}O$.

✧ The high-resolution Sumba modern *Porites* coral $\delta^{18}O$ record provides evidence of routine penetration of the South Java Current (SJC) into the Savu Sea in austral summer, and remote forced equatorial Indian Ocean Kelvin wave in autumn, which results in distinct freshening of the ocean surface during the austral autumn. By sensitively recording variability of sea surface temperature and salinity in this important exit of the Indonesian Throughflow (ITF), the Sumba coral $\delta^{18}O$ revealed active oceanic current activity in Sumba Strait. In austral winter, the current in the Sumba Strait is generally westward and the ITF brings Indonesian Inner Seas water with a Pacific source of moderate salinity. In summer, relatively saline SJC water enters the Suva Sea from the west until the current decreases in intensity around March. After March, two processes gradually lower salinity. On the one hand, the gradual weakening of the SJC owing to weakening monsoon winds might reduce the penetration of the SJC into the Sumba Strait. On the other hand, the arrival of the remotely forced Kelvin wave during April to June (during the monsoon

transition) would generate eastward flow into the Strait and result in a sudden freshening of the Savu Sea. It is possible that this input of Indian Ocean water into the Savu Sea by the summer SJC and autumn Kelvin wave could have significantly influenced the transport of the Indonesian Throughflow.

✧ The Sumba $\delta^{13}C$ shows clear annual cycles and recorded a distinct depletion in $\delta^{13}C$ during the austral summer time (December to March). Our result shows it results from the large input of terrigenous nutrients linked to local heavy summer monsoonal rainfall. A consistent annual maximum during early October in the coral $\delta^{13}C$ is supposed to be linked with the maximum of the local incoming short-wave radiation.

✧ Unique density banding in the Sumba modern coral is presented. There are two high-density bands and two low-density bands in a certain year. Detailed study on the banding and the correlation with the high-resolution $\delta^{13}C$ record indicate that the unique low-density band in summer resulted from the largely increased availability of terrigenous nutrients connected to the heavy rainfall during the north-west monsoon season. Unlike the coral $\delta^{13}C$, during off-rainfall season the coral density banding is more related to the ambient seawater temperature, rather than the local incoming short-wave radiation.

✧ Long-term trends have been shown in both the coral $\delta^{18}O$ and $\delta^{13}C$ records. The increased global warming has been attributed to the $\delta^{18}O$ trend and both the warming and the oceanic Suess effect have been attributed to the long-term trend of depletion in $\delta^{13}C$. Substantial decadal variability has been found in both the coral $\delta^{18}O$ and $\delta^{13}C$ records, and they are usually linked with the change in background climate and oceanography. Variation in input of warm, low-salinity water from the SJC into the Savu Sea in decadal time scale would also add to the decadal variability of the coral $\delta^{18}O$, such as that in the early 1990s. Large decadal variations in sea surface temperature and salinity in the Savu Sea have been

proposed and the variability is supposed up to 0.3℃ and 0.5 ups. Salinity variability in the Savu Sea during 1962 to 1998 has been reconstructed and a remarkable increase in 1974 to 1989 and rapid recover in 1989-1998 has been identified.

✧ The annual climatology of coral $\delta^{18}O$ and $\delta^{13}C$ is a very effective means to simplify and recognize the forcing agents for the variability of the records, especially in an area like Indonesia with entangled multi-systems of climate and oceanography.

Aim 3: To reconstruct Holocene climatic variability

✧ 4 high-resolution Holocene coral $\delta^{18}O$ and $\delta^{13}C$ records have been extracted from the Sumba Strait, Indonesia, where the Asian-Australian monsoon, ENSO, and the remote equatorial Indian Ocean forcing have strong impacts on the local climate and oceanography. Climatology of these coral records has been reconstructed, and the magnitude and periodicity of the interannual variability of the coral records have been achieved. Strong seasonal variation in the association between the Sumba coral records and the three prevailing climate phenomena has been found, which helps to partly disentangle the three intertwisted climate systems and makes it possible to reveal the variation of the individual climate systems since mid-Holocene.

✧ Both the coral $\delta^{18}O$ and $\delta^{13}C$ record a weakening monsoon since 5.7 ka. The monsoon was very strong in 5.7 ka and 4.8 ka, but evidently weaker in 3.7 ka. The modern time seems to have a weakest monsoon among the 4 periods of Holocene.

✧ Comprehensive analysis of the mean climatology, the magnitude and periodicity of the interannual variability of the coral $\delta^{18}Os$ indicates a very strong ENSO in 4.8 ka, a very weak ENSO in 3.7 ka, and a moderate intensity of ENSO in the present time.

- ✧ This coral evidence for variation in the Asian-Australian monsoon and ENSO is consistent with previous findings from a Chinese speleothem $\delta^{18}O$ evidence for evolution of Asian monsoon (WANG et al., 2005) and a Peruvian lake sediment evidence for ENSO evolution (MOY et al., 2002) (Figure 6.8C).

- ✧ The Sumba coral $\delta^{18}Os$ also record a variation in the equatorial Indian Ocean forcing since mid-Holocene: in comparison with the monsoon and ENSO, the remote equatorial Indian Ocean forcing was very weak in 4.8 ka, very strong in 3.7 ka, and moderate in modern time.

- ✧ The Sumba corals provide a historical perspective to understand the evolution and interplay of the three complicatedly intertwisted climate phenomena which are all of global importance. The high-resolution windows illustrate climate scenes distinctly different from the modern time in the relative intensity and variability of the three climate components in one specific location.

Aim 4: To reconstruct climate variability during background conditions distinct from the Holocene and present

- ✧ 29 years of record of fortnightly-resolution $\delta^{18}O$ and $\delta^{13}C$ was compiled for a *Porites* coral of Sumba, Indonesia. The massive coral is from a raised fossil reef with an altitude of 39 m above the mean sea level. U-series dating of a pristine part of this coral gave a conventional ^{230}Th age of 136.8 ka with an initial $\delta^{234}U$ value of 158.9‰, which suggests that the true age is slightly younger. Multiple analyses of sub-samples in the same coral suggest a model correction age of 133.6 ka, which shows that the coral grew during Termination II. Stratigraphic relationships and local uplift rate analysis on the Mondu raised reefs also support this age determination. Recent published results show that 133.6 ka coincides with an early highstand during the Termination II.

- ✧ The high-resolution isotopic record gave a mean $\delta^{18}O$ value of 4.4‰ at 133.6 ka, which is 0.6‰ higher than the local Holocene coral records, and 1.0–1.2‰ higher than the local modern coral records. Calculations based on the coral $\delta^{18}O$ shows that the mean SST at 133.6 ka was ~2.4^{o}C lower relative to the middle Holocene SST. The seawater $\delta^{18}O$ at 133.6 ka was probably similar to the enriched $\delta^{18}O$ value observed for the mid-Holocene, rather than the depleted modern warm pool $\delta^{18}O$ value.

- ✧ The high-resolution $\delta^{18}O$ record for the Termination II coral displayed a dramatic 40% decrease in the frequency of El Niño events, relative to the modern-day frequency.

- ✧ Both the high-resolution $\delta^{18}O$ climatology and the $\delta^{13}C$ climatology for the Termination II coral suggested that an intensified Asian-Australian monsoon operated at 133.6 ka. Comparison with the local Holocene coral records shows that the Termination II monsoon was stronger than the generally accepted strong mid-Holocene monsoon.

- ✧ A striking warm/fresh anomaly during October-December in the coral $\delta^{18}O$ climatology along with the May-June fresh anomaly suggests the routine incursion of Kelvin waves into the Sumba Strait during both the two monsoon transition periods (Autumn and spring) at 133.6 ka. This is in contrast to the penetration of only the austral autumn Kelvin wave into the Sumba Strait in mid-Holocene and the modern time, which is consistent with an intensified Asian-Australian monsoon during the early highstand of Termination II which should have intensified the eastward flow of the SJC with a much fresher water owing the very strong monsoon rainfall along the Indonesia coast.

- ✧ The contrast of a stronger monsoon and weaker El Niño during the different background climate state of Termination II (lower SST, higher seawater $\delta^{18}O$) provides a new perspective on the interactions between these climate systems..

9.2 FUTURE WORK

This study has demonstrated that corals from the Mondu raised reefs of Sumba are excellent recorders of changes in the past ocean-atmosphere system in the Indo-Pacific warm pool, and serve to help us understand climates of the past and improve our ability to predict future climate change. Therefore, it is important to retrieve more climate records from these reefs, especially from those periods when the mean climate was distinct from the modern time. Even though retrieving high-resolution records is time-consuming, this study has demonstrated that high-resolution coral records are capable of providing seasonally resolved records of climate system variability that is very different from the variability at the present time, or during the middle Holocene. The long cores archived at RSES, ANU include corals from reefs dated to stadial sub-stages (e.g. MIS 5b) and even glacial periods such as MIS 6. Also, targeted drilling of high-quality cores from other reefs that were U-series dated in this study is another priority for future work, especially the reefs of MIS 5a-5d, 6, and even 8.

Some corals and reefs still need to be definitively dated. Now that this study has demonstrated that the isochron model can be applied to accurately correct the ages of the Mondu raised reefs, dating multiple coral samples from the target reef or multiple sub-samples from the target coral would potentially give reliable ages.

Even though Sr/Ca has been measured for the modern and Holocene Sumba corals, Sr/Ca is yet to be measured for the Termination II coral. Finalizing these measurements and analysing Sr/Ca in more of the corals would be significant. Such measurements would be particularly helpful to further demonstrate that the Sumba coral $\delta^{18}O$ records the oceanic currents flowing through the Sumba Strait. High-resolution accelerator mass spectrometer measurements of ^{14}C in the coral skeletons would also shed light on ocean circulation patterns.

The detailed correlation between coral $\delta^{13}C$ and density banding has revealed that an extremely low density band occurring at the time of maximum monsoonal rainfall

corresponds to an annual minimum in $\delta^{13}C$ which has been attributed to the input of terrigenous nutrients linked to local heavy summer monsoonal rainfall. Therefore, measurements of Sumba coral density variability might be an economical and efficient way to reconstruct the variability of the local summer monsoon.

REFERENCES

Abram, N. J., M. K. Gagan, M. T. McCulloch, J. Chappell, and W. S. Hantoro (2003), Coral Reef Death During the 1997 Indian Ocean Dipole Linked to Indonesian Wildfires, *Science*, *301*, 952-955.

Abram, N. J. (2004), Multi-proxy coral reconstruction of Holocene climate and reef growth in the eastern Indian Ocean, PhD thesis thesis, The Australian National University, Canberra.

Abram, N. J., M. K. Gagan, Z. Y. Liu, W. S. Hantoro, M. T. McCulloch, and B. W. Suwargadi (2007), Seasonal characteristics of the Indian Ocean Dipole during the Holocene epoch, *Nature*, *445*(7125), 299-302.

Aharon, P. (1991), Recorders of reef environment histories: stable isotopes in coral, giant clams, and calcareous algae, *Coral Reefs*, *10*, 71-90.

Aissaoui, D. M., D. Buigues, and B. H. Purser (1986), Model of reef diagenesis: Mururoa Atoll French Polynesia, in *Reef diagenesis*, edited by J. H. Schroeder and B. H. Purser, pp. 27-52, Springer-Verlag.

Alibert, C., and M. T. McCulloch (1997), Strontium/calcium ratios in modern Porites corels from the great Barrier reef as a proxy for sea surface temperature: Calibration of the thermometer and monitoring of ENSO, *Paleoceanography*, *12*(3), 345-363.

Allison, N. (1996), Geochemical anomalies in coral skeletons and their possible implications for palaeoenvironmental analyses, *Marine Chemistry*, *55*(3-4), 367-379.

Allison, N., A. W. Tudhope, and A. E. Fallick (1996), Factors influencing the stable carbon and oxygen isotopic composition of Porites lutea coral skeletons from Phuket, South Thailand, *Coral Reefs*, *15*(1), 43-57.

Andersen, M. B., C. H. Stirling, E. K. Potter, and A. N. Halliday (2004), Toward epsilon levels of measurement precision on U-234/U-238 by using MC-ICPMS, *International Journal of Mass Spectrometry*, *237*(2-3), 107-118.

Andersen, M. B., C. H. Stirling, E.-K. Potter, A. N. Halliday, S. G. Blake, M. T. McCulloch, B. F. Ayling, and M. O'Leary (2008), High-precision U-series measurements of more than 500,000 year old fossil corals, *Earth and Planetary Science Letters*, *265*(1-2), 229-245.

Andrews, J. E., C. Portman, P. J. Rowe, M. R. Leeder, and J. D. Kramers (2007), Sub-orbital sea-level change in early MIS 5e: New evidence from the Gulf of Corinth, Greece, *Earth and Planetary Science Letters*, *259*(3-4), 457-468.

Ansell, T., C. J. C. Reason, and G. Meyers (2000), Variability in the tropical southeast Indian Ocean and links with southeast Australian winter rainfall., *Geophysical Research Letters*, *27*, 3977-3980.

Anthony, K. R. N. (1999), Coral suspension feeding on fine particulate matter, *Journal of Experimental Marine Biology and Ecology*, *232*(1), 85-106.

Anthony, K. R. N. (2000), Enhanced particle-feeding capacity of corals on turbid reefs (Great Barrier Reef, Australia), *Coral Reefs*, *19*(1), 59-67.

Antonioli, F., E. Bard, E.-K. Potter, S. Silenzi, and S. Improta (2004), 215-ka History of sea-level oscillations from marine and continental layers in Argentarola Cave speleothems (Italy), *Global and Planetary Change*, *43*(1-2), 57-78.

Ashok, K., Z. Y. Guan, and T. Yamagata (2001), Impact of the Indian Ocean Dipole on the relationship between the Indian monsoon rainfall and ENSO, *Geophysical Research Letters*, *28*(23), 4499-4502.

Ashok, K., Z. Y. Guan, and T. Yamagata (2003), Influence of the Indian Ocean Dipole on the Australian winter rainfall, *Geophysical Research Letters*, *30*(15), -.

Ashok, K., Z. Y. Guan, N. H. Saji, and T. Yamagata (2004), Individual and combined influences of ENSO and the Indian Ocean Dipole on the Indian summer monsoon, *Journal of Climate*, *17*(16), 3141-3155.

Ayling, B. F., M. T. McCulloch, M. K. Gagan, C. H. Stirling, M. B. Andersen, and S. G. Blake (2006), Sr/Ca and delta O-18 seasonality in a Porites coral from the MIS 9 (339-303 ka) interglacial, *Earth and Planetary Science Letters*, *248*(1-2), 462-475.

Bacastow, R. B., C. D. Keeling, T. J. Lueker, M. Wahlen, and W. G. Mook (1996), The C-13 Suess effect in the world surface oceans and its implications for oceanic uptake of CO2: Analysis of observations at Bermuda, *Global Biogeochemical Cycles*, *10*(2), 335-346.

Baquero-Bernal, A., M. Latif, and S. Legutke (2002), On dipole-like variability in the tropical Indian Ocean, *Journal of Climate*, *15*, 1358-1368.

Bar-Matthews, M., G. J. Wasserburg, and J. H. Chen (1993), Diagenesis of fossil coral skeletons: Correlation between trace elements, textures, and $^{234}U/^{238}U$, *Geochimica et Cosmochimica Acta*, *57*, 257-276.

Bard, E., B. Hamelin, and R. G. Fairbanks (1990), U-Th Ages Obtained by Mass-Spectrometry in Corals from Barbados - Sea-Level During the Past 130,000 Years, *Nature*, *346*(6283), 456-458.

Bard, E., R. G. Fairbanks, B. Hamelin, A. Zindler, and C. T. Hoang (1991), U-234 Anomalies in Corals Older Than 150,000 Years, *Geochimica Et Cosmochimica Acta*,

55(8), 2385-2390.

Bard, E., R. G. Fairbanks, and B. Hamelin (1992), How accurate are the U-Th ages obtained by Mass Spectrometry on coral terraces, in *Start of a glacial*, edited by G. J. Kukla and E. Went, p. 353, Springer-Verlag, Berlin.

Bard, E., M. Arnold, R. G. Fairbanks, and B. Hamelin (1993), ^{230}Th-^{234}U and ^{14}C ages obtained by mass spectrometry on corals, *Radiocarbon*, *35*, 191-199.

Bard, E., B. Hamelin, M. Arnold, L. Montaggioni, G. Cabioch, G. Faure, and F. Rougerie (1996a), Deglacial sea-level record from Tahiti corals and the timing of global meltwater discharge, *Nature*, *382*(6588), 241-244.

Bard, E., C. Jouannic, B. Hamelin, P. Pirazzoli, M. Arnold, G. Faure, P. Sumosusastro, and Syaefudin (1996b), Pleistocene sea levels and tectonic uplift based on dating of corals from Sumba Island, Indonesia, *Geophysical Research Letters*, *23*(12), 1473-1476.

Barnes, D. J., and J. M. Lough (1989), The nature of skeletal density banding in scleractinian corals: fine banding and seasonal patterns, *Journal of Experimental Marine Biology and Ecology*, *126*(2), 119-134.

Barnes, D. J., and R. B. Taylor (2001), On the nature and causes of luminescent lines and bands in coral skeletons, *Coral Reefs*, *19*, 221-230.

Barnes, D. J., and R. B. Taylor (2005), On the nature and causes of luminescent lines and bands in coral skeletons: II. Contribution of skeletal crystals, *Journal of Experimental Marine Biology and Ecology*, *322*(2), 135-142.

Bathurst, R. G. C. (1975), *Carbonate sediments and their diagenesis*, Elsevier, Amsterdam.

Beck, J. W., R. L. Edwards, E. Ito, F. W. Taylor, J. Recy, F. Rougerie, P. Joannot, and C. Henin (1992), Sea-Surface Temperature from Coral Skeletal Strontium Calcium Ratios, *Science*, *257*(5070), 644-647.

Beck, J. W., J. Recy, F. Taylor, R. L. Edwards, and G. Cabioch (1997), Abrupt changes in early Holocene tropical sea surface temperature derived from coral records, *Nature*, *385*(6618), 705-707.

Behera, S. K., and T. Yamagata (2003), Influence of the Indian Ocean Dipole on the southern oscillation, *Journal of the Meteorological Society of Japan*, *81*(1), 169-177.

Behera, S. K., J. J. Luo, S. Masson, S. A. Rao, H. Sakum, and T. Yamagata (2006), A CGCM study on the interaction between IOD and ENSO, *Journal of Climate*, *19*(9), 1688-1705.

Bender, M. L., R. G. Fairbanks, F. W. Taylor, R. K. Matthews, J. G. Goddard, and W. S.

Broecker (1979), Uranium-Series Dating of the Pleistocene Reef Tracts of Barbados, West-Indies, *Geological Society of America Bulletin*, *90*(6), 577-594.

Bjerknes, J. (1969), Atmospheric teleconnections from the equatorial Pacific, *Monthly Weather Review*, *97*, 163-172.

Black, D. E. (2002), CLIMATE VARIABILITY: Enhanced: The Rains May Be A-Comin', *Science*, *297*(5581), 528-529.

Black, E., J. Slingo, and K. R. Sperber (2003), An observational study of the relationship between excessively strong short rains in coastal East Africa and Indian Ocean SST, *Monthly Weather Review*, *131*(1), 74-94.

Bohm, F., A. Haase-Schramm, A. Eisenhauer, W. C. Dullo, M. M. Joachimski, H. Lehnert, and J. Reitner (2002), Evidence for preindustrial variations in the marine surface water carbonate system from coralline sponges, *Geochemistry Geophysics Geosystems*, *3*, -.

Boiseau, M., A. Juillet-Leclerc, F. Yiou, B. Salvat, P. J. Isdale, and M. Guillaume (1998), Atmospheric and oceanic evidences of El Niño-Southern Oscillation events in the south central Pacific Ocean from coral stable isotope records over the last 137 years, *Paleoceanography*, *13*, 671-685.

Boto, K., and P. J. Isdale (1985), Fluorescent bonds in massive corals result from terrestrial fulvic acid inputs to nearshore zone, *Nature*, *315*, 396-397.

Brachert, T. C., M. Reuter, T. Felis, K. F. Kroeger, G. Lohmann, A. Micheels, and C. Fassoulas (2006), Porites corals from Crete (Greece) open a window into Late Miocene (10Ma) seasonal and interannual climate variability, *Earth and Planetary Science Letters*, *245*(1-2), 81-94.

Brauer, A., J. R. M. Allen, J. Mingram, P. Dulski, S. Wulf, and B. Huntley (2007), Evidence for last interglacial chronology and environmental change from Southern Europe, *Proceedings of the National Academy of Sciences*, *104*(2), 450-455.

Bray, N. A., S. Hautala, J. Chong, and J. Pariwono (1996), Large-scale sea level, thermocline, and wind variations in the Indonesian throughflow region, *Journal of Geophysical Research-Oceans*, *101*(C5), 12239-12254.

Bray, N. A., S. E. Wijffels, J. C. Chong, M. Fieux, S. Hautala, G. Meyers, and W. M. L. Morawitz (1997), Characteristics of the Indo-Pacific throughflow in the eastern Indian Ocean, *Geophysical Research Letters*, *24*(21), 2569-2572.

Brijker, J. M., S. J. A. Jung, G. M. Ganssen, T. Bickert, and D. Kroon (2007), ENSO related decadal scale climate variability from the Indo-Pacific Warm Pool, *Earth and Planetary Science Letters*, *253*(1-2), 67-82.

Broecker, W. S. (1963), A Preliminary Evaluation of Uranium Series Inequilibrium as a Tool for Absolute Age Measurement on Marine Carbonates, *Journal of Geophysical Research*, *68*(9), 2817-&.

Broecker, W. S., and D. L. Thurber (1965), Uranium-Series Dating of Corals and Oolites from Bahaman and Florida Key Limestones, *Science*, *149*(3679), 58-&.

Buddemeier, R. W. (1974), Environmental controls over annual and lunar monthly cycles in hermatypic coral calcification, paper presented at 2nd Int. CoralReef Symp., Great Barrier Reef Committee, Brisbane, Australia.

Cane, M. A. (1986), El Niño, *Annual Review of Earth and Planetary Sciences*, *14*(1), 43-70.

Cane, M. A. (1998), CLIMATE CHANGE:A Role for the Tropical Pacific, *Science*, *282*(5386), 59-61.

Cane, M. A., and A. Clement (1999), A Role for the Tropical Pacific Coupled Ocean-Atmosphere System on Milankovitch and Millennial Timescales. Part II: Global Impacts, in *Mechanisms of Global Climate Change at Millennial Time Scales*, edited by P. U. Clark, et al., pp. 373-383, American Geophysical Union, Washington, DC.

Cane, M. A., and M. Evans (2000), CLIMATE VARIABILITY: Enhanced: Do the Tropics Rule?, *Science*, *290*(5494), 1107-1108.

Cane, M. A. (2005), The evolution of El Niño, past and future, *Earth and Planetary Science Letters*, *230*(3-4), 227-240.

Carricart-Ganivet, J. P. (2007), Annual density banding in massive coral skeletons: result of growth strategies to inhabit reefs with high microborers' activity?, *Marine Biology*, *153*(1), 1-5.

Carriquiry, J. D., M. J. Risk, and H. P. Schwarcz (1994), Stable-Isotope Geochemistry of Corals from Costa-Rica as Proxy Indicator of the El-Nino Southern Oscillation (Enso), *Geochimica Et Cosmochimica Acta*, *58*(1), 335-351.

Carton, J. A., B. S. Giese, and S. A. Grodsky (2005), Sea level rise and the warming of the oceans in the Simple Ocean Data Assimilation (SODA) ocean reanalysis, *J Geophys Res-Oceans*, *110*(C9), -.

Chakraborty, S. (2006), Coral records from the Northern Indian Ocean: Understanding the monsoon variability, *Journal of the Geological Society of India*, *68*(3), 395-405.

Chang, C. P., B. Wang, and N.-C. G. Lau (Eds.) (2004), *The Global Monsoon System: Research and Forecast. Report of the International Committee of the Third International Workshop on Monsoons (IWM-III), 2-6 November 2004, Hangzhou, China*, 512 pp., WORLD METEOROLOGICAL ORGANIZATION.

Chang, C. P., Z. Wang, J. McBride, and C. H. Liu (2005), Annual cycle of Southeast Asia - Maritime continent rainfall and the asymmetric monsoon transition, *Journal of Climate*, *18*(2), 287-301.

Charles, C. D., D. E. Hunter, and R. G. Fairbanks (1997), Interaction Between the ENSO and the Asian Monsoon in a Coral Record of Tropical Climate, *Science*, *277*(5328), 925-928.

Charles, C. D., K. Cobb, M. D. Moore, and R. G. Fairbanks (2003), Monsoon-tropical ocean interaction in a network of coral records spanning the 20th century, *Marine Geology*, *201*(1-3), 207.

Chen, J. H., R. L. Edwards, and G. J. Wasserburg (1986), U, U and Th in seawater., *Earth & Planetary Science Letters*, *80*(3-4), 241-251.

Chen, J. H., H. A. Curran, B. White, and G. J. Wasserburg (1991), Precise chronology of the last interglacial period: 234U-230Th data from fossil coral reefs in the Bahamas, *Geological Society of America Bulletin*, *103*(1), 82-97.

Cheng, H., R. L. Edwards, M. T. Murrell, and T. M. Benjamin (1998), Uranium-thorium-protactinium dating systematics, *Geochimica et Cosmochimica Acta*, *62*(21-22), 3437-3452.

Cheng, H., R. L. Edwards, J. Hoff, C. D. Gallup, D. A. Richards, and Y. Asmerom (2000), The half-lives of uranium-234 and thorium-230, *Chemical Geology*, *169*(1-2), 17-33.

Chong, J. C., J. Sprintall, S. Hautala, W. L. Morawitz, N. A. Bray, and W. Pandoe (2000), Shallow throughflow variability in the outflow straits of Indonesia, *Geophysical Research Letters*, *27*(1), 125-128.

Chung, C., and S. Nigam (1999), Asian summer Monsoon - ENSO feedback on the Cane-Zebiak model ENSO, *Journal of Climate*, *12*(9), 2787-2807.

Clark, C. O., P. J. Webster, and J. E. Cole (2003), Interdecadal variability of the relationship between the Indian Ocean Zonal Mode and East African Coastal Rainfall anomalies, *Journal of Climate*, *16*(3), 548.

Clarke, A. J., and X. Liu (1993), Observations and Dynamics of Semiannual and Annual Sea Levels near the Eastern Equatorial Indian-Ocean Boundary, *Journal of Physical Oceanography*, *23*(2), 386-399.

Clarke, A. J., and X. Liu (1994), Interannual Sea-Level in the Northern and Eastern Indian-Ocean, *Journal of Physical Oceanography*, *24*(6), 1224-1235.

Clemens, S., P. Wang, and W. Prell (2003), Monsoons and global linkages on Milankovitch and sub-Milankovitch time scales, *Marine Geology*, *201*(1-3), 1.

Clement, A. C., R. Seager, and M. A. Cane (2000), Suppression of El Niño during the mid-Holocene by changes in the Earth's orbit, *Paleoceanography*, *15*(6), 731-737.

Clement, A. C., M. A. Cane, and R. Seager (2001), An orbitally driven tropical source for abrupt climate change, *Journal of Climate*, *14*(11), 2369-2375.

CLIMAP Project Members (1976), The surface of the ice-age Earth, *Science*, *279*, 1341-1344.

Cobb, K. M., and C. D. Charles (2001), A central tropical Pacific coral demonstrates Pacific, Indian, and Atlantic decadal climate connections, *Geophysical Research Letters*, *28*(11), 2209-2212.

Cobb, K. M., C. D. Charles, H. Cheng, and R. L. Edwards (2003), El Niño/Southern Osillation and tropical Pacific climate during the last millennium, *Nature*, *424*, 271-276.

Cohen, A. L., and S. R. Hart (1997), The effect of colony topography on climate signals in coral skeleton, *Geochimica et Cosmochimica Acta*, *61*(18), 3905-3912.

Cole, J. E., and R. G. Fairbanks (1990), The Southern Oscillation recorded in the [delta]O of corals from Tarawa Atoll, *Paleoceanography*, *5*(5), 669-683.

Cole, J. E., R. G. Fairbanks, and G. T. Shen (1993), Recent Variability in the South Oscillation: Isotopic Results from a Tarawa Atoll Coral, *Science*, *260*, 1790-1793.

Coles, S. L., and P. L. Jokiel (1978), Synergistic effects of temperature, salinity and light on the hermatypic coral Montipora verrucosa, *Marine Biology*, *49*(3), 187-195.

Constanz, B. R. (1986), The primary surface area of corals and variations in their suscepibility to diagenesis, in *Reef Diagenesis*, edited by J. H. Schroeder and B. H. Purser, pp. 53-90, Springer-Verlag.

Correge, T. (2006), Sea surface temperature and salinity reconstruction from coral geochemical tracers, *Palaeogeography, Palaeoclimatology, Palaeoecology*, *232*(2-4), 408-428.

Crowley, T. J. (2000), CLIMAP SSTs re-revisited, *Climate Dynamics*, *16*, 241-255.

Cubash, U., and M. G. A. (2001), Projections of Future Climate Change. Chapter 9, IPCC Third Assessment Report.

Cutler, K. B., R. L. Edwards, F. W. Taylor, H. Cheng, J. Adkins, C. D. Gallup, P. M. Cutler, G. S. Burr, and A. L. Bloom (2003), Rapid sea-level fall and deep-ocean temperature change since the last interglacial period, *Earth and Planetary Science Letters*, *206*(3-4), 253-271.

D'Arrigo, R., R. Wilson, J. Palmer, P. Krusic, A. Curtis, J. Sakulich, S. Bijaksana, S.

Zulaikah, and L. O. Ngkoimani (2006), Monsoon drought over Java, Indonesia, during the past two centuries, *Geophysical Research Letters*, *33*(4).

da Silva, A., A. C. Young, and S. Levitus (1994), *Atlas of Surface Marine Data 1994, Volume 1: Algorithms and Procedures*, U.S. Department of Commerce, Washington, D.C.

de Villiers, S., G. T. Shen, and B. K. Nelson (1994), The Sr/Ca-temperature relationship in coralline aragonite: influence of variability in (Sr/Ca)seawater and skeletal growth parameters, *Geochimica et Cosmochimica Acta*, *58*(1), 197-208.

de Villiers, S., B. K. Nelson, and A. R. Chivas (1995), Biological controls on coral Sr/Ca and [delta]O reconstructions of sea surface temperatures, *Science*, *269*(5228), 1247-1249.

de Villiers, S. (1999), Seawater strontium and Sr/Ca variability in the Atlantic and Pacific oceans, *Earth and Planetary Science Letters*, *171*(4), 623-634.

Dodge, R. E., and G. W. Brass (1984), Skeletal Extension, Density and Calcification of the Reef Coral, Montastrea-Annularis - St-Croix, United-States Virgin Islands, *Bulletin of Marine Science*, *34*(2), 288-307.

Druffel, E. R. M., and L. M. Benavides (1986), Input of excess CO2 to the surface ocean based on 13C/12C ratios in a banded Jamaican sclerosponge, *Nature*, *321*(6065), 58-61.

Druffel, E. R. M. (1997), Geochemistry of corals: Proxies of past ocean chemistry, ocean circulation, and climate, *PNAS*, *94*(16), 8354-8361.

Dunbar, R. B., and G. M. Wellington (1981), Stable isotopes in a branching coral monitor seasonal temperature variation, *Nature*, *293*, 453-455.

Dunbar, R. B., G. M. Wellington, M. W. Colgan, and P. W. Glynn (1994), Eastern Pacific sea surface temperature since 1600 A.D.: the [delta]O record of climate variability in Galapagos corals, *Paleoceanography*, *9*(2), 291-315.

Dunbar, R. B., B. K. Linsley, and G. M. Wellington (1996), Eastern Pacific corals monitor El Niño/Southern Oscillation, precipitation, and sea surface temperature variability over the past three centuries, in *Climatic Variations and Forcing Mechanisms over the Last 2000 Years*, edited by P. D. Jones, et al., pp. 375-407, Springer, Berlin.

Dunbar, R. B., and J. E. Cole (1999), Annual records of tropical systems (ARTS). PAGES Workshop Report, Series 99-1, 72 pp.

Eakin, C. M., and A. G. Grottoli (2006), Paleo-climate changes and corals, in *Coral Reefs and Climate Change: Science and Management*, edited by J. Phinney, et al., AGU.

Edwards, R. L., J. H. Chen, and G. J. Wasserberg (1986/87), ^{238}U-$^{234}U^{230}Th$-^{232}Th systematics and the precise measurement of time over the past 500,000 years, *Earth and Planetary science Letters*, *81*, 175-192.

Edwards, R. L., J. H. Chen, T. L. Ku, and G. J. Wasserburg (1987), Precise timing of the last interglacial period from mass spectrometric determination of thorium-230 in corals., *Science*, *236*(4808), 1547-1553.

Edwards, R. L., H. Cheng, M. T. Murrell, and S. J. Goldstein (1997), Protactinium-231 Dating of Carbonates by Thermal Ionization Mass Spectrometry: Implications for Quaternary Climate Change, *Science*, *276*(5313), 782-786.

Edwards, R. L., C. D. Gallup, and H. Cheng (2003), Uranium-series dating of marine and lacustrine carbonates, in *Uranium-Series Geochemistry*, edited, pp. 363-405.

Enfield, D. B. (1989), El-Nino, Past and Present, *Reviews of Geophysics*, *27*(1), 159-187.

Enfield, D. B., and L. Cid (1991), Low-Frequency Changes in El-Nino Southern Oscillation, *Journal of Climate*, *4*(12), 1137-1146.

England, M. H., and F. Huang (2005), On the interannual variability of the Indonesian Throughflow and its linkage with ENSO, *Journal of Climate*, *18*(9), 1435-1444.

Enmar, R., M. Stein, M. Bar-Matthews, E. Sass, A. Katz, and B. Lazar (2000), Diagenesis in live corals from the Gulf of Aqaba. I. The effect on paleo-oceanography tracers, *Geochimica et Cosmochimica Acta*, *64*(18), 3123-3132.

Epstein, S., R. Buchsbaum, H. A. Lowenstam, and H. C. Urey (1953), Revised carbonate-water isotopic temperature scale., *Geological Society of America Bulletin*, *64*, 1315-1326.

Erez, J. (1978), Vital effect on stable-isotope composition seen in foraminifera and coral skeletons, *Nature*, *273*(5659), 199-202.

Esat, T. M., M. T. McCulloch, J. Chappell, B. Pillans, and A. Omura (1999), Rapid Fluctuations in Sea Level Recorded at Huon Peninsula During the Penultimate Deglaciation, *Science*, *283*(5399), 197-201.

Esat, T. M., and Y. Yokoyama (2006), Variability in the uranium isotopic composition of the oceans over glacial-interglacial timescales, *Geochimica et Cosmochimica Acta*, *70*(16), 4140-4150.

Evens, M. N., R. G. Fairbanks, and J. L. Rubenstone (1998), A proxy index of ENSO teleconnections, *Nature*, *394*, 732-733.

Fairbanks, R. G., and R. E. Dodge (1979), Annual periodicity of the O/O and C/C ratios

in the coral Montastrea annularis., *Geochimica et Cosmochimica Acta*, *43*(7), 1009-1020.

Fairbanks, R. G. (1989), A 17,000-Year Glacio-Eustatic Sea-Level Record - Influence of Glacial Melting Rates on the Younger Dryas Event and Deep-Ocean Circulation, *Nature*, *342*(6250), 637-642.

Fairbanks, R. G., M. N. Evans, J. L. Rubenstone, R. A. Mortlock, K. Broad, M. D. Moore, and C. D. Charles (1997), Evaluating climate indices and their geochemical proxies measured in corals, *Coral Reefs*, *16*, S93-S100.

Fairbanks, R. G., R. A. Mortlock, T. C. Chiu, L. Cao, A. Kaplan, T. P. Guilderson, T. W. Fairbanks, A. L. Bloom, P. M. Grootes, and M. J. Nadeau (2005), Radiocarbon calibration curve spanning 0 to 50,000 years BP based on paired Th-230/U-234/U-238 and C-14 dates on pristine corals, *Quaternary Science Reviews*, *24*(16-17), 1781-1796.

Felis, T., J. Patzold, Y. Loya, and G. Wefer (1998), Vertical water mass mixing and plankton blooms recorded in skeletal stable isotopes of a Red Sea coral, *Journal of Geophysical Research*, *103*, 30731-30739.

Felis, T., J. Patzold, Y. Loya, M. Fine, A. Nawar, and G. Wefer (2000), A coral oxygen isotope record from the northern Red Sea documenting NAO, ENSO, and North Pacific teleconnections on Middle East climate variability since the year 1750, *Paleoceanography*, *15*(6), 679-694.

Felis, T., G. Lohmann, H. Kuhnert, S. J. Lorenz, D. Scholz, J. Patzold, S. A. Al-Rousan, and S. M. Al-Moghrabi (2004), Increased seasonality in Middle East temperatures during the last interglacial period, *Nature*, *429*(6988), 164-168.

Feng, M., and G. Meyers (2003), Interannual variability in the tropical Indian Ocean: a two-year time-scale of Indian Ocean Dipole, *Deep Sea Research Part II: Topical Studies in Oceanography*, *50*(12-13), 2263-2284.

Fieux, M., C. Andrie, P. Delecluse, A. G. Ilahude, A. Kartavtseff, F. Mantisi, R. Molcard, and J. C. Swallow (1994a), Measurements within the Pacific-Indian oceans throughflow region, *Deep Sea Research Part I: Oceanographic Research Papers*, *41*(7), 1091-1130.

Fitch, T. J., and W. Hamilton (1974), Reply to "Comment on 'Plate Convergence, Transcurrent Fault, and Internal Deformation Adjacent to Southeast Asia and the Western Pacific'", *Journal of Geophysical Research*, *79*(32), 4982-4985.

Fitt, W., B. Brown, M. Warner, and R. Dunne (2001), Coral bleaching: interpretation of thermal tolerance limits and thermal thresholds in tropical corals, *Coral Reefs*, *20*(1), 51-65.

Fitt, W. K., F. K. McFarland, M. E. Warner, and G. C. Chilcoat (2000), Seasonal patterns of tissure biomass and densities of symbiotic dinoflagellates in reef corals and relation

to coral bleaching, *Limnology and Oceanography*, *45*(3), 677-685.

Fruijtier, C., T. Elliott, and W. Schlager (2000), Mass-spectrometric U-234-Th-230 ages from the Key Largo Formation, Florida Keys, United States: Constraints on diagenetic age disturbance, *Geological Society of America Bulletin*, *112*(2), 267-277.

Gagan, M. K., M. W. Sandstrom, and A. R. Chivas (1987), Restricted terrestrial carbon input to the continental shelf during Cyclone Winifred: implications for terrestrial runoff to the Great Barrier Reef Province, *Coral Reefs*, *6*(2), 113-119.

Gagan, M. K., A. R. Chivas, and P. J. Isdale (1994), High-resolution isotopic records from corals using ocean temperature and mass-spawning chronometers, *Earth & Planetary Science Letters*, *121*(3-4), 549-558.

Gagan, M. K., and A. R. Chivas (1995), Oxygen Isotopes in Western-Australian Coral Reveal Pinatubo Aerosol-Induced Cooling in the Western Pacific Warm Pool, *Geophysical Research Letters*, *22*(9), 1069-1072.

Gagan, M. K., A. R. Chivas, and P. J. Isdale (1996), Timing coral-based climatic histories using 13C enrichments driven by synchronized spawning, *Geology*, *24*(11), 1009-1012.

Gagan, M. K., L. K. Ayliffe, D. Hopley, J. A. Cali, G. E. Mortimer, J. Chappell, M. T. McCulloch, and M. J. Head (1998), Temperature and Surface-Ocean Water Balance of the Mid-Holocene Tropical Western Pacific, *Science*, *279*(5353), 1014-1018.

Gagan, M. K., L. K. Ayliffe, J. W. Beck, J. E. Cole, E. R. M. Druffel, R. B. Dunbar, and D. P. Schrag (2000), New views of tropical paleoclimates from corals, *Quaternary Science Reviews*, *19*(1-5), 45-64.

Gagan, M. K., L. K. Ayliffe, B. N. Opdyke, D. Hopley, H. Scott-Gagan, and J. Cowley (2002), Coral oxygen isotope evidence for recent groundwater fluxes to the Australian Great Barrier Reef, *Geophysical Research Letters*, *29*(20).

Gagan, M. K., E. J. Hendy, S. G. Haberle, and W. S. Hantoro (2004), Post-glacial evolution of the Indo-Pacific Warm Pool and El Niño-Southern Oscillation, *Quaternary International*, *118-19*, 127-143.

Gallup, C. D., R. L. Edwards, and R. G. Johnson (1994), The timing of high sea levels over the past 200,000 years, *Science*, *263*, 796-800.

Gallup, C. D., H. Cheng, F. W. Taylor, and R. L. Edwards (2002), Direct determination of the timing of sea level change during termination II, *Science*, *295*(5553), 310-313.

Gallup, C. D., D. M. Olson, R. L. Edwards, L. M. Gruhn, A. Winter, and F. W. Taylor (2006), Sr/Ca-Sea surface temperature calibration in the branching Caribbean coral Acropora palmata, *Geophysical Research Letters*, *33*(3), -.

Giese, B. S., S. C. Urizar, and N. S. Fuckar (2002), Southern Hemisphere Origins of the 1976 Climate Shift, *Geophysical Research Letters*, *29*(2), -.

Gill, I. P., J. A. D. Dickson, and D. K. Hubbard (2006), Daily banding in corals: Implications for paleoclimatic reconstruction and skeletonization, *Journal of Sedimentary Research*, *76*(3-4), 683-688.

Glynn, P. W., and L. D'Croz (1990), Experimental evidence for high temperature stress as the cause of El Niño-coincident coral mortality, *Coral Reefs*, *8*(4), 181-191.

Goni, M. A., K. C. Ruttenberg, and T. I. Eglinton (1997), Sources and contribution of terrigenous organic carbon to surface sediments in the Gulf of Mexico, *Nature*, *389*(6648), 275-278.

Gordon, A. L., and R. A. Fine (1996), Pathways of water between the Pacific and Indian oceans in the Indonesian seas, *Nature*, *379*, 379.

Gordon, A. L., R. D. Susanto, and A. Ffield (1999), Throughflow within Makassar Strait, *Geophysical Research Letters*, *26*(21), 3325-3328.

Gordon, A. L., R. D. Susanto, and K. Vranes (2003a), Cool Indonesian throughflow as a consequence of restricted surface layer flow, *Nature*, *425*, 824-828.

Gordon, A. L. (2005), Oceanography of the Indonesian Seas and their Throughflow, *Oceanography*, *18*(4), 14-27.

Graham, N. E. (1995), Simulation of Recent Global Temperature Trends, *Science*, *267*(5198), 666-671.

Grigg, R. W. (1997), Paleoceanography of coral reefs in the Hawaiian-Emperor Chain - revisited, *Coral Reefs*, *16*, S33-S38.

Grottoli, A. G., L. J. Rodrigues, and J. E. Palardy (2006), Heterotrophic plasticity and resilience in bleached corals, *Nature*, *440*(7088), 1186-1189.

Grottoli, A. G., and C. M. Eakin (2007), A review of modern coral delta O-18 and Delta C-14 proxy records, *Earth-Science Reviews*, *81*(1-2), 67-91.

Gruber, N., C. D. Keeling, R. B. Bacastow, P. R. Guenther, T. J. Lueker, M. Wahlen, H. A. J. Meijer, W. G. Mook, and T. F. Stocker (1999), Spatiotemporal patterns of carbon-13 in the global surface oceans and the oceanic Suess effect, *Global Biogeochemical Cycles*, *13*(2), 307-335.

Guan, Z. Y., and T. Yamagata (2003), The unusual summer of 1994 in East Asia: IOD teleconnections, *Geophysical Research Letters*, *30*(10), -.

Guilderson, T. P., R. G. Fairbanks, and J. L. Rubenstone (1994a), Tropical temperature variations since 20,000 years ago: Modulating interhemispheric climate change, *Science*,

263(5147), 663-665.

Guilderson, T. P., and D. P. Schrag (1998), Abrupt shift in subsurface temperatures in the Tropical Pacific associated with changes in El Niño, *Science*, *281*(5374), 240-243.

Guilderson, T. P., and D. P. Schrag (1999), Reliability of coral isotope records from the western Pacific warm pool: A comparison using age-optimized records, *Paleoceanography*, *14*(4), 457-464.

Guilderson, T. P., R. G. Fairbanks, and J. L. Rubenstone (2001), Tropical Atlantic coral oxygen isotopes: glacial-interglacial sea surface temperatures and climate change, *Marine Geology*, *172*(1-2), 75-89.

Gupta, S. K., and H. A. Polach (1985), Radiocarbon dating practices at ANU, ANU, Canberra.

Hamelin, B., E. Bard, A. Zindler, and R. G. Fairbanks (1991a), 234U/238U mass spectrometry of corals: How accurate is the U-Th age of the last interglacial period?, *Earth & Planetary Science Letters*, *106*, 169-180.

Hansen, J., and S. Lebedeff (1987), Global surface air temperatures: update through 1987, *Geophysical Research Letters*, *15*(4), 323-326.

Hart, S. R., and A. L. Cohen (1996), An ion probe study of annual cycles of Sr/Ca and other trace elements in corals, *Geochimica et Cosmochimica Acta*, *60*(16), 3075-3084.

Hastenrath, S. (1987), Predictability of Java Monsoon Rainfall Anomalies - a Case-Study, *Journal of Climate and Applied Meteorology*, *26*(1), 133-141.

Hastenrath, S. (2003), Comments on "Influence of the Indian Ocean dipole on the southern oscillation" by S.K. BEHERA et al. (J. Meteor. Soc. Japan, vol. 81, 169-177), *Journal of the Meteorological Society of Japan*, *81*(6), 1505-1506.

Hautala, S. L., J. Sprintall, J. T. Potemra, J. C. Chong, W. Pandoe, N. Bray, and A. G. Ilahude (2001), Velocity structure and transport of the Indonesian Throughflow in the major straits restricting flow into the Indian Ocean, *Journal of Geophysical Research-Oceans*, *106*(C9), 19527-19546.

Haylock, M., and J. McBride (2001), Spatial coherence and predictability of Indonesian wet season rainfall, *Journal of Climate*, *14*(18), 3882-3887.

Henderson, G. M., and A. S. Cohen (1993), 234U/238U ratios and 230Th ages for Hateruma Atoll corals: implications for coral diagenesis and seawater 234U/238U ratios, *Earth & Planetary Science Letters*, *115*, 65-73.

Henderson, G. M., N. C. Slowey, and M. Q. Fleisher (2001), U-Th dating of carbonate platform and slope sediments, *Geochimica et Cosmochimica Acta*, *65*(16), 2757-2770.

Henderson, G. M. (2002), Seawater (234U/238U) during the last 800 thousand years, *Earth and Planetary Science Letters*, *199*(1-2), 97-110.

Hendon, H. H. (2003), Indonesian rainfall variability: Impacts of ENSO and local air-sea interaction, *Journal of Climate*, *16*(11), 1775-1790.

Hendy, E. J., M. K. Gagan, C. A. Alibert, M. T. McCulloch, J. M. Lough, and P. J. Isdale (2002), Abrupt Decrease in Tropical Pacific Sea Surface Salinity at End of Little Ice Age, *Science*, *295*(5559), 1511-1514.

Hendy, E. J., M. K. Gagan, and J. M. Lough (2003), Chronological control of coral records using luminescent lines and evidence for non-stationary ENSO teleconnections in northern Australia, *The Holocene*, *13*(2), 187-199.

Hoerling, M. P., J. W. Hurrell, and T. Xu (2001a), Tropical Origins for Recent North Atlantic Climate Change, *Science*, *292*(5514), 90-92.

Hoerling, M. P., J. S. Whitaker, A. Kumar, and W. Q. Wang (2001b), The midlatitude warming during 1998-2000, *Geophysical Research Letters*, *28*(5), 755-758.

Holland, G. J. (1986), Interannual Variability of the Australian Summer Monsoon at Darwin - 1952-82, *Monthly Weather Review*, *114*(3), 594-604.

Huang, B. Y., and V. M. Mehta (2004), Response of the Indo-Pacific warm pool to interannual variations in net atmospheric freshwater, *J Geophys Res-Oceans*, *109*(C6), -.

Hubbard, J. A. E. B., and P. K. Swart (1982), Sequence and style in scleractinian coral preservation in reefs and associated facies, *Palaeogeogr. Palaeoclimatol. Palaeoecol.*, *37*, 165-219.

Hughen, K. A., D. P. Schrag, and S. B. Jacobsen (1999a), El Niño during the last interglacial period recorded by a fossil coral from Indonesia, *Geophysical Research Letters*, *26*(20), 3129-3132.

Hughen, K. A., D. P. Schrag, S. B. Jacobsen, and W. Hantoro (1999b), El Niño during the last interglacial period recorded by a fossil coral from Indonesia, *Geophysical Research Letters*, *26*(20), 3129-3132.

Hughen, K. A., M. G. L. Baillie, E. Bard, J. W. Beck, C. J. H. Bertrand, P. G. Blackwell, C. E. Buck, G. S. Burr, K. B. Cutler, P. E. Damon, R. L. Edwards, R. G. Fairbanks, M. Friedrich, T. P. Guilderson, B. Kromer, G. McCormac, S. Manning, C. B. Ramsey, P. J. Reimer, R. W. Reimer, S. Remmele, J. R. Southon, M. Stuiver, S. Talamo, F. W. Taylor, J. van der Plicht, and C. E. Weyhenmeyer (2004), Marine04 marine radiocarbon age calibration, 0-26 cal kyr BP, *Radiocarbon*, *46*(3), 1059-1086.

Hung, C. W., X. D. Liu, and M. Yanai (2004), Symmetry and asymmetry of the Asian and Australian summer monsoons, *Journal of Climate*, *17*(12), 2413-2426.

IPCC (2007), IPCC Fourth Assessment Report: Climate Change 2007.

Isdale, P. J. (1984), Fluorescent bands in massive corals record centuries of coastal rainfall, *Nature*, *310*, 578-579.

Isdale, P. J., B. J. Stewart, K. S. Tickle, and J. M. Lough (1998), Plaeohydrological variation in a tropical river catchment: a reconstruction using fluorescent bands in corals of the Great Barrier Reef, Australia, *The Holocene*, *8*(1), 1-8.

James, N. P. (1974), Diagenesis of scleractinian corals in the subaerial vadose environment, *Journal of Paleontology*, *48*, 785-799.

Jokiel, P. L., and S. L. Coles (1977), Effects of temperature on the mortality and growth of Hawaiian reef corals, *Marine Biology*, *43*(3), 201-208.

Jokiel, P. L., and S. L. Coles (1990), Response of Hawaiian and other Indo-Pacific reef corals to elevated temperature, *Coral Reefs*, *8*(4), 155-162.

Jones, P. D., and M. E. Mann (2004), Climate over past millennia, *Reviews of Geophysics*, *42*(2), -.

Juillet-Leclerc, A., S. Thiria, P. Naveau, T. Delcroix, N. Le Bec, D. Blamart, and T. Correge (2006), SPCZ migration and ENSO events during the 20th century as revealed by climate proxies from a Fiji coral, *Geophysical Research Letters*, *33*(17).

Kaplan, A., M. A. Cane, Y. Kushnir, A. C. Clement, M. B. Blumenthal, and B. Rajagopalan (1998), Analyses of global sea surface temperature 1856-1991, *J Geophys Res-Oceans*, *103*(C9), 18567-18589.

Keenan, T. D., S. A. Rutledge, R. E. Carbone, J. W. Wilson, T. Takahashi, M. W. Moncrieff, G. J. Holland, N. J. Tapper, C. M. R. Platt, J. M. Hacker, K. Saito, and J. Crook (2000), The Maritime Continent Thunderstorm Experiment (MCTEX): overview and early results., *Bulletin of the American Meterological Society*, *81*(10), 2433-2455.

Kerr, R. A. (2001), The Tropics Return to the Climate System, *Science*, *292*(5517), 660-661.

Kilbourne, K. H., T. M. Quinn, and F. W. Taylor (2004), A fossil coral perspective on western tropical Pacific climate similar to 350 ka, *Paleoceanography*, *19*(1).

Kirtman, B. P., and J. Shukla (2000), Influence of the Indian summer monsoon on ENSO, *Quarterly Journal of the Royal Meteorological Society*, *126*(562), 213-239.

Klein, J., J. C. Lerman, P. E. Damon, and E. K. Ralph (1982), Calibration of Radiocarbon-Dates - Tables Based on the Consensus Data of the Workshop on Calibrating the Radiocarbon Time Scale, *Radiocarbon*, *24*(2), 103-150.

Knutson, D. W., R. W. Buddemeier, and S. V. Smith (1972), Coral chronologies:

seasonal growth bands in reef corals, *Science*, *177*, 270-272.

Kortzinger, A., P. D. Quay, and R. E. Sonnerup (2003), Relationship between anthropogenic CO2 and the C-13 suess effect in the North Atlantic Ocean, *Global Biogeochemical Cycles*, *17*(1), -.

Ku, T. L., K. G. Knauss, and G. G. Mathieu (1977), Uranium in Open Ocean - Concentration and Isotopic Composition, *Deep-Sea Research*, *24*(11), 1005-1017.

Ku, T. L., M. Ivanovich, and S. Luo (1990), U-Series Dating of Last Interglacial High Sea Stands - Barbados Revisited, *Quaternary Research*, *33*(2), 129-147.

Kumar, K. K., B. Rajagopalan, and M. A. Cane (1999), On the Weakening Relationship Between the Indian Monsoon and ENSO, *Science*, *284*(5423), 2156-2159.

Laskar, J., P. Robutel, F. Joutel, M. Gastineau, A. C. M. Correia, and B. Levrard (2004), A long-term numerical solution for the insolation quantities of the Earth, *Astronomy & Astrophysics*, *428*(1), 261-285.

Lea, D. W., D. K. Pak, and H. J. Spero (2000), Climate Impact of Late Quaternary Equatorial Pacific Sea Surface Temperature Variations, *Science*, *289*(5485), 1719-1724.

Lea, D. W. (2002), PALEOCLIMATE: Enhanced: The Glacial Tropical Pacific--Not Just a West Side Story, *Science*, *297*(5579), 202-203.

Lea, D. W., P. A. Martin, D. K. Pak, and H. J. Spero (2002), Reconstructing a 350 ky history of sea level using planktonic Mg/Ca and oxygen isotope records from a Cocos Ridge core, *Quaternary Science Reviews*, *21*(1-3), 283-293.

Lea, D. W., D. K. Pak, C. L. Belanger, H. J. Spero, M. A. Hall, and N. J. Shackleton (2006), Paleoclimate history of Galapagos surface waters over the last 135,000 yr, *Quaternary Science Reviews*, *25*(11-12), 1152-1167.

Leder, J. J., P. K. Swart, A. M. Szmant, and R. E. Dodge (1996), The origin of variations in the isotopic record of scleractinian corals: I. Oxygen, *Geochimica et Cosmochimica Acta*, *60*(15), 2857-2870.

Li, T., B. Wang, C. P. Chang, and Y. S. Zhang (2003), A theory for the Indian Ocean dipole-zonal mode, *Journal of the Atmospheric Sciences*, *60*(17), 2119-2135.

Linsley, B. K., R. B. Dunbar, G. M. Wellington, and D. A. Mucciarone (1994), A coral-based reconstruction of Intertropical Convergence Zone variability over Central America since 1707, *Journal of Geophysical Research*, *99*, 9977-9994.

Linsley, B. K., R. G. Messier, and R. B. Dunbar (1999), Assessing between-colony oxygen isotope variability in the coral Porites lobata at Clipperton Atoll, *Coral Reefs*, *18*(1), 13-27.

Liu, Z., J. Kutzbach, and L. Wu (2000), Modeling Climate Shift of El Niño Variability in the Holocene, *Geophysical Research Letters*, *27*(15), 2265-2268.

Loschnigg, J., G. A. Meehl, P. J. Webster, J. M. Arblaster, and G. P. Compo (2003), The Asian monsoon, the tropospheric biennial oscillation, and the Indian Ocean zonal mode in the NCAR CSM, *Journal of Climate*, *16*(11), 1617-1642.

Lough, J. M., and D. J. Barnes (1990), Intra-annual timing of density band formation of Porites coral from the central Great Barrier Reef, *Journal of Experimental Marine Biology and Ecology*, *135*, 35-57.

Lough, J. M. (1991), Rainfall variations in Queensland, Australia: 1891-1986, *International journal of Climatology*, *11*, 745-768.

Lough, J. M., and D. J. Barnes (1992), Comparisons of Skeletal Density Variations in Porites from the Central Great-Barrier-Reef, *Journal of Experimental Marine Biology and Ecology*, *155*(1), 1-25.

Lough, J. M. (1997), Regional indices of climate variation: temperature and rainfall in Queensland, Australia., *International journal of Climatology*, *17*, 55-66.

Lough, J. M., and D. J. Barnes (1997), Several centuries of variation in skeletal extension, density and calcification in massive Porites colonies from the Great Barrier Reef: A proxy for seawater temperature and a background of variability against which to identify unnatural change, *Journal of Experimental Marine Biology and Ecology*, *211*(1), 29-67.

Lough, J. M., and D. J. Barnes (2000), Environmental controls on growth of the massive coral Porites, *Journal of Experimental Marine Biology and Ecology*, *245*(2), 225-243.

Ludwig, K. R., B. J. Szabo, J. G. Moore, and K. R. Simmons (1991), Crustal Subsidence Rate Off Hawaii Determined from U-234/U-238 Ages of Drowned Coral Reefs, *Geology*, *19*(2), 171-174.

Luo, X., M. Rehkamper, D.-C. Lee, and A. N. Halliday (1997), High precision 230Th/232Th and 234U/238U measurements using energyfiltered ICP magnetic sector multiple collector mass spectrometry, *International Journal of Mass Spectrometry and Ion Processes*, *171*(1-3), 105-117.

Lyle, M. W., F. G. Prahl, and M. A. Sparrow (1992), Upwelling and productivity changes inferred from a temperature record in the central equatorial Pacific, *Nature*, *355*(6363), 812-815.

Martin, G. D., B. H. Wilkinson, and K. C. Lohmann (1986), The role of skeletal porosity in aragonite neomorphism: Strombus and Montastrea from the Pleistocene Key Largo Limestone, Florida, *Journal of Sedimentary Petrology*, *56*, 194-203.

Martinson, D. G., N. G. Pisias, J. D. Hays, J. Imbrie, J. Moore, Theodore C., and N. J. Shackleton (1987), Age dating and the orbital theory of the ice ages: Development of a high-resolution 0 to 300,000-year chronostratigraphy*1, *Quaternary Research*, *27*(1), 1-29.

Masumoto, Y., and T. Yamagata (1993), Simulated Seasonal Circulation in the Indonesian Seas, *Journal of Geophysical Research-Oceans*, *98*(C7), 12501-12509.

Masumoto, Y., and T. Yamagata (1996), Seasonal variations of the Indonesian throughflow in a general ocean circulation model, *Journal of Geophysical Research-Oceans*, *101*(C5), 12287-12293.

McBride, J. (1998), Indonesia, Papua New Guinea, and tropical Australia, in *The Southern Hemisphere summer monsoon*, edited, pp. 89-99, Amer. Meteor. Soc.

McBride, J. L., M. R. Haylock, and N. Nichols (2003), Relationships between the maritime continent heat source and the El Niño-Southern Oscillation phenomenon, *Journal of Climate*, *16*(17), 2905-2914.

McClean, J. L., D. P. Ivanova, and J. Sprintall (2005), Remote origins of interannual variability in the Indonesian Throughflow region from data and a global Parallel Ocean Program simulation, *Journal of Geophysical Research-Oceans*, *110*(C10), -.

McConnaughey, T. (1989), C and O isotopic disequilibrium in biological carbonates: I. Patterns, *Geochimica et Cosmochimica Acta*, *53*(1), 151-162.

McConnaughey, T. A. (2003), Sub-equilibrium oxygen-18 and carbon-13 levels in biological carbonates: carbonate and kinetic models, *Coral Reefs*, *22*(4), 316-327.

McCormac, F. G., A. G. Hogg, P. G. Blackwell, C. E. Buck, T. F. G. Higham, and P. J. Reimer (2004), SHCal04 Southern Hemisphere calibration, 0-11.0 cal kyr BP, *Radiocarbon*, *46*(3), 1087-1092.

McCrea, J. M. (1950), On the isotopic chemistry of carbonates and a paleotemperature scale, *Journal of Chemical Physics*, *18*, 849-857.

McCulloch, M., G. Mortimer, T. Esat, X. Li, B. Pillans, and J. Chappell (1996), High resolution windows into early Holocene climate: coral records from the Huon Peninsula, *Earth and Planetary Science Letters*, *138*(1-4), 169-178.

McCulloch, M. T., M. K. Gagan, G. E. Mortimer, A. R. Chivas, and P. J. Isdale (1994), A high-resolution Sr/Ca and [delta]O coral record from the Great Barrier Reef, Australia, and the 1982-1983 El Niño, *Geochimica et Cosmochimica Acta*, *58*(12), 2747-2754.

McCulloch, M. T., A. W. Tudhope, T. M. Esat, G. E. Mortimer, J. Chappell, B. Pillans, A. R. Chivas, and A. Omura (1999), Coral Record of Equatorial Sea-Surface Temperatures During the Penultimate Deglaciation at Huon Peninsula, *Science*, *283*(5399), 202-204.

McCulloch, M. T., and G. E. Mortimer (2008), Applications of the U-238-Th-230 decay series to dating of fossil and modern corals using MC-ICPMS, *Aust. J. Earth Sci.*, *55*(6-7), 955-965.

McGlone, M. S., A. P. Kershaw, and V. Markgraf (1992), El Niño/Southern Oscillation and climatic variability in Australasian and South American paleoenvironmental records, in *El Niño: Historical and paleoclimatic aspects of the Southern Oscillation*, edited by H. F. Diaz and V. Markgraf, pp. 435-462, Cambridge University Press, Cambridge.

McGregor, H. V., and M. K. Gagan (2003), Diagenesis and geochemistry of Porites corals from Papua New Guinea: Implications for paleoclimate reconstruction, *Geochimica Et Cosmochimica Acta*, *67*(12), 2147-2156.

McGregor, H. V., and M. K. Gagan (2004), Western Pacific coral delta O-18 records of anomalous Holocene variability in the El Niño-Southern Oscillation, *Geophysical Research Letters*, *31*(11), -.

McPhaden, M. J., and D. X. Zhang (2002), Slowdown of the meridional overturning circulation in the upper Pacific Ocean, *Nature*, *415*(6872), 603-608.

Meehl, G. A. (1987), The Annual Cycle and Interannual Variability in the Tropical Pacific and Indian-Ocean Regions, *Monthly Weather Review*, *115*(1), 27-50.

Meehl, G. A. (1997), The south Asian monsoon and the tropospheric biennial oscillation, *Journal of Climate*, *10*(8), 1921-1943.

Meehl, G. A., and J. M. Arblaster (2002), The tropospheric biennial oscillation and Asian-Australian monsoon rainfall, *Journal of Climate*, *15*(7), 722-744.

Meehl, G. A., W. M. Washington, C. M. Ammann, J. M. Arblaster, T. M. L. Wigley, and C. Tebaldi (2004), Combinations of natural and anthropogenic forcings in twentieth-century climate, *Journal of Climate*, *17*(19), 3721-3727.

Meyers, G., R. J. Bailey, and A. P. Worby (1995), Geostrophic Transport of Indonesian Throughflow, *Deep-Sea Research Part I-Oceanographic Research Papers*, *42*(7), 1163-1174.

Meyers, G. (1996), Variation of Indonesian throughflow and the El Niño Southern Oscillation, *Journal of Geophysical Research-Oceans*, *101*(C5), 12255-12263.

Michida, Y., and H. Yoritaka (1996), Surface currents in the area of the Indo-Pacific throughflow and in the tropical Indian Ocean observed with surface drifters, *Journal of Geophysical Research-Oceans*, *101*(C5), 12475-12482.

Min, G. R., R. L. Edwards, F. W. Taylor, J. Recy, C. D. Gallup, and J. W. Beck (1995), Annual cycles of U/Ca in coral skeletons and U/Ca thermometry, *Geochimica et Cosmochimica Acta*, *59*(10), 2025-2042.

Molcard, R., M. Fieux, and F. Syamsudin (2001a), The throughflow with Ombai Strait, *Deep Sea Research Part I*, *48*, 1237-1253.

Molcard, R., M. Fieux, and F. Syamsudin (2001b), The throughflow within Ombai Strait, *Deep-Sea Research Part I-Oceanographic Research Papers*, *48*(5), 1237-1253.

Moore, W. S. (1967), Amazon and Mississippi River Concentrations of Uranium Thorium and Radium Isotopes, *Earth and Planetary Science Letters*, *2*(3), 231-&.

Morimoto, M., H. Kayanne, O. Abe, and M. T. McCulloch (2007), Intensified mid-Holocene Asian monsoon recorded in corals from Kikai Island, subtropical northwestern Pacific, *Quaternary Research*, *67*(2), 204-214.

Moy, C. M., G. O. Seltzer, D. T. Rodbell, and D. M. Anderson (2002), Variability of El Niño /Southern Oscillation activity at millennial timescales during the Holocene epoch, *Nature*, *420*, 162-165.

Muhs, D. R. (2002), Evidence for the Timing and Duration of the Last Interglacial Period from High-Precision Uranium-Series Ages of Corals on Tectonically Stable Coastlines, *Quaternary Research*, *58*(1), 36-40.

Muller, A., M. K. Gagan, and M. T. McCulloch (2001), Early marine diagenesis in corals and geochemical consequences for paleoceanographic reconstructions, *Geophysical Research Letters*, *28*(23), 4471-4474.

Muller, A., M. K. Gagan, and J. M. Lough (2004), Effect of early marine diagenesis on coral reconstructions of surface-ocean C-13/C-12 and carbonate saturation state, *Global Biogeochemical Cycles*, *18*(1), -.

Murray, S. P., and D. Arief (1988), Throughflow into the Indian Ocean through the Lombok Strait, January 1985-January 1986, *Nature*, *333*, 444-447.

Murtugudde, R., A. J. Busalacchi, and J. Beauchamp (1998), Seasonal-to-interannual effects of the Indonesian throughflow on the tropical Indo-Pacific Basin, *Journal of Geophysical Research-Oceans*, *103*(C10), 21425-21441.

Murtugudde, R., J. P. McCreary Jr., and A. J. Busalacchi (2000), Oceanic processes associated with anomalous events in the Indian Ocean with relevance to 1997?998, *Journal of Geophysical Research*, *105*(C2), 3295?3306.

Muscatine, L., L. R. McCloskey, and R. E. Marian (1981), Estimating the daily contribution of carbon from zooxanthellae to coral animal respiration., *Limnology and Oceanography*, *26*, 601-611.

Nicholls, N. (1981), Air-Sea Interaction and the Possibility of Long-Range Weather Prediction in the Indonesian Archipelago, *Monthly Weather Review*, *109*(12), 2435-2443.

Nicholls, N. (1984), The Southern Oscillation and Indonesian Sea-Surface Temperature, *Monthly Weather Review*, *112*(3), 424-432.

Nicholls, N. (1989), Sea surface temperatures and Australian winter rainfall, *Journal of Climate*, *2*, 965-973.

O'Leary, M. H. (1981), Carbon isotope fractionation in plants, *Phytochemistry*, *20*(4), 553-567.

Paillard, D., L. D. Labeyrie, and F. Yiou (1996), MacIntosh program performs time-seies analysis, *EOS, Transactions, American Geophysical Union*, *77*, 379.

Parthasarathy, B., A. A. Munot, and D. R. Kothawale (1995), Monthly and seasonal rainfall series for All-India homogeneous regions and meteorological subdivisions: 1871-1994, Pune, India.

Pelejero, C., J. O. Grimalt, S. Heilig, M. Kienast, and L. Wang (1999), High-resolution U^K37 temperature reconstructions in the South China Sea over the past 220 kyr, *Paleogeography*, *14*(2), 224.

Pfeiffer, M., W. C. Dullo, and A. Eisenhauer (2004), Variability of the Intertropical Convergence Zone recorded in coral isotopic records from the central Indian Ocean (Chagos Archipelago), *Quaternary Research*, *61*(3), 245-255.

Philander, S. G. H. (1990), *El Niño, La Nino, and the southern oscillation*, 293 pp., Academic Press, Inc., San Diego.

Phillips, H. E., S. E. Wijffels, and M. Feng (2005), Interannual variability in the freshwater content of the Indonesian-Australian Basin, *Geophysical Research Letters*, *32*(3), -.

Pierrehumbert, R. T. (2000), Climate change and the tropical Pacific: The sleeping dragon wakes, *PNAS*, *97*(4), 1355-1358.

Pirazzoli, P. A., U. Radtke, W. S. Hantoro, C. Jouannic, C. T. Hoang, C. Causse, and M. Borel Best (1991), Quaternary raised coral-reef terraces on Sumba Island, Indonesia, *Science*, *252*, 1834-1836.

Pirazzoli, P. A., U. Radtke, W. S. Hantoro, C. Jouannic, C. T. Hoang, C. Causse, and M. Borel Best (1993), A one million-year-long sequence of marine terraces on Sumba Island, Indonesia, *Marine Geology*, *109*, 221-236.

Porter, J. W., W. K. Fitt, H. J. Spero, C. S. Rogers, and M. W. White (1989), Bleaching in Reef Corals: Physiological and Stable Isotopic Responses, *PNAS*, *86*(23), 9342-9346.

Potemra, J. T., R. Lukas, and G. T. Mitchum (1997), Large-scale estimation of transport from the Pacific to the Indian Ocean, *Journal of Geophysical Research-Oceans*,

102(C13), 27795-27812.

Potemra, J. T., S. L. Hautala, J. Sprintall, and W. Pandoe (2002), Interaction between the Indonesian Seas and the Indian Ocean in observations and numerical models, *Journal of Physical Oceanography*, *32*(6), 1838-1854.

Potemra, J. T., J. Sprintall, S. L. Hautala, and W. Pandoe (2003), Observed estimates of convergence in the Savu Sea, Indonesia, *Journal of Geophysical Research-Oceans*, *108*(C1), -.

Potter, E.-K., T. M. Esat, G. Schellmann, U. Radtke, K. Lambeck, and M. T. McCulloch (2004), Suborbital-period sea-level oscillations during marine isotope substages 5a and 5c, *Earth and Planetary Science Letters*, *225*(1-2), 191-204.

Potter, E. K., C. H. Stirling, M. B. Andersen, and A. N. Halliday (2005), High precision Faraday collector MC-ICPMS thorium isotope ratio determination, *International Journal of Mass Spectrometry*, *247*(1-3), 10-17.

Potthast, I. (1992), Short-term progressive early diagenesis in density bands of recent corals: *Porites* colonies, Mauritius Island, Indian Ocean, *Facies*, *27*, 105-115.

Purser, B. H., and J. H. Schroeder (1986), The diagenesis of reefs: A brief review of our present understanding, in *Reef diagenesis*, edited by J. H. Schroeder and B. H. Purser, pp. 424-446, Springer-Verlag.

Qiu, B., M. Mao, and Y. Kashino (1999), Intraseasonal variability in the indo-pacific throughflow and the regions surrounding the Indonesian seas, *Journal of Physical Oceanography*, *29*(7), 1599-1618.

Quadfasel, D., and G. Cresswell (1992), A note on the seasonal variability of the South Java Current, *Journal of Geophysical Research-Oceans*, *97*(C3), 3685-3688.

Quay, P. D., B. Tilbrook, and C. S. Wong (1992), Oceanic uptake of fossil-fuel CO2: Carbon-13 evidence, *Science*, *256*, 74-79.

Quinn, T. M., T. J. Crowley, F. W. Taylor, C. Henin, P. Joannot, and Y. Join (1998), A multi-century stable isotope record from a New Caledonia coral: Interannual and decadal sea-surface temperature variability in the southwest Pacific since 1657 AD, *Paleoceanography*, *13*, 412-426.

Quinn, T. M., and A. W. Tudhope (2000), Science and Technology of Submerged Coral Drilling: A Workshop Report. International Submerged Coral Drilling Workshop Report, 81 pp.

Quinn, T. M., and F. W. Taylor (2006a), SST artifacts in coral proxy records produced by early marine diagenesis in a modern coral from Rabaul, Papua New Guinea, *Geophysical Research Letters*, *33*(4), -.

Quinn, T. M., and F. W. Taylor (2006b), SST artifacts in coral proxy records produced by early marine diagenesis in a modern coral from Rabaul, Papua New Guinea, *Geophysical Research Letters*, *33*(4), L04601, doi:04610.01029/02005GL024972,.

Quinn, T. M., F. W. Taylor, and T. J. Crowley (2006), Coral-based climate variability in the Western Pacific Warm Pool since 1867, *J Geophys Res-Oceans*, *111*(C11).

Rajagopalan, B., U. Lall, and M. A. Cane (1997), Anomalous ENSO occurrences: An alternate view, *Journal of Climate*, *10*(9), 2351-2357.

Ramseyer, K., T. M. Miano, V. D'Orazio, A. Wildberger, T. Wagner, and J. Geister (1997), Nature and origin of organic matter in carbonates from speleothems, marine cements and coral skeletons., *Organic Geochemistry*, *26*(5/6), 361-378.

Rao, S. A., S. K. Behera, Y. Masumoto, and T. Yamagata (2002), Interannual subsurface variability in the Tropical Indian Ocean with a special emphasis on the Indian Ocean Dipole, *Deep-Sea Research II*, *49*, 1549?1572.

Rasmusson, E. M., and T. H. Carpenter (1983), The Relationship between Eastern Equatorial Pacific Sea-Surface Temperatures and Rainfall over India and Sri-Lanka, *Monthly Weather Review*, *111*(3), 517-528.

Reimer, P. J., M. G. L. Baillie, E. Bard, A. Bayliss, J. W. Beck, C. J. H. Bertrand, P. G. Blackwell, C. E. Buck, G. S. Burr, K. B. Cutler, P. E. Damon, R. L. Edwards, R. G. Fairbanks, M. Friedrich, T. P. Guilderson, A. G. Hogg, K. A. Hughen, B. Kromer, G. McCormac, S. Manning, C. B. Ramsey, R. W. Reimer, S. Remmele, J. R. Southon, M. Stuiver, S. Talamo, F. W. Taylor, J. van der Plicht, and C. E. Weyhenmeyer (2004), IntCal04 terrestrial radiocarbon age calibration, 0-26 cal kyr BP, *Radiocarbon*, *46*(3), 1029-1058.

Reynolds, R. W., N. A. Rayner, T. M. Smith, D. C. Stokes, and W. Q. Wang (2002), An improved in situ and satellite SST analysis for climate, *Journal of Climate*, *15*(13), 1609-1625.

Richards, D. A., P. L. Smart, and R. L. Edwards (1994), Maximum Sea Levels for the Last Glacial Period from U-Series Ages of Submerged Speleothems, *Nature*, *367*(6461), 357-360.

Richter, F. M., and K. K. Turekian (1993), Simple models for the chemical response of the ocean to climatic and tectonic forcing, *Earth & Planetary Science Letters*, *119*(121-131).

Rind, D., and D. Peteet (1985), Terrestrial conditions at the last glacial maximum and CLIMAP sea surface temperature estimates: Are they consistent?, *Quaternary Research*, *24*, 1-22.

Risebrobakken, B., E. Balbon, T. Dokken, E. Jansen, C. Kissel, L. Labeyrie, T. Richter,

and L. Senneset (2006), The penultimate deglaciation: High-resolution paleoceanographic evidence from a north-south transect along the eastern Nordic Seas, *Earth and Planetary Science Letters*, *241*(3-4), 505-516.

Risk, M. J., P. W. Sammarco, and H. P. Schwarcz (1994), Cross-Continental Shelf Trends in Delta-C-13 in Coral on the Great-Barrier-Reef, *Marine Ecology-Progress Series*, *106*(1-2), 121-130.

Robinson, L. F., N. S. Belshaw, and G. M. Henderson (2004), U and Th concentrations and isotope ratios in modern carbonates and waters from the Bahamas, *Geochimica et Cosmochimica Acta*, *68*(8), 1777-1789.

Rodbell, D. T., G. O. Seltzer, D. M. Anderson, M. B. Abbott, D. B. Enfield, and J. H. Newman (1999), An similar to 15,000-year record of El Niño-driven alluviation in southwestern Ecuador, *Science*, *283*(5401), 516-520.

Ropelewski, C. F., and M. S. Halpert (1996), Quantifying Southern Oscillation - Precipitation relationships, *Journal of Climate*, *9*(5), 1043-1059.

Rosenfeld, Bresler, and Abelson (1999), Sediment as a possible source of food for corals, *Ecology Letters*, *2*(6), 345-348.

Saji, N. H., B. N. Goswami, P. N. Vinayachandran, and T. Yamagata (1999), A dipole mode in the tropical Indian Ocean, *Nature*, *401*, 360-363.

Saji, N. H., and T. Yamagata (2003a), Possible impacts of Indian Ocean Dipole mode events on global climate, *Climate Research*, *25*(2), 151-169.

Saji, N. H., and T. Yamagata (2003b), Possible impacts of Indian Ocean Dipole mode events on global climate, *Climate Research*, *25*, 151-169.

Sakova, I. V., G. Meyers, and R. Coleman (2006), Interannual variability in the Indian Ocean using altimeter and IX1-expendable bathy-thermograph (XBT) data: Does the 18-month signal exist?, *Geophysical Research Letters*, *33*(L20603), doi:10.1029/2006GL027117.

Sandweiss, D. H., J. B. Richardson III, E. J. Reitz, H. B. Rollins, and K. A. Maasch (1996), Geoarchaeological Evidence from Peru for a 5000 Years B.P. Onset of El Niño, *Science*, *273*(5281), 1531-1533.

Sandweiss, D. H., K. A. Maasch, R. L. Burger, J. B. Richardson, H. B. Rollins, and A. Clement (2001), Variation in Holocene El Niño frequencies: Climate records and cultural consequences in ancient Peru, *Geology*, *29*(7), 603-606.

Scholz, D., A. Mangini, and T. Felis (2004), U-series dating of diagenetically altered fossil reef corals, *Earth and Planetary Science Letters*, *218*(1-2), 163-178.

Scholz, D., and A. Mangini (2006), Estimating the uncertainty of coral isochron U-Th ages, *Quaternary Geochronology*, *1*(4), 279-288.

Scholz, D., and A. Mangini (2007), How precise are U-series coral ages?, *Geochimica et Cosmochimica Acta*, *71*(8), 1935-1948.

Schott, F. A., and J. P. McCreary (2001), The monsoon circulation of the Indian Ocean, *Progress in Oceanography*, *51*(1), 1-123.

Schrag, D. P., G. Hampt, and D. W. Murray (1996), Pore Fluid Constraints on the Temperature and Oxygen Isotopic Composition of the Glacial Ocean, *Science*, *272*(5270), 1930-1932.

Scoffin, T. P., A. W. Tudhope, and B. E. Brown (1989), Fluorescent and skeletal density banding in Porites lutea from Papua New Guinea and Indonesia, *Coral Reefs*, *7*, 169-178.

Scoffin, T. P., A. W. Tudhope, B. E. Brown, H. Chansang, and R. F. Cheeney (1992), Patterns and Possible Environmental Controls of Skeletogenesis of Porites-Lutea, South Thailand, *Coral Reefs*, *11*(1), 1-11.

Shen, C. C., R. L. Edwards, H. Cheng, J. A. Dorale, R. B. Thomas, S. B. Moran, S. E. Weinstein, and H. N. Edmonds (2002), Uranium and thorium isotopic and concentration measurements by magnetic sector inductively coupled plasma mass spectrometry, *Chemical Geology*, *185*(3-4), 165-178.

Shen, G. (1996), 227Th/230Th dating method: methodology and application to Chinese speleothem samples, *Quaternary Science Reviews*, *15*(7), 699-707.

Shen, G. T., and C. L. Sanford (1990), Trace element indicators of climate variability in reef-building corals, *Global ecological consequences of the 1982-83 El Niño-Southern Oscillation, Published by Elsevier; Oceanography Series, 52, Editors Glynn P.W.*, 255-283.

Shen, G. T., J. E. Cole, D. W. Lea, L. J. Linn, T. A. McConnaughey, and R. G. Fairbanks (1992), Surface ocean variability at Galapagos from 1936-1982: calibration of geochemical tracers in corals, *Paleoceanography*, *7*(5), 563-588.

Shukla, J., and D. A. Paolino (1983), The Southern Oscillation and Long-Range Forecasting of the Summer Monsoon Rainfall over India, *Monthly Weather Review*, *111*(9), 1830-1837.

Shulmeister, J., and B. G. Lees (1995), Pollen evidence from tropical Australia for the onset of an ENSO-dominated climate at c. 4000 BP, *The Holocene*, *5*, 10?18.

Siddall, M., E. Bard, E. J. Rohling, and C. Hemleben (2006), Sea-level reversal during Termination II, *Geology*, *34*(10), 817-820.

Siegel, F. R. (1960), The effect of strontium on the aragonite-calcite ratios of Pleistocene corals, *Journal of Sedimentary Petrology*, *30*(2), 297-304.

Sinclair, D. J., L. P. J. Kinsley, and M. T. McCulloch (1998), High resolution analysis of trace elements in corals by laser ablation ICP-MS, *Geochimica et Cosmochimica Acta*, *62*(11), 1889-1901.

Smart, P. L., D. A. Richards, and R. L. Edwards (1998), Uranium-series ages of speleothems from South Andros, Bahamas: implications for Quaternary sea-level history and palaeoclimate, *Cave and Karst Science*, *25*(2), 67-74.

Smith, S. V., R. W. Buddemeier, R. C. Redalje, and J. E. Houck (1979), Strontium-calcium thermometry in coral skeletons, *Science*, *204*, 404-407.

Smith, T. M., and R. W. Reynolds (2004), Improved extended reconstruction of SST (1854-1997), *Journal of Climate*, *17*(12), 2466-2477.

Sprintall, J., J. Chong, F. Syamsudin, W. Morawitz, S. Hautala, N. Bray, and S. Wijffels (1999a), Dynamics of the South Java Current in the Indo-Australian Basin, *Geophysical Research Letters*, *26*(16), 2493-2496.

Sprintall, J., J. C. Chong, F. Syamsudin, W. Morawitz, S. Hautala, N. Bray, and S. Wijffels (1999b), Dynamics of the South Java Current in the Indo-Australian basin, *Geophysical Research Letters*, *26*, 2493-2496.

Sprintall, J., A. L. Gordon, R. Murtugudde, and R. D. Susanto (2000), A semiannual Indian Ocean forced Kelvin wave observed in the Indonesian seas in May 1997, *Geophysical Research Letters*, *105, NO. C7, PAGES ,* (C7), 17,217–217,230.

Sprintall, J., J. T. Potemra, S. L. Hautala, N. A. Bray, and W. W. Pandoe (2003), Temperature and salinity variability in the exit passages of the Indonesian Throughflow, *Deep Sea Research Part II: Topical Studies in Oceanography*, *50*(12-13), 2183-2204.

Stein, M., G. J. Wasserburg, P. Aharon, J. H. Chen, Z. R. Zhu, A. Bloom, and J. Chappell (1993), Tims U-Series Dating and Stable Isotopes of the Last Interglacial Event in Papua-New-Guinea, *Geochimica Et Cosmochimica Acta*, *57*(11), 2541-2554.

Stirling, C. H., T. M. Esat, M. T. McCulloch, and K. Lambeck (1995), High-precision U-series dating of corals from Western Australia and implications for the timing and duration of the Last Interglacial, *Earth and Planetary Science Letters*, *135*(1-4), 115-130.

Stirling, C. H., T. M. Esat, K. Lambeck, and M. T. McCulloch (1998), Timing and duration of the Last Interglacial: evidence for a restricted interval of widespread coral reef growth, *Earth and Planetary Science Letters*, *160*(3-4), 745-762.

Stirling, C. H., T. M. Esat, K. Lambeck, M. T. McCulloch, S. G. Blake, D.-C. Lee, and A.

N. Halliday (2001), Orbital Forcing of the Marine Isotope Stage 9 Interglacial, *Science*, *291*(5502), 290-293.

Stoll, H. M., and D. P. Schrag (1998), Effects of Quaternary sea level cycles on strontium in seawater, *Geochimica et Cosmochimica Acta*, *62*(7), 1107-1118.

Stott, L., C. Poulsen, S. Lund, and R. Thunell (2002), Super ENSO and Global Climate Oscillations at Millennial Time Scales, *Science*, *297*(5579), 222-226.

Stuiver, M., and P. J. Reimer (1986), A Computer-Program for Radiocarbon Age Calibration, *Radiocarbon*, *28*(2B), 1022-1030.

Stuiver, M., and T. F. Braziunas (1993), Modeling atmospheric 14C influences and 14C ages of marine samples to 10,000 BC, *Radiocarbon*, *35*(1), 137-189.

Stuiver, M., and P. J. Reimer (1993), Extended C-14 Data-Base and Revised Calib 3.0 C-14 Age Calibration Program, *Radiocarbon*, *35*(1), 215-230.

Stuiver, M., P. J. Reimer, E. Bard, J. W. Beck, G. S. Burr, K. A. Hughen, B. Kromer, G. McCormac, J. Van der Plight, and M. Spurk (1998), INTCAL98 radiocarbon age calibration, 24,000-0 cal BP, *Radiocarbon*, *40*(3), 1041-1083.

Stuiver, M., P. J. Reimer, and R. W. Reimer (2005), CALIB 5.0. [WWW program and documentation]. *http://calib.qub.ac.uk/calib/*.

Stute, M., M. Forster, H. Krischkorn, A. Serejo, J. F. Clark, P. Schlosser, W. S. Broecker, and G. Bonani (1995), Cooling of Tropical Brazil (5^{o}C) During the Last Glacial Maximum, *Science*, *269*, 379-383.

Sun, D., M. K. Gagan, H. Cheng, H. Scott-Gagan, C. A. Dykoski, R. L. Edwards, and R. Su (2005), Seasonal and interannual variability of the Mid-Holocene East Asian monsoon in coral δ^{18}O records from the South China Sea, *Earth and Planetary Science Letters*, *237*(1-2), 69.

Susanto, R. D., and A. L. Gordon (2005), Velocity and transport of the Makassar Strait throughflow, *Journal of Geophysical Research-Oceans*, *110*(C1), -.

Susic, M., K. G. B. Boto, and P. J. Isdale (1991), Fluorescent humic bands in coral skeletons originate from runoff, *Marine Chemistry*, *33*, 91-104.

Suzuki, A., M. K. Gagan, P. De Deckker, A. Omura, I. Yukino, and H. Kawahata (2001), Last Interglacial coral record of enhanced insolation seasonality and seawater O-18 enrichment in the Ryukyu Islands, northwest Pacific, *Geophysical Research Letters*, *28*(19), 3685-3688.

Swart, P. K., and M. L. Coleman (1980), Isotopic data for scleractinian corals explain their palaeotemperature uncertainties, *Nature*, *283*, 557-559.

Swart, P. K. (1983), Carbon and oxygen isotope fractionation in scleractinian corals: a review, *Earth-Science Reviews*, *19*(1), 51-80.

Swart, P. K., J. J. Leder, A. M. Szmant, and R. E. Dodge (1996a), The origin of variations in the isotopic record of scleractinian corals: II. Carbon, *Geochimica et Cosmochimica Acta*, *60*(15), 2871-2885.

Swart, P. K., J. J. Leder, A. M. Szmant, and R. E. Dodge (1996b), The origin of variations in the isotopic record of scleractinian corals .2. Carbon, *Geochimica Et Cosmochimica Acta*, *60*(15), 2871-2885.

Syamsudin, F., A. Kaneko, and D. B. Haidvogel (2004), Numerical and observational estimates of Indian Ocean Kelvin wave intrusion into Lombok Strait, *Geophysical Research Letters*, *31*(24), -.

Szabo, B. J., K. R. Ludwig, D. R. Muhs, and K. R. Simmons (1994), Thorium-230 Ages of Corals and Duration of the Last Interglacial Sea-Level High Stand on Oahu, Hawaii, *Science*, *266*(5182), 93-96.

Tanaka, T., Y. W. Watanabe, S. Watanabe, S. Noriki, N. Tsurushima, and Y. Nojiri (2003), Oceanic Suess effect of delta C-13 in subpolar region: The North Pacific, *Geophysical Research Letters*, *30*(22), -.

Thompson, L. G., E. Mosley-Thompson, M. E. Davis, P.-N. Lin, K. A. Henderson, J. Cole-Dai, J. F. Bolzan, and K.-b. Liu (1995), Late glacial stage and Holocene tropical ice core records from Huascaran, Peru, *Science*, *269*, 45-50.

Thompson, W. G., M. W. Spiegelman, S. L. Goldstein, and R. C. Speed (2003), An open-system model for U-series age determinations of fossil corals, *Earth and Planetary Science Letters*, *210*(1-2), 365-381.

Thompson, W. G., and S. L. Goldstein (2005), Open-System Coral Ages Reveal Persistent Suborbital Sea-Level Cycles, *Science*, *308*(5720), 401-404.

Tomczak, M., and J. S. Godfrey (1994), *Regional Oceanography: An Introduction*, 422 pp., Pergamon, Tarryton, N.Y.

Trenberth, K. E. (1990), Recent Observed Interdecadal Climate Changes in the Northern-Hemisphere, *Bulletin of the American Meteorological Society*, *71*(7), 988-993.

Trenberth, K. E., and T. J. Hoar (1996), El Niño-Southern Oscillation event: longest on record, *Geophysical Research Letters*, *23*(1), 57-60.

Trenberth, K. E. (1997), The Definition of El Niño, *Bulletin of the American Meteorological Society*, *78*(12), 2771-2777.

Trenberth, K. E., and T. J. Hoar (1997), El Niño and climate change, *Geophysical*

Research Letters, *24*(23), 3057-3060.

Trenberth, K. E., D. P. Stepaniak, and J. M. Caron (2000), The global monsoon as seen through the divergent atmospheric circulation, *Journal of Climate*, *13*(22), 3969-3993.

Trenberth, K. E., J. M. Caron, D. P. Stepaniak, and S. Worley (2002), Evolution of El Niño-Southern Oscillation and global atmospheric surface temperatures, *Journal of Geophysical Research-Atmospheres*, *107*(D7-8), -.

Tribble, G. W. (1993), Organic-Matter Oxidation and Aragonite Diagenesis in a Coral-Reef, *Journal of Sedimentary Petrology*, *63*(3), 523-527.

Tudhope, A. W., D. W. Lea, G. B. Shimmield, C. P. Chilcott, and S. Head (1996), Monsoon climate and Arabian Sea coastal upwelling recorded in massive corals from Southern Oman, *Palaios*, *11*, 347-361.

Tudhope, A. W., C. P. Chilcott, M. T. McCulloch, E. R. Cook, J. Chappell, R. M. Ellam, D. W. Lea, J. M. Lough, and G. B. Shimmield (2001), Variability in the El Niño-Southern Oscillation Through a Glacial-Interglacial Cycle, *Science*, *291*(5508), 1511-1517.

Urban, F. E., J. E. Cole, and J. T. Overpeck (2000), Influence of mean climate change on climate variability from a 155-year tropical Pacific coral record, *Nature*, *407*(6807), 989-993.

Vecchi, G. A., B. J. Soden, A. T. Wittenberg, I. M. Held, A. Leetmaa, and M. J. Harrison (2006), Weakening of tropical Pacific atmospheric circulation due to anthropogenic forcing, *Nature*, *441*(7089), 73-76.

Villemant, B., and N. Feuillet (2003), Dating open systems by the 238U-234U-230Th method: application to Quaternary reef terraces, *Earth and Planetary Science Letters*, *210*(1-2), 105-118.

Visser, K., R. Thunell, and L. Stott (2003), Magnitude and timing of temperature change in the Indo-Pacific warm pool during deglaciation, *Nature*, *421*, 152-155.

Wainwright, L., G. Meyers, S. Wijffels, and L. Pigot (2008), Change in the Indonesian Throughflow with the climatic shift of 1976/77, *Geophysical Research Letters*, *35*(3), -.

Wajsowicz, R. C., and E. K. Schneider (2001), The Indonesian throughflow's effect on global climate determined from the COLA coupled climate system, *Journal of Climate*, *14*, 3029-3042.

Wang, P. X., S. Clemens, L. Beaufort, P. Braconnot, G. Ganssen, Z. M. Jian, P. Kershaw, and M. Sarnthein (2005a), Evolution and variability of the Asian monsoon system: state of the art and outstanding issues, *Quaternary Science Reviews*, *24*(5-6), 595-629.

Wang, Y., H. Cheng, R. L. Edwards, Y. He, X. Kong, Z. An, J. Wu, M. J. Kelly, C. A. Dykoski, and X. Li (2005b), The Holocene Asian Monsoon: Links to Solar Changes and North Atlantic Climate, *Science*, *308*(5723), 854-857.

Watanabe, T., M. K. Gagan, T. Correge, H. Scott-Gagan, J. Cowley, and W. S. Hantoro (2003), Oxygen isotope systematics in Diploastrea heliopora: New coral archive of tropical paleoclimate, *Geochimica Et Cosmochimica Acta*, *67*(7), 1349-1358.

Weber, J. N., and P. M. J. Woodhead (1970), Carbon and oxygen isotope fractionation in the skeletal carbonate of reef-building corals, *Chemical Geology*, *6*, 93-117.

Weber, J. N., and P. M. J. Woodhead (1972), Temperature dependence of oxygen-18 concentration in reef coral carbonates, *Journal of Geophysical Research*, *77*, 463-473.

Webster, P. J., and S. Yang (1992), Monsoon and Enso - Selectively Interactive Systems, *Quarterly Journal of the Royal Meteorological Society*, *118*(507), 877-926.

Webster, P. J., V. O. Magana, T. N. Palmer, J. Shukla, R. A. Tomas, M. Yanai, and T. Yasunari (1998), Monsoons: Processes, Predictability, and prospects for prediction, *Journal of Geophysical Research*, *103*(C7), 14451-14510.

Webster, P. J., A. M. Moore, J. P. Loschnlgg, and R. R. Leben (1999), Coupled ocean-atmosphere dynamics in the Indian Ocean During 1997-98, *Nature*, *401*, 356-360.

Wei, G. J., J. S. Yu, X. T. Gui, F. J. Yu, Y. W. Chen, and D. P. Liu (1998), Paleoclimate implication of oxygen and carbon isotopic composition from diagenesis coral - Discussion on the data from NY-1 core, *Sci China Ser D*, *41*(6), 609-615.

Wellington, G. M., and R. B. Dunbar (1995), Stable isotope signatures of ENSO in eastern Pacific (Panama) corals, *Coral Reefs*, *14*, 5-25.

Wellington, G. M., G. Merlen, and R. B. Dunbar (1996), Calibration of stable oxygen isotope signatures in Galapagos corals, *Paleoceanography*, *11*, 467-480.

Wijffels, S., and G. Meyers (2004), An intersection of oceanic waveguides: Variability in the Indonesian throughflow region, *Journal of Physical Oceanography*, *34*(5), 1232-1253.

Winter, A., C. Goenaga, and G. A. Maul (1991), Carbon and oxygen isotope time series from an 18- year Caribbean reef coral, *Journal of Geophysical Research*, *96*, 16673-16678.

Wolter, K., and M. S. Timlin (1998), Measuring the strength of ENSO - how does 1997/98 rank?, *Weather*, *53*, 315-324.

Woodroffe, C. D., and M. K. Gagan (2000), Coral microatolls from the central Pacific

record late Holocene El Niño, *Geophysical Research Letters*, *27*(10), 1511-1514.

Woodroffe, C. D., M. R. Beech, and M. K. Gagan (2003a), Mid-late Holocene El Niño variability in the equatorial Pacific from coral microatolls, *Geophysical Research Letters*, *30*(7), -.

Woodroffe, C. D., M. R. Beech, and M. K. Gagan (2003b), Mid-late Holocene El Niño variability in the equatorial Pacific from coral microatolls, *Geophysical Research Letters*, *30*(7).

Worum, F. P., J. P. Carricart-Ganivet, L. Benson, and D. Golicher (2007), Simulation and observations of annual density banding in skeletons of Montastraea (Cnidaria : Scleractinia) growing under thermal stress associated with ocean warming, *Limnology and Oceanography*, *52*(5), 2317-2323.

Wyrtki, K. (1973), An Equatorial Jet in the Indian Ocean, *Science*, *181*(4096), 262-264.

Wyrtki, K. (1987), Indonesian throughflow and the associated pressure gradient, *Journal of Geophysical Research*, *92*(C12), 12941-12946.

Xie, P. P., and P. A. Arkin (1997), Global precipitation: A 17-year monthly analysis based on gauge observations, satellite estimates, and numerical model outputs, *Bulletin of the American Meteorological Society*, *78*(11), 2539-2558.

Yamagata, T., S. K. Behera, J. J. Luo, S. Masson, M. R. Jury, and S. A. Rao (2004), Coupled oceanatmosphere variability in the tropical Indian Ocean, in *Earth Climate: The Ocean-Atmosphere Interaction*, edited by C. Wang, et al., pp. 189-212, AGU, Washington D. C.

Yan, X. H., C. R. Ho, Q. Zheng, and V. Klemas (1992), Temperature and Size Variabilities of the Western Pacific Warm Pool, *Science*, *258*(5088), 1643-1645.

Yasunari, T. (1990), Impact of Indian Monsoon on the Coupled Atmosphere Ocean System in the Tropical Pacific, *Meteorology and Atmospheric Physics*, *44*(1-4), 29-41.

Yu, J.-Y., C. R. Mechoso, J. C. McWilliams, and A. Arakawa (2002), Impacts of the Indian Ocean on the ENSO cycle, *Geophysical Research Letters*, *29*(8), 46.

Yu, J.-Y., and K. M. Lau (2004a), Contrasting Indian Ocean SST variability with and without ENSO influence: A coupled atmosphere-ocean GCM study, *Meteorology and Atmospheric Physics*, DOI 10.1007/s00703-00004-00094-00707.

Yu, K. F., J. X. Zhao, G. J. Wei, X. R. Cheng, and P. X. Wang (2005), Mid-late Holocene monsoon climate retrieved from seasonal Sr/Ca and delta O-18 records of Porites lutea corals at Leizhou Peninsula, northern coast of South China Sea, *Global and Planetary Change*, *47*(2-4), 301-316.

Zhu, Z., J. F. Marshall, and J. Chappell (1994), Effects of Differential Tectonic Uplift on Late Quaternary Coral-Reef Diagenesis, Huon Peninsula, Papua-New-Guinea, *Australian Journal of Earth Sciences*, *41*(5), 463-474.

Zhu, Z. R., K. H. Wyrwoll, L. B. Collins, J. H. Chen, G. J. Wasserburg, and A. Eisenhauer (1993), High-Precision U-Series Dating of Last Interglacial Events by Mass-Spectrometry - Houtman-Abrolhos Islands, Western-Australia, *Earth and Planetary Science Letters*, *118*(1-4), 281-293.

Zubair, L., S. A. Rao, and T. Yamagata (2003), Modulation of Sri Lankan Maha rainfall by the Indian Ocean dipole, *Geophysical Research Letters*, *30*(2).

APPENDICES

APPENDIX A

CORAL CORES FROM SUMBA, INDONESIA

A.1 Coral cores drilled from 1995 field trip

Reef	Core	Species	Length (m)	Sampling Date	Comments
River Site Holocene reef	RS1	*Porites*		13-11-95	Good Quality
	RS2	*Porites*	0.5	13-11-95	Good Quality
	RS3a	*Porites*		13-11-95	
	RS3b	*Porites*		13-11-95	
	RS4	*Porites*	0.27	13-11-95	
	RS5a	*Porites*	0.22	13-11-95	
	RS5b	*Porites*		13-11-95	Good Quality
	RS6	*Porites*	0.17	13-11-95	
	RS7	*Porites*		13-11-95	
Goat Site reef	GC1	*Porites*		08-11-95	
	GC2	*Porites*		08-11-95	
	GC3a	*Porites*		08-11-95	
	GC3b			08-11-95	
	GC4	*Porites*		08-11-95	
	GC5a	*Porites*		08-11-95	
	GC5b			08-11-95	
	GC6a			08-11-95	
	GC6b	*Porites*		08-11-95	
	GC6c			08-11-95	Good Quality
	GC6d			08-11-95	
	GC7	*Porites*		08-11-95	
Mondu I reef	MI1a		0.52	04-11-95	
	MI1b	*Porites*	0.49	04-11-95	
	MI1c		0.52	04-11-95	
	MI2a	*Porites*	0.52	04-11-95	
	MI2b	*Porites*	0.12	04-11-95	
	MI2c	*Porites*	0.05	04-11-95	
	MI3a		0.52	04-11-95	
	MI3b	*Porites*		04-11-95	
	MI3c		0.48	04-11-95	
	MI4	*Porites*		04-11-95	
	MI5	*Porites*		04-11-95	
	MI6a		0.49	04-11-95	
	MI6b	*Porites*	0.47	04-11-95	
	MI6c		0.50	04-11-95	
	MI6d		0.54	04-11-95	Good Quality
Mondu II reef	MII1	*Porites*		05-11-95	
	MII2a	*Porites*	0.21	05-11-95	
	MII2b	*Porites*	0.28	05-11-95	
	MII2c	*Porites*	0.51	05-11-95	Good Quality
	MII2d	*Porites*	0.50	05-11-95	
	MII3	*Porites*		05-11-95	
	MII4	*Porites*		05-11-95	
	MII5	*Porites*		05-11-95	
	MII6	*Porites*		05-11-95	
	MII7a	*Porites*	27	05-11-95	
	MII7b	*Porites*	22	05-11-95	
	MII8	*Porites*		05-11-95	
	MII9a	*Porites*	0.38	05-11-95	
	MII9b	*Porites*	0.41	05-11-95	
	MII10	*Favites*		05-11-95	

A.2 Coral cores drilled from 1998 field trip

Reef	Sample	Species	Length (m)	Sections	Sampling Date	Comments
Mutiara Site Modern reef	MSM-1	*Porites*	1.3	3	11-11-98	
	MSM-2A	*Diploastrea*	1.1	3	11-11-98	
	MSM-2B	*Porites*	1.25	3	11-11-98	
	MSM-3A	*Porites*	2.97	9	12-11-98	Good Quality
	MSM-3B	*Porites*	0.72	2	12-11-98	
	MSM-3C	*Porites*	0.7	2	12-11-98	
	MSM-4A	*Diploastrea*	1.06	3	14-11-98	
	MSM-4B	*Diploastrea*	1.14	3	14-11-98	
	MSM-5	*Diploastrea*	0.7	2	15-11-98	
	MSM-6	*Porites*	1.33	4	15-11-98	
	MSM-7	*Diploastrea*	0.66	1		
River Site Modern reef	RSM-1	*Portes*	0.99	2	12-11-98	
River Site Holocene reef	RS2.2	*Porites*	1.52	3	06-11-98	Good Quality
	RS3.2	*Porites*	0.78	2	06-11-98	
	RS4.2	*Porites*	0.88	2	07-11-98	
	RS8	*Porites*	1.72	4	06-11-98	
	RS9	*Porites*			07-11-98	
	RS10	*Porites*	1.25	3	07-11-98	
	RS11	*Porites*	0.76	3	07-11-98	
	RS12	*Porites*	0.60	1	07-11-98	
	RS13	*Porites*	1.75	4	09-11-98	
	RS14	*Porites*	1.05	3	09-11-98	
	RS15	*Porites*	1.09	2	09-11-98	
	RS16	*Porites*	0.41	1	09-11-98	
	RS17A	*Porites*			25-11-98	
	RS17B	*Porites*	0.56	3	25-11-98	
Mutiara Site Holocene reef	MS1a	*Porites*	1.43	6	04-11-98	
	MS1b	*Porites*	2.17	8	05-11-98	
	MS2	*Porites*	1.07	5	19-11-98	
	MS3	*Porites*	0.81	2	20-11-98	
	MS4	*Porites*	0.35	2	20-11-98	
	MS5	*Porites*	0.4	2	20-11-98	
	MS6A	*Diploastrea*	0.3	1	21-11-98	
	MS6B		0.66	2	21-11-98	
	MS7	*Porites*	1.12	2	21-11-98	Good Quality
	MS8	*Porites*	0.66	4	21-11-98	
	MS9	*Porites*	0.85	2	21-11-98	
	MS10	*Porites*	0.62	3	22-11-98	
Mondu I reef	MI7	*Diploastrea*	0.53	3	07-11-98	
	MI8	*Diploastrea*	0.47	2	08-11-98	
Mondu III reef	MIII1	*Diploastrea*	0.43	2	23-11-98	
	MIII2	*Porites*	0.64	4	23-11-98	
	MIII3	*Diploastrea*	0.35	2	23-11-98	
Mondu IV reef	MIV1	*Diploastrea*	0.36	2	23-11-98	
	MIV2	*Diploastrea*	0.45	2	23-11-98	Good Quality

A.3 Coral cores drilled from 2003 field trip

Reef	Core	Latitude	Longitude	Species	Length (m)	Sections	sampling date	Comments
River Site Holocene reef	RS03-1	9°27.339'S	120°4.383'E	*Porites*	0.96	3	4-9-03	
	RS03-2a	9°27.427'S	120°4.412'E	*Porites*	0.35	1	4-9-03	
	RS03-3a			*Porites*	0.45	1	5-9-03	
	RS03-3b			*Porites*	0.9	5	5-9-03	
	RS03-4	9°27.761'S	120°4.687'E	*Porites*	1.35	7	5-9-03	Good quality
Mutiara Site Holocene reef	MS03-A-1	9°28.893'S	120°8.523'E	*Porites*	0.72	3	14-8-03	
	MS03-A-2				0.4	2	6-9-03	
	MS03-B-1	9°29.079'S	120°7.434'E	*Porites*	0.58	2	3-9-03	
Goat Site reef	GC03-1a	9°29.33'S	120°7.285'E	*Porites*	0.36	2	6-9-03	
	GC03-1b	9°29.33'S	120°7.285'E	*Porites*	0.95	4	6-9-03	Good quality
Oasis reef	OA03-1a	9°29.564'S	120°7.169'E	*Porites*	0.29	3	14-8-03	
	OA03-1b	9°29.564'S	120°7.169'E	*Porites*	0.39	2	15-8-03	
	OA03-1c	9°29.564'S	120°7.169'E	*Porites*	1.79	9	15-8-03	Good quality
	OA03-2a	9°29.542'S	120°7.206'E	*Porites*	0.51	1	16-8-03	
	OA03-2b	9°29.542'S	120°7.206'E	*Porites*	0.49	2	16-8-03	
	OA03-2c	9°29.542'S	120°7.206'E	*Porites*	0.35	1	16-8-03	
	OA03-3a	9°29.547'S	120°7.193'E	*Diploastrea*	0.1	1	16-8-03	
	OA03-3b	9°29.547'S	120°7.193'E	*Diploastrea*	0.8	3	16-8-03	
	OA03-4	9°29.534'S	120°7.178'E	*Porites*	0.38	2	16-8-03	
Mondu I reef	MI03-1	9°29.379'S	120°5.879'E	*Porites*			4-9-03	
	MI03-C-1a	9°29.402'S	120°5.779'E	*Diploastrea*	0.4	1	4-9-03	
	MI03-C-1b	9°29.402'S	120°5.779'E	*Diploastrea*	0.6	2	4-9-03	
	MI03-C-1c	9°29.402'S	120°5.779'E	*Diploastrea*	0.41	2	4-9-03	
	MI-3-03a	9°29.413'S	120°5.868'E	*Porites*	0.39	1	5-9-03	
	MI-6-03	9°29.423'S	120°5.874'E	*Porites*	0.61	2	5-9-03	
Mondu I West reef	MI03-B-1a	9°29.377'S	120°5.756'E	*Diploastrea*	0.43	2	22-8-03	
	MI03-B-1b	9°29.377'S	120°5.756'E	*Diploastrea*	0.46	2	22-8-03	
	MI03-B-2a	9°29.343'S	120°5.78'E	*Porites*	0.58	2	22-8-03	
	MI03-B-3			*Diploastrea*	0.6	2	4-9-03	
Mondu IV reef	MIV03-1	9°29.479'S	120°5.704'E	*Porites*	0.43	2	21-8-03	
	MIV03-2	9°29.497'S	120°5.717'E	*Porites*	0.22	2	21-8-03	
	MIV03-2b	9°29.497'S	120°5.717'E	*Porites*	0.5	1	4-9-03	
Mondu V reef	MV03-A-1a	9°29.518'S	120°5.785'E	*Porites*	0.45	3	18-8-04	
	MV03-A-1b	9°29.518'S	120°5.785'E	*Porites*	0.54	3	18-8-03	
	MV03-A-2a	9°29.521'S	120°5.786'E	*Porites*	1.04	3	18-8-03	Good quality
	MV03-A-2b	9°29.521'S	120°5.786'E	*Porites*	0.5	1	19-8-03	
	MV03-A-2c	9°29.521'S	120°5.786'E	*Porites*	1.09	3	19-8-03	Good quality
	MV03-A-3	9°29.521'S	120°5.786'E	*Porites*	1.08	3	18-8-04	
	MV03-B-1a	9°29.539'S	120°5.744'E	*Porites*	0.62	3	20-8-03	
	MV03-B-1b	9°29.539'S	120°5.744'E	*Porites*	1.1	5	20-8-03	
	MV03-B-2a	9°29.5'S	120°5.74'E	*Porites*	0.74	4	20-8-03	
	MV03-B-2b	9°29.5'S	120°5.74'E	*Porites*	1.13	5	20-8-03	Good quality
Mondu VI reef	MVI03-1a	9°29.74'S	120°5.738'E	*Porites*	0.28	1	1-9-03	
	MVI03-1b	9°29.74'S	120°5.738'E	*Porites*	0.14	1	1-9-03	
	MVI03-2a	9°29.744'S	120°5.744'E	*Porites*	0.53	4	1-9-03	
	MVI03-2b	9°29.744'S	120°5.744'E	*Porites*	0.2	2	1-9-03	
	MVI03-2c	9°29.744'S	120°5.744'E	*Porites*	0.39	3	1-9-03	
	MVI03-3a	9°29.741'S	120°5.741'E	*Porites*	0.15	1	1-9-03	
	MVI03-3b	9°29.741'S	120°5.741'E	*Porites*	0.35	1	1-9-03	
	MVI03-4	9°29.471'S	120°5.742'E	*Porites*	0.34	6	1-9-03	
	MVI03-5a	9°29.739'S	120°5.738'E	*Porites*	0.52	5	2-9-03	
	MVI03-5b	9°29.739'S	120°5.738'E	*Porites*	0.37	3	2-9-03	

		MVI03-6a	9°29.741'S	120°5.745'E	*Porites*	0.33	2	2-9-03	
		MVI03-6b	9°29.741'S	120°5.745'E	*Porites*	0.28	2	2-9-03	
		MVI03-6c	9°29.741'S	120°5.745'E	*Porites*	0.48	2	2-9-03	
		MVI03-6d	9°29.741'S	120°5.745'E	*Porites*	0.57	2	2-9-03	
		MVI03-7a	9°29.731'S	120°5.746'E	*Porites*	0.66	4	2-9-03	Good quality
		MVI03-7b	9°29.731'S	120°5.746'E	*Porites*	0.32	2	2-9-03	
		MVI03-7c	9°29.731'S	120°5.746'E	*Porites*	0.55	2	2-9-03	Good quality
Mondu reef	II	MII03-2a	9°29.756'S	120°5.857'E	*Porites*	0.36	1	3-9-03	
		MII03-2b	9°29.756'S	120°5.857'E	*Porites*	0.35	1	3-9-03	
		MVII03-1a	9°29.744'S	120°5.679'E	*Porites*	0.75	3	2-9-03	
Mondu reef	VII	MVII03-1b	9°29.744'S	120°5.679'E	*Porites*	0.66	3	2-9-03	
		MVII03-2a	9°29.694'S	120°5.714'E	*Porites*	0.76	3	3-9-03	
		MVII03-2b	9°29.694'S	120°5.714'E	*Porites*	0.4	1	3-9-03	

APPENDIX B

RESULTS OF RADIOCARBON ANALYSIS OF SUMBA CORALS

	Sample	$\delta^{14}C$ (‰)	$\delta^{13}C$ (‰)	$D^{14}C$ (‰)	Conventional ^{14}C age (yr BP)
Holocene Corals	RS4.2	-200.6±4.6	-1.9±0.2	-237.5±4.4	2180±50
	RS13	-301.8±4.4	-1.2±2	-335±5.1	3280±70
	RS8	-345.9±4.1	-1.1±2	-377.2±4.7	3800±70
	MS7	-354.2±4.1	-0.3±0.2	-386.1±3.9	3920±60
	RS2	-358.8±4.5	0±2	-390.9±5	3980±70
	RS10	-396.2±3.9	0±2	-426.3±4.4	4460±70
	RS3	-396.5±4.3	0±2	-426.7±4.8	4470±70
	PS-1C	-402.6±3.3	0±2	-432.5±4	4550±60
	MS1b	-406.9±3.9	-0.8±0.2	-435.7±3.7	4600±60
	RS5b	-419±4.9	0±2	-448.1±5.2	4780±80
	BS-3C	-459.8±3.2	0±2	-486.8±3.7	5360±60
Late Pleistocene Coral	GC-6C	-981.6±0.8	0±2	-982.5±0.7	32490±340

The conventional radiocarbon measurements of Sumba corals were carried out by Abaz Alimanovic at the RSES Radiocarbon Dating Laboratory of the Australian National University.

APPENDIX C

RESULTS OF U-TH ANALYSES OF SOME OF SUMBA CORALS

	Sample	U (ppm)	$(230/238)_{act}$	$\delta^{234}U_{(t)}$	$\delta^{234}U_{(initial)}$	$(230/232)_{act}$	Age (cal. yr)
	RSM 4 (top)	2.5916	0.0020	146.1	146.2±2.8	81±2	193±3
Modern	RSM 4 (base)	2.6634	0.0040	144.9	145.0±3.8	208±12	384±9
Corals	RSM3 (top)	2.5963	0.0039	146.9	147.1±4.6	158±4	366±8
	RSM 3 (base)	2.4775	0.0048	149.8	150.0±3.1	142±2	455±5
	RS 2	2.2025	0.0381	144.3	145.8±3.3	913±9	3676±43
	RS 2	2.6580	0.0389	148.3	149.9±2.3	922±60	3744±58
	RS2.2	2.5648	0.0384	145.5	147.0±2.2	515±8	3702±42
Holocene	MS 7	2.5285	0.0388	148.8	150.4±2.3	373±5	3732±42
Corals	RS 3	2.8731	0.0450	143.2	144.9±2.3	430±7	4366±56
	MS-1b	2.7021	0.0489	146.1	148.1±2.4	651±6	4741±41
	RS 5b	2.9130	0.0496	149.7	151.8±2.5	2199±23	4791±40
	BS-3c	2.8430	0.0586	143.4	145.8±2.3	797.±4	5713±46
Late Pleistocene Corals	GC 6c	3.0077	1.3298	161.0		31471±294	
	MI 6D	6.5919	0.6233	100.9	129.9±4.0	40140±215	89320±86
	MII 2c	3.0969	1.3435	223.4		12744±115	
	MIV 2	2.9392	0.7604	115.7	162.9±3.2	6555±108	120800±1300

These early-stage uranium-series measurements were conducted by Dr Linda Ayliffe using the thermal ionisation mass spectrometer at the Laboratoire des Sciences du Climat et de l'Environnement, Gif-sur-Yvette Cedex, France.

APPENDIX D

Sr/Ca ANALYSIS

High precision Sr/Ca measurements were performed using thermal ionization mass spectrometry. Coral samples of approximately 100 µg were diluted in 0.5 M HNO_3 and an aliquot containing approximately 4 µg Ca was taken. This aliquot was then spiked with a Sr-Ca isotope laboratory standard and loaded onto a Ta filament. Sr/Ca ratios were measured using a MAT-261 thermal ionization multiple-collector (7 cups) mass spectrometer by Heather Scott-Gagan at the Australian National University.

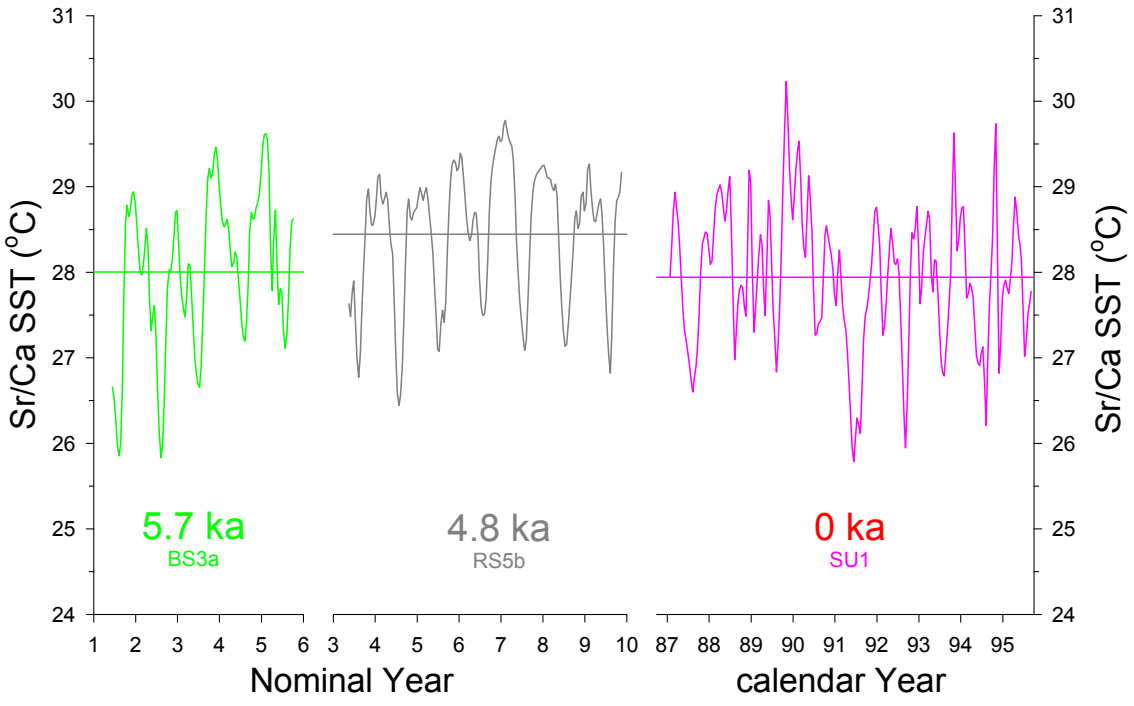

Figure A.1 Comparison of Sa/Ca SST between modern *Porites* coral SU1 and Holocene *Porites* corals from Mondu village in Sumba, Indonesia. The calibration equation between Sr/Ca ratios and SST values is SST = 168.2 – 15674 × Sr/Ca_{atomic} based on Gagan et al. [1998].

APPENDIX E

DIAGENETIC EFFECT OF ABIOTIC ARAGONITE ON $\delta^{18}O$ AND $\delta^{13}C$ OF HOLOCENE *PORITES* CORAL MS7

E.1 Background

Biogenetic coral aragonite is subject to post-depositional diagenetic alteration both in the marine and vadose environments [*James*, 1974; *Bathurst*, 1975; *Hubbard and Swart*, 1982; *Aissaoui et al.*, 1986; *Constanz*, 1986; *Martin et al.*, 1986; *Purser and Schroeder*, 1986; *Potthast*, 1992; *Bar-Matthews et al.*, 1993; *Stein et al.*, 1993; *Tribble*, 1993], and exchange and removal of elements and isotopes during the diagenetic processes have been concerned to be potential to affect the veracity of coral proxies as important tools in paleoclimate and hydrological reconstruction [*Guilderson et al.*, 1994; *McCulloch et al.*, 1996; *Esat et al.*, 1999; *Hughen et al.*, 1999; *Woodroffe and Gagan*, 2000; *Guilderson et al.*, 2001; *Tudhope et al.*, 2001; *Felis et al.*, 2004; *Brachert et al.*, 2006].

Several recent studies have investigated the paleoclimate implications of these diagenetic transformations [*Enmar et al.*, 2000; *Muller et al.*, 2001; *McGregor and Gagan*, 2003; *Muller et al.*, 2004; *Quinn and Taylor*, 2006]. McGregor and Gagan [*McGregor and Gagan*, 2003] found that diagenetic transformation of primary aragonite to calcite or addition of calcite of calcite cements in environments with meteroric water involves a negative shift in the Sr/Ca ratio, $\delta^{18}O$ and $\delta^{13}C$ composition of the diagenetically altered corals, which is consistent with early observations [*Siegel*, 1960; *Martin et al.*, 1986; *Stein et al.*, 1993; *Zhu et al.*, 1994; *Wei et al.*, 1998]. They further showed that lower Sr/Ca and $\delta^{18}O$ in diagenetically altered coral would produce up to 1.5 and 0.2 ^{o}C warmer SST artefacts for paleotemperature reconstruction, respectively [*McGregor and Gagan*, 2003]. Recent researches indicated that secondary aragonite

occurred in early marine diagenesis would bring on significant shift toward higher coral Sr/Ca, $\delta^{18}O$ and $\delta^{13}C$ relative to pristine corals [*Enmar et al.*, 2000; *Muller et al.*, 2001; *Muller et al.*, 2004; *Gallup et al.*, 2006; *Quinn and Taylor*, 2006] and conversion of these altered coral Sr/Ca and $\delta^{18}O$ to SST using standard equations yielded temperature estimates that was ~4-5 ^{o}C [*Muller et al.*, 2001] or 2.5 ($\delta^{18}O$-SST) or 6 ^{o}C (Sr/Ca-SST) [*Quinn and Taylor*, 2006] cooler than that estimated from unaltered portion of the same core.

Figure A.2 (left) X-radiograph positive image of Holocene coral core MS7. White lines represent sub-sampling transects. Notice the density alteration in the lowermost section. Yellow box indicates petrographic thin-section area and yellow dots mark spots of optical microscopic images in Figure A.4.

E.2 Coral skeletal petrological alteration

A full suite of diagenetical screening techniques have been applied to ensure the veracity of the paleoclimate reconstruction from skeletal geochemical records of Holocene coral MS7. The top 10 cm of the core is discoloured and has not been used for any further geochemical analysis. There was no calcite observed under UV light for the whole MS7 core and X-ray diffraction (XRD) results confirmed that the MS7 core contains no significant calcite. X-radiograph of the 7-mm thick slab of the core, however, revealed that the lowermost part of the core contained a 10-cm section with physical evidence of alteration showing increased skeletal density (Figure A.2).

The alteration in skeletal texture, density, and colour could also be observed by unaided eyes under natural light. Visual inspection of the petrographic thin-sections and scanning electron microscopy (SEM) images revealed that the physical alteration mainly resulted from infilling of secondary abiotic

aragonite needles in the pore space toward the base of the core (Figure A.3).

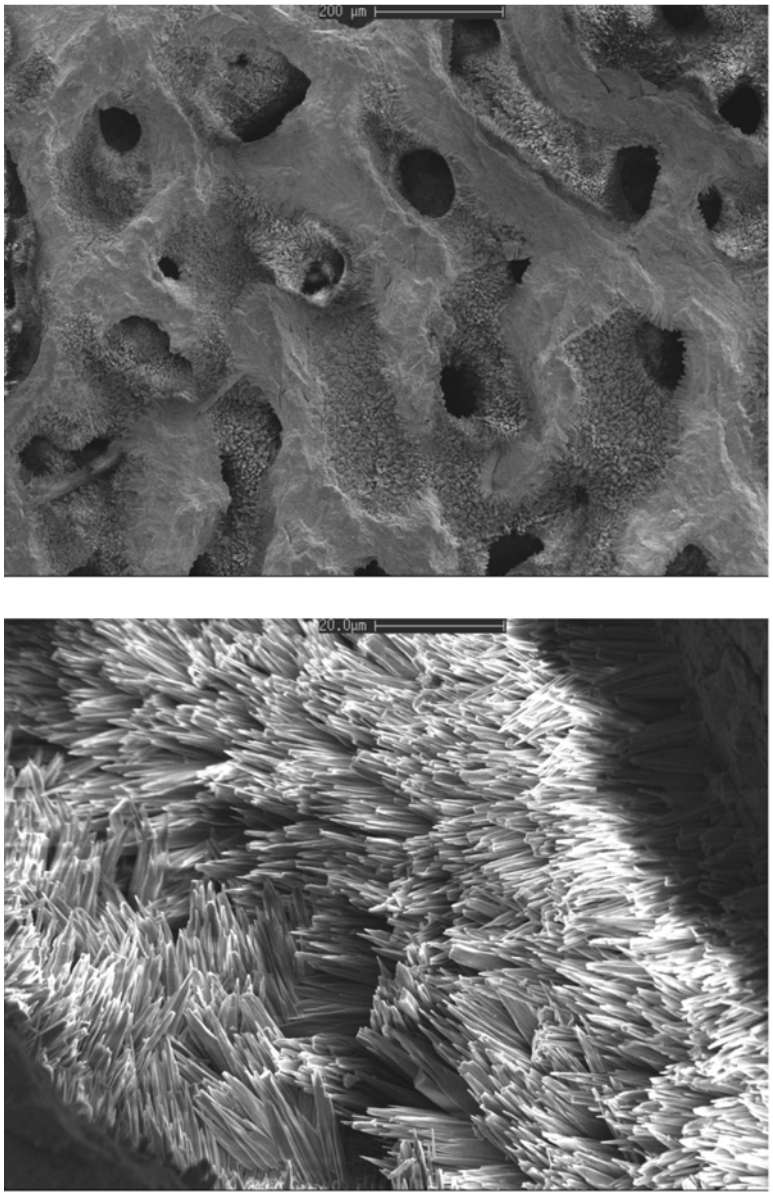

Figure A.3 SEM images exhibiting overgrowth of secondary aragonite crystals projecting into the skeletal voids in the basal section of the Holocene coral core MS7 (Photos courtesy of Gavin Dunbar).

X-radiographic image shows that coral skeletal density increases progressively toward the base of the core (Figure A.2). It might provide an opportunity for petrographic investigation on how the addition of secondary aragonite develops. To investigate the effect of abiotic aragonite on coral isotope proxies, measurement of coral $\delta^{18}O$ and $\delta^{13}C$ had been extended to the transition zone. A 65 mm by 25 mm petrographic thin-section

paralleling the geochemical sub-sampling transection C was employed (Figure A.2) and images every 15 mm paralleling the transection were shown in Figure A.4.

Figure A.4 (next page) Progressive process of coral aragonite diagenetic alteration and the effect of secondary aragonite on skeletal $\delta^{18}O$ of coral MS7 (3.7 ka). **Right panel:** optical microscopic (OM) images of coral petrographic thin-section in the diagenetic transformation transition zone parallelling the isotope sub-sampling transection III (positions of the thin-section and the OM images see Figure A.2). **Spot A:** top of the thin-section, exhibiting pristine coral skeleton. Notice the smooth septa walls, the radial-fibrous structure of aragonite fibres growing from a centre of calcification (black arrow), and the edgily micro-crannies (white arrow) in the centre of the aragonite skeleton. **Spot B:** 15 mm lower than spot A in the thin-section showing the start of the diagenetic alteration process including slight dissolution (double white arrow) of some part of the aragonite matrix and the slightly obscured radial-fibrous pattern and micro-crannies in the aragonite skeleton. **Spot C:** 15 mm lower than spot B in the thin-section showing further dissolution (double white arrow), much more obscured skeletal texture, and the occurrence of some fuzziness and thin selvages along the edges of the septa walls. The percentage of secondary aragonite is estimated to be 1~2%. **Spot D:** 15 mm lower than C spot in the thin-section exhibiting full covering of secondary aragonite needles (10 to 30 μm in size) on the surface of coral aragonite skeleton, secondary aragonite replacement of the primary skeletal aragonite, large patches of dissolution (double black arrow), and obscurity or disappearance of primary coral textures. The percentage of secondary aragonite is estimated to be 10~15%. **Spot E:** bottom of the thin-section showing bigger secondary aragonite crystal (50 to 80 μm in size) covering of voids and replacement of the primary skeletal aragonite, increasing dissolution of biotic aragonite, and further obscurity or complete disappearance of primary coral textures. The percentage of secondary aragonite is estimated to be 30~40%. **Left panel:** unresampled $\delta^{18}O$ of the core basal section. Shaded areas shows $\delta^{18}O$ sections closely linked to the presence of secondary aragonite.

Thin-section observation showed that the diagenetic alteration occurred progressively toward the base of the core within 6 cm distance from pristine biotic aragonite to severely altered aragonite skeleton and large amount of overgrowth of abiotic aragonite. In the top of the thin-section (Figure A.4 right panel-A), the coral shows all the skeletal features of modern corals including well-defined septa walls, the radial-fibrous structure of aragonite fibres growing from a centre of calcification, the edgily micro-crannies in the aragonite matrix, absence of void filling or cement formation, and no evidence of replacement of calcite or secondary aragonite. At this spot, the OM image shows no difference with any OM images from the upper part of the core. All in all, petrographic observation has proven excellent preservation above this spot for this 3.7 ka coral core.

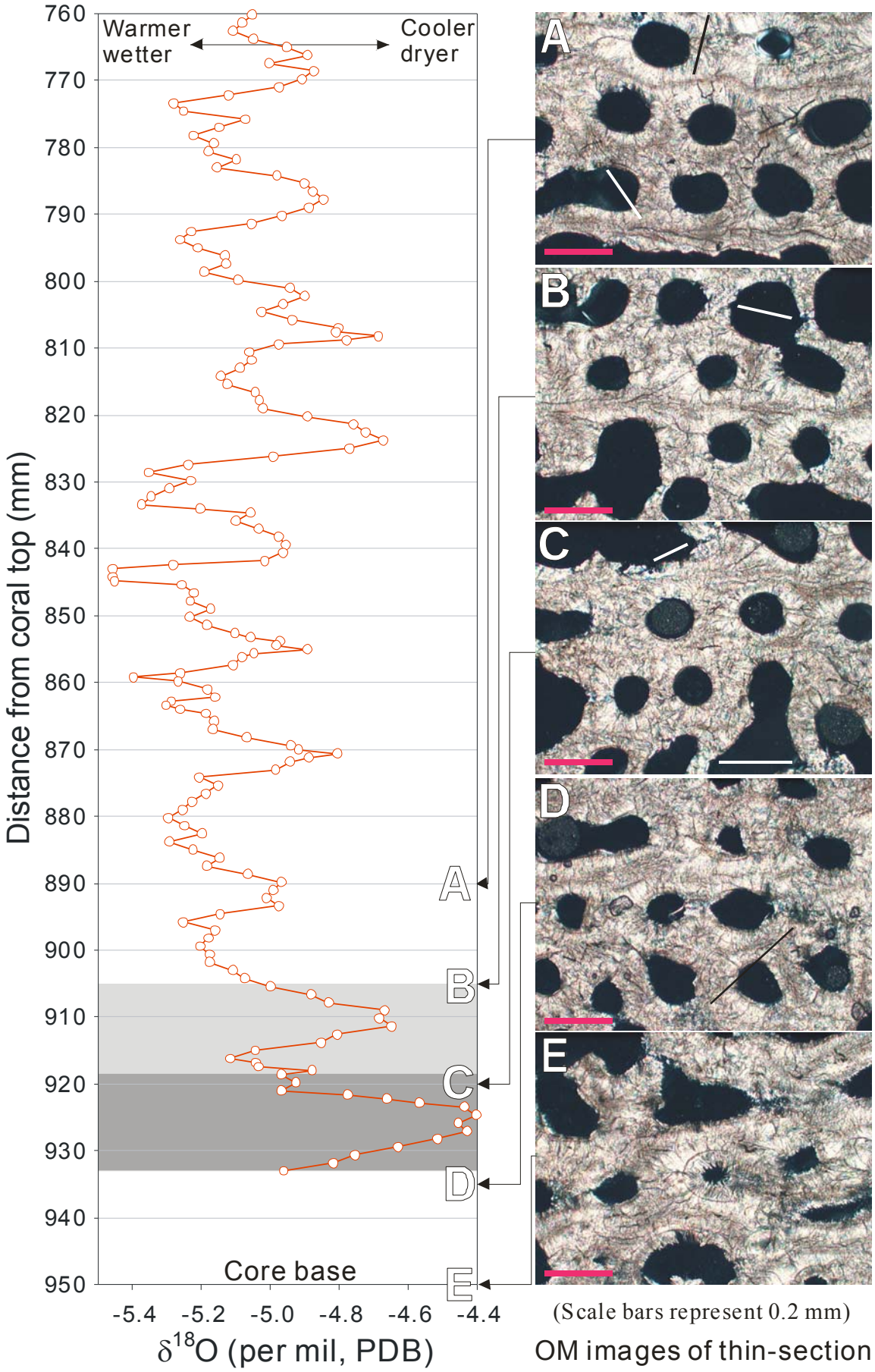
Warmer
wetter
Cooler
dryer
760
770
780
790
800
810
820
830
840
850
860
870
880
890
900
910
920
930
940
950
Distance from coral top (mm)
A
B
C
D
E
Core base
-5.4
-5.2
-5.0
-4.8
-4.6
-4.4
δ18O (per mil, PDB)
(Scale bars represent 0.2 mm)
OM images of thin-section

Even though the OM observation shows the coral in B spot is still in a good condition by preservation, the diagenesis has started because of the increased dissolution of primary aragonite (Figure A.4 right panel-B). From this spot toward the core base, the following three aspects of alteration happened progressively (Figure A.4 right panel-B, C, D, E):

a. Increasing dissolution of primary aragonite;

b. Gradual obscuring of primary aragonite skeletal structures, such as the radial-fibrous structure of aragonite fibres, the centres of calcification, and the micro-crannies in the aragonite matrix;

c. Progressive filling of the voids and replacement of primary skeletal aragonite with secondary aragonite needles and the gradual increase in the size of the secondary aragonite crystals. It was estimated by OM image observation that the percentages of the secondary aragonite in the altered coral matrix in spots C, D, and E are 1~2%, 10~15%, and 30~40%, respectively.

E.3 Influence of secondary aragonite on coral $\delta^{18}O$ and $\delta^{13}C$ records

Both $\delta^{18}O$ and $\delta^{13}C$ of the Holocene MS7 core exhibit large change in the basal sections (Figure A.5, dark shaded area). Big shifts toward higher values of isotope composition (0.25‰ for $\delta^{18}O$ and 0.7‰ for $\delta^{13}C$) compared with the neighbouring annual cycles are evident and the high values of the basal parts (dark shaded area) are much higher than any other part of the whole $\delta^{18}O$ and $\delta^{13}C$ records, implying that the geochemical variations seems not to be the result of any climate or environmental change.

Detailed petrographic research along the geochemical sub-sampling transect disclosed that the $\delta^{18}O$ and $\delta^{13}C$ variations were closely linked to presence of the secondary aragonite (Figure A.4). The combination of petrographic observation and geochemical measurement confirms the following observations:

- The altered coral $\delta^{18}O$ record still shows clear annual cycle, as shown by the dark shaded part of the coral $\delta^{18}O$ record in Figure A.4.

- Limited dissolution of primary aragonite did not produce distinguishable change in coral $\delta^{18}O$ records, as shown by OM image B in Figure 5.4 and the corresponding $\delta^{18}O$;

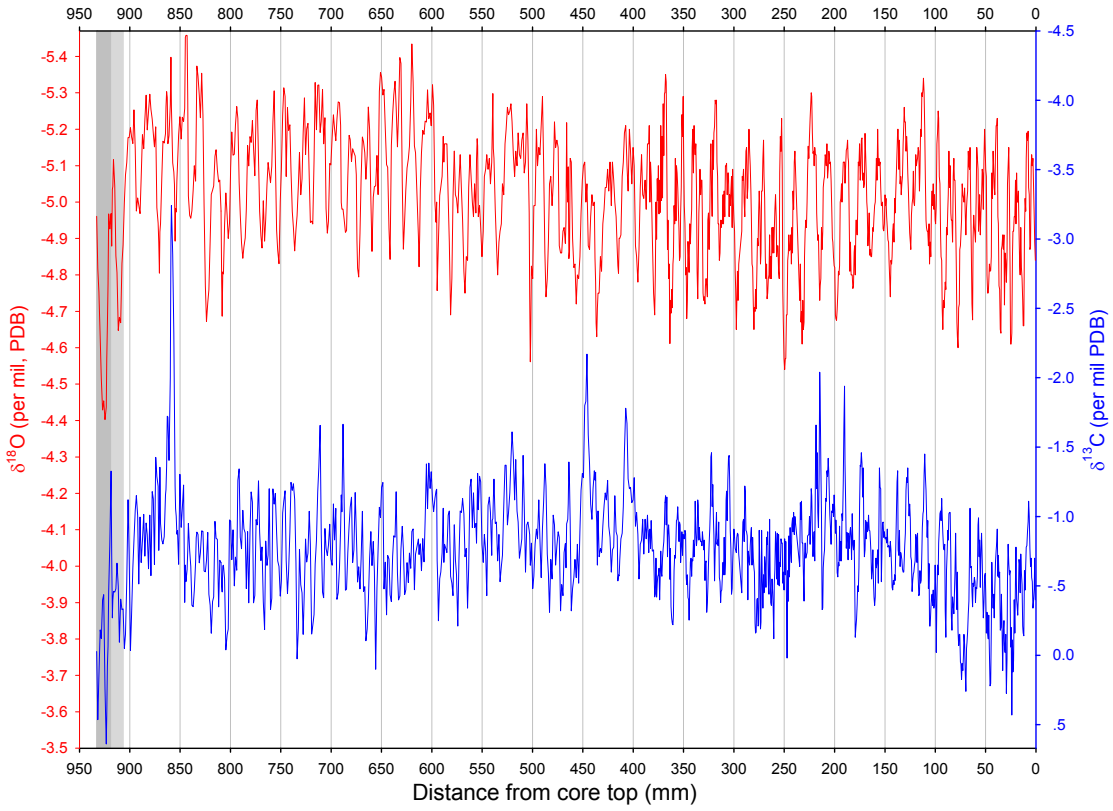

Figure A.5 Skeletal $\delta^{18}O$ (red) and $\delta^{13}C$ (blue) versus distance from core top of Holocene coral MS7. The shaded areas indicate $\delta^{18}O$ and $\delta^{13}C$ sections closely linked to the presence of secondary aragonite.

- Even a small amount of secondary aragonite could produce relatively "large" shift toward higher $\delta^{18}O$ values, indicative of sensitivity of coral $\delta^{18}O$ (and $\delta^{13}C$) to subtle infilling and replacement of original coral matrix by secondary aragonite in the marine environment. Even though there is only 1~2% secondary aragonite in spot C, the $\delta^{18}O$ seemed to have shifted to higher value since the early part of

the summer $\delta^{18}O$ has the highest summer value in the whole record. The first winter (higher $\delta^{18}O$ values between spots C and D in Figure A.4) has an average shift of 0.24‰ in $\delta^{18}O$ from the subsequent winter (between spots B and C) which has had a high average value among all the winters of this record (see Figure A.5), and the percentage of the secondary aragonite in the spot of the first winter should be less than 10% because of the progressive development of the diagenesis. Recent result of Quin and Taylor [*Quinn and Taylor*, 2006] indicated that 20% of secondary aragonite could bring a shift of 0.5‰ higher $\delta^{18}O$ value. So it is reasonable to attribute most of the 0.24‰ shift in the first winter $\delta^{18}O$ to secondary aragonite alteration. According to a $\delta^{18}O$-SST dependence of -0.189‰/ ^{o}C, the $\delta^{18}O$ shift of 0.24‰ could be converted to 1.3 ^{o}C cooler in SST.

The diagenetic alteration of coral $\delta^{18}O$ and $\delta^{13}C$ for the first annual cycle has been confirmed, but it is not so obvious for the second annual cycle. Higher $\delta^{18}O$ and $\delta^{13}C$ both in summer and winter for the second annual cycle have been observed, but the magnitudes are not big enough to distinguish them from other winter or summer interannual changes (see Figure A.5). Most of the second annual cycle is located between spots B and C (Figure A.4) and the presence of aragonite in that section should be 0~1%. Analysis of interannual variability of the MS7 coral $\delta^{18}O$ seems to support that coral $\delta^{18}O$ from this section had been altered, at least the early part of the second annual cycle.

The interannual variability of the MS7 coral $\delta^{18}O$ has been shown in Figure A.6. Since the coral $\delta^{18}O$ still has clear annual cycles in the diagenetic transition zone and the extension rates of 15.6 mm for the first two year bands are similar to the average rate in the younger section, the same chronology of the younger section has been employed to these two cycles to investigate the influence of secondary aragonite on the interannual variability of coral $\delta^{18}O$.

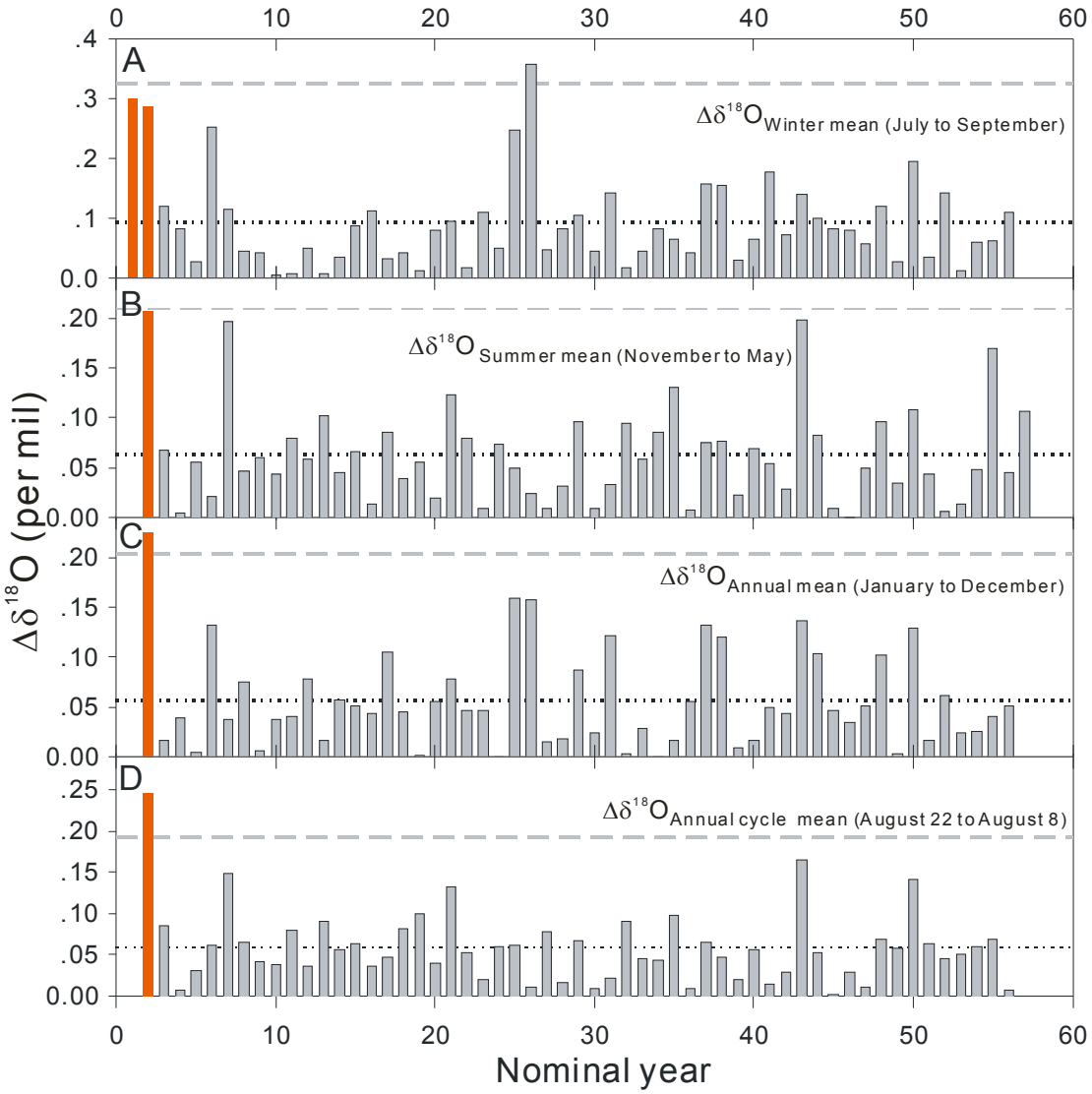

Figure A.6 Effect of secondary aragonite on the interannual variability of $\delta^{18}O$ record for the Holocene coral MS7**.** The interannual variability is expressed as the $\Delta\delta^{18}O$ which is the absolute value of the difference between the average $\delta^{18}O$ value of this year and the subsequent year for specified periods, such as winter, summer, year or annual cycle. Red bars referred as diagenetically altered coral $\Delta\delta^{18}O$. Dotted black lines are average values of the $\Delta\delta^{18}Os$ and dashed grey lines are upper control lines of 3σ standard deviation.

Figure A.6 exhibits evidently increased difference of $\delta^{18}O$ between neighbouring years during the first two annual cycles (red bars in Figure A.6). The $\Delta\delta^{18}Os$ of the first two annual cycles are 3 to 4 times of the averages of the whole core. Large $\Delta\delta^{18}O$ in both the first two winters might reflect the progressive addition of secondary aragonite. Even though the interannual variability of the winter and summer means in the second annual cycle is 3 times of the average level of the whole record, the year 2 (the second annual

cycle) is not distinguished among some years with high variation of winter and summer mean $\delta^{18}O$ (Figure A.6 A and B). However, this year could be distinguished among all the other years in the whole record by the high variations in annual mean and annual cycle mean $\delta^{18}Os$ which are 4 times of the averages and out of the 3σ standard deviation (Figure A.6 C and D).

This result shows that variation in interannual variability of coral $\delta^{18}O$ annual mean or annual cycle mean could serve as tools to help recognize diagenetic alteration of coral climate proxies, even very subtle alteration that is not so easy to be discerned by shift in winter or summer isotopic values.

This study demonstrates that clear annual cycles and small shifts from "normal" values of coral proxy records do not ensure the pristine nature of the corals. Even subtle alteration in coral skeleton, such as presence of as low as 1% of secondary aragonite, could bring large shifts in interannual variability of coral proxies which have extensive application in recognition of important historical climate events, such as ENSO, and is the base for understanding their vicissitudes by spectral analysis. Careful diagenesis screening should be performed before reconstructing paleoclimate using coral. And this study shows, even subtle diagenetical alteration in coral could be detected by combination of X-radiograph, petrographic observation, and analysis of interannual variability of coral proxies， and thereby the influence of diagenesis on coral reconstruction of paleoclimate and paleoceanography could be decreased to minimum.

The first two annual cycles in the Holocene coral MS7 were not used in climate reconstruction because of diagenetic alteration.

REFERENCES IN APPENDICES

Aissaoui, D. M., D. Buigues, and B. H. Purser (1986), Model of reef diagenesis: Mururoa Atoll French Polynesia, in *Reef diagenesis*, edited by J. H. Schroeder and B. H. Purser, pp. 27-52, Springer-Verlag.

Bar-Matthews, M., G. J. Wasserburg, and J. H. Chen (1993), Diagenesis of fossil coral skeletons: Correlation between trace elements, textures, and $^{234}U/^{238}U$, *Geochimica et Cosmochimica Acta*, *57*, 257-276.

Bathurst, R. G. C. (1975), *Carbonate sediments and their diagenesis*, Elsevier, Amsterdam.

Brachert, T. C., M. Reuter, T. Felis, K. F. Kroeger, G. Lohmann, A. Micheels, and C. Fassoulas (2006), Porites corals from Crete (Greece) open a window into Late Miocene (10Ma) seasonal and interannual climate variability, *Earth and Planetary Science Letters*, *245*(1-2), 81-94.

Constanz, B. R. (1986), The primary surface area of corals and variations in their suscepibility to diagenesis, in *Reef Diagenesis*, edited by J. H. Schroeder and B. H. Purser, pp. 53-90, Springer-Verlag.

Enmar, R., M. Stein, M. Bar-Matthews, E. Sass, A. Katz, and B. Lazar (2000), Diagenesis in live corals from the Gulf of Aqaba. I. The effect on paleo-oceanography tracers, *Geochimica et Cosmochimica Acta*, *64*(18), 3123-3132.

Esat, T. M., M. T. McCulloch, J. Chappell, B. Pillans, and A. Omura (1999), Rapid Fluctuations in Sea Level Recorded at Huon Peninsula During the Penultimate Deglaciation, *Science*, *283*(5399), 197-201.

Felis, T., G. Lohmann, H. Kuhnert, S. J. Lorenz, D. Scholz, J. Patzold, S. A. Al-Rousan, and S. M. Al-Moghrabi (2004), Increased seasonality in Middle East temperatures during the last interglacial period, *Nature*, *429*(6988), 164-168.

Gagan, M. K., L. K. Ayliffe, D. Hopley, J. A. Cali, G. E. Mortimer, J. Chappell, M. T. McCulloch, and M. J. Head (1998), Temperature and Surface-Ocean Water Balance of the Mid-Holocene Tropical Western Pacific, *Science*, *279*(5353), 1014-1018.

Gallup, C. D., D. M. Olson, R. L. Edwards, L. M. Gruhn, A. Winter, and F. W. Taylor (2006), Sr/Ca-Sea surface temperature calibration in the branching Caribbean coral Acropora palmata, *Geophysical Research Letters*, *33*(3), -.

Guilderson, T. P., R. G. Fairbanks, and J. L. Rubenstone (1994), Tropical temperature variations since 20,000 years ago: Modulating interhemispheric climate change, *Science*, *263*(5147), 663-665.

Guilderson, T. P., R. G. Fairbanks, and J. L. Rubenstone (2001), Tropical Atlantic coral oxygen isotopes: glacial-interglacial sea surface temperatures and climate change, *Marine Geology*, *172*(1-2), 75-89.

Hubbard, J. A. E. B., and P. K. Swart (1982), Sequence and style in scleractinian coral preservation in reefs and associated facies, *Palaeogeogr. Palaeoclimatol. Palaeoecol.*, *37*, 165-219.

Hughen, K. A., D. P. Schrag, S. B. Jacobsen, and W. Hantoro (1999), El Nino during the last interglacial period recorded by a fossil coral from Indonesia, *Geophysical Research Letters*, *26*(20), 3129-3132.

James, N. P. (1974), Diagenesis of scleractinian corals in the subaerial vadose environment, *Journal of Paleontology*, *48*, 785-799.

Martin, G. D., B. H. Wilkinson, and K. C. Lohmann (1986), The role of skeletal porosity in aragonite neomorphism: Strombus and Montastrea from the Pleistocene Key Largo Limestone, Florida, *Journal of Sedimentary Petrology*, *56*, 194-203.

McCulloch, M., G. Mortimer, T. Esat, X. Li, B. Pillans, and J. Chappell (1996), High resolution windows into early Holocene climate: coral records from the Huon Peninsula, *Earth and Planetary Science Letters*, *138*(1-4), 169-178.

McGregor, H. V., and M. K. Gagan (2003), Diagenesis and geochemistry of Porites corals from Papua New Guinea: Implications for paleoclimate reconstruction, *Geochimica Et Cosmochimica Acta*, *67*(12), 2147-2156.

Muller, A., M. K. Gagan, and M. T. McCulloch (2001), Early marine diagenesis in corals and geochemical consequences for paleoceanographic reconstructions, *Geophysical Research Letters*, *28*(23), 4471-4474.

Muller, A., M. K. Gagan, and J. M. Lough (2004), Effect of early marine diagenesis on coral reconstructions of surface-ocean C-13/C-12 and carbonate saturation state, *Global Biogeochemical Cycles*, *18*(1), -.

Potthast, I. (1992), Short-term progressive early diagenesis in density bands of recent corals: *Porites* colonies, Mauritius Island, Indian Ocean, *Facies*, *27*, 105-115.

Purser, B. H., and J. H. Schroeder (1986), The diagenesis of reefs: A brief review of our present understanding, in *Reef diagenesis*, edited by J. H. Schroeder and B. H. Purser, pp. 424-446, Springer-Verlag.

Quinn, T. M., and F. W. Taylor (2006), SST artifacts in coral proxy records produced by

early marine diagenesis in a modern coral from Rabaul, Papua New Guinea, *Geophysical Research Letters*, *33*(4), -.

Siegel, F. R. (1960), The effect of strontium on the aragonite-calcite ratios of Pleistocene corals, *Journal of Sedimentary Petrology*, *30*(2), 297-304.

Stein, M., G. J. Wasserburg, P. Aharon, J. H. Chen, Z. R. Zhu, A. Bloom, and J. Chappell (1993), Tims U-Series Dating and Stable Isotopes of the Last Interglacial Event in Papua-New-Guinea, *Geochimica Et Cosmochimica Acta*, *57*(11), 2541-2554.

Tribble, G. W. (1993), Organic-Matter Oxidation and Aragonite Diagenesis in a Coral-Reef, *Journal of Sedimentary Petrology*, *63*(3), 523-527.

Tudhope, A. W., C. P. Chilcott, M. T. McCulloch, E. R. Cook, J. Chappell, R. M. Ellam, D. W. Lea, J. M. Lough, and G. B. Shimmield (2001), Variability in the El Nino-Southern Oscillation Through a Glacial-Interglacial Cycle, *Science*, *291*(5508), 1511-1517.

Wei, G. J., J. S. Yu, X. T. Gui, F. J. Yu, Y. W. Chen, and D. P. Liu (1998), Paleoclimate implication of oxygen and carbon isotopic composition from diagenesis coral - Discussion on the data from NY-1 core, *Sci China Ser D*, *41*(6), 609-615.

Woodroffe, C. D., and M. K. Gagan (2000), Coral microatolls from the central Pacific record late Holocene El Nino, *Geophysical Research Letters*, *27*(10), 1511-1514.

Zhu, Z., J. F. Marshall, and J. Chappell (1994), Effects of Differential Tectonic Uplift on Late Quaternary Coral-Reef Diagenesis, Huon Peninsula, Papua-New-Guinea, *Australian Journal of Earth Sciences*, *41*(5), 463-474.